Recombinant expression and initial characterisation of two *Plasmodium falciparum* copper binding proteins: Cox11 and Cox19

by

Abdulmalik Abdullahi Salman

BSc (Hons), MSc. Biochemistry (ABUZ)

Submitted in fulfilment of the academic requirements for the degree of Philosophy of Science in the School of Life Sciences

University of KwaZulu-Natal

Pietermaritzburg

Preface

The experimental work described in this thesis was carried out in the Discipline of Biochemistry, School of Life Science, University of KwaZulu-Natal, Pietermaritzburg from August 2015 to November 2018 under the supervision of Prof. J.P.D. Goldring.

These studies represent original work by the author and have not otherwise been submitted in any form to another University. Where use has been made of the work by other authors it has been duly acknowledged in the text.

Signed:

_____

Date:

_____

Declaration – Plagiarism

I, Abdulmalik Abdullahi Salman, declare that:

1. The research reported in this thesis, except where otherwise indicated, is my original research.

2. This thesis has not been submitted for any other degree or examination at any other University.

3. This thesis does not contain other persons' data, pictures, graphs or other information, unless specifically acknowledged as being sourced from other persons.

4. This thesis does not contain other persons' writing, unless specifically acknowledged as being sourced from other researchers. Where other written sources have been quoted, then:
   a. Their words have been re-written but the general information attributed to them has been referenced.
   b. Where their exact words have been used, then their writing has been placed in italics and inside quotation marks, and referenced.

5. This thesis does not contain text, graphics or tables copied and pasted from the internet, unless specifically acknowledged, and the source being detailed in the thesis and in the References sections.

Signed:

_____

Date:

_____

Declaration Plagiarism 22/05/08 FHDR Approved

Acknowledgements

"In the name of Allah, the Most Gracious, the Most Merciful".

All glory and venerations are to the Creator of the universe and that in it.

I would like to express my earnest appreciation to the following people for their contribution to this study:

Firstly, my supervisor, Professor J.P. Dean Goldring for his support, mentorship, guidance and criticism throughout my research.

Dr Robert G.E. Krause for his guidance and support, and the rest of my malaria lab colleagues: Eugene Katapazi, Kajal Fowdar, Mark Hatton, Mlondi Shezi, Zainab Baig, Sheldon Sookai and Sinothile Khuzwayo for the good times in and out of the lab.

Professor Theresa H.T. Coetzer for access to her lab and equipment.

The technical staff, Jessica Moodley and Yegan Pillay. Charmaine Schofield-Ahrens, Natalie Jones and Tanya Karalic for their help with the administrative duties.

The South African Malaria Initiative, the National Research Foundation of South Africa, the Medical Research Council and the University of KwaZulu-Natal for funding the research.

My parents, Mr (late) and Mrs Abdullahi Salman, for their overwhelming support and kindness from the cradle to date. The rest of my family members for their support.

Dr Mohammed Auwal Ibrahim and Murtala Isah Bindawa for facilitating my PhD. admission.

My employer, Ahmadu Bello University Zaria, for awarding me a study fellowship. The head of biochemistry, Ahmadu Bello University Zaria, Professor M. Nasiru Shuaibu for his support.

My Professors, secondary and primary school teachers in Nigeria who mentored and gave me the much-needed head start to succeed in the field of science.

Dr Aliyu Salihu for the correspondence while I was away.

Finally, my friends, for their support and goodwill.

Abstract

Emerging drug resistance hinders the efforts to control malaria and so novel antimalarial drugs are required. Copper is essential for the survival of plasmodial parasites but the proteins involved in copper homeostasis are not well characterised. This study looked at plasmodial copper homeostasis by identifying and partially characterising two *P. falciparum* copper metallochaperones, Cox11 and Cox19. The Basic Local Alignment Search Tool (BLASTp) screen of the *Plasmodium* database (www.plasmodb.org) identified Cox11 and Cox19 gene orthologues in nine *Plasmodium* spp. The plasmodial Cox11 amino acid sequence contained a single N-terminus membrane-spanning region and three conserved cysteine residues, two of which are in a CFCF motif. These features are found in mammalian and yeast Cox11 amino acid sequences. The plasmodial Cox19 amino acid sequence has a domain containing a twin Cx_9C motif, and a conserved Tyr-Leu dipeptide between the pair of cysteine of one Cx_9C motif, similar to the amino acid sequences of human and yeast Cox19. The cloned and expressed recombinant MBP-*Pf*Cox11Ct and MBP-*Pf*Cox19 fusion proteins resolved on SDS-PAGE gels as ~62 kDa and ~66 kDa proteins respectively. Polyclonal IgY antibodies raised in chickens against rMBP-*Pf*Cox11Ct and rMBP-*Pf*Cox19 detected the native murine parasite, *P. berghei*, proteins on a western blot. Both recombinant proteins bound copper in the form of the cuprous ion *in vitro* and *in vivo* using the: bicinchoninic acid release, ascorbic acid oxidation, atomic absorption spectroscopy, and differential scanning fluorimetry assays. Three *P. falciparum* Cox11 mutants (two single- and a double-mutant) were engineered with site-directed mutagenesis, where an alanine replaced the corresponding cysteine residue and the mutant proteins were expressed as MBP fusion proteins. The two *P. falciparum* Cox11 cysteines, Cys155 and Cys157, in a CFCF motif were shown to be essential for the binding of copper in several assays. *P. falciparum* Cox11 and Cox19 bind copper *in vitro* and in an *in vivo* environment. Both rMBP-*Pf*Cox11Ct and rMBP-*Pf*Cox19 bound copper in an *in vivo* environment, enabling the growth of *E. coli* host cells expressing the proteins in the presence of toxic concentrations of copper. The localisation of the plasmodial Cox11 and Cox19 proteins suggested by proteomic data to be mitochondrial requires experimental confirmation. This study provides the foundation for further experiments to study *P. falciparum* Cox11 and Cox19 biochemistry and the evaluation of the two proteins as possible drug targets.

Graphical Abstract

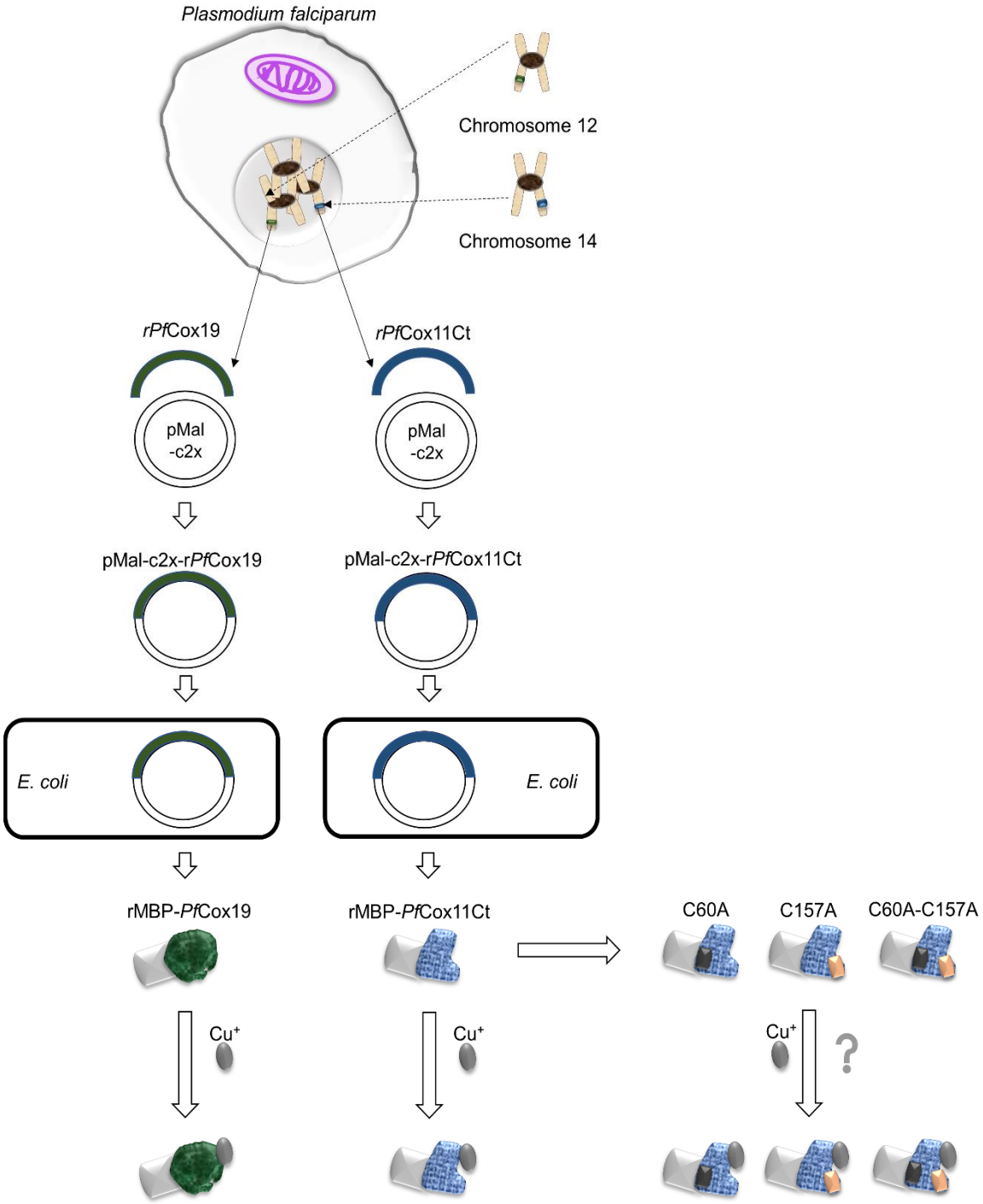

Contents

List of Figures

List of Tables

Abbreviations and symbols

Abbreviation	Explanation
2xYT	2x yeast extract, tryptone
3'-UTR	3'-untranslated region
3D	Three dimensional
A + X	Artemisinin with a partner drug
AAS	Atomic absorption spectroscopy
ABTS	2,2'-azino-bis(3-ethylbenzothiazoline sulfonate
Ace1	Ace1 transcription factor
ACT	Artemisinin-based combination therapy
ANOVA	Analysis of variance
Atox1	Antioxidant 1 copper chaperone
ATP	Adenosine triphosphate
ATP7A	ATPase copper transporter Alpha
ATP7B	ATPase copper transporter Beta
b.i.d	Twice daily
BCA	Bicinchoninic acid
BCKDH	Branch chain ketoacid dehydrogenase
BLASTp	Basic local alignment search tool for proteins
bp	Base pairs
BSA	Bovine serum albumin
C157A	Mutant pMal-c2x-r*Pf*Cox11Ct plasmid with Ala codon substituting that of Cys157
C60A	Mutant pMal-c2x-r*Pf*Cox11Ct plasmid with Ala codon substituting that of Cys60
C60A-C157A	Mutant pMal-c2x-r*Pf*Cox11Ct plasmid with Ala codon substituting that of Cys60 and Cys157
CcO	Cytochrome *c* oxidase
CCS	Copper chaperone for superoxide dismutase
CREBBP	CREB-binding protein
Crs5	Metallothionein-like protein Crs5
C-terminus	Carboxy terminus
Ctr1	Copper transporting protein 1
Ctr2	Copper transporting protein 2
Cup1	Copper metallothionein 1
CuP-ATPase	Copper-transporting P-type ATPase
Cyt*b*	Cytochrome *b*
Cyt*c*	Cytochrome *c*
DDC	Diethyldithiocarbamate
DHODH	Dihydroorotate dehydrogenase
DMSO	Dimethyl sulfoxide
DNA	Deoxyribonucleic acid
dNTP	Deoxyribonucleoside triphosphate
DTT	Dithiothreitol
ECL	Enhanced chemiluminescence
EDTA	Ethylenediaminetetraacetic acid
eEF2	Eukaryotic elongation factor 2
ELISA	Enzyme linked immunosorbent assay
EtBr	Ethidium bromide
FCA	Freund's complete adjuvant
FIA	Freund's incomplete adjuvant
FRE1	Cu^{2+}/Fe^{3+} metalloreductase component 1
FRE2	Cu^{2+}/Fe^{3+} metalloreductase component 2
GAPDH	Glyceraldehyde-3- phosphate dehydrogenase
gDNA	Genomic DNA
GSH	Reduced glutathione

Abbreviation	Explanation
hnDNA	Heterogenous nuclear DNA
HRP-2	Histidine-rich protein-2
HRPO	Horse radish peroxidase
Ig	Immunoglobulin
IM	Inner mitochondrial membrane
IMS	Mitochondrial intermembrane space
IPTG	Isopropyl-β-D-1-thiogalactopyranoside
IPTp	Intermittent preventive treatment in pregnancy
IRS	Indoor residual spray
ITS	IMS-targeting signal
KAT	Lysine acetyltransferase
kDa	kiloDaltons
LAMP	Loop-mediated isothermal amplification
LDH	Lactate dehydrogenase
LLIN	Long-lasting insecticide nets
Mac1	Metal-binding activator 1
MBP	Maltose binding protein
MBS	Maleimidobenzoyl-N-hydroxysuccinimide ester
MCF	Mitochondrial carrier proteins
MEC	Molecular exclusion chromatography
MISS	Mitochondrial IMS-sorting signal
MMV	Medicine for malaria venture
ms	Microsatellite
MT	Metallothionein
mtDNA	Mitochondrial DNA
MTF1	Metal transcription factor 1
MWCO	Molecular weight cut-off
nDNA	Nuclear DNA
NMCPs	National malaria control programs
NMD	Nonsense-mediated mRNA decay
NMR	Nuclear magnetic resonance
N-terminal	Amino terminal
OD	Optical density
ORF	Open reading frame
PBS	Phosphate buffered saline
PCR	Polymerase chain reaction
PDB	Protein data bank
PEG	Polyethylene glycol
*Pf*ATP4	P-type Na^+ ATPase
*Pf*crt	*P. falciparum* chloroquine resistance marker
*Pf*cytb	*P. falciparum* cytochrome *b*
*Pf*dhfr	*P. falciparum* dihydrofolate reductase
*Pf*mdr1	*P. falciparum* multidrug resistance-1
*Pf*mrp1	*P. falciparum* multidrug resistance protein-1
*Pf*nhe1	*P. falciparum* Na^+/H^+ exchanger
pGEM®-T Easy-r*Pf*Cox11Ct	Recombinant pGEM®-T Easy cloning vector with r*Pf*Cox11Ct coding sequence
PI4K	Lipid phosphatidylinositol 4-kinase
pMal-c2x-r*Pf*Cox11Ct	Recombinant pMal-c2x expression vector with r*Pf*Cox11Ct coding sequence
pMal-c2x-r*Pf*Cox19	Recombinant pMal-c2x expression vector with r*Pf*Cox19
PMT	Phosphoethanolamine-N-methyltransferase
pTZ57R/T-r*Pf*Cox19	Recombinant pTZ57R/T cloning vector with r*Pf*Cox19 coding sequence
q.d	Once daily
RDTs	Rapid diagnostic tests

Abbreviation	Explanation
rMBP-*Pf*Cox11Ct	Recombinantly expressed MBP fused *P. falciparum* Cox11 carboxy terminal domain
rMBP-*Pf*Cox19	Recombinantly expressed MBP fused *P. falciparum* Cox19
RNA	Ribonucleic acid
r*Pf*Cox11Ct	Recombinant *P. falciparum* Cox11 carboxy terminal coding sequence
r*Pf*Cox19	Recombinant *P. falciparum* Cox19 coding sequence
RT	Room temperature
S.E	Standard error
SAP	Shrimp alkaline phosphatase
SCC	Small copper carrier
SD	Standard deviation
SDS	Sodium dodecyl sulphate
SDS-PAGE	Sodium dodecyl sulphate polyacrylamide gel electrophoresis
SMC	Seasonal malaria chemoprevention
SOC	Super optimal broth with catabolite repression
SOD	Cu/Zn superoxide dismutase
SPR	Surface plasmon resonance
TAE	Tris, acetic acid, EDTA buffer
TCA	Tricarboxylic acid
TEMED	N,N'N'N'-tetramethylethylenediamine
TGN	Trans-Golgi network
Tm	Melting temperature
WHO	World Health Organisation
X	α-aminobutyric acid (replacing Cys in the synthetic peptide)
X-gal	5-bromo-4-chloro-3-indolyl-β-D-galactopyranoside

Chapter 1

Introduction and literature review

1.1 An overview of malaria

1.1.1 The malaria burden

Malaria, a mosquito-borne parasitic disease caused by a protozoan of the genus *Plasmodium*, is a public health problem and a leading cause of death from infectious diseases in 91 countries (Murray *et al.*, 2014; WHO, 2017). Only five species of the over 100 *Plasmodium* spp.; *Plasmodium falciparum, P. vivax, P. malariae, P. ovale* and *P. knowlesi* are known to infect humans, with *P. falciparum* responsible for the largest burden followed by *P. vivax* (Ashley *et al.*, 2018; Daneshvar *et al.*, 2009). About 90% of the 216 million cases reported in 2016 were in Africa, accounting for the 91% of the 445000 deaths globally, most of which were children under five years old (WHO, 2017). The clinical manifestations of malaria may vary from mild (fever) to severe (severe anaemia, and organ failure) and cerebral (coma) malaria (Miller *et al.*, 1994a; White *et al.*, 2014). Considerable success has been recorded in the global control and eradication of malaria since the beginning of the millennium, with a 41% and 62% reduction in incidence and death from malaria respectively (WHO, 2016). This success is threatened by the increasing emergence of parasites resistant to the available antimalarial drugs including artemisinin (Ashley *et al.*, 2014; Cui *et al.*, 2015; Hyde, 2005). Therefore, there is a need to develop new antimalarial drugs (Burrows *et al.*, 2017; Flannery *et al.*, 2013; Le Roch *et al.*, 2003).

1.1.2 A brief history of malaria

The discovery of human malaria parasite antigens in mummified individuals from ancient Egypt who lived between 3200 BC and 1085 BC showed that malaria is an ancient disease (Miller *et al.*, 1994b). Before the discovery that malaria is caused by a *Plasmodium* spp. infection by Alphonse Laveran in 1880, the disease was thought to be associated with "bad air" (*mal'aria* in Latin) emanating from swamps (Laveran, 1881). The discovery of the avian and human malaria vectors, the culicine and the anopheline mosquitoes were made in two separate studies by Sir Ronald Ross and a group of Italian scientists respectively (Grassi, 1901; Ross, 1898). The discovery in 1947 by Henry Shortt and Cyril Garnham that the liver phase precedes the intraerythrocytic phase of the parasite was significant to the understanding of the parasite life cycle (Shortt and Garnham, 1948). The dormant liver phase was subsequently

discovered by Wojciech Krotoski in 1982 (Krotoski *et al.*, 1982). The identification of the *Plasmodium* spp. with certitude was only possible in 1907. Most of the human-infecting species were identified in the 1920s and 1930s, while the first rodent malaria parasite, *P. berghei*, was identified in 1948 (Cox, 2010; Vincke and Lips, 1948).

1.1.3 A brief description of the *Plasmodium* life cycle

The human-infecting malaria parasite infects two hosts, the human and the female *Anopheles* mosquito (Figure 1.1). An infected *Anopheles* mosquito transmits malaria during a blood meal by inoculating about 20 sporozoites into the avascular tissue of the skin, marking the beginning of a cycle in the human host (Baldacci and Ménard, 2004; Kappe *et al.*, 2010). Within three hours of inoculation, the sporozoites exit the inoculation site and penetrate a blood vessel to enter the blood and eventually the liver (Cowman *et al.*, 2016; Ponnudurai *et al.*, 1991). In the liver, the sporozoites access the liver by traversing the sinusoidal barrier targetting Kupffer and endothelial cells (Cha *et al.*, 2015; Tavares *et al.*, 2013). Once inside the hepatocytes, asexual replication commences with the transformation and division of sporozoites into exo-erythrocytic forms (liver stage) over two to ten days leading to the release of 10000 to 30000 merozoites per hepatocyte into the bloodstream (Fujioka and Aikawa, 2002; Sturm *et al.*, 2006; White *et al.*, 2014).

The merozoites invade erythrocytes within two minutes of contact in a rapid, energetic, and multi-step process (Gilson and Crabb, 2009; Weiss *et al.*, 2015). When erythrocyte invasion is established, 16 to 32 merozoites are formed by cell division (schizogony) over 24 (*P. knowlesi*), 48 (*P. falciparum*, *P. vivax*, *P. ovale*) or 72 (*P. malariae*) hours (White *et al.*, 2014). The merozoites are then released into the bloodstream following the destruction of the erythrocyte membrane. The newly infective merozoites go on to infect naïve erythrocytes.

Following a variable number (often three to ten) of completed asexual cycles, a small proportion of the merozoites differentiate into male and female gametocytes which are capable of transmitting malaria to mosquitoes (Bousema and Drakeley, 2011; Josling and Llinas, 2015). The sexual stage of the parasite life cycle commences upon ingestion of the gametocytes in a blood meal by the mosquito. The gametocytes in the midgut fuse to form a zygote which then matures into mobile ookinetes which pass through the midgut cell wall and transform into an oocyst. The oocysts then undergo sporogony, releasing sporozoites which migrate to the mosquito salivary glands where they remain, and ready for onward transmission in the next blood meal (Lee *et al.*, 2014).

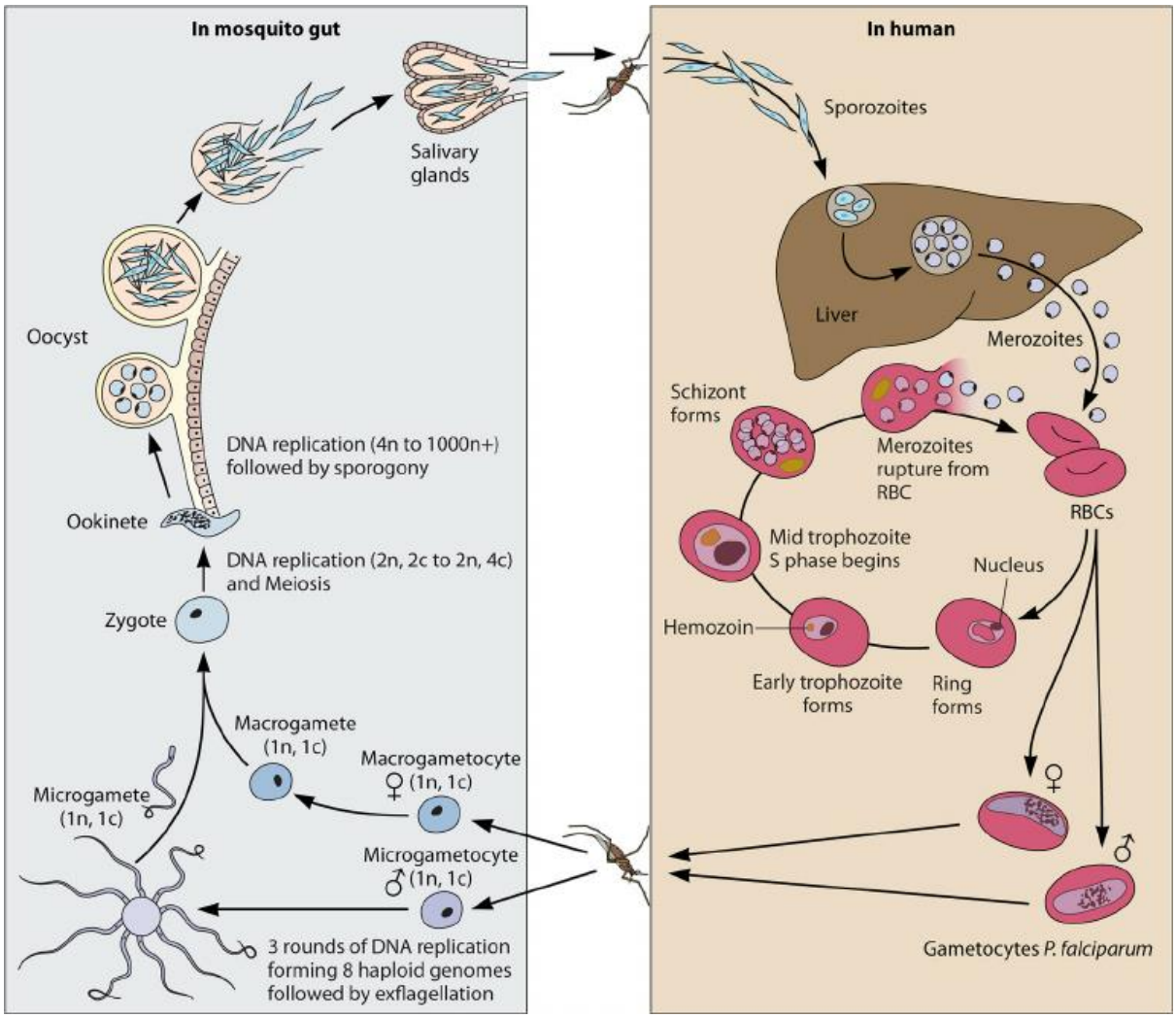

Figure 1.1. The *Plasmodium* life cycle
The malaria parasite life cycle is complex and occurs within the mosquito vector (left side of the cycle) and the human host (right side of the cycle). Malaria infection begins upon parasite transmission by a female *Anopheles* mosquito to a human host. The parasites undergo sexual (in mosquito) and asexual (in a human host) development. Number of cells, n; set of chromosomes in a cell, c. Taken from Lee *et al.* (2014).

1.1.4 Geographical distribution of malaria

Malaria is endemic to 91 countries in the tropical and subtropical regions of the world (Figure 1.2) (WHO, 2017). Malaria transmission depends on environmental factors – mainly temperature, the efficiency of *Anopheles* mosquito to support parasite growth alongside other factors like poverty, natural disasters, war and the implementation of control measures (Ashley *et al.*, 2018; Balogun *et al.*, 2016; Cowman *et al.*, 2016; White *et al.*, 2014). Only a few of the over 400 anopheline mosquitoes are vectors, and they are indigenous to specific geographical regions (Massey *et al.*, 2016; Sinka *et al.*, 2012).

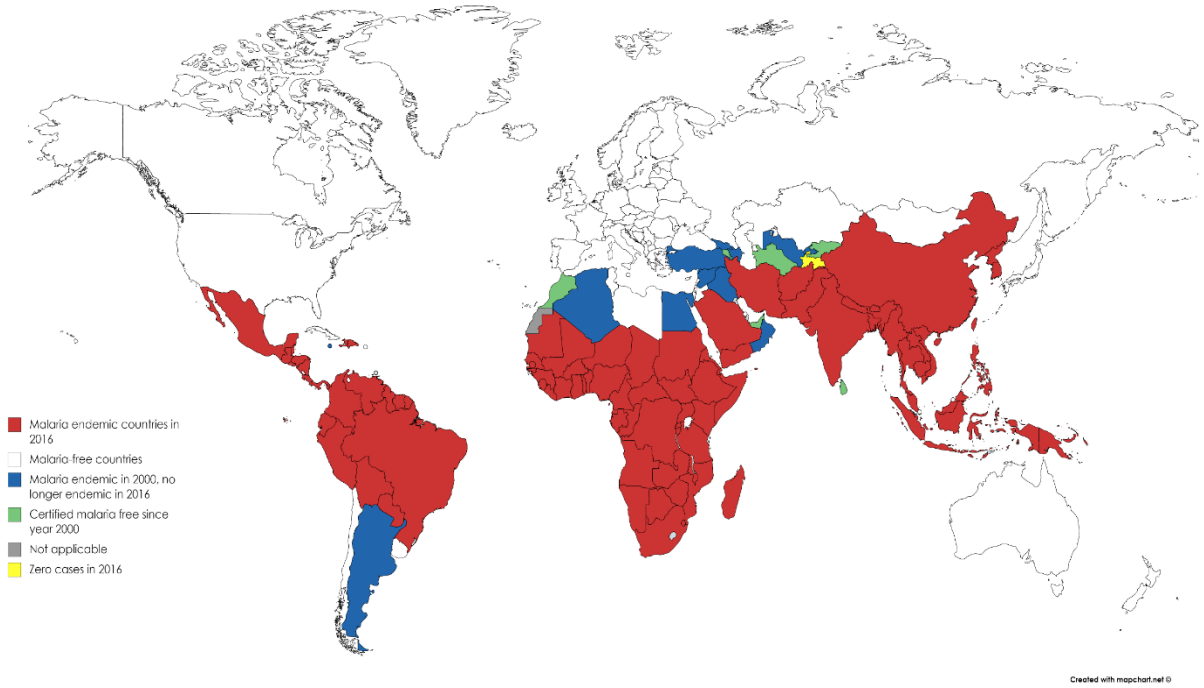

Figure 1.2. Countries with indigenous cases in 2000 and their status by 2016
Malaria endemicity was determined by the number of indigenous cases. Countries with no indigenous cases reported to the WHO over the past three consecutive years are considered to have eliminated malaria. This map was created using the online MapChart tool (https://mapchart.net/). Adapted from WHO (2017).

P. falciparum and *P. vivax* are the prepotent species of the human malaria parasites, accounting for about 95% and 4% respectively of the global cases of malaria in 2016 (Ashley *et al.*, 2018; WHO, 2017). *P. falciparum* is responsible for the vast majority of malaria cases (99%) in Africa with a substantial variation in prevalence within and among countries (Nkumama *et al.*, 2017; Snow *et al.*, 2017), while *P. vivax* malaria is less common. Conversely, *P. vivax* malaria is predominant in the Americas (64%), South-East Asia (30%) and in the Eastern Mediterranean regions (40%) (WHO, 2017). The two malaria species, *P. malariae* and *P. ovale*, accounted for about 1% of the global malaria burden in 2016, a low incidence despite their global distribution (WHO, 2017). *P. ovale* is largely indigenous to Africa and South-East Asia. The last of the five human-infecting malaria parasites hitherto ascribed to primate malaria, *P. knowlesi*, was only recently found to infect humans in South-East Asia (Cox-Singh *et al.*, 2008; Singh *et al.*, 2004). The lack of *P. knowlesi* transmitting vectors in Africa and the Americas is preventing its global distribution (Kar *et al.*, 2014; Singh and Daneshvar, 2013).

In South Africa, malaria endemicity is restricted to the low-altitude border regions of three of the nine provinces; KwaZulu-Natal, Mpumalanga and Limpopo (Morris *et al.*, 2013). The containment of the disease to three provinces is the product of effective malaria control strategies initiated in the 1940s (Coetzee *et al.*, 2013). Despite the steady progress towards

eradicating malaria since South Africa adopted the elimination strategy in 2012, an increase of about 4900 cases were reported between 2013 and 2014 mainly in Mpumalanga and Limpopo provinces (Raman *et al.*, 2016). Malaria transmission in South Africa is seasonal often between the months of October and May. About 4.9 million persons (~10% of the population) are at risk of malaria infection in South Africa (http://www.health.gov.za/index.php/introduction, accessed 14/09/18).

1.1.5 Malaria control

A renewed interest in the eradication of malaria, backed by an increase in international funding since the turn of the millennium, has led to the adoption and upscale of malaria control interventions in endemic countries (Kesteman *et al.*, 2017). The intervention strategies include the use of rapid diagnostic tests in malaria diagnosis, indoor residual spraying (IRS), long-lasting insecticide nets (LLIN) for mosquito control. Drug interventions include mass drug administrations (MDAs), intermittent preventive treatment in pregnancy (IPTp) and in infants (IPTi), seasonal malaria chemoprevention (SMC). Changes in drug administration include artemisinin-based combination therapy (ACT) as the first-line treatment of uncomplicated malaria and monitoring the efficacy and safety of antimalarial drugs and resistance among others (WHO, 2015). The adoption and implementation of these interventions are controlled by national malaria control programs of each malaria endemic country.

1.1.6 Malaria diagnosis

Microscopy (thick and thin blood film) and rapid diagnostic tests are the two diagnostic methods with the most impact on malaria control. Microscopy remains the gold standard of malaria diagnosis for evaluating any new diagnostic test (Alam *et al.*, 2011; Wongsrichanalai *et al.*, 2007). The visual identification of parasites within the erythrocytes under the microscope relies on the staining of parasite DNA molecules by the Giemsa and other stains (Barcia, 2007; Warhurst and Williams, 1996). Since peripheral blood erythrocytes lack DNA, only the parasitised erythrocytes contain the stained DNA. In addition to the Giemsa stain, the Wright's, Field's and Leishman stains are used (Sathpathi *et al.*, 2014; Warhurst and Williams, 1996). A skilled microscopist can detect about 5 parasites/µl of blood, while an average microscopist detects about 50 to 100 parasites/µl of blood (Kasetsirikul *et al.*, 2016; Tangpukdee *et al.*, 2009). Microscopy is laborious, dependent on a skilled microscopist, prone to misdiagnosis of

morphologically closely related species (like *P. knowlesi and P. malariae*), and an underestimation of infection in asymptomatic malaria (Kasetsirikul *et al.*, 2016).

1.1.7 Rapid diagnostic tests

Rapid diagnostic tests (RDTs) are based on the immunological detection of a number of malaria antigens like histidine-rich protein-2 (HRP-2), lactose dehydrogenase (LDH) and aldolase in blood on an immunochromatographic test strip impregnated with the respective colloidal gold-labelled antibody and a control. Recently two constitutively expressed plasmodial proteins, glyceraldehyde-3-phosphate dehydrogenase (GAPDH) (Krause *et al.*, 2017) and phosphoethanolamine-N-methyltransferase (PMT) (Krause and Goldring, 2018) were shown to be potential malaria diagnostic biomarkers. In a bid to enhance the applicability of rapid diagnostic tests for malaria detection, specific aptamers targetting malaria LDH were recently shown to discriminately bind their targets (Frith *et al.*, 2018). With rapid diagnostic tests, the confirmation of infection is timely, cost-effective, and little or no expertise is required (Boyce *et al.*, 2015; Hansen *et al.*, 2015). However, rapid diagnostic tests are expensive and liable to false-positive diagnosis owing to the presence of malaria antigens like HRP-2 in the blood after parasite clearance (Mayxay *et al.*, 2001; Swarthout *et al.*, 2007).

In addition to the two diagnostic tests – microscopy and RDTs described above, PCR-based tests are also common. PCR-based tests provide higher specificity and sensitivity (<5 parasites/µl of blood) compared to the RDTs and can differentiate different plasmodial species (Lee *et al.*, 2015; Ongagna-Yhombi *et al.*, 2013). Though the PCR-based tests have low limits of detection, they take a longer time to perform, are dependent on electricity and are often laboratory-based and so are not suited for point of care application in the field. The PCR-based tests can be grouped into nested, single, multiplex, real-time and quantitative PCR. The least technically demanding among the PCR-based tests is the loop-mediated isothermal amplification (LAMP) (Cook *et al.*, 2015). LAMP uses isothermal amplification directly from blood samples by a mutant *Taq* DNA polymerase resistant to the PCR inhibitors in the blood (Kermekchiev *et al.*, 2009; Kersting *et al.*, 2014). LAMP is suited for field application and could take less time than the conventional PCR reactions using heat-blocks and viewed under UV light without the requirement for imaging equipment.

1.1.8 Treatment of malaria

To effectively treat malaria, the disease has to be correctly diagnosed and promptly treated with the appropriate antimalarial drug. The management of malaria requires the use of safe, cheap and accessible, effective, well tolerated, and easy to administer antimalarials (Kremsner and Krishna, 2004). Antimalarials are classified based on their structure (Cui *et al.*, 2015; Schlitzer, 2008) or the parasite life-cycle stage target (Bruce-Chwatt, 1962) (Table 1.1). Based on the parasite life-cycle stage target, antimalarial drugs are either; tissue schizontocides, blood schizontocides, gametocytocides, sporontocides, or anti-relapse drugs (Bruce-Chwatt, 1962; Frederich *et al.*, 2002). Despite their differing modes of action, almost all the currently antimalarials in use are blood schizontocides. Primaquine is the only licensed anti-relapse drug of all the antimalarials in use for treating hypnozoites in *P. vivax* and *P. ovale* infections. Structurally, antimalarial drugs are grouped as 4-aminoquinolines, arylamino alcohols, 8-aminoquinolines, artemisinin derivatives, antifolates, naphthoquinone, or antibiotics (Antony and Parija, 2016; Cui *et al.*, 2015; Schlitzer, 2008).

The treatment regimens for the two prepotent malaria parasites, *P. falciparum* and *P. vivax*, are different chiefly due to their varying pathophysiology. Owing to the emergence and spread of resistance against the established antimalarial drugs, artemisinin-based combination therapy (ACT) has now been adopted as the first-line treatment for uncomplicated *falciparum* malaria in endemic regions (Nosten and White, 2007). The combination of chloroquine for treating blood stage and primaquine for hypnozoites (dormant liver stages) clearance, stands as the first-line treatment for *P. vivax* malaria (WHO, 2010). The primary aim of adopting ACTs as the first-line treatment for malaria was to curb the emergence of drug-resistant parasites. ACTs comprise a fast-acting artemisinin component and a long-acting partner drug that clears the residual parasites evading artemisinin clearance, thus, arresting the emergence of possible artemisinin resistance (Egan and Kaschula, 2007; Nosten and White, 2007). Therefore, the long-acting partner drug in ACTs compensates for the poor pharmacokinetics of the artemisinin component (Egan and Kaschula, 2007; Nosten and White, 2007). Both component drugs in an ACT-regimen have different modes of action. The blood stages of non-*falciparum* malaria are also cleared by ACTs. With the exception of the artemether-lumefantrine combination therapy, which is a six-dosage regimen (twice daily for three days), all the WHO-approved ACTs in use are taken as a three-dosage regimen (once daily for three days) (Table 1.2) (WHO, 2015). Due to an elongation effect of piperaquine on the electrical repolarisation and depolarisation of the ventricles (QT interval) (Darpo *et al.*, 2015;

Vanachayangkul *et al.*, 2017), an electrocardiogram is required before prescribing the dihydroartemisinin-piperaquine combination therapy to a patient (WHO, 2015). In endemic regions in Africa, intermittent preventive treatment is recommended for pregnant mothers and infants (with sulfadoxine/pyrimethamine), and in areas with high seasonal malaria transmission (with amodiaquine + sulfadoxine/pyrimethamine) (WHO, 2015). Travellers from nonendemic to high-risk areas are advised to take malaria chemoprophylaxis (Cui *et al.*, 2015; Schlagenhauf and Petersen, 2008). The antimalarials; mefloquine, atovaquone/proguanil (Malarone) or doxycycline are the recommended chemoprophylactic for long-term travellers (Schlagenhauf and Petersen, 2008; WHO, 2015).

Table 1.1. Classification and drug-resistance status of available antimalarials.

Class	Drug	Parasite life-cycle stage target	Drug resistance	Drug-resistance marker gene
4-Aminoquinoline	Chloroquine	Blood-stage schizontocide*, sporontocide,	Yes	*Pfcrt*, *Pfmdr1*, *Pfmrp1*
	Amodiaquine	Blood-stage schizontocide*	Yes	*Pfmdr1*
	Piperaquine	Blood-stage schizontocide*	Yes	plasmepsin 2-3, exo-E415G
8-Aminoquinoline	Primaquine	Tissue-stage schizontocide, sporontocide, gametocide, anti-relapse	Yes	Not yet identified
Arylamino alcohol	Quinine	Blood-stage schizontocide*, gametocide¶	Yes	*Pfcrt*, *Pfmdr1*, *Pfmrp1*, *Pfnhe1*
	Lumefantrine	Blood-stage schizontocide*	Yes	*Pfmdr1*
	Mefloquine	Blood-stage schizontocide*	Yes	*Pfmdr1*
Sesquiterpene lactone endoperoxides	Artemether	Blood-stage schizontocide*, gametocide	Yes	*Pfmdr1*, *Kelch13*
	Artesunate	Blood-stage schizontocide*, gametocide	Yes	*Pfmdr1*, *Kelch13*
	Dihydroartemisinin	Blood-stage schizontocide*, gametocide	Yes	*Pfmdr1*, *Kelch13*
Antifolate	Sulfadoxine	Blood-stage schizontocide#, tissue schizontocide, sporontocide	Yes	*Pfdhps*
	Pyrimethamine	Blood-stage schizontocide#, tissue schizontocide, sporontocide	Yes	*Pfdhfr*
	Proguanil	Blood-stage schizontocide#, tissue schizontocide, sporontocide	Yes	*Pfdhfr*
Naphthoquinone	Atovaquone	Blood-stage schizontocide#, sporontocide	Yes	*Pfcytb*
Antibiotics	Doxycycline	Blood-stage schizontocide#	No	-
	Clindamycin	Blood-stage schizontocide#	No	-

* Quick onset, ¶ *P. vivax* and *P. ovale only*, # Slow onset, *Pfcrt*; *P. falciparum* chloroquine resistance marker, *Pfmdr1*; *P. falciparum* multidrug resistance-1, *Pfmrp1; P. falciparum* multidrug resistance protein-1, *Pfnhe1; P. falciparum* Na^+/H^+ exchanger, *Pfdhps*; *P. falciparum* dihydropteroate synthase, *Pfdhfr*; *P. falciparum* dihydrofolate reductase, *Pfcytb*; *P. falciparum* cytochrome *b*. Information from this table was from; (Amato *et al.*, 2017; Bruce-Chwatt, 1962; Cui *et al.*, 2015; WHO, 2015; Witkowski *et al.*, 2017).

Table 1.2. WHO approved artemisinin-based combination therapies (ACTs) for treating uncomplicated malaria

Drug components	Formulation / Tablet (A + X)	Bodyweight (kg) (dose)	Prescription	Comment(s)
Artemether + Lumefantrine	20 mg + 120 mg [#] 40 mg + 240 mg	5 – <15 (20 mg +120 mg) 15 – 25 (40 mg + 240 mg) 25 – <35 (60 mg + 360 mg) ≥35 (80 mg + 480 mg)	3 x b.i.d. (total, 6 doses)	- Lumefantrine absorption is enhanced by fat intake. - Lumefantrine is not available as a monotherapy.
Artesunate + Amodiaquine	25 mg + 67.5 mg 50 mg + 135 mg 100 mg + 270 mg	4.5 – <9 (25 mg + 67.5 mg) 9 – <18 (50 mg + 135 mg) 18 – <36 (100 mg + 270 mg) ≥36 (200 mg + 540 mg)	3 x q.d. (total, 3 doses)	- Pharmacokinetics of amodiaquine is not affected by age or pregnancy.
Artesunate + Mefloquine	25 mg + 50 mg 100 mg + 200 mg	5 – <9 (25 mg + 50 mg) 9 – <18 (50 mg + 100 mg) 18 – <30 (100 mg + 200 mg) ≥30 (200 mg + 400 mg)	3 x q.d. (total, 3 doses)	- Symptoms due to mefloquine include nausea, vomiting, dizziness, dysphoria and sleep disturbances. - Co-administration with rifampicin results in decreased mefloquine bioavailability.
Artesunate + Sulfadoxine-Pyrimethamine	50 mg + 500 mg +25 mg*	5 – <10 (25 mg + 250 mg + 12.5 mg) 10 – <25 (50 mg + 500 mg + 25 mg) 25 – <50 (100 mg + 1000 mg + 50 mg) ≥50 (200 mg + 1500 mg + 75 mg)	3 x q.d. (total, 3 doses)	- Not available as a fixed dose combination.
Dihydroartemisinin + Piperaquine	20 mg + 160 mg 40 mg + 320 mg	5 – <8 (20 mg + 160 mg) 8 – <11 (30 mg + 240 mg) 11 – <17 (40 mg + 320 mg) 17 – <25 (60 mg + 480 mg) 25 – <36 (80 mg + 640 mg) 36 – <60 (120 mg + 960 mg) 60 – <80 (160 mg + 1260 mg) ≥80 (200 mg + 1600 mg)	3 x q.d. (total, 3 doses)	- Electrocardiogram is required before prescription, as piperaquine prolongs QT interval (electrical repolarisation and depolarisation of the ventricles).

Dispersible formulation; * not available as a single dose combination; b.i.d. twice daily; q.d. once daily; A artemisinin component; X partner drug.
Information from this table was from WHO (2015).

1.1.9 Antimalarial drug resistance

The goals to control and possibly eradicate malaria are threatened by emerging resistance to the available antimalarials. *P. falciparum* is proficient at acquiring and spreading resistance to antimalarials often from low-transmission areas (Southeast Asia and South America) to high-transmission areas in sub-Saharan Africa (White, 2004). The acquisition of antimalarial drug resistance is a consequence of genetic modifications that confer reduced drug susceptibility to the parasite. The genetic modifications are either point mutations or changes to the copy number of genes encoding or associated with the drug's parasite target, or transport proteins regulating the intraparasitic drug level (Menard and Dondorp, 2017; White, 2004). These modifications can arise at any of the developmental stages of the parasite (Pongtavornpinyo *et al.*, 2009). The genetic modifications must not be at the cost of the parasite's fitness (Menard and Dondorp, 2017; White, 2004). The identification of an antimalarial drug-resistance gene marker is vital to understanding the extent and spread of antimalarial drug resistance. So far, the antimalarial drug-resistance gene markers (Table 1.1) identified are; *P. falciparum* chloroquine resistance transporter (*Pfcrt*), *P. falciparum* multidrug resistance-1 (*Pfmdr1*), *P. falciparum* multidrug resistance-associated protein-1 (*Pfmrp1*), *P. falciparum* Na^+/H^+ exchanger (*Pfnhe1*), dihydropteroate synthase (*Pfdhps*), *P. falciparum* dihydrofolate reductase (*Pfdhfr*), *P. falciparum* cytochrome b (*Pfcytb*), and, most recently, Kelch K13 propeller domain (*Kelch13*), *plasmepsin 2-3* and an exonuclease gene polymorphism on chromosome 13 (*exo-E415G*). Together, these antimalarial drug-resistance gene markers are responsible for the poor efficacy of the available antimalarial drugs.

1.1.9.1 Modifications to the antimalarial drug-resistance markers

The development of resistance to an antimalarial drug is a consequence of either a single or concerted molecular changes to some of the known antimalarial drug-resistance markers. These changes are either amino acid substitutions or changes to the gene copy number. The substitution of lysine 76 in *Pf*CRT to threonine (K76T) in both clinical and field isolates is implicated in *P. falciparum* chloroquine resistance (Durand *et al.*, 2001; Fidock *et al.*, 2000). The K76T mutation renders chloroquine inactive by preventing its accumulation and actively transporting it out of the food vacuole (Martin and Kirk, 2004). *Pf*MDR1 like the *Pf*CRT is a transmembrane transport protein, and both mutation and variation in gene copy number of the *Pfmdr1 gene* has been associated with resistance to some 4-aminoquinoline and arylamino alcohol antimalarials, and artemisinin derivatives *in vitro* (Table 1.1) (Foote *et al.*, 1990; Price

et al., 1999; 2006; Reed *et al.*, 2000; Sidhu *et al.*, 2005). The single amino acid substitutions in *Pf*MDR1 protein implicated in multidrug-resistance are; N86Y, S1034C, Y184F, D1246Y and N1042D. Two single amino acid substitutions, Y191H and A437S in *Pf*MRP, also a transmembrane transport protein, are linked to chloroquine and quinine resistance (Antony and Parija, 2016; Mu *et al.*, 2003). The gene knockout of *Pfmrp1* gene in chloroquine-resistant parasites not only increased their sensitivity to chloroquine and quinine, but also to multiple antimalarial drugs (Raj *et al.*, 2009). Repeat polymorphisms (DNNND and NHNDNHNNDDD motifs) in the microsatellite region (ms4760) of the *P. falciparum* transmembrane proton efflux protein, *Pf*NHE1, was demonstrated to be associated with quinine resistance (Ferdig *et al.*, 2004). However, two subsequent independent *in vitro* studies on field isolates in Africa demonstrated the lack of association between the repeat polymorphisms of the two motifs to quinine resistance (Andriantsoanirina *et al.*, 2010; Briolant *et al.*, 2011). Therefore, the *Pfnhe1* gene cannot serve as a global marker for quinine-resistance. Resistance to the antifolate antimalarial drugs is the result of a mutation to the gene markers *Pfdhfr* (proguanil and pyrimethamine) and *Pfdhps* (sulfadoxine) of the folate synthesis pathway (Cowman *et al.*, 1988; Gregson and Plowe, 2005). Pyrimethamine resistance results from triple mutations in the *Pfdhfr* gene coding for N51I, C59R and S108N single amino acid substitutions (Peterson *et al.*, 1988). Sulfadoxine resistance results from multiple combinations of the single amino acid substitutions; S/A436F, A437G, K540E, A581G, and A613S/T in *Pf*DHPS (Brooks *et al.*, 1994). Resistance to atovaquone is conferred by mutations in *Pfcytb* gene coding single amino acid substitutions of Y268N/S (Fivelman *et al.*, 2002; Korsinczky *et al.*, 2000). Whole-genome sequencing of artemisinin-resistant isolates from Africa and Cambodia revealed a strong association between artemisinin resistance and the single amino acid substitutions, Y493H, R539T, I543T, and C580Y, in the Kelch13 (Ariey *et al.*, 2014). Most recently, the two gene markers for piperaquine-resistance, *plasmepsin 2-3* and *exo-E415G*, were identified (Amato *et al.*, 2017; Witkowski *et al.*, 2017). The amplification of *plasmepsin 2-3* gene and mutation in the *exo-E415G* gene confers reduced primaquine susceptibility to the parasite (Amato *et al.*, 2017; Dondorp, 2017; Witkowski *et al.*, 2017). To date, the lone *P. vivax* malaria resistance to have emerged is against chloroquine (Rieckmann *et al.*, 1989) and its molecular marker is yet to be identified (Menard and Dondorp, 2017).

1.1.10 Potential antimalarial drug targets

With the efficacy of the current antimalarial drugs being limited by drug resistance, concerns about their long-term usefulness are raised. This then emphasises the need for developing new drugs with different or similar molecular targets to the existing antimalarial drugs in order to realise malaria control and eradication goals. To this end, a number of public-private partnerships like Medicines for Malaria Venture (MMV) were initiated to advance the use of medicinal chemistry-based approaches and high-throughput drug screens for identifying new promising antimalarial drug targets. A number of potential drug candidates, as well as new drug targets, have been identified in high-throughput whole-cell screens of compounds against the parasite (Table 1.3) (Blasco *et al.*, 2017; Cowman *et al.*, 2016; Flannery *et al.*, 2013). The new antimalarial drug targets identified so far for the new drug candidates at different developmental stages are; i) P-type Na^+ ATPase (*Pf*ATP4), ii) lipid phosphatidylinositol 4-kinase (PI4K), iii) dihydroorotate dehydrogenase (DHODH) iv) eukaryotic elongation factor 2 (eEF2), and v) phenylalanyl-tRNA synthetase (Blasco *et al.*, 2017; Cowman *et al.*, 2016).

1.1.11 Novel antimalarial drug candidates

Cipargamin (KAE609), a spiroindolone compound currently in advanced clinical trials, was identified from whole-cell screens of asexual stages of *P. falciparum*. Cipargamin inhibits the parasite asexual blood-stage progression and transmission to mosquitoes by targetting *Pf*ATP4, which results in the disruption of sodium homeostasis (Rottmann *et al.*, 2010; Spillman *et al.*, 2013). Two other *Pf*ATP4 inhibitors, a dihydroisoquinolone, SJ733, currently in clinical trials (Jiménez-Díaz *et al.*, 2014) and a pyrazoleamide compound, PA21A092, a preclinical drug candidate (Vaidya *et al.*, 2014), have also been identified. Like cipargamin, SJ733 and PA21A092 block the asexual blood-stage progression and transmission of the parasite (Jiménez-Díaz *et al.*, 2014; Vaidya *et al.*, 2014). Two classes of compounds targetting PI4K, imidazopyrazines (McNamara *et al.*, 2013) and a 2-aminopyridine (MMV390048) (Paquet *et al.*, 2017) were identified from whole-cell screens. Imidazopyrazines alters the intracellular phosphatidylinositol-4-phosphate distribution by interacting with the ATP-binding pocket of PI4K to inhibit the blood-stages of *P. falciparum* and *P. vivax* as well as the hypnozoites of *P. cynomolgi* (McNamara *et al.*, 2013). Unlike the imidazopyrazines, MMV390048 inhibits all life-stages of the parasite but the hypnozoites (Paquet *et al.*, 2017). DSM265, a triazolopyrimidine compound currently in clinical trials is a long-acting antimalarial drug inhibiting both the blood- and liver-stages by targetting DHODH (McCarthy

et al., 2017; Phillips *et al.*, 2015). DSM265 is suited for use as a partner drug in a single-dose combination treatment (McCarthy *et al.*, 2017). A 2,6-disubstituted quinoline-4-carboxamide scaffold, DDD107498, and a bicyclic azetidine (BRD3444) identified from whole-cell screens inhibit protein synthesis by targetting eEF2 and phenylalanyl-tRNA synthetase respectively (Baragaña *et al.*, 2015; Kato *et al.*, 2016). The imidazolopiperaquine, KAF156, currently in clinical trials is also active against multiple life-cycle stages, however, its molecular target is yet to be identified (Kuhen *et al.*, 2014; Meister *et al.*, 2011).

Table 1.3. Potential antimalarial drugs and targets.

Drug target	Drug name	Previous name(s)	Parent structure	Efficacy	Status*	Reference
*Pf*ATP4	Cipargamin	NITD609, KAE609	Spiroindolone	- Asexual blood stage - Blocks transmission	- Completed first phase IIa (short duration monotherapy POC in patients) - Phase II study in patients started in February 2018 to be completed 2019/20	Rottmann *et al*., 2010; Spillman *et al*., 2013
	SJ733	(+)- SJ000557733	Dihydroisoquinolone	- Asexual blood stage - Blocks transmission	- First-in-human study recruiting	Jiménez-Díaz *et al*., 2014
	PA21A092	-	Pyrazoleamide	- Asexual blood stage - Blocks transmission	Pre-clinical	Vaidya *et al*., 2014
PI4K	KA1407, KA1715 and KDU691	-	Imidazopyrazines	- Blood-stages - Hypnozoites of P. cynomolgi	Pre-clinical	McNamara *et al*., 2013
	MMV390048	-	2-aminopyridine	- Liver and blood stages	Pre-clinical	Paquet *et al*., 2017
DHODH	DSM265		Triazolopyrimidine	- Asexual blood stage - Chemoprotection	- Phase IIa in Peru with P. *falciparum* or P. *vivax* completed - Controlled human malaria infection study of combination with OZ439 completed	McCarthy *et al*., 2017; Phillips *et al*., 2015
eEF2	DDD107498	-	2,6-disubstituted quinoline-4-carboxamide	- Liver and blood stages	Pre-clinical	Baragaña *et al*., 2015
Phenylalanyl-tRNA synthetase	BRD3444	-	Bicyclic azetidines	- Liver and blood stages	Pre-clinical	Kato *et al*., 2016
Unknown	KAF156	GNF156	Imidazolopiperaquine	- Liver and blood stages	- Phase IIb combination study ongoing to be completed in 2019	Kuhen *et al*., 2014; Meister *et al*., 2011

* Clinical status obtained from https://www.mmv.org/research-development/mmv-supported-projects.
*Pf*ATP4; *P. falciparum* P-type Na^+ ATPase, PI4K; lipid phosphatidylinositol 4-kinase, DHODH; dihydroorotate dehydrogenase, eEF2; eukaryotic elongation factor 2, POC; point of care.

1.2 Biological role of copper

Copper is an indispensable component of a large range of essential biochemical processes in living organisms. Examples of copper-dependent processes are; oxidative respiration, neurological function (synthesis of neurotransmitters as well as neuromodulation), defence against oxidative damage, tissue repair, skin pigmentation, peptide hormone production and iron homeostasis among others (Kaplan and Maryon, 2016; Kim *et al.*, 2008; Lutsenko, 2010; Scheiber *et al.*, 2014). Several of these processes exploit the dual redox states of copper, Cu(I) and Cu(II), for its structural, regulatory and catalytic roles. Cu^{2+} and Cu^{+} coordination to the prion protein and the human copper chaperone for superoxide dismutase (CCS) respectively, results in conformational changes in the proteins (Kim *et al.*, 2008). However, the redox activity of copper when left unchecked could potentially lead to oxidative stress from free-radical (reactive oxygen species) production. The damaging effect of copper stems from its propensity under aerobic conditions to produce the highly reactive hydroxyl radical which causes damage to the macromolecules via the Fenton ($Cu^{+} + H_2O_2 \rightarrow Cu^{2+} + OH^{-} + \cdot OH$) and Haber-Weiss ($Cu^{2+} + \cdot O_2 \rightarrow Cu^{+} + O_2$) reactions (Halliwell and Gutteridge, 1984; Hodgkinson and Petris, 2012). Oddly, copper can potently inhibit many biological processes as it reacts indiscriminately with the sulphur, nitrogen and oxygen atoms of a diverse spectrum of protein side chains (Kaplan and Maryon, 2016). Selective damage via radical formation can arise from copper binding at side-chains (containing O, S or N) of catalase, BSA, thyrotropin-releasing hormone, glutamine synthetase and amyloid precursor proteins (Davies, 2016; Levine, 1983; Marx and Chevion, 1986; Multhaup *et al.*, 1998; Rivett and Levine, 1990). Therefore, free cellular copper must be tightly regulated. In line with this, organisms have evolved mechanisms to keep intracellular copper content within the required threshold and ensure copper delivery to the target site. The human pathologies, Menkes and Wilson's diseases, are directly linked to disturbed copper metabolism from the mutations of ATP7A and ATP7B genes, respectively (Scheiber *et al.*, 2014). Other human pathologies like cancer, Alzheimer's, Parkinson's and Huntington's are indirectly linked to an imbalance of copper metabolism (Dudzik *et al.*, 2013; Hung *et al.*, 2010; Millhauser, 2007; Tisato *et al.*, 2010; Xiao *et al.*, 2013). About 100 mg of copper is present in an average human adult (Kim *et al.*, 2008). Most of the copper present in the blood plasma is bound to ceruloplasmin (~70%), and the rest is bound to albumin (~18%) and other components, but none of the copper is free (Linder, 2001; Tapiero *et al.*, 2003).

1.2.1 Copper uptake

The processes involved in the intracellular copper utilisation including signalling, transport across biological membranes, delivery and insertion of copper at the targetted destination are regulated with a high degree of specificity (Argüello *et al.*, 2012; Kim *et al.*, 2008; Turski and Thiele, 2009). Together, these processes regulate copper acquisition from the immediate surrounding of the cell (Nevitt *et al.*, 2012). The high-affinity copper transport protein 1, Ctr1, is responsible for the bulk (~70%) of copper uptake in eukaryotic cells (Lee *et al.*, 2002a), while other low-affinity divalent metal transporters contribute to the cellular demand for copper (~30%) (Arredondo *et al.*, 2014; Lee *et al.*, 2002b; Liu *et al.*, 1997; Nevitt *et al.*, 2012). High-affinity copper acquisition is triggered when the copper levels of the immediate surrounding of the cell are below the binding threshold of the ever-present low-affinity metal transporters on the cell surface (Nevitt *et al.*, 2012).

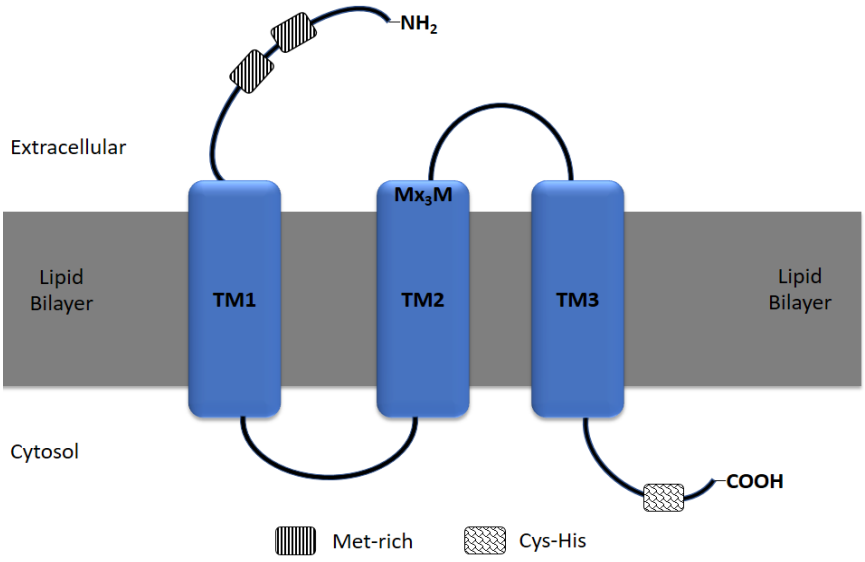

Figure 1.3. Structural model for copper transport proteins
Copper transport proteins (Ctr1 and Ctr2) are characterised by three transmembrane domains (TM), with the essential copper uptake motif, Mx_3M, in the second TM. The Met-rich N-terminal domain is localised extracellularly, while the Cys-His cluster-containing C-terminal tail is localised intracellularly.

Ctr1, an integral membrane protein (Figure 1.3), is composed of three membrane-spanning domains, an extracellular methionine-rich N-terminal domain, a conserved Mx_3M motif in the second transmembrane domain, and an intracellular C-terminal tail (Eisses and Kaplan, 2002; Wang *et al.*, 2011). The several methionine motifs within the N-terminal domain, although not essential for copper transport, bind and coordinate copper to facilitate high-affinity transfer (Eisses and Kaplan, 2005; Puig *et al.*, 2002). Functional studies demonstrated the essentiality of the Mx_3M motif for copper uptake via the formation of Cu-S

linkages (De Feo *et al.*, 2009; Puig *et al.*, 2002). Copper transport relies on the oligomerisation of Ctr1 to a homotrimer (Figure 1.4), which forms a copper-permeable pore through which copper is ferried across the membrane (Aller and Unger, 2006; De Feo *et al.*, 2009). Ctr1 is specific to Cu^{+}, therefore, copper uptake is subject to a preliminary reduction of Cu^{2+} to Cu^{+} by the cell surface Cu^{2+}/Fe^{3+} metalloreductases (Figure 1.5), Fre1 and Fre2 in yeast, and the Steap family metalloreductases in mammals (Georgatsou *et al.*, 1997; Hassett and Kosman, 1995; Martins *et al.*, 1998; Ohgami *et al.*, 2006; Rees and Thiele, 2007). Small copper carriers (SCC) in the mammalian plasma and liver are thought to be extracellular ligands from which copper is delivered to Ctr1 (Cabrera *et al.*, 2008; Gray *et al.*, 2012; Linder, 2016). The high-affinity copper transport by Ctr1 is not ATP-dependent (Lee *et al.*, 2002a). Prior to copper transport across the membrane by Ctr1 in yeast, the detection of cellular copper status is mediated by the reciprocal activities of the two copper-binding transcription factors, Ace1 and Mac1, which are activated in copper-replete and copper-deficient cells respectively (Keller *et al.*, 2005; Rutherford and Bird, 2004). Under copper shock, cells show a rapid activation of Ace1 and a corresponding rise in Mac1 inactivation leading to accumulation of cellular copper. The activation of Ace1 and Mac1 results in the upregulation and downregulation, respectively, of copper homeostatic proteins. In mammals, the metal transcription factor 1 (MTF1) helps with the regulation of cellular copper content in response to starvation or repletion (Heuchel *et al.*, 1994).

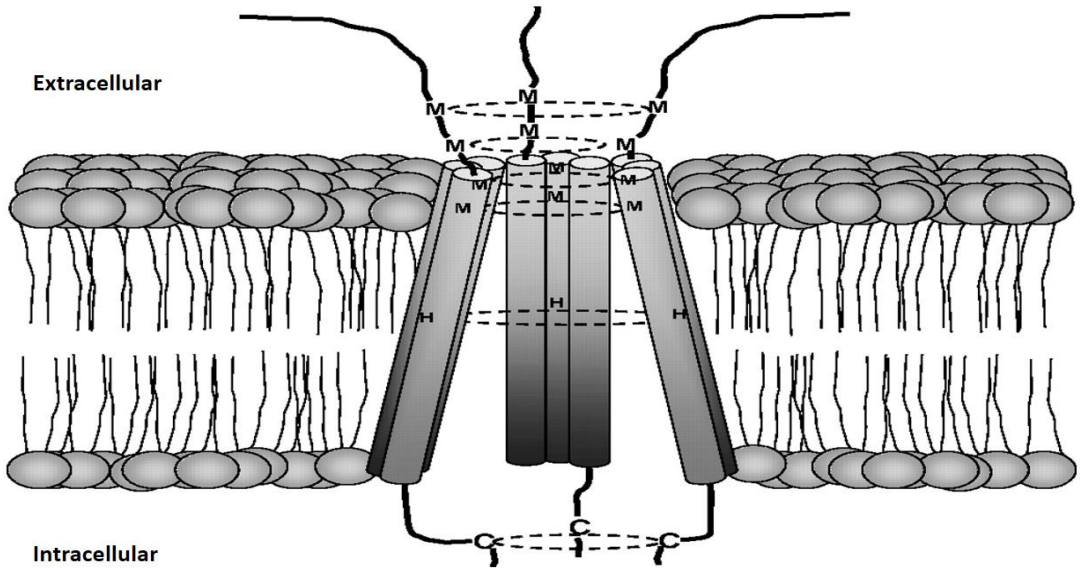

Figure 1.4. Schematic of the trimeric pore of copper transport proteins
Nine transmembrane domains from a homotrimer of Ctr1 forms a pore of stacked rings of Met, His, and Cys in the bilayer that participates in the transchelation – a successive chelation of Cu^{+} between the Met residues along the homotrimeric pore of Ctr1 protein during Cu^{+} uptake through the Ctr1 protein. Taken from Howell *et al.* (2010).

The second copper transport protein, Ctr2, in yeast and mammals, is structurally similar to Ctr1 with a high degree of sequence similarity (Rees *et al.*, 2004; Zhou and Gitschier, 1997). In contrast to Ctr1, Ctr2 is a low-affinity (van den Berghe *et al.*, 2007) vacuolar membrane transporter in yeast which releases copper from the intracellular stores during copper starvation and delivers it to different chaperones (Rees *et al.*, 2004). The human Ctr2 has is localised to the intracellular organelles, lysosome and endosomes (van den Berghe *et al.*, 2007). However, the main physiological role of the human Ctr2 remains unresolved (Öhrvik and Thiele, 2015).

1.2.2 Intracellular copper delivery

The intracellular handling and distribution of copper is a tightly regulated mechanism which keeps the undesirable redox activity of copper in check. Evidence from several studies has demonstrated that almost no free intracellular copper is present within a cell (Linder, 2001; Tapiero *et al*., 2003). The two cytosolic copper chaperones, copper chaperone for superoxide dismutase (CCS) and Antioxidant 1 copper chaperone (Atox1) (Atx1 in yeast) supply copper to Cu/Zn superoxide dismutase (SOD1) and membrane-bound copper-transporting P-type ATPases in the secretory pathway, respectively (Figure 1.5) (Field *et al.*, 2002). Examples of the copper-transporting P-type ATPases (CuP-ATPase) are ATP7A and ATP7B in mammals, and Ccc2 in yeast. The P-type ATPases are mainly located in the terminal compartment of the Golgi apparatus, the trans-Golgi network. Atox1 and CCS were demonstrated to engage the negatively charged lipid bilayer and directly interact with the copper-bound Ctr1 (Flores and Unger, 2013; Pope *et al.*, 2013). These findings support the model that copper release from Ctr1 is effected by protein-protein interaction between the chaperones and the transporter (Lutsenko, 2016). Conversely, an independent study demonstrated glutathione (GSH) to be the initial Cu^{+} acceptor after its translocation through Ctr1 (in human Ctr1), which then delivers copper to the chaperones from a Cu-GSH complex (Maryon *et al.*, 2013). The metalloreductase, Fre6, together with Ctr2 in yeast mobilises vacuolar copper (Rees *et al.*, 2004). Copper is also required in the mitochondria for cytochrome *c* oxidase (CcO) assembly and SOD1 activity. The mechanism by which copper is delivered to the mitochondria is yet to be resolved, however, a low molecular weight carrier (L) is implicated (Cobine *et al.*, 2004; 2006). In a copper-depleted environment, copper is made available to critical biological processes from a pool of intracellular copper partly maintained by the chaperones, metallothioneins (MTs) (Cup1 and Crs5 in yeast), and GSH (Nevitt *et al.*, 2012).

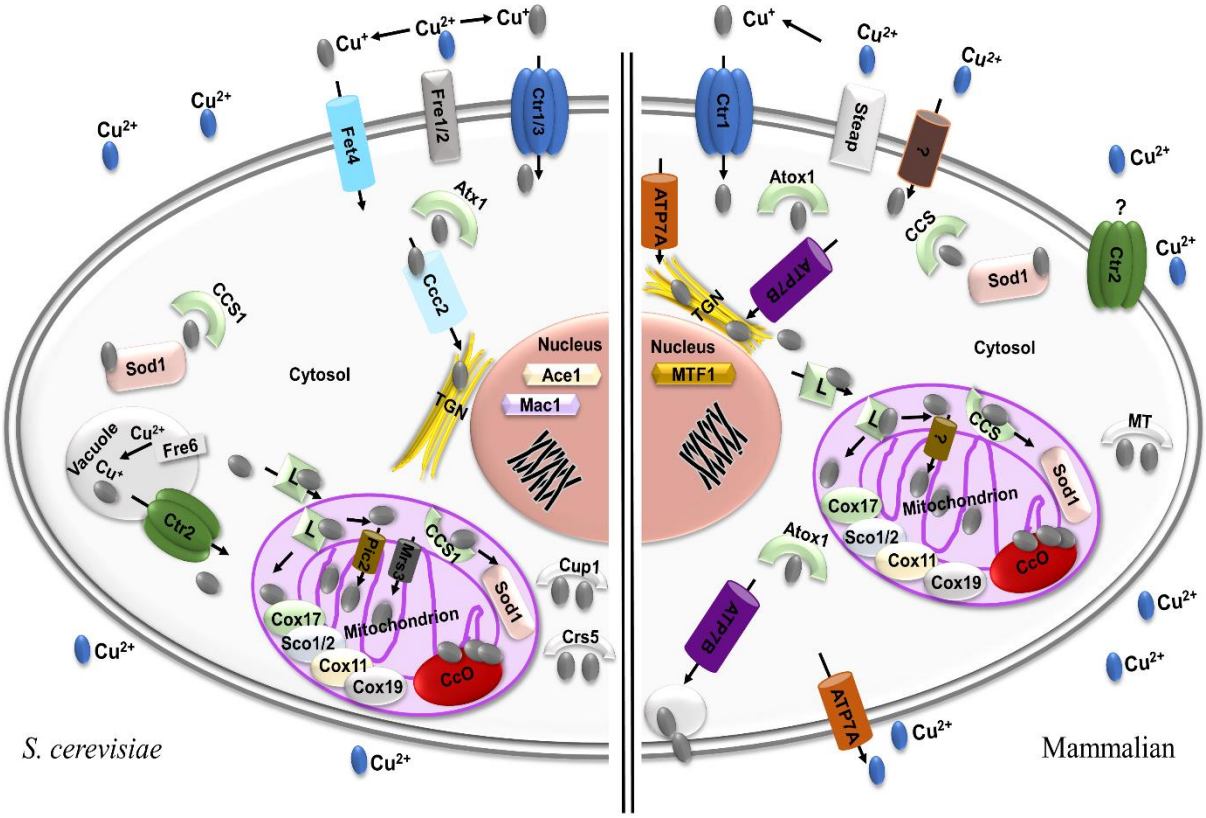

Figure 1.5. Copper homeostasis in eukaryotes
A synopsis of copper sensing, acquisition, intracellular distribution, sequestration and mobilisation in eukaryotes. Both the *S. cerevisiae* (left) and the generic mammalian (right) models for copper homeostasis are depicted. The importance of these proteins to copper homeostasis are discussed in the text. Image modified from Nevitt *et al.* (2012).

1.2.3 Copper delivery to the mitochondria

Copper in the mitochondria is primarily needed for SOD1 activation and CcO assembly (Fontanesi *et al.*, 2006). The mitochondrial matrix copper content is about an order of magnitude above the expected threshold for the activation of the CcO (Cobine *et al.*, 2004). This suggests that mitochondria contain a pool of copper not associated with the copper-dependent CcO assembly, hence, possibly serving as a copper storage organelle. This now leaves the question of how the mitochondrion acquires copper. As stated earlier, the mechanism by which copper gets to the mitochondria is not well described, however, it is mediated by four mitochondrial copper chaperones; Cox17, Cox11, Sco1 and Sco2. Cox17 was first identified in yeast as an essential component of CcO when mutant cells were unable to respire despite having all the CcO components (Glerum *et al.*, 1996). Cox17 supplies copper to two inner mitochondrial membrane (IM)-associated copper-binding proteins (Maxfield *et al.*, 2004), Sco1 and Cox11, which are responsible for the metallation of the Cu_A and Cu_B centres of Cox2

and Cox1 respectively (Hiser *et al.*, 2000; Horng *et al.*, 2004; Lode *et al.*, 2000; Timón-Gómez *et al.*, 2018). Initially, Cox17 was thought to convey copper from the cytosol into the mitochondrial intermembrane space (IMS) owing to its dual localisation in both compartments. However, Cox17 was demonstrated in experiments tethering it to the inner mitochondrial membrane to serve a copper chaperone role to the CcO assembly without having to leave the mitochondrial intermembrane space (Maxfield *et al.*, 2004). So far, the only clue with regards copper entry into the mitochondria is the low molecular weight carrier (L) which is thought to bind copper in the cytosol and the complex (CuL) is ferried across the outer mitochondrial membrane (Cobine *et al.*, 2004; 2006). Thereafter, the mitochondrial Cox17 obtains copper from the complex for onward supply to Cox11 and Sco1 respectively. Vest *et al.* (2013) demonstrated that the mitochondrial carrier family (MCF) protein, Pic2, supplies the pool of copper in the mitochondrial matrix in yeast by transporting copper as CuL complex across the inner mitochondrial membrane. Mrs3, an IM-associated high-affinity iron transporter was subsequently demonstrated in yeast to complement Pic2 in the generation of the mitochondrial matrix copper pool by transporting CuL across the inner mitochondrial membrane (Vest *et al.*, 2016). Despite the lack of evidence of a bi-directional copper transport across the inner mitochondrial membrane by Pic2 and Mrs3 (Baker *et al.*, 2017; Vest *et al.*, 2013; 2016), an unidentified protein mobilises copper from the matrix copper pool into the mitochondrial intermembrane space (Baker *et al.*, 2017).

1.2.4 Role of copper in the malaria parasite

Copper has been shown to be important for *P. falciparum* in red blood cells (Asahi *et al.*, 2014). The chelation of copper ions in the parasite growth medium resulted in the inhibition of the progression of the ring-trophozoite-schizont stages of erythrocytic development (Asahi *et al.*, 2013). Similarly, when the copper-binding proteins in the *P. falciparum* were inhibited with neocuproine (a copper chelator) the parasite ceased to grow (Asahi *et al.*, 2014). In two separate studies, the presence of the membrane transport proteins, CuP-ATPase and Ctr1 in *P. falciparum* (Choveaux *et al.*, 2012; Rasoloson *et al.*, 2004) were reported (Figure 1.6). CuP-ATPase is expressed in all *Plasmodium* life cycle stages and localised in the cell to unidentified vesicle-like structures as shown in Figure 1.6 (Kenthirapalan *et al.*, 2014). Gene knock-out of the CuP-ATPase and Ctr1 genes in *P. berghei*, severely affected parasite fertility and transmission through the mosquito vector but did not affect the exponential propagation of asexual blood stages (Kenthirapalan *et al.*, 2014; 2016). The poor parasite transmission in the

mosquito host arising from the loss of function of the two copper transporting proteins, CuP-ATPase and Ctr1, implied copper homeostasis in *Plasmodium* spp. could be targetted in transmission-blocking strategies (Kenthirapalan *et al.*, 2014; 2016). The critical role of copper in the liver stage of *P. cynomolgi* was demonstrated when neocuproine treatment of hepatocytes showed a pronounced effect on the viability of both liver schizonts and hypnozoites (Voorberg-van der Wel *et al.*, 2017). Together, this evidence suggests the requirement for copper and a copper-homeostatic mechanism in the parasite. However, the strategy employed by the parasite to acquire extracellular copper is yet to be elucidated (Asahi *et al.*, 2016). Rasoloson *et al.* (2004) demonstrated that extracellular copper is made available to the parasite following degradation of the host Cu/Zn superoxide dismutase in the parasite's food vacuole. Using a bioinformatics approach, four putative copper metallochaperones, Cox11, Cox17, Cox19 and Sco1 were identified in *Plasmodium falciparum* (Choveaux *et al.*, 2015). Two of the four metallochaperones, Cox11 and Cox19, were chosen for characterisation in this study.

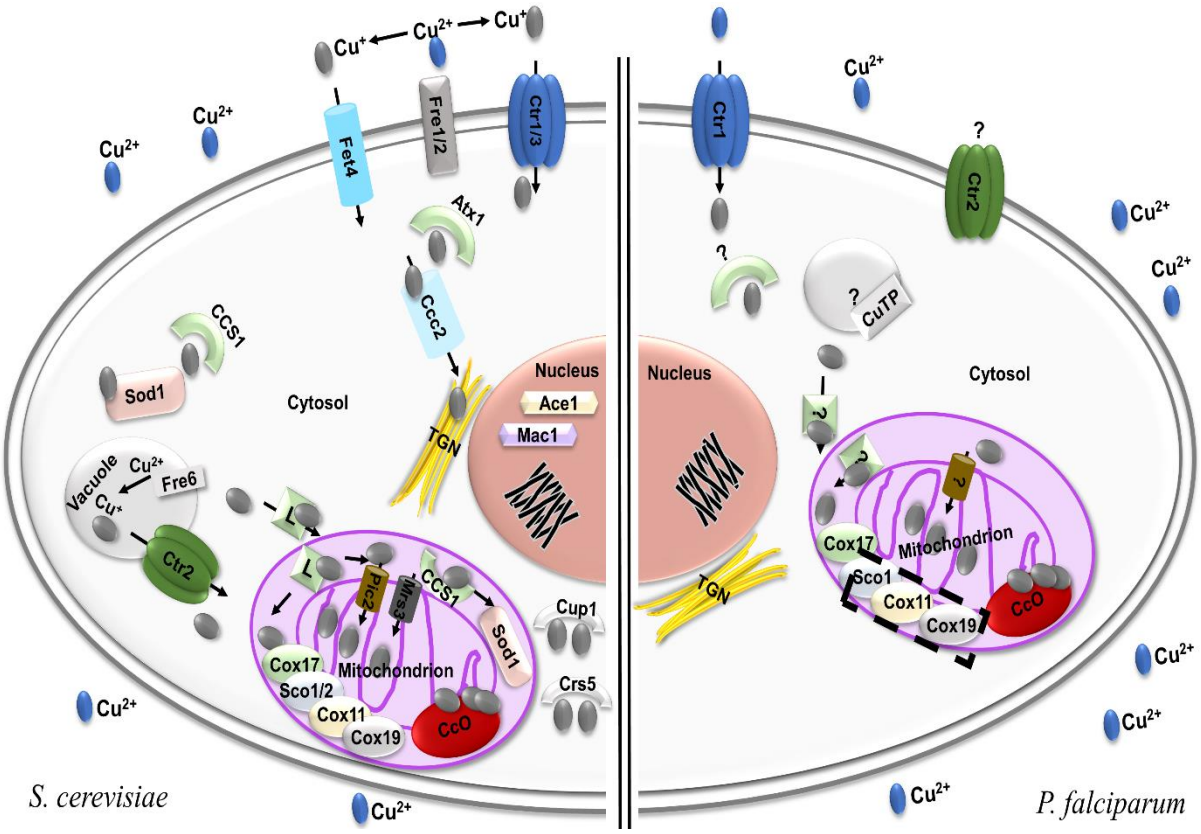

Figure 1.6. Current understanding of plasmodial copper homeostasis
A synopsis of the current understanding of plasmodial copper homeostasis relative to the established yeast copper homeostasis. Both *S. cerevisiae* (left) and the *P. falciparum* (models) for copper homeostasis are depicted. *P. falciparum* Cox11 and Cox19 (▭) are characterised in this study. *P. falciparum* Sco1 has been identified using bioinformatics but has not yet been characterised. The importance of these proteins to copper homeostasis are discussed in the text. Leftside image modified from Nevitt *et al.* (2012).

1.3 Role of oxidative respiration in *Plasmodium*

Despite glycolysis being preferred over oxidative respiration in *Plasmodium* spp. (Vander Jagt *et al.*, 1990), all tricarboxylic acid (TCA) cycle enzymes are encoded in the *Plasmodium* genome (Gardner *et al.*, 2002) and expressed in asexual stages (Bozdech *et al.*, 2003). The *Plasmodium* mitochondrion lacks pyruvate dehydrogenase (Foth *et al.*, 2005), an enzyme that catalyses acetyl CoA production from pyruvate, thus implying a deviation from the canonical oxidative TCA cycle. However, isotopic labelling studies demonstrated an active oxidative TCA cycle with glutamine and glucose as the two primary carbon sources in *P. falciparum* (Cobbold *et al.*, 2013; MacRae *et al.*, 2013). Subsequently, a branched chain ketoacid dehydrogenase (BCKDH) was implicated in the production of acetyl CoA from pyruvate (Oppenheim *et al.*, 2014). The electrons in the form of reducing equivalents are channelled into the mitochondrial electron-transport chain solely for the regeneration of ubiquinone for pyrimidine biosynthesis, atypical of the canonical oxidative respiration in eukaryotes (Painter *et al.*, 2007). To some extent, oxidative phosphorylation takes place with minimal contribution to the overall ATP required by the parasite (Balabaskaran Nina *et al.*, 2011; Uyemura *et al.*, 2004). However, the mitochondrial electron transport chain is indispensable to the parasite, as the antimalarial drug, atovaquone targets the cytochrome bc_1 complex (Fry and Pudney, 1992; Mather *et al.*, 2005).

1.4 Cytochrome c oxidase (CcO)

Cytochrome *c* oxidase (CcO) (also termed complex IV) is a multimeric enzyme of eleven in yeast or thirteen in mammals (Capaldi, 1990), nuclear and mitochondrially encoded subunits assembled by more than 30 accessory proteins (Tzagoloff and Dieckmann, 1990). The three subunits of yeast CcO constituting the catalytic core; Cox1, Cox2 and Cox3, are mitochondrially encoded, and the remaining subunits are nuclear-encoded proteins (Fontanesi *et al.*, 2006). In *Plasmodium* spp., Cox1, Cox3 and Cyt*b* are the three mitochondrially encoded proteins (Vaidya and Mather, 2009). The catalytic core in yeast is a complex of integral membrane proteins lacking significant extramembrane domains except the IMS-extending β-barrel of Cox2 that binds soluble cytochrome *c* (Cyt*C*). Cox1 consists of two redox centres; i) a low-spin haem *a* centre, and ii) a heterobimetallic centre of a high-spin haem a_3 and Cu_B. The Cu_B is a mononuclear copper site situated about 13 Å below the membrane surface (Tsukihara *et al.*, 1995), which is metallated by the copper chaperone, Cox11 (Hiser *et al.*, 2000). A third redox centre, Cu_A, is a binuclear centre formed by two copper ions within the Cox2 subunit.

The Cu_A centre is metallated by the copper metallochaperone Sco1 (Lode *et al.*, 2000). Conversely, the third member of the catalytic core of CcO, Cox3, has no prosthetic groups.

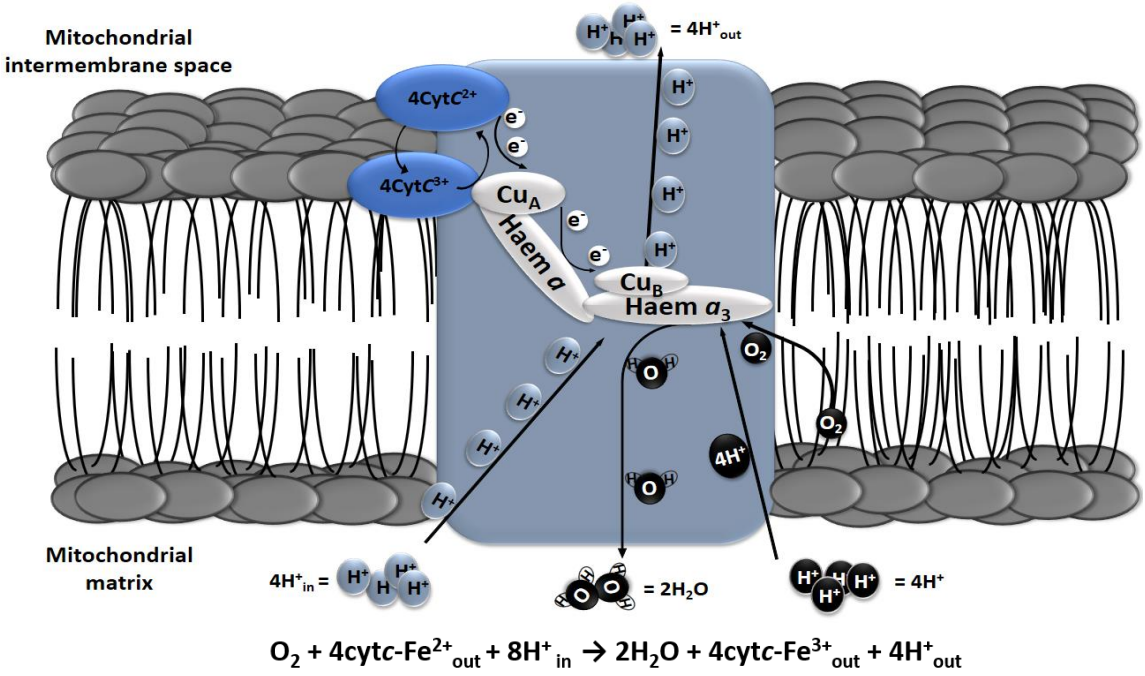

Figure 1.7. Redox-driven electron transfer and proton pumping by CcO
A synopsis of the electron transduction along the CcO subunits. In each catalytic cycle, two molecules of water are produced from the reduction of an oxygen molecule by four electrons furnished by four protons. Only four of the eight protons are translocated across the IM per catalytic cycle.

CcO is the terminal electron acceptor of oxidative respiration in eukaryotes and many bacteria. Oxidative respiration in aerobic organisms involves electron transfer to oxygen via a chain of membrane-associated protein complexes. The electron flow sustains a transmembrane electrochemical proton gradient that drives ATP synthesis. CcO accepts electrons from reduced Cyt*C* (cyt*c*-Fe^{2+}) (Wang *et al.*, 1999) to catalyse the four-electron reduction of oxygen to water via its redox centres; haems *a* and a_3, Cu_A and Cu_B (Figure 1.7). The Cu_A centre of Cox2 first accepts the electrons from Cyt*C*. The electrons flow to haem *a* of Cox1 and then the haem a_3-Cu_B centre where oxygen is reduced to water (Babcock and Wikström, 1992). For each catalytic cycle, eight protons are involved – four protons are translocated across the inner mitochondrial membrane while two pairs of electron from four other protons are transferred through CcO to reduce oxygen to water (Wikstrom, 1977). Conversely, the terminal electron from CcO in *Plasmodium* is used for the regeneration of ubiquinone (Painter *et al.*, 2007; Vaidya and Mather, 2009).

Table 1.4. Homologues of CcO assembly factors in *S. cerevisiae* and *P. falciparum*

Components	Yeast	*P. falciparum*	PlasmoDB ID	Role in yeast
Catalytic core subunit (mtDNA encoded structural subunits)				
Cox1	+	+	mal_mito_2	Catalytic core subunit
Cox2*	+	+	PF3D7_1430900	
Cox3	+	+	mal_mito_1	
Core protective shield (nDNA encoded structural subunits)				
Cox4	+	-	-	CcO assembly and function subunits
Cox5a	+	-	-	
Cox5b	+	+	PF3D7_0927800	
Cox6a	+	-	-	
Cox6b	+	+	PF3D7_0928000.1	
Cox7	+	-	-	
Cox7a	+	-	-	
Cox8	+	-	-	
Expression of catalytic core subunits				
Mss116	+	+	PF3D7_1307300.1	Helicase required for Cox1 and Cyt*b* intron splicing Component of the RNA degradosome
Suv3	+	+	PF3D7_0623700.1	Stabilises the Cox1 and Cyt*b* primary transcripts (hnRNA) Helicase required for Cox1 aI5β intron splicing Component of the RNA degradosome
Mrs1	+	-	-	Cox1 aI5β intron splicing Excision of the Cyt*b* b13 intron
Mne1	+	-	-	Cox1 aI5β intron splicing
Mss18	+	-	-	Cox1 aI5β intron splicing
Cox24	+	-	-	Splicing of aI2 and aI3 Cox1 introns Cox1 mRNA translation
Nam2	+	+	PF3D7_0828200.1	Cox1 aI4 intron splicing
Ccm1	+	-	-	Cox1 aI4 intron splicing
Pet309	+	-	-	Activation of Cox1 mRNA translation
Mss51	+	-	-	Activation of Cox1 mRNA translation
Ygr021w	+	-	-	Not yet identified
Pet111	+	-	-	Activation of Cox2 mRNA translation
Pet54	+	-	-	Activation of Cox3 mRNA translation Cox1 aI5β intron splicing and translation
Pet122	+	-	-	Activation of Cox3 mRNA translation
Pet494	+	-	-	Activation of Cox3 mRNA translation
Membrane insertion and processing of catalytic core subunits				
Oxa1	+	+	PF3D7_0828400.1	Membrane insertion of CcO subunits Cyt*b* and ATPase proteolipid
Cox20	+	-	-	Cox2 chaperone
Cox18	+	-	-	Export of the Cox2 C-terminus to the IMS
Mss2	+	-	-	Export of the Cox2 C-terminus to the IMS
Pnt1	+	-	-	Export of the Cox2 C-terminus to the IMS
Imp1	+	-	-	Maturation of Cox2 precursor
Imp2	+	+	PF3D7_0730400.1	Imp1 stability and activation
Som1	+	-	-	Component of the IMP complex
Copper metabolism and insertion into catalytic core subunits				
Cox17	+	+	PF3D7_1025600	Copper delivery to Cox11 and Sco1
Sco1	+	+	PF3D7_0708900	Copper delivery to the Cu_A site of Cox2
Cox11	+	+	PF3D7_1475300	Copper delivery to the Cu_B site of Cox1
Cox19	+	+	PF3D7_1201800	Interact with Cox11 to facilitate copper delivery to the Cu_B site of Cox1
Cox23	+	-	-	Copper trafficking and distribution to CcO. Mia40-dependent IMS import
Pet191	+	+	PF3D7_0825600.1	
Cmc1	+	+	PF3D7_0729600.1	
Cmc2	+	-	-	
Haem A biosynthesis				
Cox10	+	+	PF3D7_0519300.1	Protoheme IX farnesylation
Cox15	+	+	PF3D7_1435000.1	biosynthesis of haem *a* from haem *o*
Yah1	+	+	PF3D7_1214600.1	Haem *a* biosynthesis
Arh1	+	+	PF3D7_1139700.1	Haem *a* biosynthesis
Assembly/unknown				
Cox16	+	-	-	Could be involved in the merging of Cox1 and Cox2
Pet117	+	+	PF3D7_1458100.1	Not yet identified
Pet100	+	-	-	Assembly of the Cox7, Cox8 and Cox9 intermediates
Shy1	+	-	-	Formation Mss51-Cox14 complex for Cox1 translation
Cox14	+	+	PF3D7_1422000.1	Stability, maturation and assembly of Cox1
Coa1	+	-	-	Stability, maturation and assembly of Cox1
Coa2	+	-	-	Stability, maturation and assembly of Cox1
Coa3	+	-	-	Stability, maturation and assembly of Cox1
Coa4	+	-	-	CcO assembly and stability

*Nuclear-encoded in *P. falciparum*. +; present, -; absent, CcO; cytochrome c oxidase, mtDNA; mitochondrial DNA, nDNA; nuclear DNA, Cyt*b*; cytochrome *b*, IMS; mitochondrial intermembrane space, hnRNA; heterogenous nuclear RNA. The structure and some components of the table were adapted from Soto *et al.* (2012). Other information from this table was from; (Aurrecoechea *et al.*, 2009; Chen *et al.*, 2017; Pundir *et al.*, 2017).

The orthologues of some genes encoding components of the CcO assembly in *Plasmodium* have been identified (Table 1.4) (Choveaux *et al.*, 2015; Feagin, 1992; Gardner *et al.*, 2002; Vaidya *et al.*, 1989), and the presence of CcO confirmed in the *P. berghei* (Howells et al., 1969), *P. yoelii* and *P. falciparum* genomes (Fry and Beesley, 2009). However, only a few of these plasmodial orthologues have so far been characterised. Native *P. berghei* CcO has been partially purified and characterised (Krungkrai *et al.*, 1993).

1.5 Cox11

Cox11 is a nuclear-encoded mitochondrial protein tethered to the inner mitochondrial membrane by a single membrane-spanning domain in eukaryotes and bacteria (Banci *et al.*, 2004; Carr *et al.*, 2002; Timón-Gómez *et al.*, 2018; Tzagoloff *et al.*, 1990). The N- and C-terminal domains are exposed within the mitochondrial matrix and the mitochondrial intermembrane space respectively (Banci *et al.*, 2004; Carr *et al.*, 2002; Hiser *et al.*, 2000; Tzagoloff *et al.*, 1990). Cox11 is a copper-binding protein critical for the metallation of the Cu_B centre of the Cox1 in the assembly of CcO (Hiser *et al.*, 2000). Copper is supplied to Cox11 by the copper chaperone, Cox17 (Maxfield *et al.*, 2004). Cox11 is characterised by three conserved cysteines within the C-terminal domain in the mitochondrial intermembrane space. A pair of the conserved cysteine residues are in a CFCF motif implicated in copper coordination, while the third cysteine is a short distance away and few residues from the transmembrane domain (Banci *et al.*, 2004; Carr *et al.*, 2002; Thompson *et al.*, 2010). The lone cysteine residue by the transmembrane domain facilitates the transfer of bound Cu(I) to the Cu_B centre from the Cu(I)-Cox11 cluster (Thompson *et al.*, 2010; Timón-Gómez *et al.*, 2018). Cox11 adopts an immunoglobulin-like fold (Banci *et al.*, 2004), and its soluble C-terminal domain forms a homodimer that binds one Cu(I) per monomer via thiolate bonds (Banci *et al.*, 2004; Carr *et al.*, 2002). The coordinated Cu(I) is stabilised by the dimeric C-terminal domain structure until inserted in the Cu_B centre (Banci *et al.*, 2004). Cox11 transiently interacts with Cox19 via its lone cysteine residue at the inner mitochondrial membrane interface to facilitate a vectorial metallation of Cu_B centre without forming a stable complex (Bode *et al.*, 2015). Cox11 null yeast cells were respiratory deficient, had low levels of Cox1 devoid of a Cu_B centre with an inactive CcO (Hiser *et al.*, 2000; Tzagoloff *et al.*, 1990). In what seems to be an auxiliary function, Cox11 is required for the stable accumulation of Cox19 in the mitochondrial intermembrane space, while the biogenesis of Cox11 is not influenced by the Cox19 (Bode *et al.*, 2015). In an attempt to identify a secondary role of Cox11, analysis of the yeast Cox11

gene promoter for peroxidase-responsiveness at stationary phase using the LacZ assay failed to establish any correlation between the expression level of Cox11 with time in culture and β-galactosidase activity or peroxide concentration (Dubinski *et al.*, 2018). Thus, implying Cox11 has no functional role in the growth of the yeast cells at stationary phase.

1.6 Cox19

Cox19 is a nuclear-encoded mitochondrial protein found in eukaryotes and contains a twin Cx_9C sequence motif, which adopts a helical hairpin structure like the copper chaperone, Cox17 (Arnesano *et al.*, 2005; Rigby *et al.*, 2007). Cox19 is characterised by a [Coiled coil 1]-[Helix 1]-[Coiled coil 2]-[Helix 2] (CHCH) domain, where each helix contains two cysteine residues separated by nine amino acids. Cox19 is an essential CcO assembly accessory protein which is essential for the survival of yeast cells (Bode *et al.*, 2015; Nobrega *et al.*, 2002; Rigby *et al.*, 2007). Cox19 transiently accumulates in the cytosol in yeast and humans following synthesis, before localising to the IMS by a membrane potential driven Mia40-dependent import across the mitochondrial outer membrane (Fischer *et al.*, 2013). The Mia40 gene was not found in *P. falciparum* genome, while the sulfhydryl oxidase in *P. falciparum*, *Pf*Erv1 (essential for the Mia40 shuttle in yeast and humans), did not complement the yeast Erv1 orthologue (Eckers *et al.*, 2013). Perhaps a yet to be identified protein is involved in shuttling the plasmodial IMS protein across the mitochondrial outer membrane into the IMS (Allen *et al.*, 2008; Carrie and Soll, 2017). Cox19 has been shown to partition between the cytosol and IMS in a copper-dependent manner in fibroblast cells, where the cytosolic Cox19 level is proportional to the intracellular copper content (Leary *et al.*, 2013). Cox19 was demonstrated to exist as a fully oxidised molecule with two disulphides (Bien *et al.*, 2010; Fischer *et al.*, 2013; Rigby *et al.*, 2007) after import into the IMS by Mia40 (Fraga *et al.*, 2014).

The specific role of Cox19 in CcO assembly remains unclear. The recombinant Cox19 protein has been shown to bind copper in a 1:1 stoichiometry via its cysteine residues, while the native protein binds a variable amount of copper in the IMS (Rigby *et al.*, 2007). Thus, implying a possible copper-binding role in the mitochondria. However, the copper-binding role of Cox19 is questionable since all four cysteine residues are oxidised, and Cox19 lacks the Cu(I)-binding CCxC motif found in Cox17 (Rigby *et al.*, 2007). This could be an indication of Cox19 possibly having a moonlighting role – a secondary role other than the suggested Cu(I) binding role in the CcO assembly (Leary *et al.*, 2013). Recent studies implicate Cox19 in keeping the Cys111 (Cys60 in *P. falciparum*) in yeast Cox11 reduced (Bode *et al.*, 2015;

Mansilla *et al.*, 2018) to facilitate copper insertion at the Cu_B centre of Cox1 subunit (Thompson *et al.*, 2010; Timón-Gómez *et al.*, 2018). There seems to be a synergy between Cox11 and stable accumulation of Cox19 in the IMS (Bode *et al.*, 2015). The buildup of Cox19 in the cytosol was demonstrated to be a signal for copper overload, potentially regulating copper efflux from the ATP7A copper-transporting ATPase of the trans-Golgi network (Leary *et al.*, 2013). Cox19 null yeast cells were more susceptible to oxidative damage than the wild-type strains (Bode *et al.*, 2015) due to copper reactivity. Yeast Cox19 mRNA was recently demonstrated to be directly regulated in response to copper availability by a nonsense-mediated mRNA decay (NMD) pathway (Murtha *et al.*, 2018; Peccarelli *et al.*, 2016), a pathway responsible for degrading aberrant mRNAs (Celik *et al.*, 2017; Guan *et al.*, 2006; He *et al.*, 2003). The regulatory action of the NMD pathway on yeast Cox19 mRNA is facilitated by an atypically long 3'-untranslated region (3'-UTR) (Peccarelli *et al.*, 2016). Cox19 mRNA accumulates under high copper conditions in NMD mutant cells compared to the wild-type cells, further suggesting a role of Cox19 in copper homeostasis (Murtha *et al.*, 2018). Cox19 like most of the mitochondrial intermembrane space proteins was recently demonstrated to be degraded in wild-type yeast cells by the ubiquitin-proteasome system but remained stable in mutant cells lacking the proteasomal function (Kowalski *et al.*, 2018).

1.7 The aims and objectives of the current study

This study sought to contribute to the understanding of the plasmodial copper homeostasis by identifying and characterising two novel copper metallochaperones. The study addressed the following:

1) The genes coding for copper metallochaperones in *Plasmodium* spp., Cox11 and Cox19, were identified and characterised using bioinformatics tools.
2) The genes for two *P. falciparum* copper metallochaperones, Cox11 and Cox19, were cloned, recombinantly expressed and polyclonal antibodies against the recombinant proteins raised in chickens.
3) The copper binding abilities of *P. falciparum* Cox11 and Cox19 copper metallochaperones, *in vitro* and *in vivo* were tested using; the bicinchoninic acid release assay, the ascorbic acid oxidation assay, atomic absorption spectroscopy, differential scanning fluorimetry, and assessing the influence of the copper chaperones on the growth of *E. coli* host cells expressing them in the presence of toxic levels of copper.

4) The copper binding motifs of *P. falciparum* Cox11 were assessed by mutational studies using site-directed mutagenesis.

Chapter 2

Materials and Methods

2.1 Introduction

This chapter describes the general materials and methods used for bioinformatics, parasitological, molecular, immunochemical and biochemical techniques in this study.

2.2 Equipment

The following the equipment were purchased from Bio-Rad (California, USA): T100™ Thermal cycler, Basic Powerpac™, Miniprotean®3 system with 1 mm spacer; Thermo Scientific™ NanoDrop 2000 from Thermo Fisher Scientific (Massachusetts, USA); PCR Rotorgene 6000 from Corbett Research (Massachusetts, USA). BG-subMINI horizontal electrophoresis from Baygenebiotech (China); TEZZ Mighty Small Transphor Unit from Hoefer Inc. (California, USA); VersaMax™ ELISA plate reader from Molecular Devices Corporation (California, USA); Minis Pro DNR Bio-imaging Systems (Israel); Syngene G:Box system (UK). The centrifuges: Avanti™ J-26 XPI and Allegra™ X-22R were purchased from Beckman Coulter (California, USA); Virsonic™ cell disruptor from VirTis (New York, USA); Micro Tube Peristaltic pump MP-3 from EYELA Tokyo Rikakikai Co. Ltd. (Tokyo, Japan); Orbital shaking incubator from New Brunswick Scientific (New Jersey, USA); UV-1800 Shimadzu spectrophotometer from Shimadzu Corporation (Kyoto, Japan); Water bath from GFL (Burgwedel, Germany); benchtop orbital shaker and Spectrafuge bench top centrifuge from Labnet International Inc. (USA); weigh balance from Denver Instruments (USA); pH meter from HANNA instruments; magnetic stirrers from Velp Scientifica (Europe); Agilent Varian AA280FS was purchased from Agilent (California, USA).

2.3 Bioinformatics

This section describes the bioinformatics tools employed in the identification and structural characterisation of the two *Plasmodium falciparum* putative copper chaperones.

2.3.1 Sequence identification and characterisation

The need for copper by *Plasmodium* has been established by the identification of copper-requiring protein orthologues in the *P. falciparum* genome (Choveaux *et al.*, 2015; Gardner *et al.*, 2002). Herein, the *in silico* analysis of two of eleven copper-requiring protein orthologues, putative Cox11 and Cox19 are described.

Cox11 and Cox19

From the *P. falciparum* Cox11 (PF3D7_1475300) and Cox19 (PF3D7_1201800) orthologues, similar orthologues of both proteins in eight other *Plasmodium* spp. were identified by the Basic Local Alignment Search Tool for proteins (BLASTp) search of the PlasmoDB site (www.plasmodb.org/). *Plasmodium* spp. Cox11 nucleotide sequences were aligned with five characterised Cox11 sequences: *Homo sapiens* (Accession No. NP_004366.1), *Mus musculus* (Accession No. NP_950173.1), *Saccharomyces cerevisiae* (Accession No. NP_015193.1), *Arabidopsis thaliana* (Accession No. NP_171743.1) and *Sinorhizobium meliloti* (GenBank: KKA13892.1) obtained from NCBI (ncbi.nlm.nih.gov) and aligned using Clustal Omega (http://www.ebi.ac.uk/Tools/msa/clustalo/). The single transmembrane region of the Cox11 protein sequence was identified using the TMHMM 2.0 program (http://www.cbs.dtu.dk/services/TMHMM/). As with Cox11, Cox19 orthologues in eight other *Plasmodium* spp. were identified by the BLASTp search of PlasmoDB site (www.plasmodb.org/). The sequence identity of the *Plasmodium* spp. Cox19 nucleotide sequences to five characterised Cox19 sequences from NCBI (ncbi.nlm.nih.gov) was assessed by sequence alignment, using Clustal Omega (http://www.ebi.ac.uk/Tools/msa/clustalo/). The five characterised nucleotide sequences obtained from NCBI (ncbi.nlm.nih.gov) were: *Homo sapiens* (Accession No. NP_932097.1), *Mus musculus* (Accession No. NP_001243736.1), *Gallus gallus* (Accession No. NP_001243736.1), *Arabidopsis thaliana* (Accession No. NP_564879.1) and *Saccharomyces cerevisiae* (GenBank: GAX71665.1). The characteristic [Coiled coil1]-[Helix 1]-[Coiled coil 2]-[Helix 2] (CHCH) domain feature in Cox19 was verified in *Plasmodium* sequence using the conserved domain search tool (https://www.ncbi.nlm.nih.gov/Structure/cdd/wrpsb.cgi).

A query for both plasmodial Cox11 and Cox19 orthologues for the parasite-specific signal peptide was made on PlasmoAP (http://v4-4.plasmodb.org/restricted/PlasmoAPcgi.shtml) and iSMP-Grey (http://www.jci-bioinfo.cn/iSMP-Grey) servers. The sequences of both Cox11 and

Cox19 orthologues were screened for the presence of ubiquitylation and acetylation post-translational modification sites using the UbiProber (http://bioinfo.ncu.edu.cn/UbiProber.aspx) and GPS-PAIL 2.0 (http://pail.biocuckoo.org/online.php) online servers.

2.3.2 Homology modelling

Homology models of the *P. falciparum* Cox11 (Pf3D7_1475300) and Cox19 (Pf3D7_1201800) sequences were constructed using NMR-solved structures of *Sinorhizobium meliloti* Cox11 (1SO9) and *Homo sapiens* Mia40 (2K3J) templates respectively. Each of these templates was used to model the malaria protein using the Swiss-Pdb DeepView program (Guex *et al.*, 2009).

2.3.3 Predict7™

The Cox11 copper binding site peptide sequence with 90% conservation in amino acid composition in *Plasmodium* was identified using Predict7™ (Cármenes *et al.*, 1989). Predict7™ analyses amino acid sequences based on hydrophilicity, surface probability, antigenicity, and flexibility to identify immunogenic peptide sequences for antibody production.

2.4 Propagation and cryopreservation of *P. berghei* parasites in BALB/c mice

Parasites were propagated in male BALB/c mice by intraperitoneal injection of the parasite stabilate (1 x 10^7 parasitised mouse red blood cells) (Burns *et al.*, 1989; Suckow *et al.*, 2001). Parasitaemia was monitored daily on a Giemsa-stained thin blood smear of tail blood (Warhurst and Williams, 1996). The number of infected RBC was expressed as a percentage of total RBC. Once parasitemia reached a suitable level, mice were bled, and the blood collected in a heparinised vacuum test tube. Parasite-infected red blood cells were preserved in 10% glycerol-PBS at 1 x 10^7 parasitised-RBC (pRBC) per 100 µl of stabilate. The stabilate was labelled, flash-frozen and immediately stored in a liquid nitrogen cryo-tank.

2.5 Generation of expression constructs

This section describes the techniques employed to generate recombinant gene fusion constructs of *P. falciparum* Cox11 and Cox19.

2.5.1 Reagents

Agarose, T4 DNA ligase, 10x T4 DNA ligase buffer, DNA MassRuler™, 6X MassRuler DNA Loading Dye, 10 mM dNTP mix, *Sal*1, *Pst*I, Buffer O™, shrimp alkaline phosphatase (SAP), *Alu*I, Platinum™ *Taq* DNA polymerase High fidelity, 10x high fidelity buffer, 50 mM $MgSO_4$, GeneJET™ Plasmid Miniprep Kit, GeneJET™ Gel Extraction Kit, 5-bromo-4-chloro-3-indolyl-β-D-galactopyranoside (X-gal) and unstained protein molecular weight marker ranging from 14.4 to 116 kDa were purchased from Fermentas (Vilinius, Lithuania). pGEM®-T-Easy Cloning vector was purchased from Promega (Madison, WI, USA). Ethidium bromide (EtBr) and isopropyl-β-D-thiogalactopyranoside (IPTG) were purchased from Sigma-Aldrich-Fluka (Steinheim, Germany). The Zymo Research Clean and Concentrator™ Kit was purchased from Zymo Research (Orange, CA, USA). The following molecular biology reagents were purchased from Solis Biodyne (Tartu, Estonia): 10x PCR buffer ($MgCl_2$ and detergent-free), PCR $MgCl_2$ stock solution (25 mM) and FIREpol® *Taq* polymerase. The pMal-c2x expression system, Q5® High fidelity DNA polymerase, 5x Q5 reaction buffer, 5x Q5 High GC enhancer and Quick-Load® 100 bp DNA Ladder purchased from New England Biolabs (Massachusetts, USA). Tryptone, bacteriological agar, yeast extract, D(+) glucose anhydrous, magnesium chloride hexahydrate, magnesium sulphate, and calcium chloride were from Merck (Darmstadt, Germany). All oligonucleotide primers used in this study were synthesised by the Molecular and Cell Biology synthetic DNA unit at the University of Cape Town (Cape Town, South Africa). The *Escherichia coli* host cells: BL21 and JM109 glycerol stocks purchased from Novagen (Darmstadt, Germany). Bovine serum albumin (BSA) purchased from Roche (Mannheim, Germany).

2.5.2 Agarose gel electrophoresis

The purity of the isolated genomic and plasmid DNA, PCR amplicons, or restriction digestion products were analyzed on agarose gels. A 1 or 3% (w/v) agarose (0.6 or 1.8 g agarose respectively) in TAE buffer (2 M Tris; 50 mM EDTA; 0.95 M glacial acetic acid; pH 8.0) was heated until dissolved. Once the solution had cooled to ~45ºC, EtBr (1% (w/v) 0.5 µg/ml) was added. The molten agarose was poured and allowed to set in an assembled gel cassette with a comb in place. The cassette was placed in the BG-subMINI horizontal electrophoresis system containing TAE buffer. Samples were prepared in sample loading buffer (0.25% (w/v) bromophenol blue and

40% (w/v) sucrose in TAE buffer) and loaded into the wells. The gels were run at 70 V for 45 min, and images captured under UV light using a Syngene G:Box system. The sizes of the DNA bands (bp) of interest were extrapolated from a graph of relative distance travelled from the loading well to log size of DNA standards (bp) (DNA MassRuler™, Fermentas)

2.5.3 Isolation of *Plasmodium falciparum* genomic DNA (gDNA)

The *P. falciparum* genomic DNA (gDNA) was isolated using the Fermentas™ DNA Purification Kit as per manufacturer's instruction. The yield and purity of DNA were assessed by spectrophotometry and on 0.5% (w/v) agarose electrophoresis gel. The isolated *P. falciparum* genomic DNA (gDNA) served as the DNA template for the PCR-amplification of the *Pf*Cox11 and the *Pf*Cox19 sequences.

2.5.4 Primers for r*Pf*Cox11Ct and r*Pf*Cox19

Primers amplifying the sequences of the *Pf*Cox11 (PF3D7_1475300) and the *Pf*Cox19 (PF3D7_1201800) genes were designed with the Primer3 software (http://bioinfo.ut.ee/primer3-0.4.0/primer3/). The primers included additional restriction endonuclease sites to facilitate subsequent subcloning, and a stop codon was added to the 3' end to exclude the β-galactosidase α fragment. Primer characteristics are listed in Table 2.2.

2.5.5 Primers for r*Pf*Cox11Ct mutant clones

Overlap extension PCR (Heckman and Pease, 2007; Ho *et al.*, 1989) was used to introduce the desired point mutations in the recombinant plasmid (pMal-c2x-r*Pf*Cox11Ct). A set of four primers: two internal and two flanking (external), was required for each mutation. These primers were designed with the aid of PrimerX software (http://www.bioinformatics.org/primerx/). The two internal primers are complementary and contain the desired mutant codon with overlapping nucleotides sequence. The mutant codon is flanked on both 5' and 3' ends with a minimum of nine nucleotides. The two external primers contained a minimum of eighteen pMal-c2x expression vector nucleotides flanking the *Pf*Cox11Ct gene. The primers and their characteristics are listed in Table 2.2.

2.5.6 Polymerase chain reaction (PCR)

All PCR reactions were performed in a 20 µl reaction volume with the T100™ Thermal cycler. Unless otherwise stated the PCR reaction components were mixed (Table 2.1) and the PCR reactions were run. DNA inserts cloned into TA cloning vector (pGEM®-T-Easy), were amplified from the *P. falciparum* gDNA with Platinum™ *Taq* DNA polymerase High fidelity. The identification of recombinant plasmids by colony PCR was carried out with FIREpol® *Taq* polymerase.

Table 2.1. Components of a PCR reaction mixture

Reaction component	Concentration
5x PCR buffer	1x
$MgSO_4$ / $MgCl_2$	2 mM / 2.5 mM
dNTP mix	0.2 mM (each)
Forward primer	0.5 µM
Reverse primer	0.5 µM
Sterile dH_20	-
Template DNA	1-100 ng
DNA polymerase*	1 U

**Taq* or Phusion DNA polymerases.
PCR reaction volume was 20 µl.

The PCR reaction conditions are represented in Figure 2.1. The annealing temperatures used for each reaction were determined by the melting temperatures for the set of primers used (Table 2.2). The PCR products were resolved on a 1% (w/v) agarose gel and images captured under UV light using the Syngene G:Box system.

Table 2.2. Primer sequences used for PCR amplifications

Primer	Sequence	% GC	T_m (°C)	Annealing temp. (°C)	Application
r*Pf*Cox11Ct-Fwd[a]	*cc* ***GTC GAC*** CAA TTA TTT TGT CAA TCC ACA GG	45	70.9	65	PCR-amplification of the carboxy-terminus of *P. falciparum* Cox11. Expected size is 505 bp.
r*Pf*Cox11Ct-Rev[b]	*tt* ***CTG CAG*** TCA GGA AAT AGC CCT TGA GAG G	60	72.1		
r*Pf*Cox11Ct$_{C60A}$-F$_1$	GAA AGA CGC GCA GAC TAA TTC GAG CTC	52	69.9	65	Site-directed mutagenesis in a two-stage PCR step. Amplification of a C60A mutant of *P. falciparum* Cox11. The expected sizes of the lagging and leading fragments from the first PCR are 129 bp and 519 bp respectively. The expected size of the full-length fragment from the second PCR is 648 bp.
r*Pf*Cox11Ct$_{C60A}$-R$_1$	GGC CAG TGC CAA GCT TGC CTG CAG	67	72.2		
r*Pf*Cox11Ct$_{C60A}$-f$_2$[c]	GTC GAC CAA TTA TTT GCG CAA TCC ACA GG	48	70.3		
r*Pf*Cox11Ct$_{C60A}$-r$_2$[c]	CC TGT GGA TTG CGC AAA TAA TTG GTC GAC	48	70.3		
r*Pf*Cox11Ct$_{C157A}$-F$_1$	GAA TTC GGA TCC TCT AGA GTC	48	59.5	52.4	Site-directed mutagenesis in a two-stage PCR step. Amplification of a C157A mutant of *P. falciparum* Cox11. The expected sizes of the lagging and leading fragments from the first PCR are 337 bp and 210 bp respectively. The expected size of the full-length fragment from the second PCR is 547 bp.
r*Pf*Cox11Ct$_{C157A}$-R$_1$	TGC CAA GCT TGC CTG CAG	61	58.4		
r*Pf*Cox11Ct$_{C157A}$-f$_2$[c]	CAA TGT TTT GCC TTT GAA GAA C	36	56.4		
r*Pf*Cox11Ct$_{C157A}$-r$_2$[c]	G TTC TTC AAA GGC AAA ACA TTG	36	56.4		
r*Pf*Cox19-Fwd[a]	*at* ***GTC GAC*** AGG CAG CTT GTT AAG AAG CC	50	70.1	65	PCR-amplification of the *P. falciparum* Cox19. Expected size is 575 bp
r*Pf*Cox19-Rev[b]	*at* **CTG CAG** TCA CAG CTA AAT AAC CCT CAG C	47	70.8		

[a] bold bases are *Sal*1 restriction sites
[b] bold bases are *Pst*1 restriction sites
[c] underlined bases are degenerate alanine codons

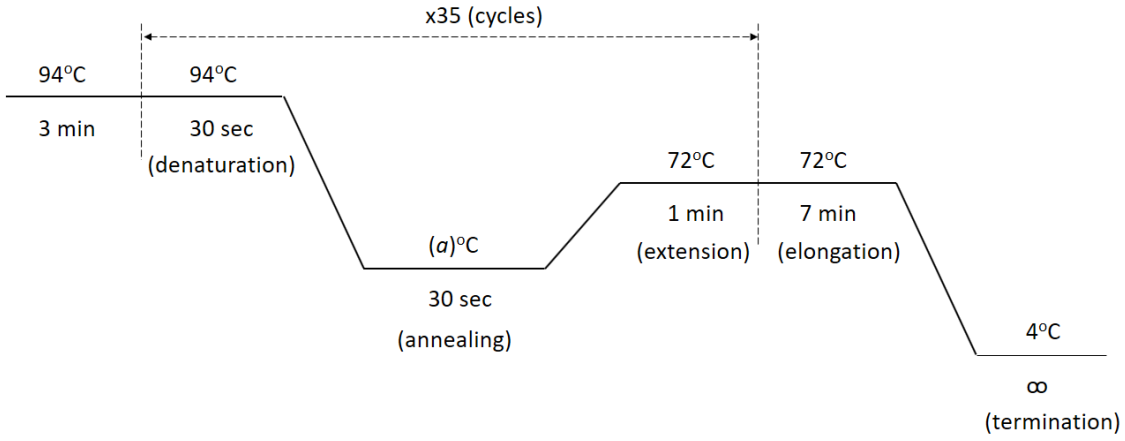

Figure 2.1. PCR conditions
The annealing temperature "*a*" used in each run was determined by the melting temperatures (T_m) of each set of primers.

All PCR products, except for colony PCR, were cleaned and concentrated with Zymo Research Clean and Concentrator™ Kit as per manufacturer's instructions. The DNA bound to the agarose in the mini-spin column was washed with ethanol and subsequently eluted in TE buffer (10 mM Tris; 1 mM EDTA; pH 8.0). The cleaned DNA was quantified with Thermo Scientific™ NanoDrop 2000 at 260 nm. The PCR products were further confirmed by *Alu*I restriction digestion before sequencing (section 2.5.12).

2.5.7 Ligation of DNA fragments by T4 DNA ligase

Ligation is a molecular technique used in joining two nucleotide fragments via phosphodiester bond between the 3'-hydroxyl of one DNA strand with the 5'-phosphoryl of another. Ligation is an energy driven process catalysed by T4 DNA ligase. PCR products or excised genomic DNA fragments are ligated into a plasmid vector for downstream molecular applications.

2.5.7.1 Ligation of purified DNA fragments into the cloning vector

Both the pGEM®-T Easy and pTZ57R/T cloning vectors were employed in the propagation of the recombinant genes in this study. The pGEM®-T Easy and pTZ57R/T (Figure 2.2) are linearised, high copy number vectors with 3'-terminal thymidines at both ends. The efficiency of ligation of PCR products amplified by a *Taq* polymerase, to the vector DNA is enhanced by the T-overhangs that prevent recircularization of the vector. The multiple cloning regions are flanked by T7 and SP6 RNA polymerase promoters within the α-peptide coding

region of β-galactosidase. The α-peptide is inactivated upon insertion of a foreign DNA, thereby allowing the identification of recombinants by blue/white colony screening.

The cleaned *P. falciparum* Cox11 and Cox19 PCR-amplicons (section 2.5.6), were ligated into the pGEM®-T Easy and pTZ57R/T vectors respectively in a ratio of 3:1. The ligation reaction mixture contained: 1x ligation buffer; 50 ng cloning vector; 25 ng gene insert and 1U T4 DNA ligase made up to 10 µl with sterile dH_2O. The reaction was kept at 4ºC overnight (16 h). Subsequently, recombinant plasmids were propagated in JM109 *E. coli* host (section 2.5.8), selected, purified (section 2.5.9) and digested (section 2.5.10) with *Sal*I and *Pst*I respectively. The resulting sticky ended gene fragments were ligated with the pMal-c2x expression vector digested with *Sal*I and *Pst*I restriction enzymes.

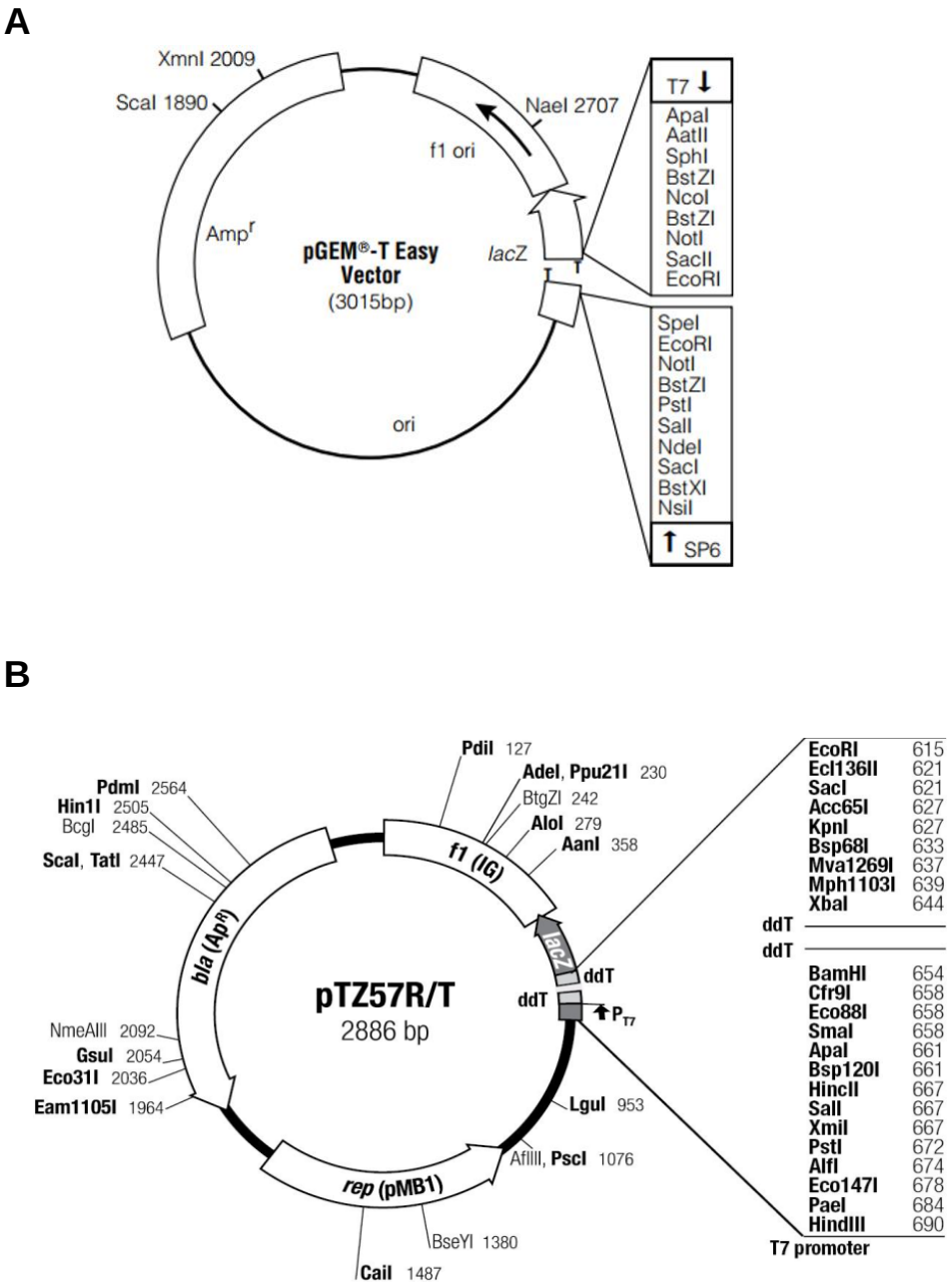

Figure 2.2. Map of the pGEM®-T Easy and pTZ57R/T cloning vectors
Features of (A) pGEM®-T Easy, a 3015 bp vector, and (B) pTZ57R/T, a 2886 bp vector. The features include a gene coding for β-galactosidase (*Lac*Z); ampicillin resistance gene (Amp^r or *bla* (Ap^r)); RNA polymerase promoters (T7 and SP6); multiple cloning sites *Apa*I – *Nsi*I (pGEM® T Easy) and *Eco*RI – *Hin*dIII (pTZ57R/T); T-overhangs for ligation of the insert. (*Adapted from the Promega pGEM®-T and pGEM®-T Easy vector systems technical manual and Thermo Scientific InsTAclone PCR Cloning Kit product information manual*).

2.5.7.2 Ligation of DNA fragments into the pMal-c2x expression vector

The pMal-c2x is a 6646 bp expression vector containing the *malE* gene of *E. coli* which encodes the maltose-binding protein gene sequence (MBP) (Figure 2.3). The *malE* gene in pMal-c2x is lacking its periplasm-specific signal sequence, leading to the cytoplasmic expression of MBP fusion proteins. The vector uses the strong "tac" promoter and *malE* translation signal to give a high-level of protein expression. DNA inserts are cloned downstream from the *malE* gene inactivating the β-galactosidase's α-peptide. The gene fragments (section 2.5.10) of the r*Pf*Cox11Ct clones and r*Pf*Cox19 were ligated ratio 3:1 into pMal-c2x digested with the *Sal*I and *Pst*I. The ligation reaction mixture contained: 1x ligation buffer; 50 ng digested pMal-c2x; 11.4 ng r*Pf*Cox11Ct (for each clone) insert or 13 ng r*Pf*Cox19; 1U T4 DNA ligase and made up to 10 µl with sterile dH_2O. The reaction was kept at 4°C overnight (16 h). The recombinant plasmids were transformed (section 2.5.8) into *E. coli* BL21 host cells. The pMal-c2x constructs of r*Pf*Cox11Ct and r*Pf*Cox19 are referred to as pMal-c2x-r*Pf*Cox11Ct and pMal-c2x-r*Pf*Cox19 respectively.

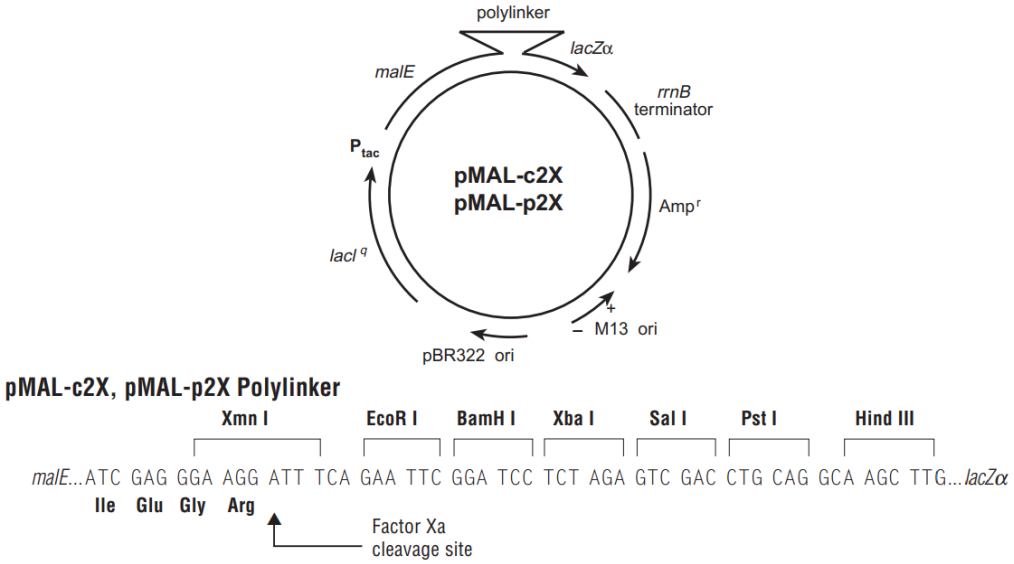

Figure 2.3. Map of the pMal-2x expression vector
Features of pMal-2x expression vectors and include a gene coding for β-galactosidase (*Lac*Z); ampicillin resistance gene (Amp^r); maltose-binding protein gene (*malE*); tac promoter (P_{tac}); multiple cloning sites (polylinker). (*Adapted from NEB pMal™ protein fusion and purification system manual*).

2.5.8 Transformation of competent *E. coli* host cells with plasmid DNA

The recombinant plasmids generated above were transformed into competent *E. coli* JM109 or BL21 host cells (Cohen *et al.*, 1972; Sambrook *et al.*, 1989). A single *E. coli* colony was grown overnight (16 h) in 2xYT media (1.6% (w/v) tryptone, 1% (w/v) yeast extract,

85 mM NaCl, 11 mM glucose) at 37ºC, 200 rpm. A 1:100 dilution of the overnight culture was made in 50 ml 2xYT media and grown at 37ºC, 200 rpm until an optical density measured at 600 nm (OD_{600}) of between 0.3-0.4 was reached. The culture was cooled on ice for 10 min. Thereafter, 45 ml of the culture was transferred into ice-cold tubes and pelleted (4500 x *g*, 4ºC, 10 min) in a pre-cooled centrifuge (Allegra™ X-22R). The cells were resuspended in 20 ml ice-cold sterile 100 mM $CaCl_2$ and pelleted again (4500 x *g*, 4ºC, 10 min). The resulting cells were resuspended in 1 ml of ice-cold sterile 100 mM $CaCl_2$ and kept on ice. The competent cells (50 µl) were added to the ligation mix (5 µl), incubated on ice for 30 min and then heat shocked at 42ºC for 20 s. The transformed cells were immediately incubated on ice for 5 min. The cells were incubated in pre-warmed 250 µl SOC media (2% (w/v) tryptone, 0.5% (w/v) yeast extract, 10 mM NaCl, 2.5 mM $MgCl_2$, 10 mM $MgSO_4$ and 20 mM glucose) at 37ºC, 200 rpm for an hour. Thereafter, the cells (100 µl) were plated on pre-warmed 2xYT agar plates (1.6% (w/v) tryptone, 1% (w/v) yeast extract, 85 mM NaCl, 11 mM glucose, 1.5% (w/v) bacteriological agar, 100 µg/ml ampicillin) and incubated overnight at 37ºC. For transformations with recombinant pGEM®-T Easy plasmid, the 2xYT agar plates, in addition, contain 0.16 mM IPTG and 32 µg/ml X-gal for the blue/white colony selection. The recombinant pGEM®-T Easy and pMal-c2x plasmids were transformed into *E. coli* JM109 and *E. coli* (BL21) hosts cells respectively.

Single transformed colonies were picked and incubated overnight (16 h) in 5ml 2xYT media containing 100 µg/ml ampicillin at 37ºC, 200 rpm. Glycerol stocks of the transformed cells were prepared in glycerol (7.5% (v/v) and kept at -80ºC.

To confirm the identity of recombinant clones, plasmids were isolated (section 2.5.9) and colony PCR performed with the appropriate gene primers (Table 2.2). The recombinant plasmids were sequenced (section 2.5.12) and aligned with the sequences obtained from the PlasmoDB site (www.plasmodb.org/).

2.5.9 Plasmid DNA isolation

A single *E. coli* colony with the plasmid of interest was grown overnight (16 h) in 5 ml 2xYT containing ampicillin (100 µg/ml) at 37ºC, 200 rpm. The cells were pelleted in a centrifuge (12000 x *g*, RT, 1 min), and the plasmid DNA isolated using the GeneJET™ Plasmid Miniprep Kit as per manufacturer's instructions.

2.5.10 Restriction digestion of plasmids

The purified plasmid (section 2.5.9) was digested in a 30 µl reaction volume containing: 1x buffer O; 5 U *Sal*I; 5 U *Pst*I; 1-1.5 µg plasmid and incubated overnight (16 h at 37^{o}C). The reaction was stopped by incubation at 65^{o}C for 20 min. For pMal-c2x digestion, the 5'-phosphoryl group was removed by adding 0.5 U shrimp alkaline phosphatase (SAP) to the digestion mix and incubated at 37^{o}C, 20 min, and the reaction stopped by incubation at 75^{o}C for 5 min. The digested products were electrophoresed on agarose gel electrophoresis and viewed in the presence of crystal violet under white light. The products were excised from the gel and gel purified with GeneJET™ Gel Extraction Kit as per manufacturer's instructions. The cleaned DNA was quantified with the Thermo Scientific™ NanoDrop 2000.

2.5.11 Site-directed mutagenesis by overlap extension polymerase chain reaction

Two of the three conserved cysteines (Cys60 and Cys157) were investigated for their possible roles in copper binding in r*Pf*Cox11Ct. Either Cys60 and Cys157 or both cysteines were mutated to alanine by employing the method earlier outlined in two separate studies (Heckman and Pease, 2007; Ho *et al*., 1989) with some modifications. The cysteine codon (TGT) was mutated to two degenerate alanine codons: GCG or GCC at positions C60 and C157 respectively. The mutations were designated as C60A, C157A, and C60A-C157A for the double mutant respectively.

Overlap extension PCR (Figure 2.4) was used to introduce a point mutation by site-directed mutagenesis in r*Pf*Cox11Ct. Two PCRs: first and second PCR with similar reaction conditions (section 2.5.6) were required for the reactions. A Phusion (Q5® High fidelity) DNA polymerase was used. In the first PCR, two pairs of primers: a flanking forward (F_1) with an internal reverse (r_2), and internal forward (f_2) with flanking reverse (R_1) primers were used. To construct C60A and C157A recombinant plasmids, the pMal-c2x-r*Pf*Cox11Ct plasmid DNA served as template in the first PCR generating two contiguous gene fragments. The C60A plasmid DNA served as a template for C60A-C157A mutagenesis. In the leading and lagging fragments, the mutant codon was overlapped with nucleotides at the 3' and 5' ends respectively. In the second PCR reaction, F_1 and R_1 primers were used to amplify the entire r*Pf*Cox11Ct with flanking vector nucleotides (pMal-c2x). An equimolar concentration of the two fragments served as DNA template in the second PCR. Samples of the first and second PCR products were resolved on a 3% (w/v) agarose gel respectively. Images were captured under UV light using Syngene G:Box system. Both PCR products were then cleaned and

concentrated with Zymo Research Clean and Concentrator™ Kit as per manufacturer's instructions. The cleaned products were quantified with Thermo Scientific™ NanoDrop 2000 at 260 nm.

The amplified product from the second PCR was digested with *Sal*1 and *Pst*1 (section 2.5.10) and ligated (section 2.5.7.2) into the pMal-c2x vector digested with *Sal*1 and *Pst*1.

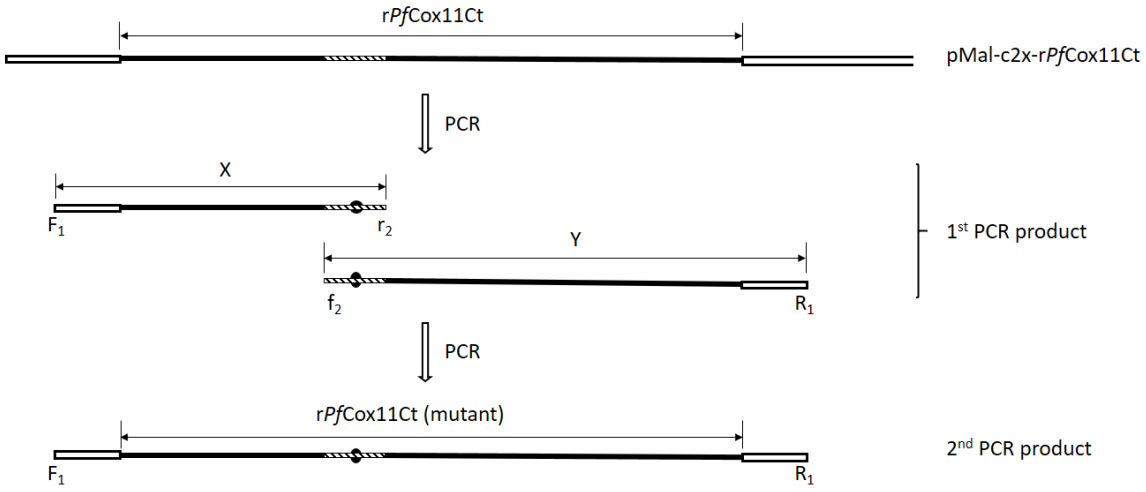

Figure 2.4. Overlap extension PCR
A schematic of site-directed mutagenesis by overlap extension PCR. The first PCR produces two contiguous fragments with flanking pMal-c2x expression vector nucleotide on both ends of the gene. The second PCR produces the entire gene flanked by pMal-c2x nucleotide sequences. Open horizontal bars (pMal-c2x nucleotide sequence); solid bars (r*Pf*Cox11Ct coding sequence); hatched bars (contiguous nucleotides); black circle (point mutation); X (lagging fragment) and Y (leading fragment).

2.5.12 Sequencing

The recombinant pMal-c2x-r*Pf*Cox11Ct and pMal-c2x-r*Pf*Cox19 plasmid sequences were confirmed by sequencing (Central Analytical Facility, Stellenbosch University). For all r*Pf*Cox11Ct clones, the primers r*Pf*Cox11Ct$_{c60A}$-F$_1$ and r*Pf*Cox11Ct$_{c60A}$-R$_1$ were used for the sequencing reaction, while the primers for r*Pf*Cox19 listed on Table 2.2 were used for the sequencing of the pMal-c2x-r*Pf*Cox19 plasmid.

2.6 Recombinant protein expression and purification

The techniques used in the recombinant expression, purification and partial characterisation of *Pf*Cox11Ct clones and *Pf*Cox19 are described in this section.

2.6.1 Reagents

The following were purchased from Merck (Darmstadt, Germany): Tryptone, bacteriological agar, yeast extract, D(+) glucose anhydrous, glycerol, dipotassium hydrogen orthophosphate, potassium chloride, sodium hydroxide, sodium chloride, disodium hydrogen orthophosphate anhydrous, maltose, and an Amicon® Ultra-15 Centrifugal Filter Units (10 kDa MWCO). The following were purchased from Sigma-Aldrich-Fluka (Steinheim, Germany): Bradford reagent, N,N'-methylenebisacrylamide, bromophenol blue, β-mercaptoethanol, acrylamide, glycine, Coomassie Brilliant Blue R-250 as well as G-250, sodium dodecyl sulphate (SDS), Tris, ammonium persulfate, ovalbumin, Sephacryl S200, N,N',N',N'-tetramethylethylenediamine (TEMED), SYPRO® Orange, ampicillin, isopropyl-β-D-thiogalactopyranoside (IPTG), acid (EDTA), copper(II) chloride dihydrate and L(+)-ascorbic acid. Amylose resin was purchased from New England Biolabs (Massachusetts, USA). Snake skin™ dialysis membrane (10 kDa MWCO) was purchased from Pierce Perbio Science (Erembodegem, Belgium). 0.22 and 0.45 µm syringe filters were from PALL Life Sciences (Ann Arbor, MI, USA).

2.6.2 Expression of recombinant proteins

All recombinant proteins were expressed as MBP-fusion proteins. Unless otherwise stated, bacteria cultures were grown in 2xYT media (30ºC, 200 rpm) containing ampicillin (100 µg/ml) in culture volumes not exceeding 20% of the flask volume. A single bacterial colony was grown overnight (16 h) in 2xYT media. A 1:100 dilution of the overnight culture was made in 400 ml 2xYT media and grown to OD_{600} between 0.5-0.6. Recombinant protein expression was induced for 4 h with 0.5 mM IPTG and the culture had additional ampicillin (100 µg/ml) added. The bacterial cells were pelleted by centrifugation (4000 x *g*, 4ºC, 10 min) in the Avanti™ J-26 XPI (Rotor, JLA-10.500) and the supernatant discarded.

2.6.3 Affinity purification of recombinant proteins

All recombinant proteins in lysed bacterial culture in this study were affinity purified with an amylose resin. Bacterial pellets (section 2.6.2) were resuspended in 10% of the original culture volume in column buffer (20 mM Tris, 200 mM NaCl, 1 mM EDTA, pH 7.4). Cell suspensions were lysed with nine freeze-thaw cycles (-196ºC and 37ºC) followed by sonication on ice (3 cycles, 30 s/burst, 30 s between bursts). The cell lysates were then centrifuged (12000 x *g*, 4ºC, 25 min). The supernatant was added to a 1 ml amylose resin pre-equilibrated

with 10 ml column buffer. The resin was washed with column buffer until an OD_{280} absorbance of ≤ 0.02 was observed and the resin was washed with two more column volumes of buffer (100 mM NaH_2PO_4, 200 mM NaCl, pH 7.4). Recombinant proteins were eluted with elution buffer (100 mM NaH_2PO_4, 200 mM NaCl, 0.3 mM maltose, pH 7.4) and 1 ml fractions were collected. Protein fractions were pooled and concentrated with an Amicon® Ultra-15 Centrifugal Filter Units (10 kDa MWCO) by centrifugation (5000 x *g*, 4°C, at 10 min intervals). The proteins were dialysed at 4°C against three buffer changes (16-2-2 h) in an appropriate buffer (200 x protein volume). Finally, the dialysed protein sample was quantified by the Bradford method (section 2.6.4) and stored at -20°C.

2.6.4 Bradford protein assay

Protein samples were quantified using the Bradford assay from triplicate readings using BSA as the standard protein (Bradford, 1976; Goldring, 2015). Refer to the image (Figure 2.5). Protein samples were also quantified using absorbance at 280 nm.

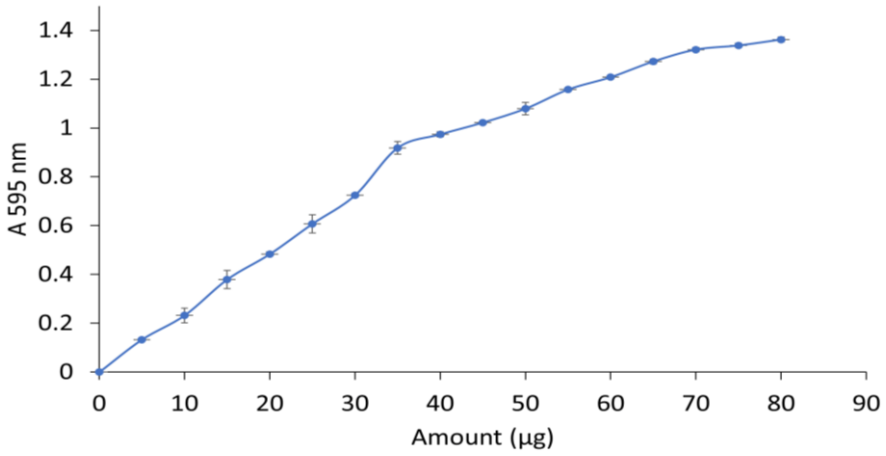

Figure 2.5. Bradford calibration curve
All values are average values of triplicate readings with standard deviations shown.

2.6.5 Sodium dodecyl sulphate polyacrylamide gel electrophoresis (SDS-PAGE)

The purity and size of protein samples were assessed using SDS-PAGE as described by Laemmli (1970). Protein samples were resolved on a 12.5% separating gel and 4% stacking gel prepared according to Table 2.3. The reagents used in preparing the SDS-PAGE gel were: monomer solution (4.1 M acrylamide, 52 mM N,N'-methylenebisacrylamide); separating gel buffer (1.5 M Tris, pH 8.8) and stacking gel buffer (0.5 M Tris, pH 6.8). The solution was mixed (Table 2.3) and poured into an assembled Bio-Rad Miniprotean®3 gel-casting cassettes

and overlaid with dH_2O. The water was decanted, and the stacking gel solution was poured on top of the polymerised separating gel. A ten or fifteen well comb was inserted, and the gel allowed to polymerise. The polymerised gel was assembled according to the manufacturer's instructions and submerged in tank buffer (25 mM Tris, 192 mM glycine and 0.1% (w/v) SDS).

Table 2.3. Recipe to prepare three gels for SDS-PAGE

Reagent	Separating gel	Stacking gel
Monomer solution	6.25 ml	940 µl
Separating gel buffer	3.75 ml	-
Stacking gel buffer	-	1.75 ml
10% SDS	150 µl	70 µl
Distilled water	4.75 ml	4.3 ml
10% Ammonium persulfate	75 µl	35 µl
TEMED	7.5 µl	15 µl

Samples were prepared in 2x sample buffer (125 mM stacking gel, 20% glycerol, 4% (w/v) SDS, bromophenol blue) for non-reducing gels. For reducing gels, β-mercaptoethanol (1:10) was added to the sample buffer before mixing with the samples. The samples were boiled for 5 min, loaded into the wells and electrophoresed at 20 mA per gel.

2.7 Immunochemical techniques

This section describes the protocols used in the production, isolation and affinity purification of chicken IgY antibodies, ELISA, western blotting, and enhanced chemiluminescence.

2.7.1 Reagents

The following were purchased from Sigma-Aldrich-Fluka (Steinheim, Germany): Ellman's reagent, Dimethyl sulfoxide (DMSO), Dimethylformamide (DMF), Freund's complete adjuvant (FCA), Freund's incomplete adjuvant (FIA), maleimidobenzoyl-N-hydroxysuccinimide ester (MBS), rabbit albumin (RA), L-cysteine, sodium azide, Sodium cyanoborohydride solution, Sephadex G-25, Sephadex G-104-chloro-1-naphthol, Biomax® X-ray film, p-iodophenol, luminol, Ponceau S and Tween-20. Polyethylene glycol 6000 (PEG 6000), citrate and hydrogen peroxide were purchased from Merck (Darmstadt, Germany). Molecular biology grade DTT was purchased from Fermentas (Vilinius, Lithuania). 2,2'-azino-bis(3- ethybenzothiazolinesulfonate) (ABTS) was purchased from Boehringer (Mannheim, Germany). SulfoLink™ and AminoLink™ resins were purchased from Pierce Perbio Science (Erembodegem, Belgium). Synthetic *Pf*Cox11 peptide (KIQXFXFEEQMLNAKEEM) was

synthesised by GL Biochem (Shanghai, China). Hybond-CTM Extra nitrocellulose membrane was purchased from GE Healthcare (Buckinghamshire, England). Peroxidase-conjugated rabbit anti-IgY and peroxidase conjugated goat anti-mouse IgG antibodies were from Jackson Immunochemicals (Pennsylvania, USA). Nunc MaxiSorp™ 96-well ELISA plates were from Nunc products (Roskilde, Denmark).

Affinity purified MBP fused r*Pf*Cox11Ct and r*Pf*Cox19 were used in the construction of the AminoLink™ affinity matrices.

2.7.2 Antibody production

This section describes the protocols used in the preparation of proteins and peptides for the immunisation of chickens and the isolation and affinity purification of chicken IgY.

2.7.2.1 Peptide synthesis

The selected *Pf*Cox11 peptide (section 2.3.3) was synthesised by replacing the two internal cysteines with α-aminobutyric acid and a C-terminal cysteine added to the original sequence to allow for coupling to rabbit albumin (section 2.7.2.2) or the SulfoLink™ resin (section 2.7.2.6).

2.7.2.2 Coupling peptide to rabbit albumin

The *Pf*Cox11 peptide was coupled to rabbit albumin, to improve its immunogenicity (Saravanan and Satish, 2010). The coupling was achieved with maleimidobenzoyl-N-hydroxysuccinimide ester (MBS), using the terminal cysteine sulfhydryl group of the peptide and free amine group on the rabbit albumin. The coupling of 4 mg of the peptide involved two steps: 1) Activation of the rabbit albumin carrier protein with MBS, and 2) reduction of the peptide's cysteine sulfhydryl group.

1) *Activation of the rabbit albumin carrier protein with MBS*

The peptide was coupled to rabbit albumin at a ratio of 40:1. The mass of the rabbit albumin required for the coupling was determined using the formula below, where the molecular mass of the rabbit albumin is 68.2 kDa.

$$68200 \times \frac{1}{40} \times \frac{4 \times 10^{-3}\ \mathrm{g}\ (peptide)}{Mr\ (peptide)} \times 1000 = carrier\ (mg)$$

The rabbit albumin carrier was activated with MBS at a ratio of 1:40. The mass of the MBS required for coupling was determined using the formula below, where the molar mass of the MBS is 314.26 g/mol.

$$314.26 \times 40 \times \frac{carrier\ (mg)}{68200} \times 1000 = MBS\ (mg)$$

The calculated amount of MBS was dissolved in 200 µl dimethylformamide (DMF) and made up to 500 µl with PBS and mixed with an equal volume of PBS containing the rabbit albumin, and the solution was left to stand at room temperature for 30 min. The incubation was started 30 min into the peptide incubation with DTT. Then, the solution was loaded onto a Sephadex G-25 molecular exclusion chromatography (MEC) column previously washed with two column volumes of 0.2 M NaOH and pre-equilibrated in MEC buffer (100 mM NaH_2PO_4, 0.02% (w/v) NaN_3, pH 7.0). The MBS-rabbit albumin complex was eluted with MEC buffer and 1 ml fractions were collected. Fractions with $A_{280} \geq 0.3$ were pooled.

2) *Reduction of the peptide's cysteine sulfhydryl group*

Peptide (4 mg) was dissolved in 50 µl DMSO and made up to 500 µl in reducing buffer (100 mM Tris, 1 mM EDTA, 0.02% (w/v) NaN_3, pH 8.0). Then, 500 µl 10 mM DTT was added to the peptide solution, mixed and incubated at 37^{o}C in a water bath for 90 min. The reduced peptide was separated from DTT on a Sephadex G-10 MEC column pre-equilibrated in MEC buffer. Then, 500 µl fractions were collected and the presence of reduced peptide determined by adding freshly prepared Ellman's reagent. Fractions containing reduced peptide produced a yellow reaction with the Ellman's reagent were pooled.

The activated rabbit albumin fractions were combined with the reduced peptide fractions and incubated at room temperature for 3 h with gentle stirring. The conjugated peptide was aliquoted into four equal volumes and stored at -20^{o}C until required for immunisation.

2.7.2.3 Preparation of immunogen for chicken immunisation

Chickens were immunised four times (weeks zero, two, four and six). For each immunisation, 50 µg of recombinant protein in PBS or the conjugated peptide sample were triturated 1:1 with Freund's complete adjuvant (1st immunisation) or Freund's incomplete adjuvant (2nd, 3rd and 4th immunisations) was injected intramuscularly in the breast muscles of each chicken.

2.7.2.4 Isolation of IgY from chicken egg yolk

Chicken eggs were collected throughout the immunisation schedule up to 16 weeks post-immunisation and kept at 4°C. IgY from a single egg before immunisation (non-immune) and eggs collected at the end of each week post-immunisation were isolated to monitor antibody production by ELISA.

The egg yolk was carefully separated from the albumin fraction and rinsed with water. The yolk content was obtained by puncturing the yolk sac and the yolk volume noted. An equivalent of two yolk volumes of phosphate buffer (100 mM NaH_2PO_4, 0.2% (w/v) NaN_3, pH 7.6) was added to the yolk. Then, 3.5% (w/v) PEG was added and the mixture stirred to equilibrate and centrifuged (4420 x g, 4°C, 30 min). The supernatant was filtered through cotton wool to trap the floating fat cake and the volume of the filtrate noted. The PEG concentration in the filtrate was increased to 12% (w/v), allowed to equilibrate and centrifuged (12000 x *g*, 4°C, 10 min). The supernatant was discarded and the pellet resuspended in a volume of phosphate buffer equivalent to the original egg yolk volume. Then, 12% (w/v) PEG was added, equilibrated and centrifuged (12000 x *g*, 4°C, 10 min). The final pellet was resuspended in one-sixth of the initial egg yolk volume in storage buffer (100 mM NaH_2PO_4, 0.1% (w/v) NaN_3 at pH 7.6) and stored at 4°C. The final IgY concentration was determined using the extinction coefficient $E_{280\ nm}^{1\ mg/ml}$ = 1.25 (Polson *et al.*, 1985).

2.7.2.5 Coupling of recombinant proteins to AminoLink™ resin

AminoLink™ resin contains aldehyde groups that spontaneously react with primary amines on proteins to allow for the covalent immobilisation of proteins.

A suspension of 2 ml AminoLink™ (50% slurry) in storage buffer was poured into a BioRad affinity column and the storage buffer drained. The resin was equilibrated with 6 ml coupling buffer (100 mM NaH_2PO_4, 300 mM NaCl, 0.05% (w/v) NaN_3, pH 7.2) and drained. Then, 1.5 mg recombinant protein in 2 ml coupling buffer was added to the resin. The slurry was mixed end-over-end for 4 h. The resin was then washed with 6 ml of the coupling buffer and drained. Then, 2 ml coupling buffer and 40 µl cyanoborohydride solution (5 M $NaCNBH_3$, 1 M NaOH) were added to the resin in a fume hood, and the column was mixed end-over-end for 4 h at RT. The column was drained in the fume hood, and the resin washed with 4 ml of quenching buffer (1 M Tris-HCl, pH 7.4). Then, 2 ml of quenching buffer and 40 µl of cyanoborohydride solution were added to the resin and mixed gently for 30 min and drained.

The column was washed with 10 ml of washing buffer (100 mM NaH_2PO_4, 0.2% (w/v) NaN_3, pH 6.5) followed by two column volumes of storage buffer and stored at 4ºC until needed. Coupling efficiency was assessed by measuring the protein concentration bound to the column from the retained flow-through after coupling and expressing it as a ratio of the initial protein concentration passed over the column.

2.7.2.6 Coupling of the *Pf*Cox11 peptide to a SulfoLink™ resin

SulfoLink™ resin contains iodoacetyl groups that react with free sulfhydryls to form irreversible thioether bonds attaching peptides or proteins to the resin.

The *Pf*Cox11 peptide (5 mg) was reduced as described above (section 2.7.2.2). Fractions containing the reduced peptide were pooled and added to 1 ml SulfoLink™ resin pre-equilibrated in coupling buffer (50 mM Tris-HCl, 50 mM EDTA, pH 8.5), mixed for 15 min, and left to stand for 30 min, then drained. Following washes with three column volumes in coupling buffer, 1 ml of 50 mM L-cysteine solution was added to the resin, mixed for 15 min on an end over end mixer and left to stand for 30 min. The column was drained and washed with 16 column volumes washing buffer followed by two column volumes of storage buffer and stored at 4ºC until required.

2.7.2.7 Affinity purification of IgY

The pool of isolated IgY from eggs from weeks with high antibody titres was circulated through the affinity resin overnight at room temperature. The column was washed with PBS until the A_{280} was ≤ 0.02. Bound antibodies were eluted with 950 µl elution buffer (100 mM glycine, 0.02% (w/v) NaN_3, pH 2.8) into a 1.5 ml tube containing 50 µl neutralization buffer (1 M NaH_2PO_4, 0.02% (w/v) NaN_3, pH 8.5). Fractions with $A_{280} \geq 0.2$ were pooled and the IgY concentration was calculated. The affinity purified IgY was stored at 4ºC until use.

2.7.3 ELISA

Each of the wells in a 96-well microtiter plate was coated with 150 µl of 1 µg/ml antigen prepared in PBS (137 mM NaCl, 3 mM KCl, 7 mM Na_2HPO_4, pH 7.2). The plate was incubated at 37ºC for 1 h, then overnight (16 h) at 4ºC to allow for coating of the wells. All subsequent incubations were done at 37ºC, except for the addition of substrate, which was left at room temperature. The plates were washed between incubations with PBS containing 0.1% (v/v) Tween 20 at RT. The plates were blocked with 200 µl 0.5% (v/v) BSA-PBS per well and

incubated for 1 h, and then washed three times. Plates were incubated for 2 h with 100 µl primary antibody and washed three times. The plate was then incubated with 120 µl of the rabbit-anti-chicken HRPO secondary antibody (1:15000) for 1 h and washed three times. Antibodies were prepared in 0.5% (w/v) BSA-PBS. The plates were incubated with 150 µl substrate (0.05% (w/v) ABTS, 0.0015% (v/v) H_2O_2 prepared in a 0.15 M citrate-phosphate buffer at pH 5.0) per well. The plate was read in an ELISA-plate reader at 405 nm. Background controls included: no antigen (or no coat), no primary antibody and no detection antibody in separate wells during each of the respective ELISA incubation steps. All results were corrected for background. Positive controls included a no blocking control.

2.7.4 Western blotting

The western blotting method used in this study was described by (Towbin *et al.*, 1979). After resolving the protein samples as described in an SDS-PAGE gel, the proteins were electrophoretically transferred to a nitrocellulose membrane. The gel and nitrocellulose membrane were sandwiched between blotting paper and sponges in a blotting cassette. The gel, nitrocellulose membrane and blotting papers were soaked in blotting buffer (50 mM Tris, 192 mM glycine, 20% (w/v) methanol) for 10 min before assembling the apparatus. Proteins were transferred to the nitrocellulose membrane overnight at 20 mA, stained with Ponceau S stain (0.2% (w/v) Ponceau S in 1% (v/v) acetic acid) and the position of the molecular weight marker proteins marked with a pencil. The membrane was washed in dH_2O to remove the stain and blocked with 10 ml of 5% (w/v) low-fat milk powder in TBS (20 mM Tris, 200 mM NaCl, pH 7.4) for 1 h at 4^{o}C. The nitrocellulose membrane was washed three times in 10 ml TBS for 5 min/wash, followed by a 2 h incubation with the primary antibody in 0.5% (w/v) BSA-TBS. The nitrocellulose membrane was again washed three times in 10 ml TBS for 5 min/wash and incubated with the secondary antibody 1:12000 in 0.5% (w/v) BSA-TBS, followed by three washes in 10 ml TBS for 5 min/wash. The nitrocellulose membrane was developed for 5-20 min using a substrate solution (0.06% (w/v) 4-chloro-1-naphthol, 0.012% (v/v) H_2O_2 prepared in TBS). Finally, the developed nitrocellulose membrane was washed with dH_2O, dried and the image taken.

2.7.5 Enhanced chemiluminescence

The enhanced chemiluminescence (ECL) (Mruk and Cheng, 2011) follows a similar procedure as the western blotting (section 2.7.4) with the following modifications; TTBS (0.1%

(v/v) Tween 20 was added to the TBS buffer), blocking was performed with 8% (w/v) low-fat milk powder in TTBS, and the wash steps were increased to 8 min/wash in 10 ml TTBS. After blocking for 1 h and washing three times, the nitrocellulose membrane was incubated for 2 h with the primary antibody in 0.5% (w/v) BSA-TTBS and washed three times. The nitrocellulose membrane was then incubated with the secondary antibody (1:12000 in 0.5% (w/v) BSA-TTBS), followed by three washes. The chemiluminescent reagent (0.2 mg/ml luminol, 0.25 mM p-iodophenol, 0.075% (v/v) H_2O_2 prepared in a 0.1 M Tris-HCl buffer at pH 8.5) was poured directly onto the nitrocellulose membrane and exposure time was optimised per sample.

2.8 Copper binding studies

The binding of copper to the recombinant proteins was evaluated using the following techniques.

2.8.1 Bicinchoninic acid (BCA) release assay

The BCA release assay (Brenner and Harris, 1995), was employed to assess presence of copper attached to the recombinant protein. The method exploits BCA complexation with Cu(I) (Cu(I)-BCA) at alkaline pH to give a purple colour detectible at 562 nm which absorbs with a higher intensity than at 354 nm. Although oxygen was not excluded in the experiment, incubation of the recombinants protein with copper was done under reduced (with ascorbate) or non-reduced (without ascorbate) conditions to allow for recombinant protein complexation with Cu(I) and Cu(II) respectively. In this assay, protein-copper complexes are disrupted by denaturation with trichloroacetic acid to release copper into a reducing solution which facilitates the Cu(I)-BCA complex formation. Cu(II) in the reaction medium must be reduced to Cu(I) by a reducing agent for the Cu(I)-BCA complex to be formed.

For the BCA assay, 10 µM recombinant protein in phosphate buffer (100 µM NaH_2PO_4, 0.01% (w/v) NaN_3, pH 7.5) was denatured with 30% (w/v) trichloroacetic acid. The protein precipitates formed were pelleted by centrifugation (12000 x *g*, RT, 2 min), and the supernatant aliquoted (4 x 250 µl) into clean microfuge tubes. Then, 50 µl of 2 mM ascorbic acid or distilled water (dH_2O) was added to two samples. The four reactions were neutralized with 200 µl 0.15 mM BCA, 0.9 M NaOH, 0.2 M HEPES, mixed and allowed to stand for 2 min at RT before reading the absorbance at 354 nm. The assay was used to assess the binding of copper by recombinant proteins *in vivo* and *in vitro*. The potential influence of azide in the assay was

minimalized by the molar excesses of copper present. An independent control with azide was included.

In vitro copper binding by recombinant proteins

For the *in vitro* copper binding by recombinant proteins, duplicate samples of 10 µM purified recombinant protein were mixed with 200 µM $CuCl_2$ (ratio 1:20). Then, 10 mM ascorbic acid was added to one sample, while distilled water was added to the other. The samples were briefly mixed and allowed to stand at RT for 15 min. The excess unbound copper was removed by dialysis as described. Bound copper was then determined by BCA release assay.

In cellulo copper binding by recombinant proteins

In vivo copper binding by the recombinant proteins was measured by adding 0.5 mM $CuCl_2$ to the bacterial growth media. This copper concentration has been shown to be tolerated by growing *E. coli* cells with no significant effect on the growth rate (Lutsenko *et al.*, 1997). Expression of recombinant proteins was induced (section 2.6.2), and the proteins affinity purified (section 2.6.3). The bound copper was determined by BCA release assay.

2.8.2 Ascorbate oxidation assay

The inhibition of copper-catalysed ascorbic acid oxidation by the recombinant proteins was measured *in vitro*. A 1 ml reaction with 120 µM ascorbic acid, 8 µM copper(II) chloride and 5 µM recombinant protein (variable) was set up at RT. The reaction was started with the addition of the ascorbic acid solution to the rest of the reaction components. The OD_{255} of the solution was monitored at pH 4.5 for 300 s, at 5 s intervals and the rate of inhibition of ascorbic acid oxidation followed in a UV-1800 Shimadzu spectrophotometer. The experiment was repeated thrice.

2.8.3 Atomic absorption spectroscopy

The amount of copper bound to the recombinant proteins was quantified by atomic absorption spectroscopy (AAS) using an Agilent Varian AA280FS atomic absorption spectrophotometer. Samples were prepared as described for the *in vitro* copper binding assessment using BCA release assay (section 2.8.1).

2.8.4 Differential scanning fluorimetry

The recombinant protein samples were prepared as described for the *in vivo* copper binding assessment (section 2.8.1). Differential scanning fluorimetry using the fluorescent dye SYPRO® Orange dye (Lo *et al.*, 2004) was employed to assess the melting temperature (T_m) of the recombinant malaria proteins. The assay was performed in 25 µl reaction volume containing 500 ng recombinant protein and 10x SYPRO® orange and phosphate buffer (pH 7.4) using the Rotorgene® 6000. The T_m of the recombinant protein over a temperature range of 25 to 90ºC at a ramp of 0.3ºC/min was monitored by SYPRO® fluorescence at λ_{ex} 470 nm and λ_{em} 570 nm. The data obtained was transformed to a negative first derivative (-d(RFU)/dT) and the melting temperature extrapolated from the curve.

2.8.5 Effect of copper on the growth of *E. coli* host cells expressing the recombinant proteins

E. coli host cells expressing the recombinant proteins were grown in the presence of varying copper concentrations to assess the effect of the recombinant proteins on the copper tolerance of *E. coli* host cells during growth. The concentration of copper inhibiting 50% cell growth (IC_{50}) was determined.

Overnight (16 h) cultures of single colonies of naïve or transformed *E. coli* (BL21) cells with pMal-c2x and recombinant pMal-c2x plasmids were grown in 2xYT media (30ºC, 200 rpm) containing ampicillin (100 µg/ml). The cultures were diluted 1:100 into fresh 2xYT media containing ampicillin (100 µg/ml) and grown in the same conditions. At an OD_{600} between 0.5-0.6, recombinant expression was induced with 0.5 mM IPTG and additional ampicillin (100 µg/ml) and in the presence of varying copper concentrations (0-20 mM). The cultures were then incubated for 6 h. The growth rate was monitored at hourly intervals at OD_{600}.

2.9 Ethical clearance for the use of experimental animals

The use of experimental animals for this study was approved by the animal ethics committee of the University of Kwa-Zulu Natal (UKZN) (Ethics no.:004/15//Animal). Mice were housed and cared for at the School of Life Sciences animal house, Pietermaritzburg. Chickens were housed and cared for at the UKZN farms at Ukulinga, Pietermaritzburg. Two chickens were used per immunogen.

Chapter 3

In silico analysis of *Plasmodium falciparum* Cox11 and Cox19 copper metallochaperones

3.1 Introduction

Advances in the field of biomedicine are attributable to the application of genomics, proteomics and structural biology to understanding diseases hitherto untreatable or unmanageable. These studies are facilitated with the application of bioinformatics, a tool integrating computer science, mathematics, engineering and biology to analyse and interpret biological data (Martin-Sanchez *et al.*, 2004). The bioinformatics tools employed to characterise two novel putative *P. falciparum* copper metallochaperones earlier identified in the *P. falciparum* genome (Choveaux *et al.*, 2015; Gardner *et al.*, 2002) are described in this chapter.

3.1.1 Mitochondrial cytochrome c oxidase of the malaria parasite

Cytochrome c oxidase (CcO) is the terminal enzyme of the mitochondrial electron transport chain situated in the inner mitochondrial membrane. CcO is a complex of eleven (in yeast) or thirteen (in mammals) subunits (Capaldi, 1990) with other accessory proteins involved in its assembly. An active CcO contains five cofactors: two haems, three copper ions, magnesium, zinc and sodium ions (Carr and Winge, 2003; Tsukihara *et al.*, 1995). In yeast, the catalytic core of CcO is comprised of Cox1, Cox2 and Cox3 transmembrane subunits encoded by the mitochondrial genome (mtDNA), while other subunits are encoded by the nuclear genome (Fontanesi *et al.*, 2006). *Plasmodium* parasites have limited mitochondria of highly reduced gene content encoding only three proteins, Cox1, Cox3 and Cyt*b* (Vaidya and Mather, 2009). Cox1 has two redox centres, one formed by haem A, and the other by haem a_3 and a Cu_B centre containing one copper atom. The Cox2 subunit has the binuclear Cu_A centre, containing two copper atoms. Since Cox1 is synthesised in the mitochondria, the copper atoms must be imported from outside the organelle. The accessory proteins in mammalian and yeast systems implicated in the delivery of copper to CcO are Cox11, Cox17, Cox19 and Sco1 respectively (Beers *et al.*, 2002; Bode *et al.*, 2015; Hiser *et al.*, 2000; Nobrega *et al.*, 2002; Timón-Gómez *et al.*, 2018). Using a bioinformatics approach, four putative copper metallochaperones, Cox11, Cox17, Cox19 and Sco1 were identified in the *Plasmodium falciparum* genome (Table 3.1) (Choveaux *et al.*, 2012). Two of the four metallochaperones, Cox11 and Cox19, were chosen for initial characterisation in this study.

Presence of the two copper metallochaperones, Cox11 and Cox19 orthologues in eight other *Plasmodium* spp. was confirmed in a BLASTp search of the malaria genome at PlasmoDB (Aurrecoechea *et al.*, 2009) using PF3D7_1475300 and PF3D7_1201800 protein as the query sequence. Both the *P. falciparum* Cox11 and the *P. falciparum* Cox19 protein sequences were characterised and antibodies raised in chickens.

Table 3.1. Copper-dependent protein orthologues found in the *P. falciparum* genome

Protein name	PlasmoDB ID	Chromosome (#)	Characterised	Function in *Plasmodium*	Reference
S-adenosyl-L-homocysteine hydrolase	PF3D7_0520900	5	No	No data	N/A
Copper-transporting ATPase (CuP-ATPase)	PF3D7_0904900	9	Yes	Copper efflux malaria fertility.	Rasoloson *et al*., 2004; Kenthirapalan *et al*., 2014.
Ctr1	PF3D7_1439000	14	Yes	Copper binding	Choveaux *et al*., 2012.
Ctr2	PF3D7_1421900	14	Yes	Copper binding	Choveaux *et al*., 2012.
Cox1	mal_mito_2	Not assigned	No	No data	N/A
Cox2	PF3D7_1361700 PF3D7_1430900	13 14	No No	No data	N/A
Cox3	mal_mito_1	Not assigned	No	No data	N/A
Cox5B	PF3D7_0927800	9	No	No data	N/A
Cox6B	PF3D7_0928000.1	9	No	No data	N/A
Cox11	PF3D7_1475300	14	No	No data	N/A
Cox17	PF3D7_1025600	10	Yes	Copper binding	Choveaux *et al*., 2015.
Cox19	PF3D7_1201800	12	No	No data	N/A
Sco1	PF3D7_0708900	7	No	No data	N/A

Table modified from Choveaux *et al.*, 2012

3.2 Results

3.2.1 Bioinformatic characterisation of the putative *P. falciparum* Cox11 protein

The role and contribution of the TCA cycle to the bioenergetics of the erythrocytic stages of malaria parasites has been a long-standing debate (Vaidya and Mather, 2009). For a functional CcO protein, Cox11 is required for the formation of the Cu_B centre (Hiser *et al.*, 2000). Choveaux *et al*., (2012) identified a putative Cox11 alongside 13 copper-dependent protein orthologues in *P. falciparum* from a BLASTp search of the PlasmoDB genome database (Aurrecoechea *et al.*, 2009). Of the 14 *P. falciparum* copper-binding protein orthologues identified, only four have been characterised to date as shown in

Table **3.1**. Despite the increasing evidence suggestive of the importance of copper homeostasis to the malaria parasite, not much has been studied on malaria parasite copper homeostasis (Asahi *et al.*, 2013; 2014; Choveaux *et al.*, 2012; 2015; Kenthirapalan *et al.*, 2014; 2016; Rasoloson *et al.*, 2004).

The putative *P. falciparum* Cox11 (PF3D7_1475300) protein sequence (~45% identity to human Cox11) having met the minimum identity (>30%) (Pearson, 2013) to make a homologue, the sequence was used in a BLASTp search of the PlasmoDB genome database (Aurrecoechea *et al.*, 2009) to identify Cox11 in eight plasmodial species. The Cox11 sequences were from; *P. vivax* (PVX_118645), *P. knowlesi* (PKNH_1245600), *P. reichenowi* (PRCDC_1474400), *P. cynomolgi* (PCYB_127810), *P. yoelii* (PY17X_1304500), *P. chabaudi* (PCHAS_1304100), *P. berghei* (PBANKA_1300900) and *P. gallinaceum* (PGAL8A_00196000). To identify common characteristics, the amino acid sequence of Cox11 from nine *Plasmodium* sequences were aligned with five well characterised Cox11 sequences, including Cox11 from, *Homo sapiens* (NP_004366.1), *Mus musculus* (NP_950173.1), *Saccharomyces cerevisiae* (NP_015193.1), *Arabidopsis thaliana* (NP_171743.1) and *Sinorhizobium meliloti* (GenBank: KKA13892.1). The aligned sequences (Figure 3.1), showed that 48 to 67 amino acids are missing from the N-terminal sequence in *Plasmodium* compared to the human, mouse, yeast and plant Cox11 orthologues. However, in comparison with the bacterial orthologue, *Plasmodium* has 17 extra amino acids at the N-terminus. The intergenic region upstream of the suspected initiation codon for each gene sequence was assessed for the presence of a nearby open reading frame (ORF). The nearest ORF to *Plasmodium* spp. Cox11 was 460 nucleotide bases away in *P. berghei*. Similarly, downstream

amino acid deletions in *Plasmodium* spp., at residues eight, 27, 73 and 96 of *P. falciparum* in relation to the human sequence were found. The alignment shows amino acid conservation within the predicted transmembrane and the C-terminal domains of all 14 sequences. The sequences all contained three cysteine residues (Figure 3.1). Two of the three cysteines are in a conserved CFCF motif, and the third a short distance from this motif. The cysteines are at residue 60, 155 and 157 in *P. falciparum* sequence, with the cysteines 155 and 157 included in the CFCF motif.

Each of the putative *Plasmodium* Cox11 sequences alongside the five characterised sequences was submitted to the GPS-PAIL online server to predict potential acetylation sites (Deng *et al.*, 2016). At the highest threshold, a minimum of two internal lysine acetylation sites (Figure 3.1) were predicted in *Plasmodium* spp. In the two mammalian and yeast Cox11 sequences, no acetylation sites were predicted. However, the plant and bacterial Cox11 were predicted to have one and three acetylation sites respectively. The predicted sites are predicted to be acetylated by the two lysine acetyltransferases (KAT), EP300 and CREBBP. A third is lone KAT2B site predicted in the plant Cox11 sequence. In the *Plasmodium* spp., the predicted EP300 acetylation sites are at the N-terminus within the predicted mitochondrial matrix domain, while the CREBBP acetylation sites are within the C-terminal domain in the mitochondrial intermembrane space (Figure 3.2). The *P. falciparum* Cox11 was predicted to have three EP300 acetylation sites. In furtherance of the search for possible post-translation modification sites, the prevalence of lysine in the *P. falciparum* Cox11 sequence prompted the query for ubiquitination site. The UbiProber server (Chen *et al.*, 2013) predicting the ubiquitination site did not identify any site in any of the *Plasmodium* sequences. Also, no signal peptide was predicted in *Plasmodium* Cox11 sequences by the PlasmoAP and iSMP-Grey servers (Lin *et al.*, 2012).

The *Plasmodium* Cox11 sequences were analysed for a membrane-spanning region using the TMHMM (Krogh *et al.*, 2001) transmembrane (TM) prediction server. A common 23-amino acid membrane-spanning domain tethering Cox11 to the inner mitochondrial membrane (IM) was predicted in all *Plasmodium* sequences. Figure 3.2 illustrates the predicted orientation of *P. falciparum* Cox11 as it relates to the *S. meliloti* Cox11 reference sequence. The position of the transmembrane domain in *Plasmodium* spp. is variable, contained between amino acid residue 33 to 59 (Figure 3.1). The *P. falciparum* transmembrane domain is located between amino residues 34 to 56.

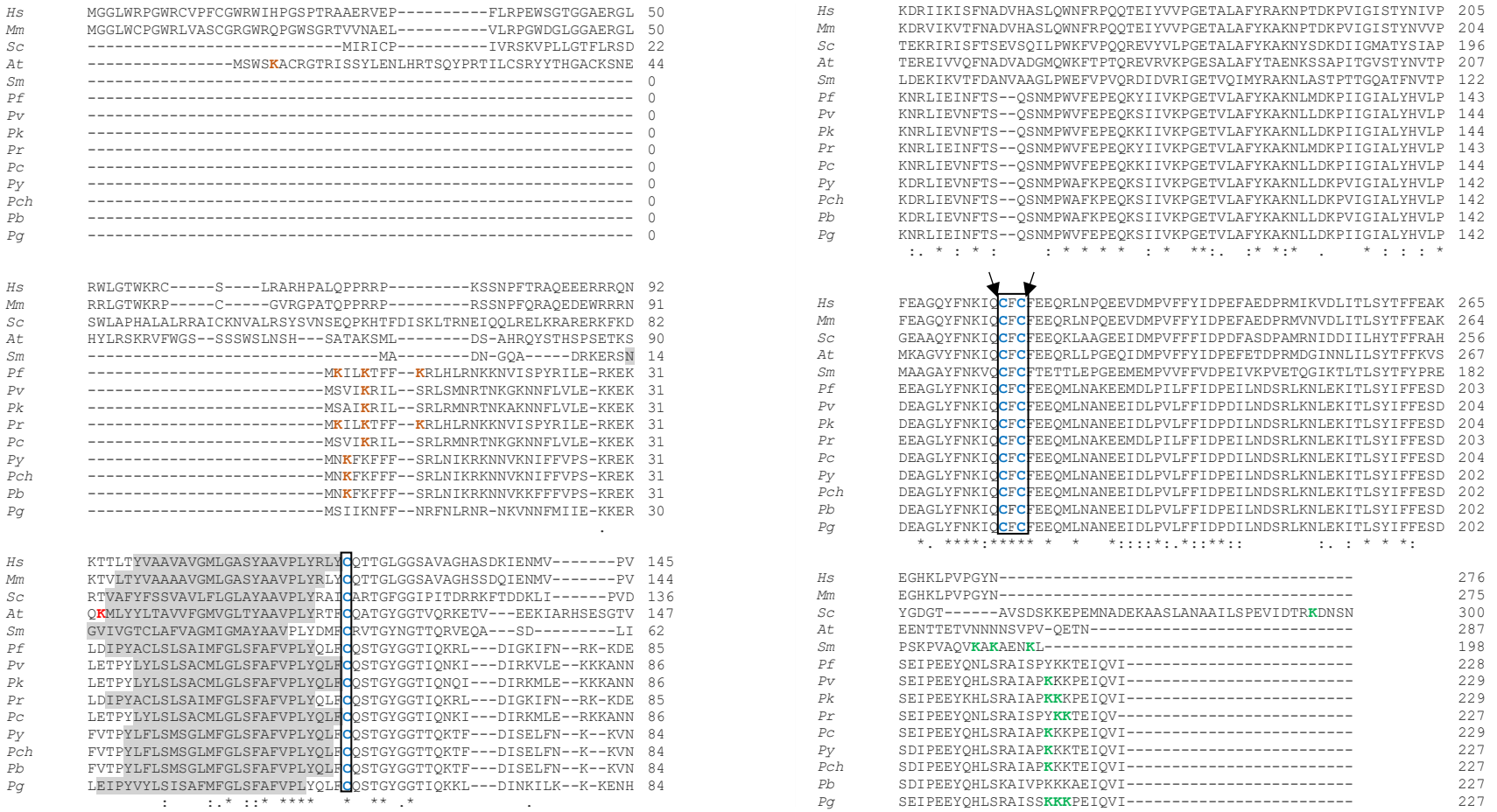

Figure 3.1. Alignment of nine putative *Plasmodium* and five established Cox11 amino acid sequences

Clustal Omega was used to align the plasmodial Cox11 sequence with Cox11 from: *Hs*, *Homo sapiens* (NP_004366.1); *Mm*, *Mus musculus* (NP_950173.1); Sc, *Saccharomyces cerevisiae* (NP_015193.1); *At*, *Arabidopsis thaliana* (NP_171743.1); *Sm*, *Sinorhizobium meliloti* (GenBank: KKA13892.1); *Pf*, *P. falciparum* (PF3D7_1475300); *Pv*, *P. vivax* (PVX_118645); *Pk*, *P. knowlesi* (PKNH_1245600); *Pr*, *P. reichenowi* (PRCDC_1474400); *Pc*, *P. cynomolgi* (PCYB_127810); *Py*, *P. yoelii* (PY17X_1304500); *Pch*, *P. chabaudi* (PCHAS_1304100); *Pb*, *P. berghei* (PBANKA_1300900); *Pg*, *P. gallinaceum* (PGAL8A_00196000). The annotation "*****", denote conserved residue, while "**:**"and "**.**" denote conserved and semi-conserved substitutions respectively. The three conserved cysteine residues are shown in blue by the box region. Arrow indicates the two cysteines implicated in copper binding. The brown, green and red Lys residues denote the predicted acetylation sites for EP300, CREBBP and KAT2B acetyltransferases respectively. Predicted transmembrane regions are highlighted in grey.

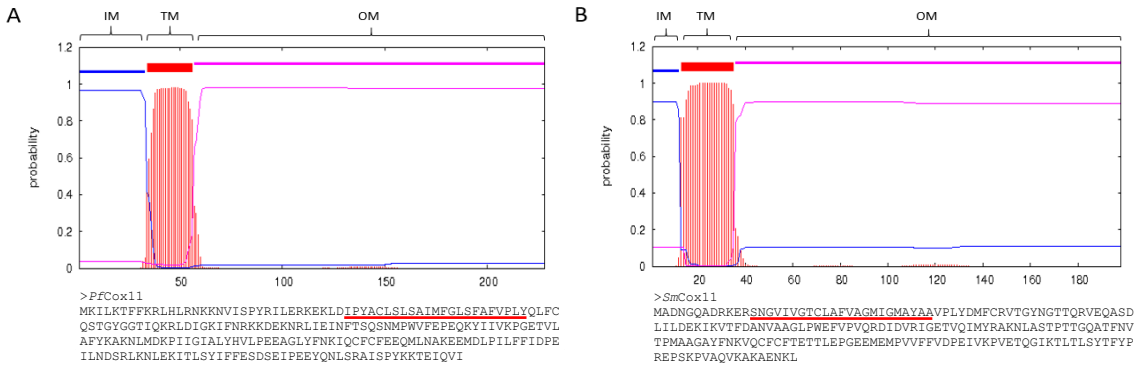

Figure 3.2. Predicting membrane-spanning regions in *P. falciparum* Cox11
The TMHMM plots with the amino acid sequences for *P. falciparum* (A) and the reference characterised *S. meliloti* Cox11 (B). Sections of the sequences of the proteins are predicted to be on the outer surface of the inner mitochondrial membrane, OM (pink horizontal line), a transmembrane domain, TM (red horizontal line and underlined sequences) or within the mitochondrial matrix, IM (blue horizontal line).

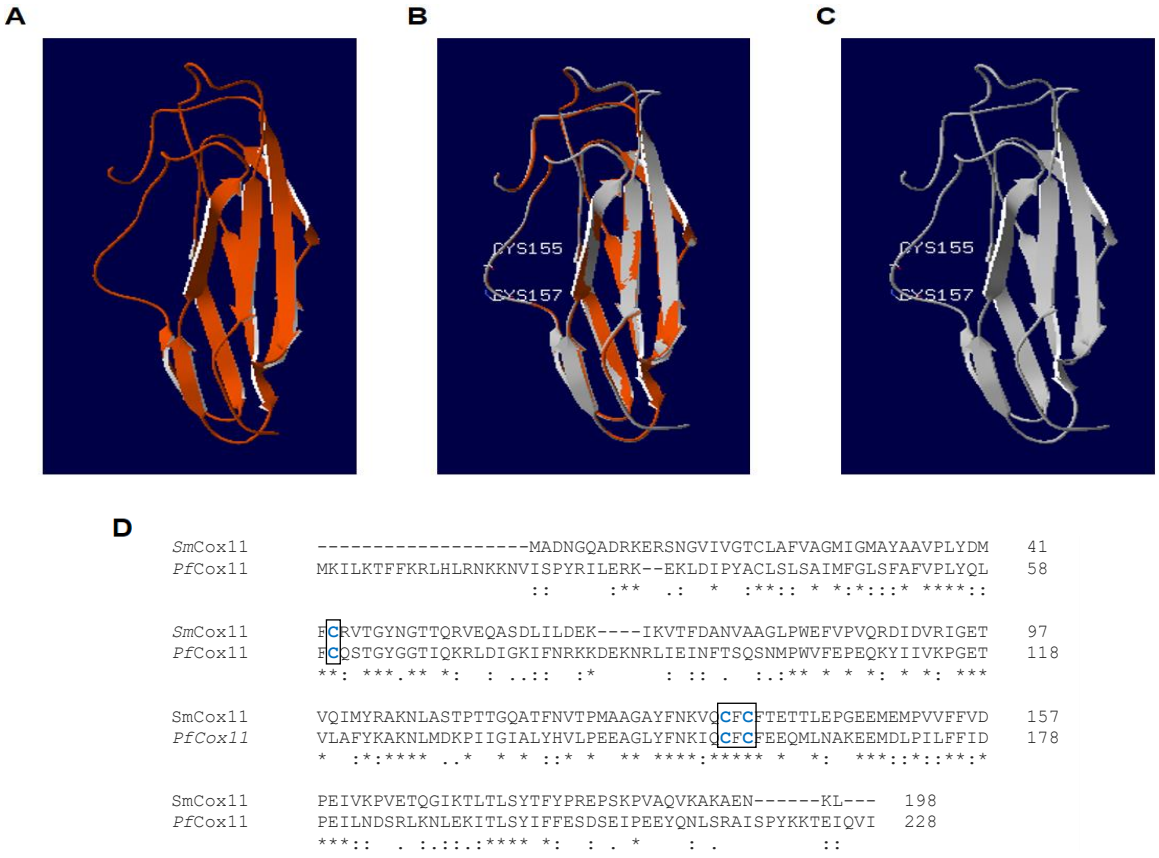

Figure 3.3. *Plasmodium falciparum* Cox11 modelled on the *Sinorhizobium meliloti* Cox11 structure
The NMR-solved structure of *S. meliloti* (PDB: 1so9) Cox11 (A) (Banci *et al*., 2004) amino acid sequence served as a template (brown ribbon) for homology modelling of the *P. falciparum* Cox11 amino acid sequence (grey ribbon) (B). The *Pf*Cox11 model shows two of three conserved cysteines (Cys155 and Cys157) (blue structures) implicated in copper coordination (C) (Carr *et al*., 2002). The annotation "*****", denote conserved residue, while "**:**"and "**.**" denote conserved and semi-conserved substitutions respectively. The model was constructed by sequence alignment (D). The three conserved cysteines residues are in blue by the box region.

The *P. falciparum* Cox11 structure (Figure 3.3C) was modelled on the *S. meliloti*, *Sm*Cox11 (Figure 3.3A) NMR structure (PDB: 1so9) (Banci *et al.*, 2004) template using the Swiss-Pdb DeepView program (Guex *et al.*, 2009). Both *Sm*Cox11 and *Pf*Cox11 have a similar structure of the β-immunoglobulin (Ig)-like fold (Figure 3.3B) (Banci *et al*., 2004). The distinctive feature between them is a 30 amino acid residue extension in the *Pf*Cox11 sequence (Figure 3.3D). The modelled *Pf*Cox11 structure fitted well into the *Sm*Cox11 structure.

3.2.2 Bioinformatic characterisation of the putative *P. falciparum* Cox19 protein

As with Cox11, the *P. falciparum* Cox19 (PF3D7_1201800) protein sequence (40% identity to human Cox19) having met the minimum identity (>30%) (Pearson, 2013) to make a homologue, the sequence was used to identify eight *Plasmodium* spp. Cox19 sequences from a BLASTp search of the PlasmoDB (Aurrecoechea *et al.*, 2009). The sequences identified were; *P. vivax* (PVX_084115), *P. knowlesi* (PKNH_1301700), *P. reichenowi* (PRCDC_1201200), *P. cynomolgi* (PCYB_131060), *P. yoelii* (PY17X_0603400), *P. chabaudi* (PCHAS_0602700), *P. berghei* (PBANKA_0600800) and *P. gallinaceum* (PGAL8A 00319900). To identify common characteristics, all nine *Plasmodium* spp. sequences were aligned using Clustal Omega (Li *et al.*, 2015) with five characterised Cox11 sequences; *Homo sapiens* (NP_001026788.1), *Mus musculus* (NP_932097.1), *Gallus gallus* (NP_001243736.1), *Arabidopsis thaliana* (NP 564879.1) and *Saccharomyces cerevisiae* (GenBank: GAX71665.1).

From the sequence alignment (Figure 3.4) six and 22 N-terminal amino acid deletions in *Plasmodium* spp. relative to the vertebrate and plant Cox19 sequences respectively were revealed. The C-termini of all malaria species had 116 to 129 extra amino acids relative to the five other species. Within the *Plasmodium* spp., there were some amino acid deletions and insertions. Two conserved deletions of six and four amino acids were found in the three murine malaria parasites, between residues 128 to 135, and 162 to 167 compared to the *P. falciparum* sequence. Four conserved cysteines were found within the [Coiled coil 1]-[Helix 1]-[Coiled coil 2]-[Helix 2] (CHCH) domain in a twin Cx_9C motif. The cysteines are at positions 24, 34, 45 and 55 respectively in the *P. falciparum* amino acid sequence. These cysteines form two disulphide bonds, between Cys34 – Cys45 and Cys24 – Cys55 respectively in the yeast and human sequences (Fischer *et al.*, 2013; Rigby *et al.*, 2007). Also present is an Arg residue adjacent to the carboxy-proximal cysteine,

which is conserved in all 14 Cox19 sequences (Figure 3.4). This Arg is at position 56 in the *P. falciparum* amino acid sequence.

As with Cox11, each of the putative *Plasmodium* spp. Cox19 sequences alongside the five characterised sequences was submitted to the GPS-PAIL online server for predicting acetylation sites (Deng *et al.*, 2016). Using the most stringent criteria, *Plasmodium* spp. had a minimum of one predicted acetylation site. In contrast to the predictions in Cox11, acetylation sites were predicted in the mammalian and yeast Cox19 sequences but none in the plant sequence. The lysine acetyltransferase sites predicted were specific to EP300, CREBBP and KAT2B respectively. The EP300 acetylation site predicted at position four in *P. falciparum* sequence is conserved in 12 of the 14 sequences but not *A. thaliana* and *S. cerevisiae*. All predicted acetylation sites are outside the CHCH domain. No ubiquitination site in *Plasmodium* spp. was predicted by the UbiProber server (Chen *et al.*, 2013). Subjecting the sequences to the PlasmoAP and iSMP-Grey servers (Lin *et al.*, 2012) found no signal sequences.

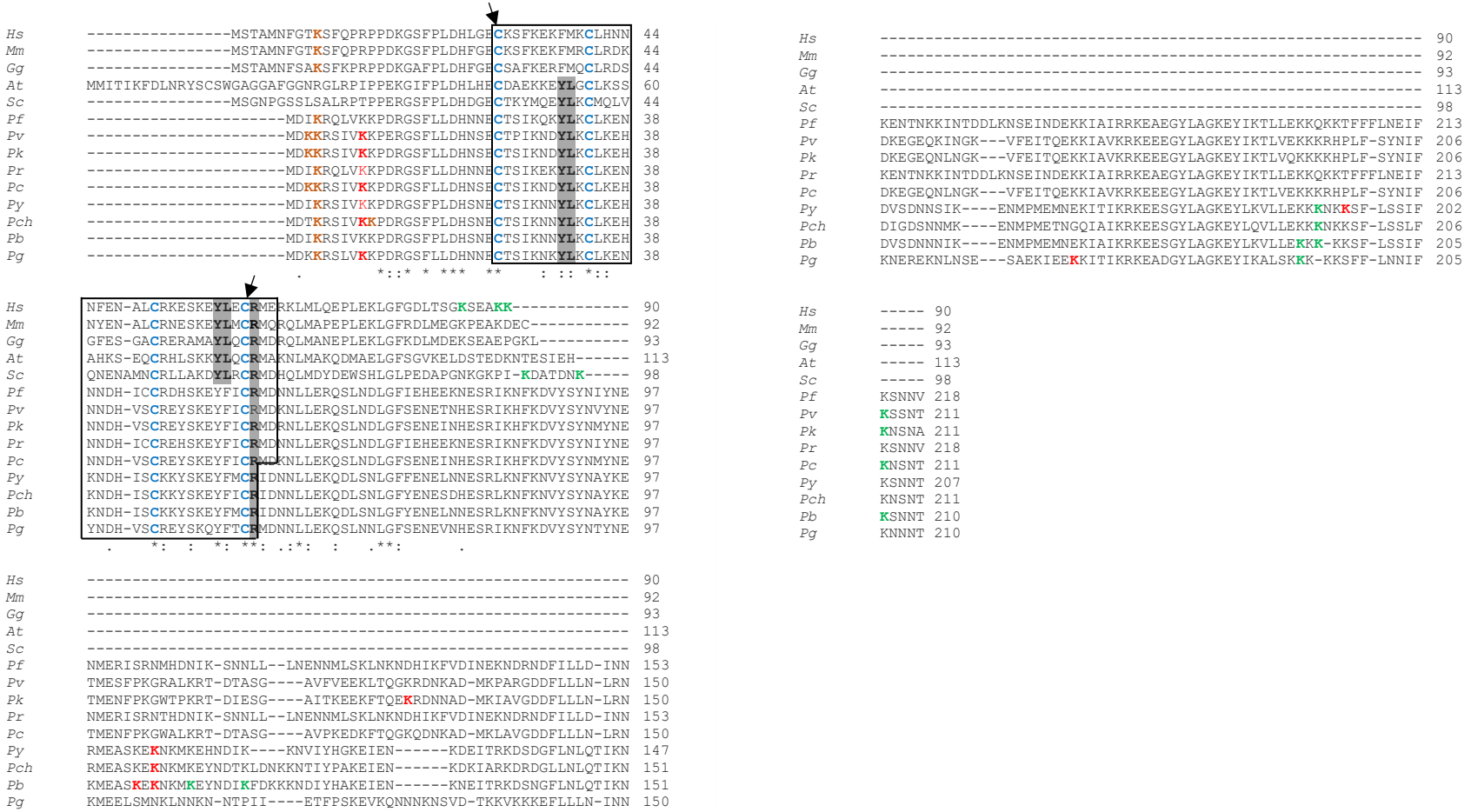

Figure 3.4. Alignment of nine putative *Plasmodium* and five characterised Cox19 amino acid sequences

Clustal Omega was used to align plasmodial and human and other Cox19 sequences. The sequences are: *Hs*, *Homo sapiens* (NP_001026788.1); *Mm*, *Mus musculus* (NP_932097.1); *Gg*, *Gallus gallus* (NP_001243736.1); *At*, *Arabidopsis thaliana* (NP_564879.1); *Sc*, *Saccharomyces cerevisiae* (GenBank: GAX71665.1); *Pf*, *P. falciparum* (PF3D7_1201800); *Pv*, *P. vivax* (PVX_084115); *Pk*, *P. knowlesi* (PKNH_1301700); *Pr*, *P. reichenowi* (PRCDC_1201200); *Pc*, *P. cynomolgi* (PCYB_131060); *Py*, *P. yoelii* (PY17X_0603400); *Pch*, *P. chabaudi* (PCHAS_0602700); *Pb*, *P. berghei* (PBANKA_0600800); *Pg*, *P. gallinaceum* (PGAL8A_00319900). The annotation "*****", denote conserved residue, while "**:**"and "**.**" denote conserved and semi-conserved substitutions respectively. The [Coiled coil1]-[Helix 1]-[Coiled coil 2]-[Helix 2] (CHCH) domain is shown by the box region. The conserved cysteine residues in Cx_9C motif within the CHCH domain are shown in blue. Arrows indicate the two cysteines implicated in copper binding. The brown, green and red Lys residues denote the predicted acetylation sites for EP300, CREBBP and KAT2B acetyltransferases respectively. The conserved residues essential for an active Cox19 in yeast; Tyr-Leu dipeptides and Arg are highlighted in grey.

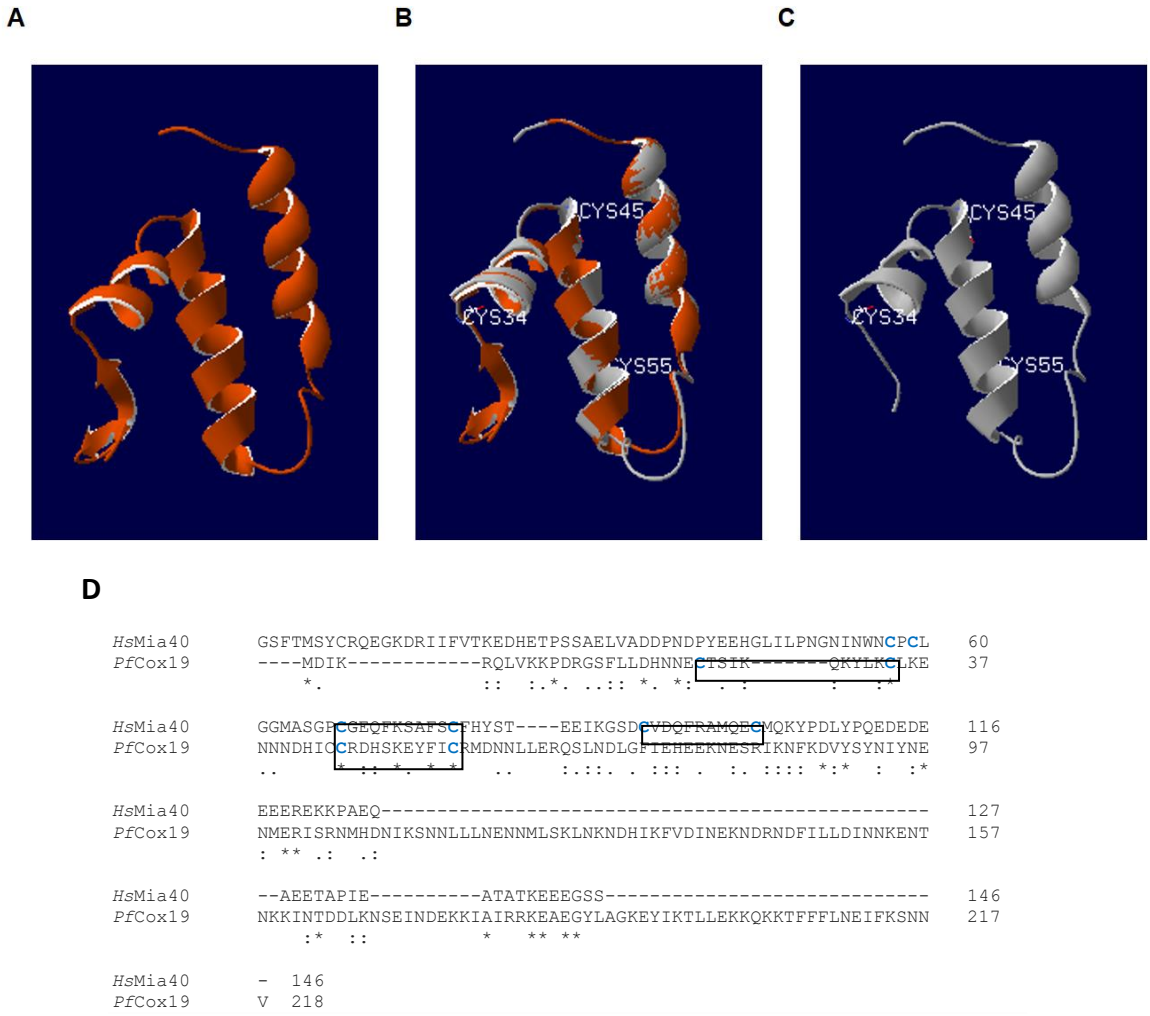

Figure 3.5. *Plasmodium falciparum* Cox19 modelled on *Homo sapiens* Mia40 structure
The NMR-solved structure of *Homo sapiens* Mia40 (PDB: 2K3J) (A) amino acid sequence (Banci *et al.*, 2009) served as a template (brown ribbon) for homology modelling of the *P. falciparum* Cox19 (grey ribbon) (B). The *Pf*Cox19 model shows three of the four conserved cysteines (Cys34, Cys45 and Cys55) in twin Cx_9C motif (C). The model was constructed by sequence alignment (D). Only the overlapping sequence was modelled on the *Hs*Mia40 structure. The annotation "*****", denote conserved residue, while "**:**"and "**.**" denote conserved and semi-conserved substitutions respectively. The conserved cysteines residues are in blue, while the Cx_9C motif is shown by the box region.

Like Cox11, an attempt was made to construct a hypothetical *P. falciparum* Cox19 (*Pf*Cox19) structure. However, no Cox19 structure was found at the protein data bank. To this end, the NMR-solved *H. sapiens* Mia40 (*Hs*Mia40) structure (PDB:2K3J) (Banci *et al.*, 2009) (Figure 3.5A) was used to model the putative *Pf*Cox19 which has been used for yeast Cox19 (Bode *et al.*, 2015; Timón-Gómez *et al.*, 2018). Mia40 is a twin Cx_9C protein that catalyses the oxidative folding and import of twin Cx_9C and Cx_3C substrates into the mitochondrial intermembrane space via a conserved CPC motif (Banci *et al.*, 2009; Bien *et al.*, 2010; Fraga *et al.*, 2014; Koch and Schmid, 2014). Mia40 like twin Cx_9C proteins has a CHCH domain. Cox19 is thought to have structure similar to Mia40 that has a conserved critical twin Cx_9C

domain that forms a helix-loop-helix fold in which the two antiparallel α-helices are connected by two parallel disulfide bonds. The homology modelling was done using the Swiss-Pdb DeepView program. As shown in Figure 3.5B, both *Hs*Mia40 and *Pf*Cox19 have a similar structure. However, the first 28 *P. falciparum* residues are not included in the present model. Only the overlapping sequence that fit into the *Hs*Mia40 structure was included in the modelling. *P. falciparum* Cys24 was not included in the model. Thus, only three conserved cysteines residues were included in the modelled structure assuming the CHCH conformation (Figure 3.5B and C).

3.2.3 Selection of immunogenic Cox11 peptide for antibody production in chickens

A peptide of 18 amino acid residues was selected (Figure 3.6) around the putative *P. falciparum* Cox11 binding domain using Predict7™ (Cármenes *et al.*, 1989) for synthesis. Antibodies against the synthetic peptide, KIQXFXFEEQMLNAKEEM were raised in chickens for copper binding competition assays. The "X" in the synthetic peptide denotes α-aminobutyric acid. To improve antibody specificity, chickens were immunised with the KIQXFXFEEQMLNAKEEM peptide epitope coupled to a carrier protein, rabbit albumin (Hurdayal *et al.*, 2010; Tomar *et al.*, 2006). The two internal cysteines were substituted with α-aminobutyric acid, and a C-terminal cysteine added to allow for specific N-terminal coupling to rabbit albumin via maleimidobenzoyl-N-hydroxysuccinimide ester (MBS).

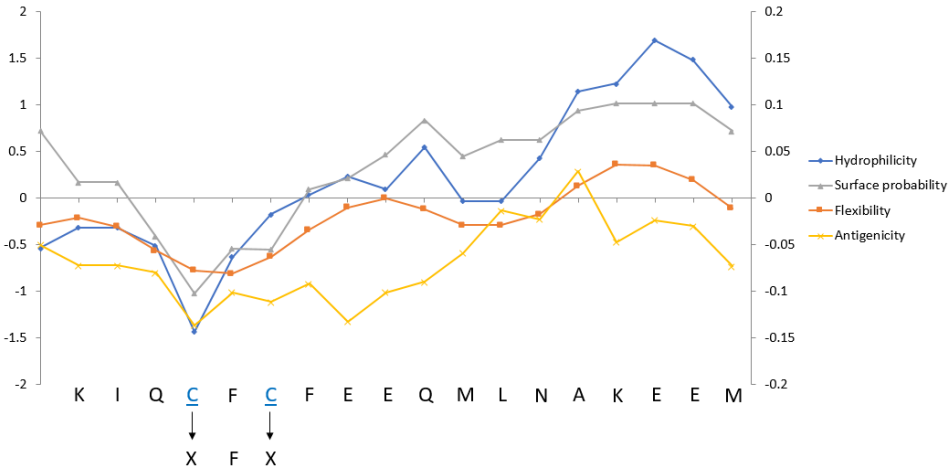

Figure 3.6. Peptide around the putative *P. falciparum* Cox11 copper binding domain
Predict7™ analysis showing hydrophilicity, surface probability, flexibility and antigenicity of the selected *P. falciparum* Cox11 peptide (KIQXFXFEEQMLNAKEEM), containing the implicated copper-binding site. The two internal cysteines (C) residues were replaced with α-aminobutyric acid (X) in the synthetic peptide. A C-terminus cysteine was added to the synthetic peptide for peptide conjugation to MBS.

3.3 Discussion

The membrane potential generated across the inner mitochondrial membrane forms the driving force for the ATP synthesis in most eukaryotes. In contrast, glycolysis is preferred over oxidative respiration in *Plasmodium* spp. (Vander Jagt *et al.*, 1990). However, oxidative respiration is essential for the regeneration of ubiquinone for pyrimidine biosynthesis required by the actively dividing parasite. The turnover of the electron transfer cascade is maintained by CcO, the terminal enzyme of the mitochondrial electron transport chain. A functional CcO requires three copper residues within its Cox1 and Cox2 subunits, which have been demonstrated in yeast to be supplied by the metallochaperones Cox11, Cox17, Cox19 and Sco1 (Beers *et al.*, 2002; Glerum *et al.*, 1996; Nobrega *et al.*, 2002). Plasmodial Cox11 and Cox19 were characterised *in silico*.

3.3.1 Bioinformatic characterisation of the putative *P. falciparum* Cox11 protein

In an attempt to add to the existing knowledge on the *Plasmodium* copper pathways and homeostasis, the Cox11 sequence was analysed. The Cox11 orthologues were present in the genome of all the nine *Plasmodium* spp., implying a significant role of the protein for the parasite. The multiple sequence alignments of the *Plasmodium* sequences with other characterised Cox11 sequences revealed sizeable N-terminal differences. Deletions in two regions within the C-terminal domain of *Plasmodium* spp. were revealed. These deletions, in part, could be attributed to the substantial reduction in the genome and gene sizes accompanied in the evolution of parasitism in apicomplexans (Jackson *et al.*, 2016; Vivares *et al.*, 2002; Wolf and Koonin, 2013). The reductions could be explained as a loss of functional redundancy with an increased functional complexity. As shown in Figure 3.1, the N-terminal sequence (the region predicted to be in the mitochondrial matrix) of the extant *Plasmodium* spp. genes lack amino acid conservation in relation to the characterised Cox11 orthologues in other organisms. Earlier, mutational analysis of the *S. cerevisiae* Cox11 demonstrated the lack of essential function of the N-terminal domain within the mitochondrial matrix (Banting and Glerum, 2006; Carr *et al.*, 2005). The importance of the transmembrane domain was however demonstrated in a study where the matrix and transmembrane domains of Cox11 were supplanted with those of Sco1, resulting in a respiratory deficiency in yeast (Khalimonchuk *et al.*, 2005). Three-conserved cysteines, a feature of Cox11 was observed with two cysteines in a conserved CFCF motif and the third a short distance from the motif. Yeast Cox11 has been shown to form a dimer that binds one mole equivalent of Cu(I) per monomer via three thiolate bonds (Carr *et*

al., 2002). The NMR-solved structure of *S. meliloti* Cox11 revealed Cu(I) coordination via two thiolate bonds by the two cysteines in the CFCF motif per monomer, while the third cysteine was proposed to be in a disulphide bond with a cysteine from another monomer forming a dimer (Banci *et al.*, 2004). Subsequent studies proposed the third cysteine to be involved in the transfer of Cu(I) from the Cu(I)-Cox11 cluster to the Cu_B centre, and not required for dimerisation (Thompson *et al.*, 2010). All three cysteines are conserved suggesting their importance.

3.3.2 Predicting the topology of *P. falciparum* Cox11

The outcome of the predicted topology (Figure 3.2) in all putative *Plasmodium* spp. Cox11 is in concordance with the knowledge of the presence of a membrane-spanning helix tethering the protein to the inner mitochondrial membrane (Banci *et al.*, 2004; Carr *et al.*, 2002; Hiser *et al.*, 2000; Tzagoloff *et al.*, 1990). As expected, *Plasmodium* spp. Cox11 orthologues do not have a signal peptide or a motif for targetting to the apicoplast. The homology model for *P. falciparum* Cox11, shows the protein adopting a similar conformational orientation to the corresponding *S. meliloti* Cox11 template (Figure 3.3B). This structural similarity suggests that *Plasmodium* Cox11 may employ a similar mode of operation, which is the transfer of copper to the Cu_B of the Cox1 subunit.

3.3.3 Predicting acetylation sites in the *P. falciparum* Cox11 sequence

Protein lysine acetylation is a reversible, highly regulated post-translational modification (PTM) crucial in regulating a wide range of cellular function in eukaryotes and some prokaryotes. Before the discovery of lysine acetylation in p53, a nonhistone protein, lysine acetylation was ascribed to histones (Gu and Roeder, 1997). Subsequently, over 2000 acetylated proteins involved in diverse cellular processes in mammalian and bacteria cells were identified from four independent studies (Choudhary *et al.*, 2009; Kim *et al.*, 2006; Wang *et al.*, 2010; Zhao *et al.*, 2010). Although some acetylated lysines were predicted in the *Plasmodium* spp. Cox11 sequence, none of these lysines is surrounded by any of the established predicted motif patterns known to be associated with acetylated lysines in mitochondrial proteins. (Choudhary *et al.*, 2009; Miao *et al.*, 2013).

3.3.4 Bioinformatic characterisation of the putative *P. falciparum* Cox19 protein

To study copper homeostasis in *Plasmodium*, the Cox19 orthologue was also analysed. Cox19 orthologues were present in the genome of all nine *Plasmodium* spp. In contrast to Cox11, the multiple sequence alignment of Cox19 amino acid sequences revealed C-terminus amino acid insertions in *Plasmodium* spp., about the same size as the extant Cox19 orthologues in the five other organisms (Figure 3.4). This implied the *Plasmodium* Cox19 sequences are twice as large as their orthologues in other organisms. This observed size variation, however, raises a question on the evolution of parasitism accompanied by loss of functional redundancy. Upon closer examination of all Cox19 genes, *Plasmodium* Cox19 amino acid sequences are the product of one exon from a mRNA transcript, while the characterised Cox19 sequences are formed by three to four exons contained on the mRNA transcript. Thus, implying that *Plasmodium* spp. have deleted the non-coding DNA within the Cox19 gene, leaving a small functional gene over the course of parasitism. Hence, the apparent C-terminal insertions in *Plasmodium* spp. are resultant of loss of functional redundancy with an increased functional complexity (Jackson *et al.*, 2016; Vivares *et al.*, 2002; Wolf and Koonin, 2013). The identification of the CHCH domain with all four conserved cysteines, a characteristic of Cox19 in the *Plasmodium* sequences imply the formation of two disulphides is probable within the protein structure (Bode *et al.*, 2015; Fischer *et al.*, 2013; Rigby *et al.*, 2007). Only the proximal disulphide (Cys24 – Cys55) is essential for an active Cox19, as double mutations of Cys34 and Cys45 in yeast had no significance to the functionality (*in vivo*) and copper binding (*in vitro*) of the protein (Rigby *et al.*, 2007). Two conserved Tyr-Leu dipeptides at positions seven and eight between the cysteine residues (twin Cx_6YLxC) (Bode *et al.*, 2015) and an adjacent Arg to the carboxy-proximal cysteine (Nobrega *et al.*, 2002) were shown to be essential to the functionality of Cox19 in yeast. One of the two essential Tyr-Leu dipeptides in yeast Cox19 has its Leu residue substituted with Phe in the *Plasmodium* Cox19 sequences (Figure 3.4). The mammalian and avian Cox19 sequences have only one Tyr-Leu dipeptide in the second Cx_9C motif.

The conformation of the putative *Pf*Cox19 model (Figure 3.5) is in concord with the proposed Cox19 structure, of having distal and proximal disulphide (Fischer *et al.*, 2013; Rigby *et al.*, 2007). An extended model would position the omitted Cys24 in place for a proximal disulphide with Cys55. This suggests that *Plasmodium* Cox19 is likely to bind copper.

3.3.5 Predicting acetylation sites in *P. falciparum* Cox19 sequence

Recent studies have implicated dysfunctional KATs and lysine deacetylases (KDACs) in diseases such as Asthma, diabetes, retroviral pathogenesis, neurodegenerative disorders among others (Drazic *et al.*, 2016; Kaypee *et al.*, 2016; Selvi and Kundu, 2009). Currently, KATs and KDACs inhibitors are being explored in the treatment of diseases like cancer (Gajer *et al.*, 2015; Shrimp *et al.*, 2017). Like the *P. falciparum* Cox11 sequence, none of the predicted acetylated lysines in the *Plasmodium* spp. Cox19 sequence is surrounded by any of the established predicted motif patterns around acetylated lysines in mitochondrial proteins or *Plasmodium* spp. (Choudhary *et al.*, 2009; Miao *et al.*, 2013).

3.3.6 Selecting a Cox11 peptide for antibody production

To assist with the characterisation of *Pf*Cox11, anti-peptide antibodies against the putative copper-binding domain were raised in chickens. A 19-amino acid peptide was selected, synthesised and conjugated to a rabbit albumin carrier protein for immunisation into chickens. The antibodies raised against the peptides were to be used for immunochemical studies and characterisation of *Pf*Cox11.

3.3.7 Conclusion

Both of the *P. falciparum* Cox11 and Cox19 sequences were found to contain features common to other characterised orthologues in yeast and other higher organisms. Therefore, to establish the putative functions of both malaria copper metallochaperones, the genes were recombinantly cloned, expressed and characterised.

Chapter 4

The *Plasmodium falciparum* putative Cox11 copper metallochaperone: Recombinant protein copper binding studies

4.1 Introduction

Copper, a transition metal, is an essential micronutrient required by living organisms. As a transition metal, copper ions exist between Cu(I) and Cu(II) redox states. The redox activity makes copper a suitable cofactor for enzymes in diverse biological processes like cellular respiration, iron mobilisation, antioxidant defence and immune responses (Nevitt *et al.*, 2012; Samanovic *et al.*, 2012). Unregulated copper activity generates reactive oxygen species (ROS) which can result in cellular oxidative damage. Organisms have evolved complex regulatory mechanisms to keep cellular copper concentrations in check (Nevitt *et al.*, 2012). The identification of copper-dependent protein orthologues in *Plasmodium* (Choveaux *et al.*, 2015; Gardner *et al.*, 2002; Rasoloson *et al.*, 2004), implies similar regulatory mechanisms may be in place in the parasite. The *P. falciparum* Cox11 gene was characterised *in silico.* Here the PCR-amplified gene was cloned, and the recombinant protein expressed and characterised.

4.1.1 Recombinant protein expression

The characterisation of a putative native protein from natural host cells is often a difficult task to undertake. This entails enrichment of the protein from a large pool of the natural host cells. Often, recombinant protein expression has been undertaken in a significant number of expression hosts. Of the numerous hosts, *Escherichia coli* is preferentially used owing to the well-studied genetics, rapid growth, ease of expression, cheap and rapid high-density cultivation (Singha *et al.*, 2017; Sørensen and Mortensen, 2005). Since the expression vector used in the entire study uses a “tac” promoter (section 2.5.7.2), the *E. coli* (BL21) host was used as the expression host. The BL21 host lacks the *ompT* and *lon* proteases that are capable of degrading the recombinantly expressed proteins (Overton, 2014; Sørensen and Mortensen, 2005). The bulk of the solved 3D-structure of proteins curated at the protein data bank (PDB) were recombinantly expressed in *E. coli* (Sørensen and Mortensen, 2005). Likewise, about 30% of the current biopharmaceuticals on the market are produced in bacterial hosts (Overton, 2014). Earlier, our laboratory successfully used the *E. coli* system to characterise two malaria copper metallochaperones (Choveaux *et al.*, 2012; 2015) and other constitutive malaria proteins (Krause and Goldring, 2018; Krause *et al.*, 2017).

4.1.2 Copper delivery to the plasmodial mitochondria

Copper from the external milieu destined for the mitochondria is ferried across the plasma membrane into the cytoplasm as Cu(I) via a copper transport protein (Ctr1) (Dancis *et al.*, 1994; Lee *et al.*, 2001; Zhou and Gitschier, 1997). Ctr1 is a high-affinity transporter that functions as a pore-forming homotrimer complex, facilitating translocation of Cu(I) across the plasma membrane (Aller and Unger, 2006; De Feo *et al.*, 2009). The exact mechanism by which Cu(I) gets to the mitochondria in *Plasmodium* is yet to be identified, perhaps Cox17 is involved (Choveaux *et al.*, 2015). In mammalian and yeast cells, copper in the mitochondria could either be delivered to Cu/Zn superoxide dismutase (SOD) or used in the assembly of the cytochrome *c* oxidase (CcO) complex at the Cu_A and Cu_B centres respectively. *Plasmodium* spp. lack the SOD and the copper chaperone for SOD (CCS) orthologues (Choveaux *et al.*, 2015; Gardner *et al.*, 2002). Eukaryotic CCS is a trimeric protein required for the delivery and insertion copper into SOD (Nevitt *et al.*, 2012). The lack of plasmodial SOD and CCS could imply the parasite does not utilise these proteins, or their roles have been supplanted by other proteins. Therefore, copper within the plasmodial mitochondria would likely be utilised for the formation of the CcO complex. Copper from the cytoplasm is attached to Cox17, which then delivers copper to the two inner mitochondria membrane-associated proteins (Maxfield *et al.*, 2004), Sco1 and Cox11, implicated in the metallation of the Cu_A and Cu_B centres of the Cox2 and Cox1 subunits of the CcO complex respectively (Hiser *et al.*, 2000; Horng *et al.*, 2004; Lode *et al.*, 2000; Timón-Gómez *et al.*, 2018).

4.2 Results

4.2.1 Identification of the presence of a Cox11 copper metallochaperone sequence in the *Plasmodium falciparum* genome

The PF3D7_1475300 gene encoding the putative Cox11 in *P. falciparum* from a monocistronic mRNA is predicted to be localised between bases 3 085 496 to 3 086 182 of chromosome 14 (Figure 4.1A). A 486 bp sequence encoding the C-terminal domain of the putative *P. falciparum* Cox11 of the 687 bp coding domain (Figure 4.1C), was cloned and recombinantly expressed (Figure 4.1D). Two restriction sites, a stop codon and two adapter gene nucleotides at the 5' end of the restriction enzyme to enhance the specificity of the primers to the DNA template were added to the primer design. A 505 bp PCR-amplicon was expected.

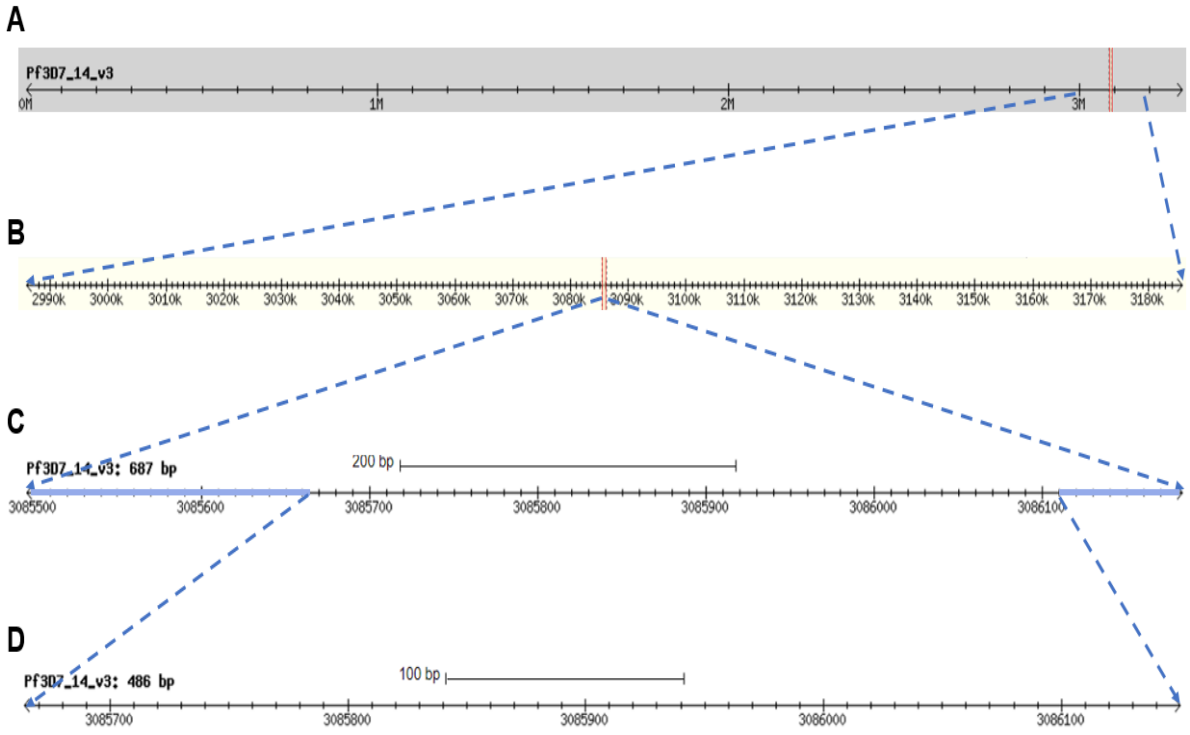

Figure 4.1. Localisation of the Cox11 coding domain in *P. falciparum* chromosome 14
PF3D7_1475300 coding domain localisation on *P. falciparum* chromosome 14 (A). An expanded view of the chromosome 14 gene organization relative to PF3D7_1475300 (B). An exploded PF3D7_1475300 gene, 687 bp, encoding the complete protein (C). The recombinantly cloned putative C-terminal domain, 486 bp (D). ▬ denotes the excluded gene segments at both N- and C-termini.

The C-terminal domain of *P. falciparum* Cox11 was PCR-amplified and cloned into a pMal-c2x expression vector for characterisation. Figure 4.2 illustrates the steps taken in the PCR-amplification, cloning and subcloning of the *Pf*Cox11 C-terminal domain (r*Pf*Cox11Ct). Agarose gel analysis of the PCR-amplicons revealed a product of about 506 bp (Figure 4.2A), corresponding to the size predicted from the gene sequence. The amplicon was cloned into a

pGEM®-T Easy cloning vector, and colonies harbouring the recombinant plasmid (pGEM®-T Easy-r*Pf*Cox11Ct) selected. Colony-PCR of each colony produced amplicons of about the same size as the gene insert from all three colonies (Figure 4.2B). The pGEM®-T Easy-r*Pf*Cox11Ct and pMal-c2x expression plasmid were digested with *Sal*I and *Pst*I. The agarose gel (Figure 4.2C) showed the pGEM®-T Easy-r*Pf*Cox11Ct plasmid at ~2000 bp. The product of enzyme digestion was two DNA fragments at ~3000 bp and ~500 bp corresponding to the predicted sizes for pGEM®-T Easy plasmid (3015 bp) and r*Pf*Cox11Ct respectively.

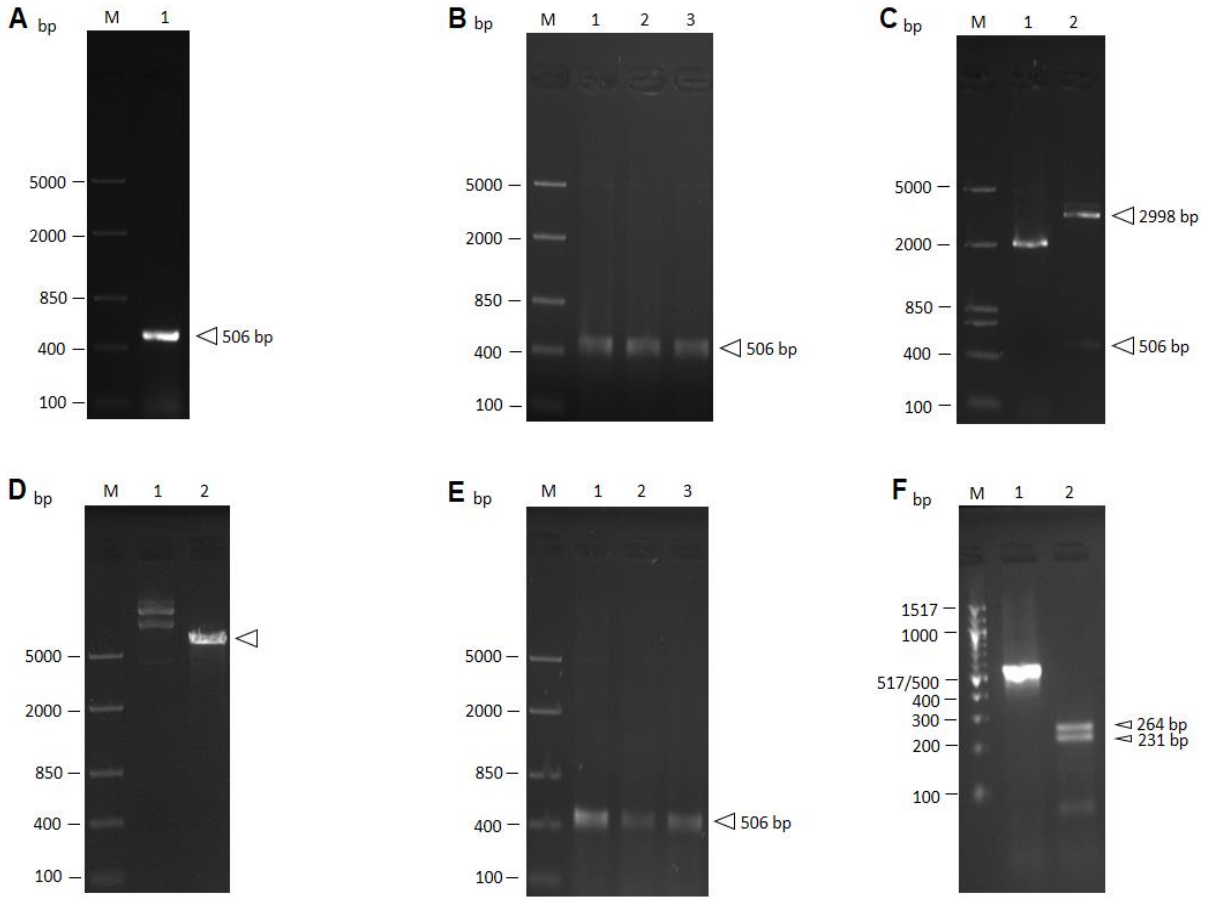

Figure 4.2. PCR-amplification, cloning and restriction enzyme digestion of r*Pf*Cox11Ct
(A) r*Pf*Cox11Ct amplification product from the *P. falciparum* gDNA (lane 1). (B) r*Pf*Cox11Ct amplified from three pGEM®-T Easy-r*Pf*Cox11Ct plasmid-containing bacterial colonies (lanes 1-3). (C) pGEM®-T Easy-r*Pf*Cox11Ct plasmid alone (lane 1) and digested with *Sal*I and *Pst*I (lane 2). (D) pMal-c2x plasmid alone (lane 1) and digested with *Sal*I and *Pst*I (lane 2). (E) r*Pf*Cox11Ct amplified from three pMal-c2x-r*Pf*Cox11Ct plasmid-containing bacterial colonies (lanes 1-3). (F) r*Pf*Cox11Ct alone (lane 1) and digested with *Alu*I. Samples in A-E were analysed on a 1%, and F on a 3% (w/v) agarose gel. M in all images refers to the DNA ladder. The arrows refer to the key molecular weight band in each stance.

In a similar experiment (Figure 4.2D), the digested pMal-c2x plasmid resolved as a ~6550 bp molecule, similar to the predicted size. The r*Pf*Cox11Ct was cloned into the pMal-c2x expression vector at the *Sal*I and *Pst*I sites, transformed, and colonies harbouring the recombinant plasmid (pMal-c2x-r*Pf*Cox11Ct) selected. Colony-PCR analysis for three

colonies resulted in three ~500 bp amplicons (Figure 4.2E). A unique *Alu*I site, AGCT occurred once in the r*Pf*Cox11Ct sequence enabling the *Alu*I product of ~280 bp and ~230 bp to be produced (Figure 4.2F).

```
PfCox11Ct_vect      CCGTCGACCAATTATTTTGTCAATCCACAGGTTATGGTGGTACAATACAAAAGCGATTGG      60
PfCox11Ct_pldb      --------CAATTATTTTGTCAATCCACAGGTTATGGTGGTACAATACAAAAGCGATTGG      52
                            **************************************************

PfCox11Ct_vect      ATATAGGTAAAATATTTAATAGGAAAAAGGATGAAAAGAATAGATTAATTGAAATAAATT      120
PfCox11Ct_pldb      ATATAGGTAAAATATTTAATAGGAAAAAGGATGAAAAGAATAGATTAATTGAAATAAATT      112
                    ************************************************************

PfCox11Ct_vect      TTACTAGTCAATCTAATATGCCATGGGTATTTGAACCTGAACAAAAATATATTATAGTAA      180
PfCox11Ct_pldb      TTACTAGTCAATCTAATATGCCATGGGTATTTGAACCTGAACAAAAATATATTATAGTAA      172
                    ************************************************************

PfCox11Ct_vect      AGCCAGGAGAAACAGTATTAGCTTTTTATAAGGCAAAAAATTTAATGGATAAGCCTATTA      240
PfCox11Ct_pldb      AGCCAGGAGAAACAGTATTAGCTTTTTATAAGGCAAAAAATTTAATGGATAAGCCTATTA      232
                    ************************************************************

PfCox11Ct_vect      TTGGAATTGCTTTATATCATGTATTACCAGAAGAAGCTGGACTATATTTTAATAAAATTC      300
PfCox11Ct_pldb      TTGGAATTGCTTTATATCATGTATTACCAGAAGAAGCTGGACTATATTTTAATAAAATTC      292
                    ************************************************************

PfCox11Ct_vect      AATGTTTTTGTTTTGAAGAACAAATGTTAAATGCTAAAGAAGAAATGGATTTACCTATAC      360
PfCox11Ct_pldb      AATGTTTTTGTTTTGAAGAACAAATGTTAAATGCTAAAGAAGAAATGGATTTACCTATAC      352
                    ************************************************************

PfCox11Ct_vect      TCTTTTTTATCGATCCAGAAATATTAAATGATTCAAGATTAAAAAATTTAGAAAAAATTA      420
PfCox11Ct_pldb      TCTTTTTTATCGATCCAGAAATATTAAATGATTCAAGATTAAAAAATTTAGAAAAAATTA      412
                    ************************************************************

PfCox11Ct_vect      CACTATCATATATTTTTTTTGAATCCGATTCAGAAATACCTGAAGAATACCAAAACCTCT      480
PfCox11Ct_pldb      CACTATCATATATTTTTTTTGAATCCGATTCAGAAATACCTGAAGAATACCAAAACCTCT      472
                    ************************************************************

PfCox11Ct_vect      CAAGGGCTATTTCCTGACTGCAGAA   505
PfCox11Ct_pldb      CAAGGGCTATTTCC-----------   486
                    **************
```

Figure 4.3. Alignment of *P. falciparum* Cox11Ct cloned sequence with the PlasmoDB gene sequence
The *P. falciparum* Cox11Ct cloned sequence in pMal-c2x-r*Pf*Cox11Ct plasmid (*Pf*Cox11Ct_vect) and the PlasmoDB sequence (*Pf*Cox11Ct_pldb) (PF3D7_1475300) were aligned using Clustal Omega. The underlined nucleotide bases at the 5' and 3' ends indicate the primer sequences used to amplify *Pf*Cox11Ct from the *P. falciparum* gDNA. The reverse complement of the underlined sequence at the 3' end was used as the reverse primer.

The r*Pf*Cox11Ct coding region cloned into a pMal-c2x-r*Pf*Cox11Ct plasmid was sequenced and found to be identical to the PlasmoDB sequence, except for the additional stop codon at the 3' end (Figure 4.3).

4.2.2 Site-directed mutagenesis to replace Cys60 and Cys157 with Ala in the *P. falciparum* Cox11 sequence

Two of the three conserved cysteine residues in Cox11 corresponding to Cys60 and Cys157 in the *P. falciparum* sequence were investigated for their roles in copper binding in *Pf*Cox11. Overlap extension PCR was employed to mutate either Cys60 and Cys157 or both

cysteines to alanine (Figure 4.4). Substituting a cysteine with an alanine at position 155 – the third conserved cysteine, was not possible owing to constraints in the design of the two internal primers for the mutant codon.

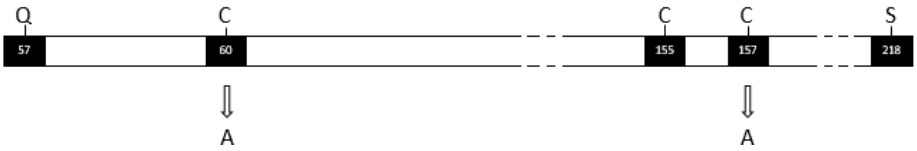

Figure 4.4. Sites on the gene for site-directed mutagenesis
Residues Cys60 and Cys157 were mutated to Ala on the *P. falciparum* Cox11Ct.

Figure 4.5 summarises the steps taken to substitute a cysteine with an alanine at position 60. The process involved a two-step PCR reaction (Figure 4.5A). Agarose gel analysis of the first PCR amplicons (Figure 4.5B) showed lagging and leading fragments with estimated sizes of ~130 bp and ~500 bp, which correspond to their predicted sizes of 131 bp and 519 bp respectively. The second PCR amplicon (Figure 4.5C) ran as ~620 bp, similar to the predicted size of 648 bp. This amplicon was digested with *Sal*I and *Pst*I restriction endonucleases and cloned into the pMal-c2x expression vector at the corresponding restriction sites. The recombinant plasmid harbouring the desired mutant codon "GCG" corresponding to Ala60 (C60A) was sequenced and was identical to the curated PlasmoDB sequence, barring the mutation and the stop codon as expected (Figure 4.5D).

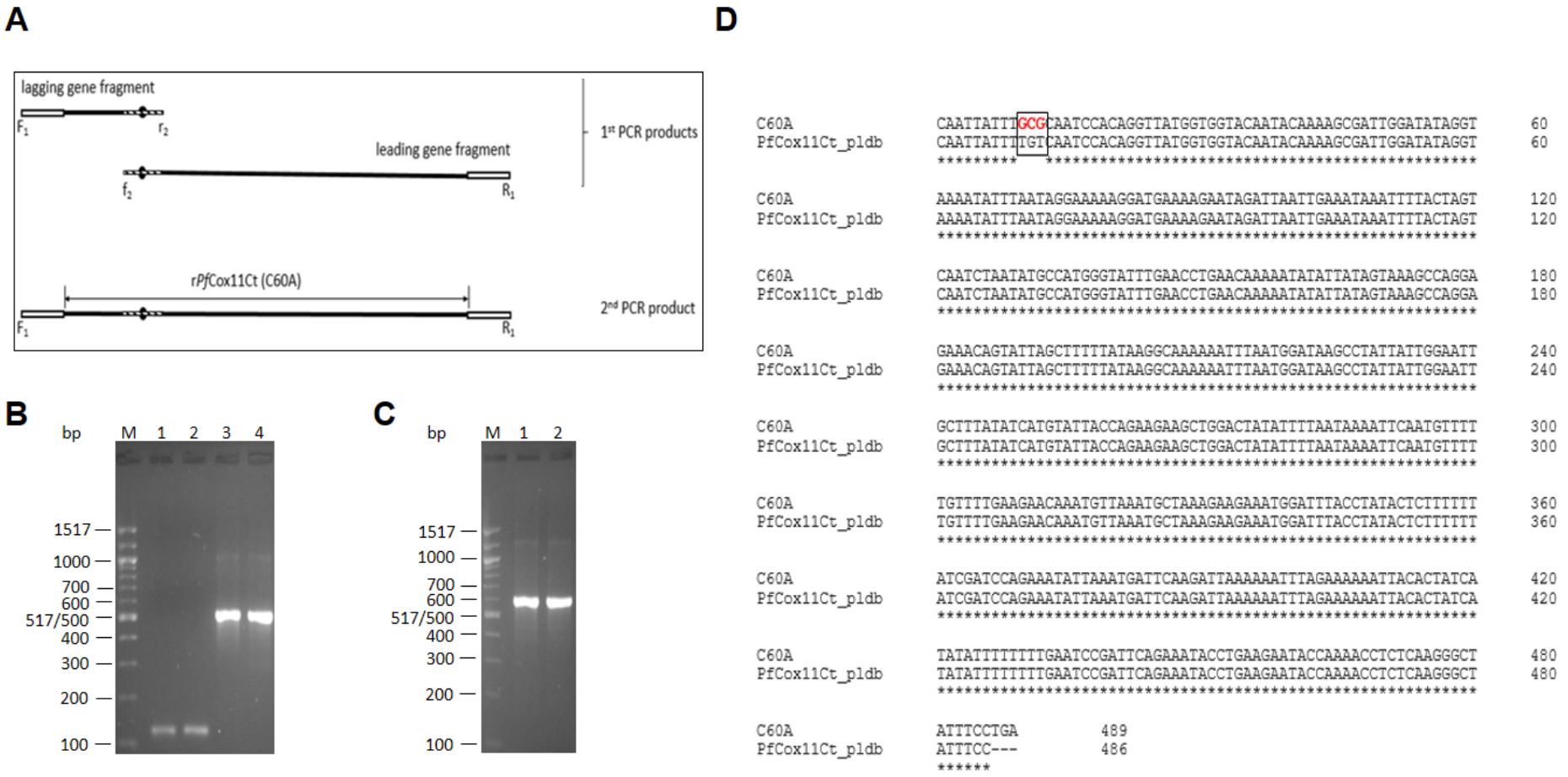

Figure 4.5. Site-directed mutagenesis using overlap extension PCR amplification to substitute Cys60 with Ala

The overlap extension PCR was conducted in a two-step PCR reaction substituting Cys60 with Ala using the pMal-c2x-r*Pf*Cox11Ct plasmid as the template DNA. (A) A diagram of the two PCR products in overlap extension PCR. Open bars, pMal-c2x nucleotide sequence; solid bar, *Pf*Cox11Ct; hatched bar, contiguous overlap; black circle, point mutation; F_1 and r_2, lagging gene fragment primers; f_2 and R_1, leading gene fragment primers. (B) First PCR products were; a lagging gene fragment (lanes 1, 2), and a leading gene fragment (lanes 3, 4). (C) The full-length mutated gene including pMal-c2x fragment was amplified in the second PCR from the two fragments. Lanes 1 and 2, full-length mutated gene including pMal-c2x fragment. PCR products were analysed on a 3% (w/v) agarose gel. DNA ladders are designated M. (D) Sequence alignment of the C60A mutant with PlasmoDB sequence (*Pf*Cox11Ct_pldb) (PF3D7_1475300) using Clustal Omega. The box indicates the site of mutagenesis with the mutant codon in red.

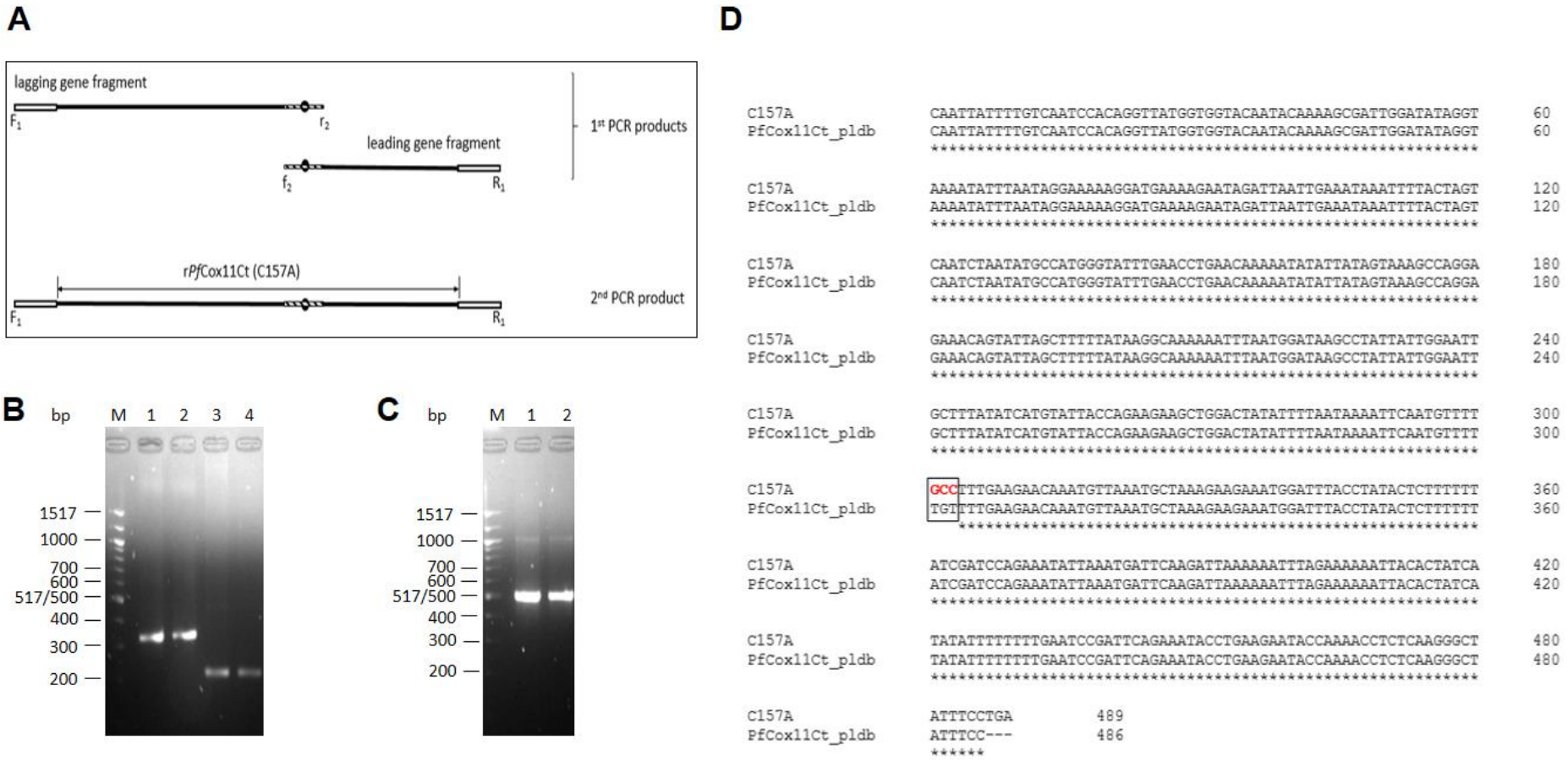

Figure 4.6. Site-directed mutagenesis using overlap extension PCR amplification to substitute Cys157 with Ala

The overlap extension PCR was conducted in a two-step PCR reaction substituting Cys157 with Ala using the pMal-c2x-r*Pf*Cox11Ct plasmid as the template DNA. (A) A diagram of the two PCR products in overlap extension PCR. Open bars, pMal-c2x nucleotide sequence; solid bar, *Pf*Cox11Ct; hatched bar, contiguous overlap; black circle, point mutation; F_1 and r_2, lagging gene fragment primers; f_2 and R_1, leading gene fragment primers. (B) First PCR products were; a lagging gene fragment (lanes 1, 2), and a leading gene fragment (lanes 3, 4). (C) The full-length mutated gene including pMal-c2x fragment was amplified in the second PCR from the two fragments. Lanes 1 and 2, full-length mutated gene including pMal-c2x fragment. PCR products were analysed on a 3% (w/v) agarose gel. DNA ladders are designated M. (D) Sequence alignment of the C157A mutant with PlasmoDB sequence (*Pf*Cox11Ct_pldb) (PF3D7_1475300) using Clustal Omega. The box indicates the site of mutagenesis with the mutant codon in red.

A similar experiment substituting alanine for cysteine at position 157 from overlap extension PCR was conducted (Figure 4.6). Agarose gel analysis of the first PCR amplicons (Figure 4.6B) revealed lagging, and leading fragments sizes estimated as ~330 bp and ~210 bp which are in agreement with the predicted 337 bp and 210 bp sizes respectively. The full-length mutant gene including the pMal-c2x fragment was analysed on an agarose gel and ran as ~530 bp, which is similar to the predicted size of 547 bp (Figure 4.6C). The mutated gene sequence was cloned into pMal-c2x at the *Sal*I and *Pst*I sites. The recombinant plasmid with the desired mutant codon "GCC" corresponding to Ala157 (C157A) was sequenced and was shown to be identical to the curated PlasmoDB sequence, barring the mutation and the stop codon (Figure 4.6D).

Like C60A and C157A, the double mutant plasmid (C60A-C157A) was engineered from the overlap extension PCR (Figure 4.7A). Agarose gel analysis of the first PCR amplicons (Figure 4.7B) revealed an estimated size of about 340 bp and 220 bp for the lagging and leading fragments corresponding to the predicted sizes of 337 bp and 210 bp respectively. The full-length mutant gene including the pMal-c2x fragment was analysed on agarose gel and ran as ~550 bp corresponding to predicted size, 547 bp (Figure 4.7C). The sequenced plasmid contains the desired "GCG" and "GCC" Ala codons corresponding to position 60 and 157 in the amino acid sequence, and again the sequences were identical to the curated PlasmoDB sequence, apart from the stated mutations and the stop codon (Figure 4.7D).

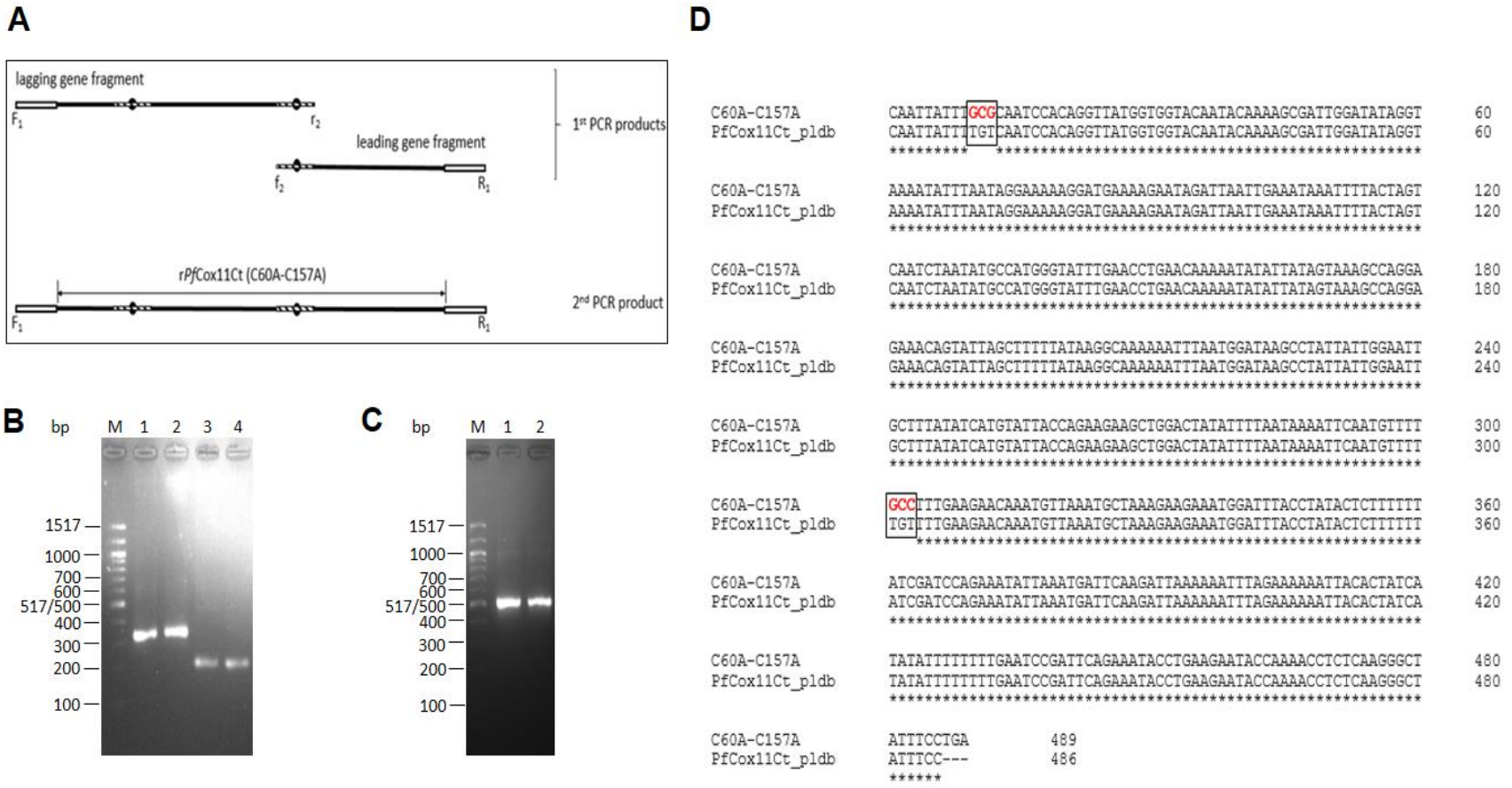

Figure 4.7. Site-directed mutagenesis using overlap extension PCR amplification to substitute Cys60 and Cys157 with Ala

The overlap extension PCR was conducted in a two-step PCR reaction substituting Cys60 and C157 with Ala using the pMal-c2x-r*Pf*Cox11Ct plasmid as the template DNA. (A) A diagram of the two PCR products in overlap extension PCR. Open bars, pMal-c2x nucleotide sequence; solid bar, *Pf*Cox11Ct; hatched bar, contiguous overlap; black circle, point mutation; F_1 and r_2, lagging gene fragment primers; f_2 and R_1, leading gene fragment primers. (B) First PCR products were; a lagging gene fragment (lanes 1, 2), and a leading gene fragment (lanes 3, 4). (C) The full-length mutated gene including pMal-c2x fragment was amplified in the second PCR from the two fragments. Lanes 1 and 2, full-length mutated gene including pMal-c2x fragment. PCR products were analysed on a 3% (w/v) agarose gel. DNA ladders are designated M. (D) Sequence alignment of the C60A-C157A double mutant with PlasmoDB sequence (*Pf*Cox11Ct_pldb) (PF3D7_1475300) using Clustal Omega. The box indicates the site of mutagenesis with the mutant codon in red.

The cloned 486 bp encodes 162 amino acids within the putative C-terminal domain of the *P. falciparum* Cox11 amino acid sequence, excluding the first 56 and last ten amino acid (Figure 4.8).

A

>*Pf*Cox11
MKILKTFFKRLHLRNKKNVISPYRILERKEKLDIPYACLSLSAIMFGLSFAFVPLY**QLFC**
QSTGYGGTIQKRLDIGKIFNRKKDEKNRLIEINFTSQSNMPWVFEPEQKYIIVKPGETVL
AFYKAKNLMDKPIIGIALYHVLPEEAGLYFNKIQCFCFEEQMLNAKEEMDLPILFFIDPE
ILNDSRLKNLEKITLSYIFFESDSEIPEEYQNLSRAISPYKKTEIQVI

B

>rMBP-*Pf*Cox11Ct
MKIEEGKLVIWINGDKGYNGLAEVGKKFEKDTGIKVTVEHPDKLEEKFPQVAATGDGPDI
IFWAHDRFGGYAQSGLLAEITPDKAFQDKLYPFTWDAVRYNGKLIAYPIAVEALSLIYNK
DLLPNPPKTWEEIPALDKELKAKGKSALMFNLQEPYFTWPLIAADGGYAFKYENGKYDIK
DVGVDNAGAKAGLTFLVDLIKNKHMNADTDYSIAEAAFNKGETAMTINGPWAWSNIDTSK
VNYGVTVLPTFKGQPSKPFVGVLSAGINAASPNKELAKEFLENYLLTDEGLEAVNKDKPL
GAVALKSYEEELAKDPRIAATMENAQKGEIMPNIPQMSAFWYAVRTAVINAASGRQTVDE
ALKDAQTNSSSNNNNNNNNNLGIEGRISEFGSSRVD**QLFCQSTGYGGTIQKRLDIGKIF**
NRKKDEKNRLIEINFTSQSNMPWVFEPEQKYIIVKPGETVLAFYKAKNLMDKPIIGIALY
HVLPEEAGLYFNKIQCFCFEEQMLNAKEEMDLPILFFIDPEILNDSRLKNLEKITLSYIF
FESDSEIPEEYQNLSRAISLQ

Figure 4.8. *P. falciparum* Cox11 amino acid sequence
(A) The cloned *Pf*Cox11 soluble C-terminal amino acid sequence derived from the *P. falciparum* gDNA is shown in bold print. (B) The recombinant MBP-*Pf*Cox11Ct protein amino acid sequence derived from the pMal-c2x-r*Pf*Cox11Ct plasmid. The three conserved Cys are in blue. The selected peptide sequence for antibody production is underlined.

4.2.3 Optimising conditions for the recombinant expression of MBP-*Pf*Cox11Ct

To establish the optimum conditions for recombinant MBP-*Pf*Cox11Ct expression, firstly, different growth medium were tested (Figure 4.9). The rMBP-*Pf*Cox11Ct cell lysate grown in Luria-Bertani (LB) (Figure 4.9A), and 2xYT (Figure 4.9B) media after a 6 h induction period was analysed on an SDS-PAGE gel. A similar protein profile of increasing concentration of all proteins of different sizes with time was observed on both gels. A 60 kDa band of low intensity in the uninduced sample had increased in intensity over time upon induction on both gels. This band corresponds to the predicted size for rMBP-*Pf*Cox11Ct of

62.7 kDa. The expressed band intensity was more in 2xYT than that in LB medium. 2xYT medium and a time of 4 h induction time were chosen for subsequent expression.

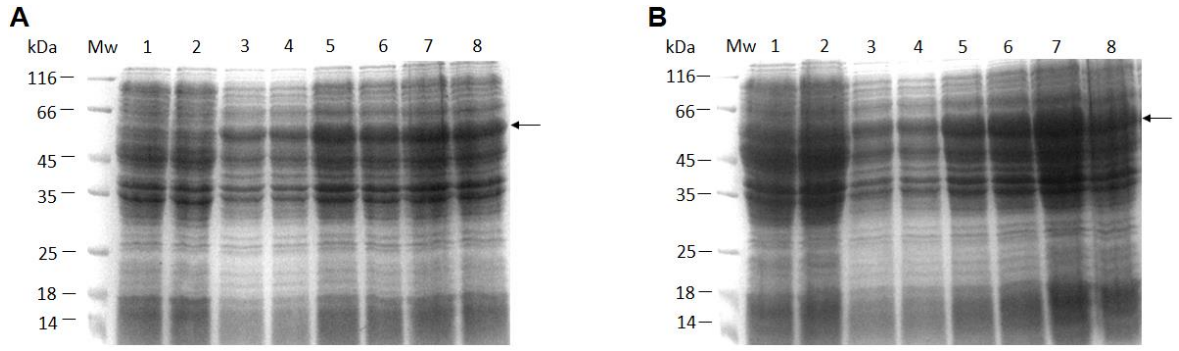

Figure 4.9. Effect of 2xYT and LB media on the recombinant expression of MBP-*Pf*Cox11Ct
E. coli cells harbouring the pMal-c2x-r*Pf*Cox11Ct plasmid were grown in (A) LB and (B) 2xYT media at 30ºC and analysed on a 12.5% reducing SDS-PAGE gel. Recombinant protein expression was induced with 0.5 mM IPTG. Uninduced lysate after 6 h (lanes 1 and 2), expression was monitored at 2 h (lanes 3 and 4), 4 h (lanes 5 and 6) and 6 h (lanes 7 and 8) post-induction. Molecular weight marker, M; arrow indicates rMBP-*Pf*Cox11Ct.

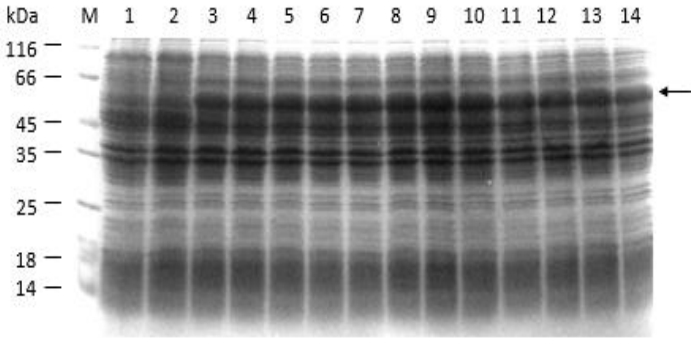

Figure 4.10. Recombinant expression of MBP-*Pf*Cox11Ct with varying IPTG concentration
E. coli cells harbouring the pMal-c2x-r*Pf*Cox11Ct plasmid grown in 2xYT media at 30ºC and induced for 4 h with 0 to 1 mM IPTG were analysed on a 12.5% SDS-PAGE. Molecular weight marker, M; Lanes 1 and 2, no IPTG added; lanes 3 and 4, 0.1 mM IPTG; lanes 5 and 6, 0.2 mM IPTG; lanes 7 and 8, 0.3 mM IPTG; lanes 9 and 10, 0.4 mM IPTG; lanes 11 and 12, 0.5 mM IPTG; lanes 13 and 14, 1 mM IPTG; arrow indicates rMBP-*Pf*Cox11Ct.

As was shown in Figure 4.10, a 60 kDa protein appeared after induction with IPTG. The intensity of the expressed band increased with the IPTG concentration up to 0.4 mM. There was no apparent increase in the concentration of the protein above 0.4 mM IPTG.

4.2.4 Isolation of the recombinant MBP-*Pf*Cox11Ct protein

After expressing rMBP-*Pf*Cox11Ct (see section 2.6.2), the protein was isolated using an amylose affinity resin. A maltose gradient was used to elute the protein, 0.3 mM was chosen for subsequent purifications. A ~62 kDa protein and a 45 kDa protein corresponding to the size

of the MBP forming portion were observed (Figure 4.11B). A form of the cleaved MBP fusion does often occur (pMAL™ Protein Fusion and Purification System, Instruction manual), and the addition of glucose to the bacterial growth medium did not change the expression the MBP protein.

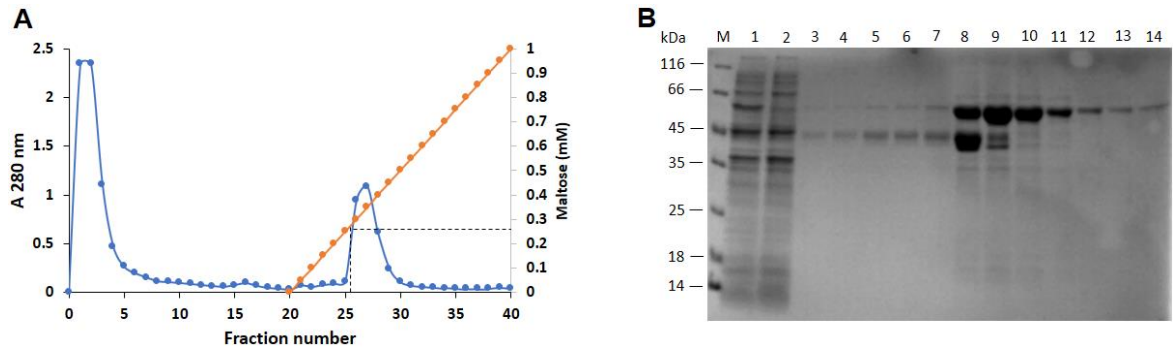

Figure 4.11. Recombinant expression and affinity purification of the MBP-*Pf*Cox11Ct
The rMBP-*Pf*Cox11Ct was purified with an amylose affinity column. (A) Elution profile from the amylose affinity matrix showing the maltose gradient. (B) Samples from the purification steps were analysed on a 12.5% reducing SDS-PAGE. Molecular weight marker (M); soluble cell lysate (lane 1); unbound fraction from the amylose affinity matrix (2); final wash (lane 3); eluents from the amylose affinity matrix (lanes 4 to 14).

Table 4.1 is a protein purification table showing protein yield from the purification steps of the rMBP-*Pf*Cox11Ct protein from duplicate 400 ml cultures. About 122 mg protein was obtained in the soluble lysate from the lysis of ~2.91 g bacterial pellet, corresponding to a yield of ~42 mg/g bacterial pellet. About 0.49 mg/g bacterial pellet of rMBP-*Pf*Cox11Ct was obtained.

Table 4.1. Purification table for the affinity purified rMBP-*Pf*Cox11Ct

	Total vol. (ml)	**Total protein* (mg)**	**Yield (%)**	**Yield (mg/g bacterial pellet)**
Soluble cell lysate	30.15 ± 1.91	122.41 ± 2.20	100	42.07 ± 0.76
Unbound fraction	27.46 ± 2.06	103.33 ± 0.70	84.41 ± 2.09	35.51 ± 0.24
Washes	58.50 ± 7.78	11.08 ± 1.10	9.04 ± 0.74	3.81 ± 0.38
Affinity purified rMBP-*Pf*Cox11Ct	23.59 ± 1.47	1.43 ± 0.19	1.17 ± 0.18	0.49 ± 0.06

Data presented are Mean ± SD values from duplicate purifications.
Bacterial pellet = 2.91 ± 0.22 g
* Determined with Bradford assay

The identity of the purified rMBP-*Pf*Cox11Ct protein was confirmed on a western blot probed with a mouse monoclonal anti-MBP antibody (Figure 4.12). Both a ~62 kDa protein rMBP-*Pf*Cox11Ct and a 45 kDa MBP protein with some minor proteins were detected by the anti-MBP antibody (Figure 4.12B).

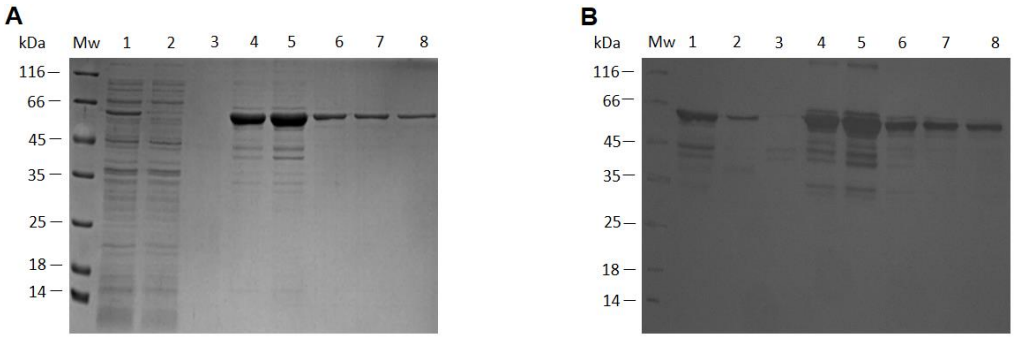

Figure 4.12. Detection of rMBP-*Pf*Cox11Ct by anti-MBP antibodies in a western blot
The rMBP-*Pf*Cox11Ct was identified on a western blot. (A) Coomassie-stained 12.5% reducing SDS-PAGE reference gel. (B) Western blot probed with mouse monoclonal anti-MBP IgG. Molecular weight marker (M); lane 1, soluble cell lysate; lane 2, unbound fraction from the amylose affinity matrix; lane 3, final wash; lanes 4 to 8, eluents from the amylose affinity matrix. Antibodies were; mouse monoclonal anti-MBP IgG (1:12000) and goat anti-mouse IgG-HRPO (1:12000).

4.2.5 IgY antibodies were raised in chickens against rMBP-*Pf*Cox11Ct

Two chickens were immunised four times with purified rMBP-*Pf*Cox11Ct and IgY was isolated from the eggs of the chickens. Antibody titres in eggs were monitored by ELISA over a 16-week period (Figure 4.13A). Antibody responses increased from week two and remained high from week three to week 16. IgY was isolated from eggs and affinity purified with a rMBP-*Pf*Cox11Ct AminoLink™ affinity matrix (Figure 4.13B). About 21 mg of affinity purified anti-rMBP-*Pf*Cox11Ct IgY was obtained from a chicken. The chicken affinity-purified antibodies detected rMBP-*Pf*Cox11Ct and lower proteins but did not detect any protein in the uninfected red blood cell lysate or *E. coli* host cell (Figure 4.13C).

The purified recombinant MBP from the pMal-c2x plasmid was expressed with the β-galactosidase α fragment as a ~50 kDa protein.

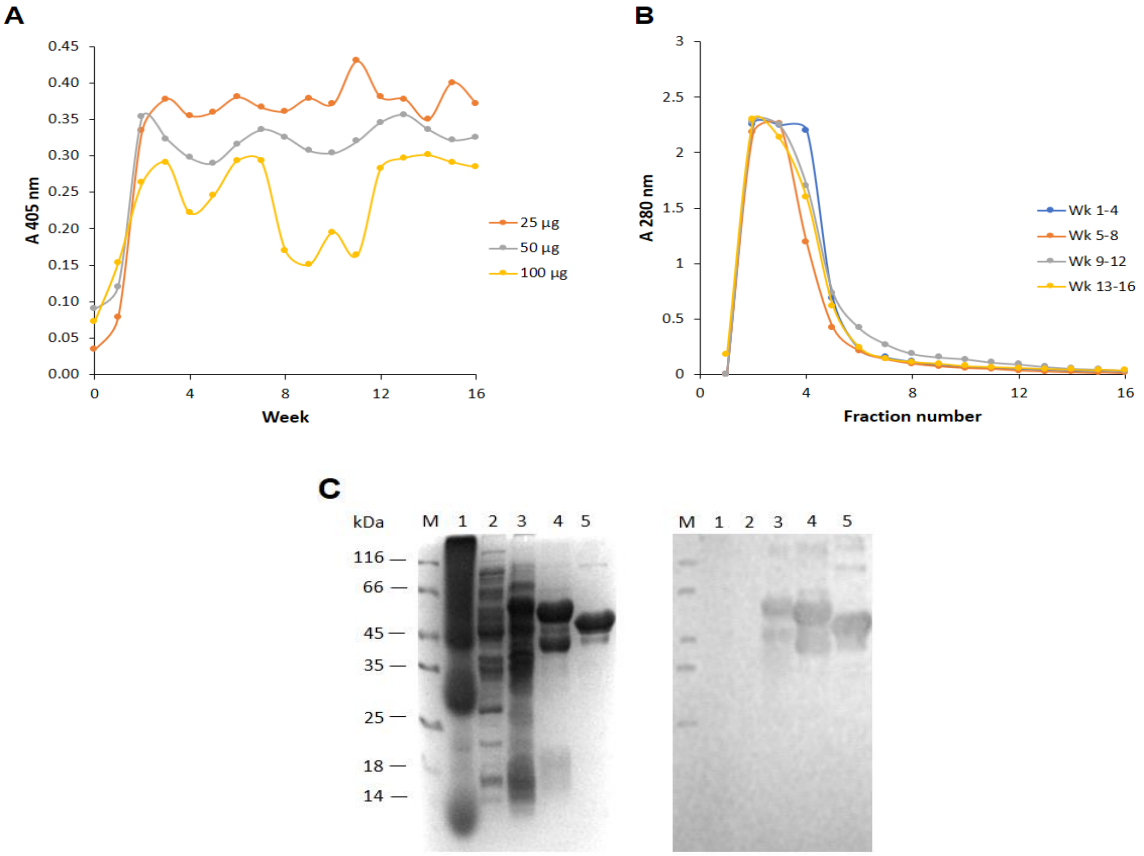

Figure 4.13. Affinity purified antibodies detected rMBP-*Pf*Cox11Ct
Antibodies against rMBP-*Pf*Cox11Ct were monitored in chicken eggs by ELISA over 16 weeks. (A) Plates were coated with 150 ng/well rMBP-*Pf*Cox11Ct. IgY (25, 50 and 100 µg/ml) primary antibody and rabbit anti-chicken IgG-HRPO (1:15 000), and plates read at OD_{405}. (B) Pools of isolated IgY from eggs were affinity purified with a rMBP-*Pf*Cox11Ct AminoLink™ column. (C) A 12.5% reducing SDS-PAGE Coomassie-stained reference gel (left panel). Affinity-purified IgY detected rMBP-*Pf*Cox11Ct on a western blot (right panel). Molecular weight marker (M); lane 1, uninfected human red blood cell lysate; lane 2, untransformed *E. coli* (BL21) lysate; lane 3, soluble rMBP-*Pf*Cox11Ct lysate; lane 4, affinity purified MBP-*Pf*Cox11Ct; lane 5, recombinant MBP.

4.2.6 IgY antibodies was raised in chickens against a *Pf*Cox11 peptide

An antibody against *Pf*Cox11 targetting a selected peptide sequence (KIQXFXFEEQMLNAKEEM) within the putative copper binding site (see section 2.3.3) was also raised in two chickens and the IgY isolated from the eggs of the chickens. The antibody titres in chickens over a 16-week period was monitored by ELISA (Figure 4.14A). Antibodies against the KIQXFXFEEQMLNAKEEM peptide were generated from week three to four in both chickens, remained high for six weeks and then slowly decreased. The pool of IgY was affinity purified with a KIQXFXFEEQMLNAKEEM SulfoLink™ affinity matrix (Figure 4.14B). About 21 mg of affinity purified anti-KIQXFXFEEQMLNAKEEM peptide IgY was obtained from each chicken. The chicken affinity-purified antibodies detected rMBP-*Pf*Cox11Ct and did not detect any protein in the uninfected red blood cell lysate, *E. coli* host lysate or recombinant MBP (Figure 4.14C).

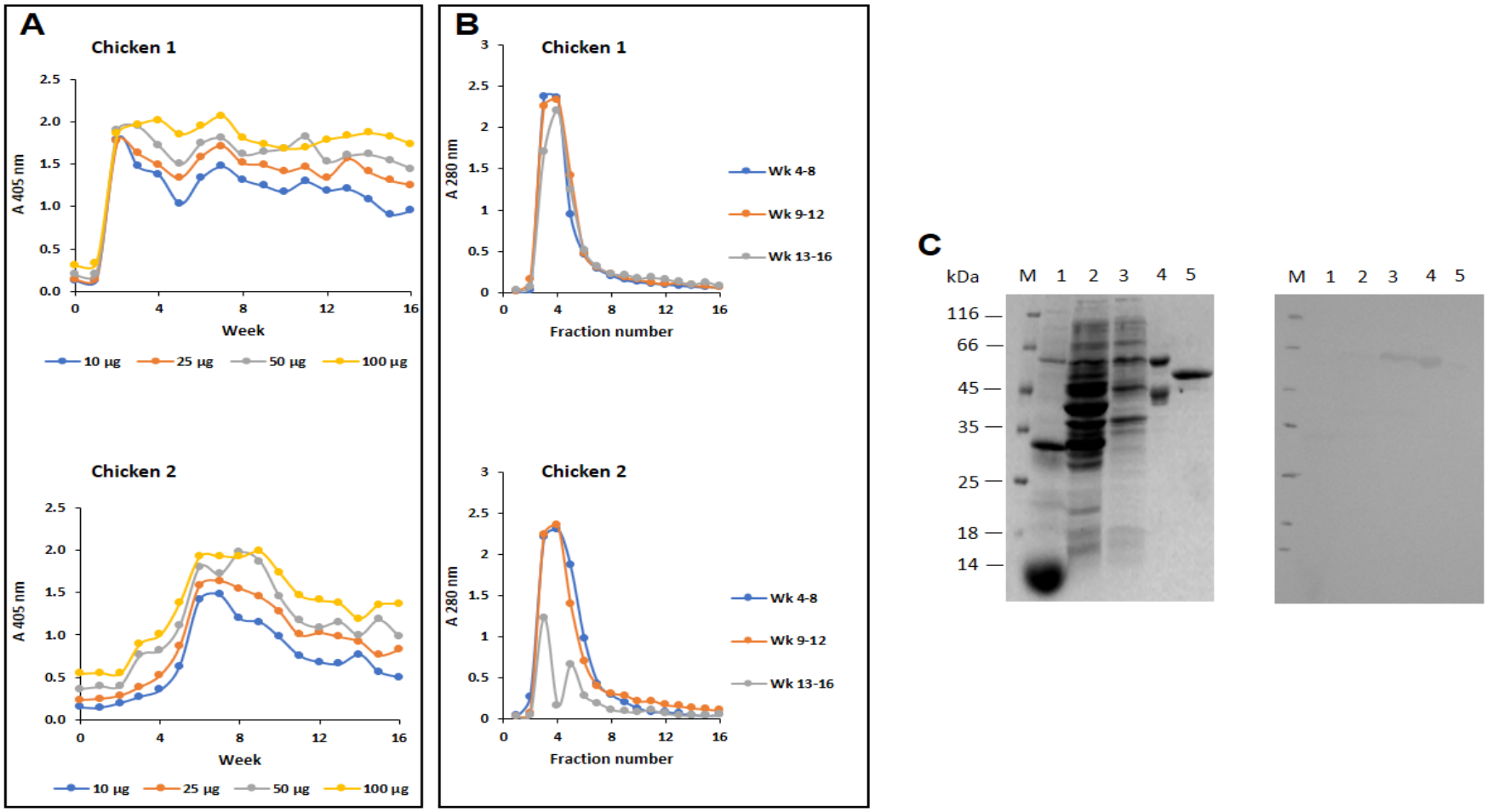

Figure 4.14. Affinity purified anti-peptide (KIQXFXFEEQMLNAKEEM) antibodies detected rMBP-*Pf*Cox11Ct

Antibodies against the peptide, KIQXFXFEEQMLNAKEEM, were monitored in chicken eggs by ELISA over 16 weeks. (A) Plates were coated with 150 ng/well rMBP-*Pf*Cox11Ct. IgY (10, 25, 50 and 100 µg/ml) primary antibody and rabbit anti-chicken IgG-HRPO (1:15 000), and plates read at OD_{405}. (B) Pools of isolated IgY from eggs were affinity purified with a KIQXFXFEEQMLNAKEEM SulfoLink™ column. "X", α-aminobutyric acid. (C) A 12.5% reducing SDS-PAGE Coomassie-stained reference gel (left panel). Affinity-purified IgY detected rMBP-*Pf*Cox11Ct on a western blot (right panel). Molecular weight marker (M); lane 1, uninfected human red blood cell lysate; lane 2, untransformed *E. coli* (BL21) lysate; lane 3, soluble rMBP-*Pf*Cox11Ct lysate; lane 4, affinity purified MBP-*Pf*Cox11Ct; lane 5, recombinant MBP.

4.2.7 Detection of the *P. berghei* Cox11 with antibodies against rMBP-*Pf*Cox11Ct

Owing to an 85% amino acid sequence identity between the soluble C-terminal of *P. falciparum* and *P. berghei* Cox11 (Figure 4.15A), the anti-rMBP-*Pf*Cox11Ct antibody was used to detect the expression of native Cox11 in the murine malaria parasite cell lysate. Detection of lactate dehydrogenase (LDH) with LDH antipeptide (APGKSDKEWNRDDL) antibody in the parasite lysate served as a reference and internal control.

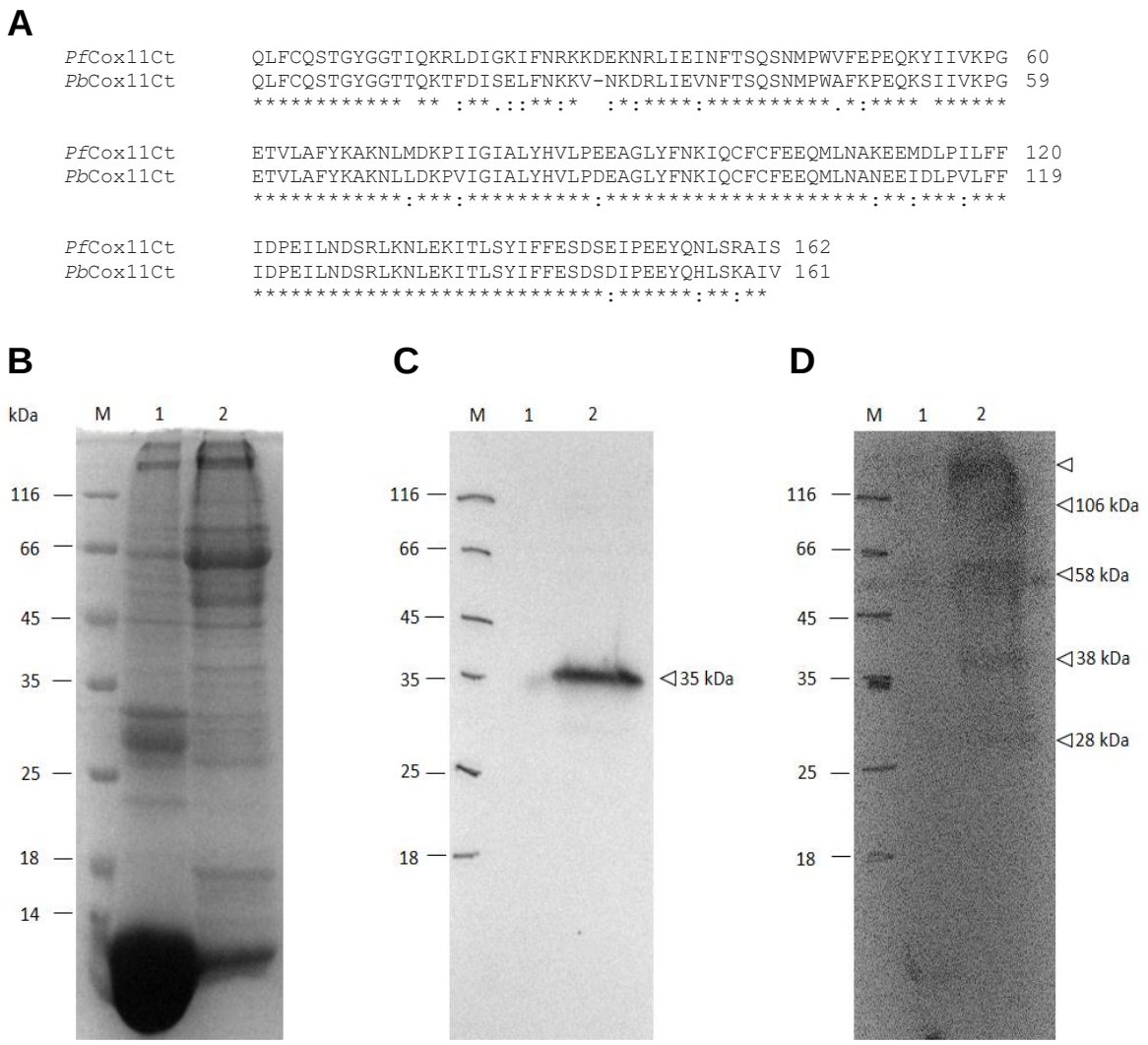

Figure 4.15 Anti-rMBP-*Pf*Cox11Ct antibody detection of the Cox11 in *P. berghei* infected mouse red blood cell lysate

(A) Alignment of the *P. falciparum* and *P. berghei* Cox11 soluble C-terminal amino acid sequences. The annotation "*****", denote conserved residue, while "**:**"and "**.**" denote conserved and semi-conserved substitutions respectively. Cox11 was detected in *P. berghei* infected BALB/c mouse red blood cell lysate using enhanced chemiluminescence (ECL). (B) A 12.5% reducing SDS-PAGE Coomassie-stained reference gel. (C) Western blots probed with lactate dehydrogenase antipeptide antibody or (D) IgY anti-rMBP-*Pf*Cox11Ct, and goat anti-mouse IgG-HRPO (1:12000). Molecular weight marker (M); uninfected (lane 1) and infected (lane 2) *P. berghei* BALB/c mouse red blood cell lysates.

The pan-specific LDH antipeptide control antibody detected a 35 kDa protein corresponding to the *P. berghei* LDH in the *P. berghei* infected BALB/c mouse red blood cell lysate (Figure 4.15B). The anti-rMBP-*Pf*Cox11Ct antibody detected the protein in the *P. berghei* infected BALB/c mouse red blood cell. The anti-rMBP-*Pf*Cox11Ct detected proteins at 106 kDa, 58 kDa, 38 kDa and a ~28 kDa within a kDa of the expected *P. berghei* Cox11 size, 26.5 kDa, and a large molecular weight aggregate above the 116 kDa protein marker. Excluding the 38 kDa band, the proteins correspond to a dimer, tetramer and higher oligomeric forms of the *P. berghei* Cox11.

4.2.8 Binding of copper to rMBP-*Pf*Cox11Ct measured with the bicinchoninic acid (BCA) release assay

The BCA release assay exploits the BCA complexation with Cu(I) (Cu(I)-BCA) at alkaline pH producing an intense purple colour detectable at 354 nm (Brenner and Harris, 1995). Protein-copper complexes were disrupted by acid denaturation to release copper into the reducing solution containing ascorbate to facilitate Cu(I)-BCA complexation (Figure 4.16A).

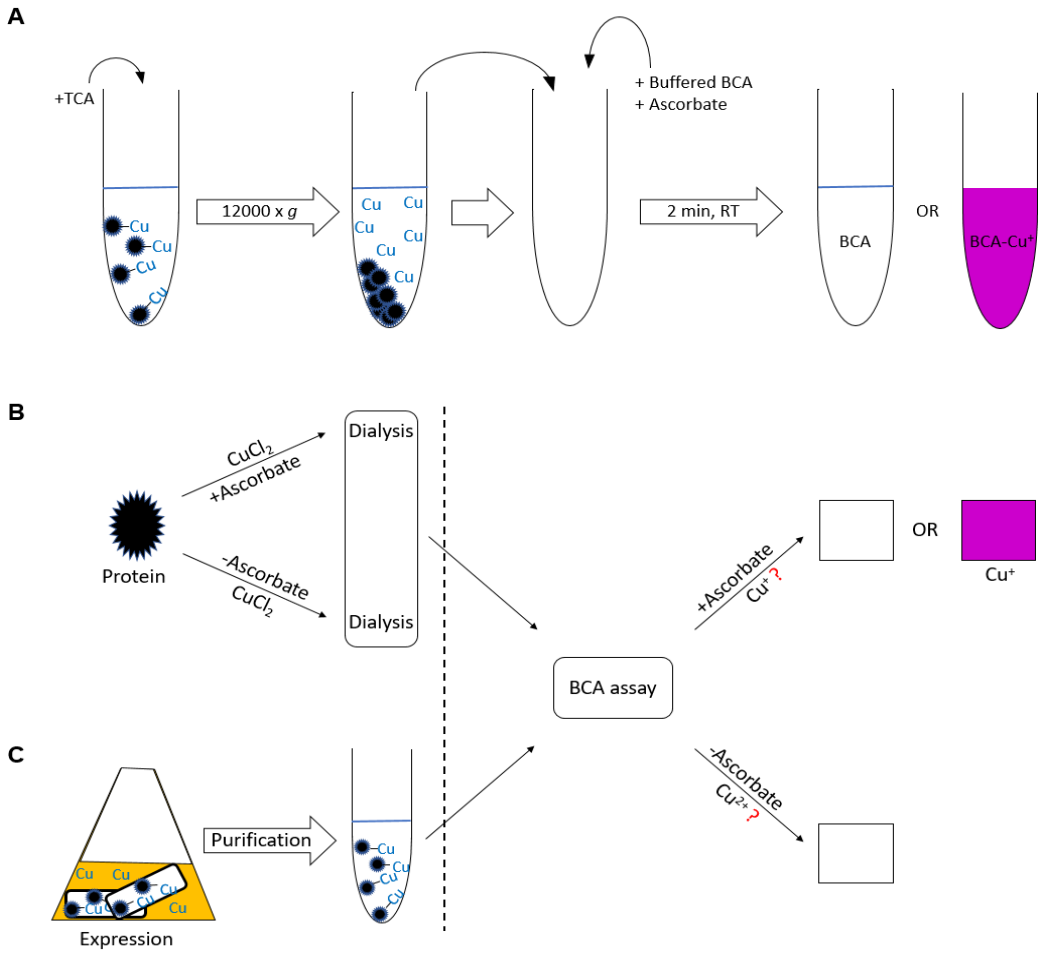

Figure 4.16. Diagram of the copper determined with the BCA release assay
(A) Protocol for the BCA assay. (B) Diagram of the copper binding *in vitro* to a recombinant protein in the presence or absence of ascorbic acid. (C) Diagram of recombinant protein expressed with copper in the growth medium (*in vivo*). A modified BCA assay was used to determine the oxidation state of protein-bound copper.

The *in vitro* copper binding characteristics of the rMBP-*Pf*Cox11Ct were assessed by incubating the purified recombinant proteins with a 20-fold molar excess of copper in the presence or absence of ascorbic acid and dialysis (16-2-2 h) (Figure 4.16B). The addition of ascorbic acid, a reducing agent, was to ascertain the oxidation state of bound copper. Copper was detected by the BCA assay using ascorbic acid to facilitate the formation of the purple Cu(I)-BCA complex. An experiment conducted showed that the unbound copper was removed from the reaction mixture in the first 16 h of dialysis (data not shown).

Figure 4.17 illustrates the *in vitro* binding of copper to rMBP-*Pf*Cox11Ct and all three mutant proteins measured with the BCA release assay. The rMBP-*Pf*Cox11Ct and all three mutant proteins bind Cu(I) and not Cu(II) as indicated in the absence and presence of ascorbate *in vitro*. The MBP control binds less copper. There was no significant difference in the *in vitro* copper binding between the rMBP-*Pf*Cox11Ct and the three mutant proteins.

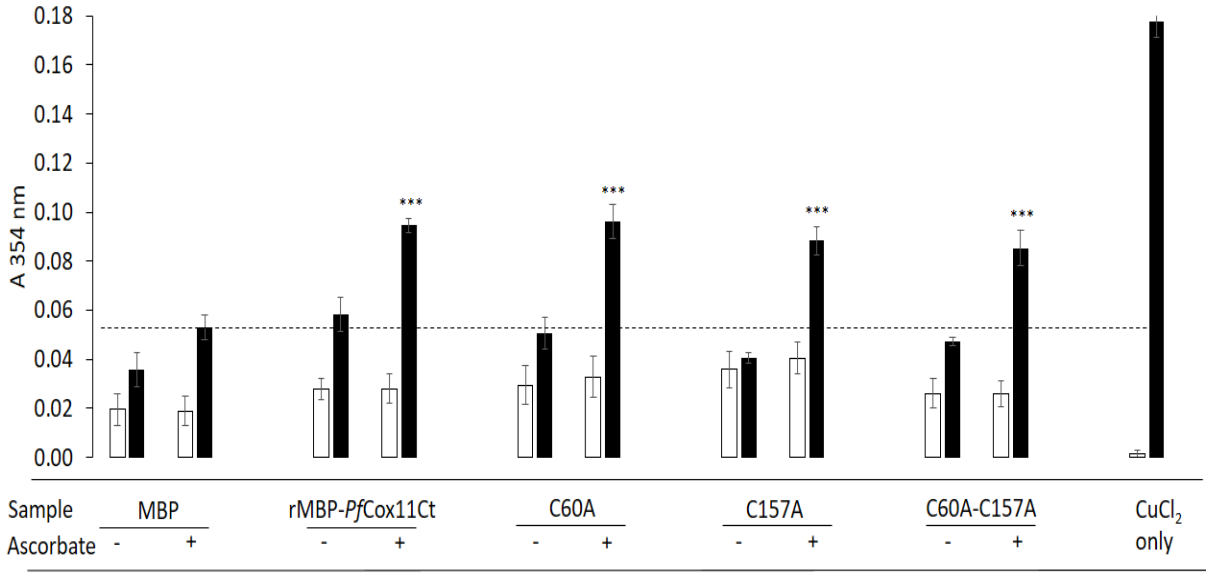

Figure 4.17. Binding of copper to rMBP-*Pf*Cox11Ct and mutant proteins *in vitro* measured by BCA release assay

Affinity-purified rMBP-*Pf*Cox11Ct and mutant proteins (C60A, C157A and C60A-C157A) or MBP alone were incubated with $CuCl_2$ in the absence (–) or presence (+) of ascorbic acid *in vitro*. The BCA release assay was used to detect copper without (open bars) or with (solid bars) the addition of ascorbic acid. The copper standard ($CuCl_2$) was equimolar to the amount of protein. The horizontal broken line represents the cut-off for copper bound to MBP. Results are means ± S.E. of triplicate measurements from duplicate samples. A two-way ANOVA with Bonferroni multiple comparison tests were conducted on samples incubated with $CuCl_2$ in the presence of ascorbate (+). Comparison between MBP and rMBP-*Pf*Cox11Ct/C60A/C157A/C60A-C157A is illustrated with "*". Data were considered significant at $P<0.05$ (*), $P<0.01$ (**), $P<0.001$ (***).

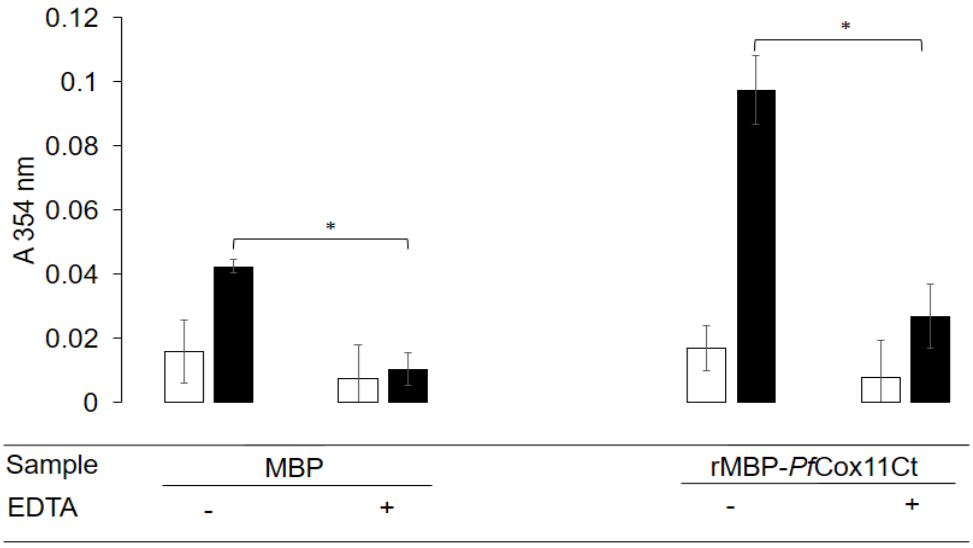

Figure 4.18. The effect of EDTA on copper binding to rMBP-*Pf*Cox11Ct *in vitro*

Affinity-purified rMBP-*Pf*Cox11Ct and MBP was incubated with $CuCl_2$ and ascorbate in the absence (-) or presence (+) of EDTA. Copper was detected without (open bars) or with (solid bars) the addition of ascorbic acid in BCA release assay at 354 nm. The data presented are mean ± SD of a duplicate. "*" denotes statistical significance ($P<0.05$) as determined by Student's *t*-test.

An additional control showed that EDTA, which chelates copper, inhibited the Cu(I)-BCA complexation (Figure 4.18).

In vivo copper binding of rMBP-rPfCox11Ct

To see if the rMBP-*Pf*Cox11Ct bound copper *in vivo*, copper was added to the growth medium of *E. coli* cells expressing the rMBP-*Pf*Cox11Ct and the three mutant proteins. The recombinant proteins were affinity purified and the presence of copper assessed (Figure 4.16C). The oxidation state of copper binding to rMBP-*Pf*Cox11Ct could not be assessed *in vivo*, however, copper is reported (Davis and O'Halloran, 2008) to be reduced inside cells. As seen with the *in vitro* results, the rMBP-*Pf*Cox11Ct bound copper *in vivo* ($P<0.001$) compared to the MBP control (Figure 4.19). Two single mutants, C60A and C157A ($P<0.001$), and the C60A-C157A ($P<0.05$) double mutant significantly bound copper. Both rMBP-*Pf*Cox11Ct and C60A mutant bound copper equally well *in vivo*. The C157A bound copper less well and the C60A-C157A mutant poorly, but above the levels shown by the MBP control.

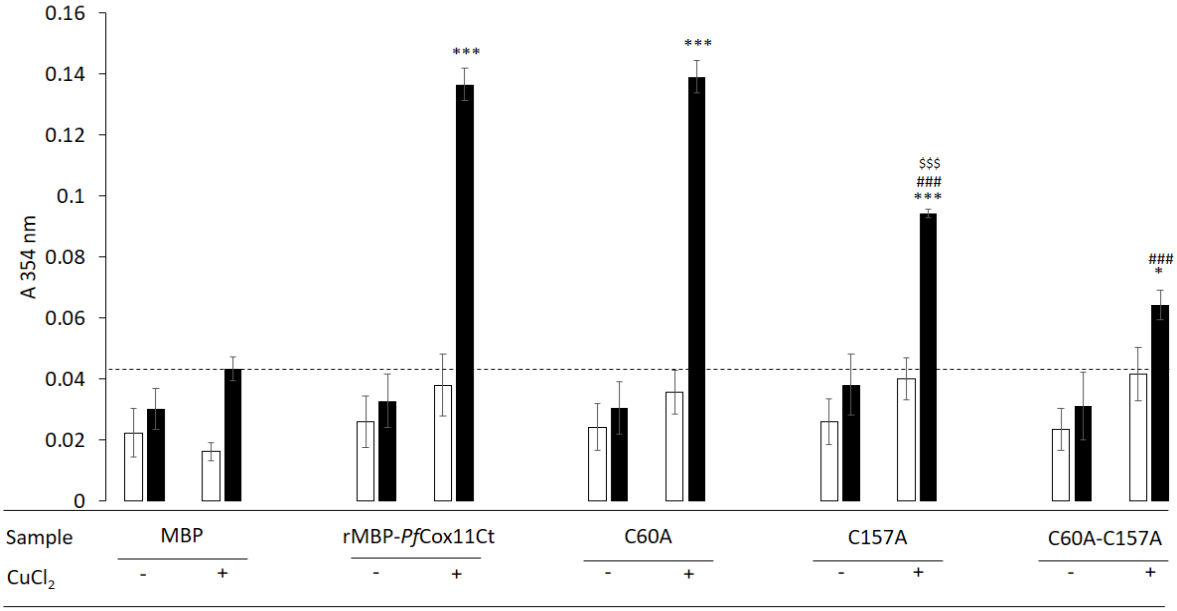

Figure 4.19. Binding of copper to rMBP-*Pf*Cox11Ct and mutant proteins *in vivo* measured by the BCA release assay

0.5 mM $CuCl_2$ was added to the *E. coli* growth medium after the induction of recombinant protein expression. Following affinity purification of the recombinant proteins, copper bound *in vivo* was detected by the BCA release assay without (open bars) or with (solid bars) the addition of ascorbic acid. The BCA-Cu^+ complex was detected at 354 nm. The horizontal broken line represents the cut-off for copper bound to MBP. Results are mean ± S.E. of triplicate measurements from duplicate samples. A two-way ANOVA with Bonferroni multiple comparison tests were conducted on samples expressed with $CuCl_2$ (+). Data were considered significant at $P<0.05$ (*, $^{\#}$ or $^{\$}$), $P<0.01$ (**, $^{\#\#}$ or $^{\$\$}$), $P<0.001$ (***, $^{\#\#\#}$ or $^{\$\$\$}$). Comparison between MBP and rMBP-*Pf*Cox11Ct and mutant proteins is illustrated with "*" and comparison of mutants to rMBP-*Pf*Cox11Ct is illustrated with "#", whereas, "$" signifies comparison between C157A and C60A-C157A.

4.2.9 rMBP-*Pf*Cox11Ct inhibition of the copper-catalysed oxidation of ascorbic acid

The effect of the rMBP-*Pf*Cox11Ct and mutant proteins on the copper-catalysed ascorbic acid oxidation was investigated (Figure 4.20). Ascorbic acid had a relatively stable absorbance reading over 300 s. The addition of 8 µM copper to ascorbic acid produced a rapid and progressive ascorbic acid oxidation. The inhibition of this oxidation was examined with the addition of 5 µM of the rMBP-*Pf*Cox11Ct and mutant proteins or MBP. MBP had little effect on the oxidation. rMBP-*Pf*Cox11Ct inhibited the oxidation. The C60A mutant inhibited the oxidation less well, while the C157A and the C60A-C157A mutants poorly inhibited the oxidation.

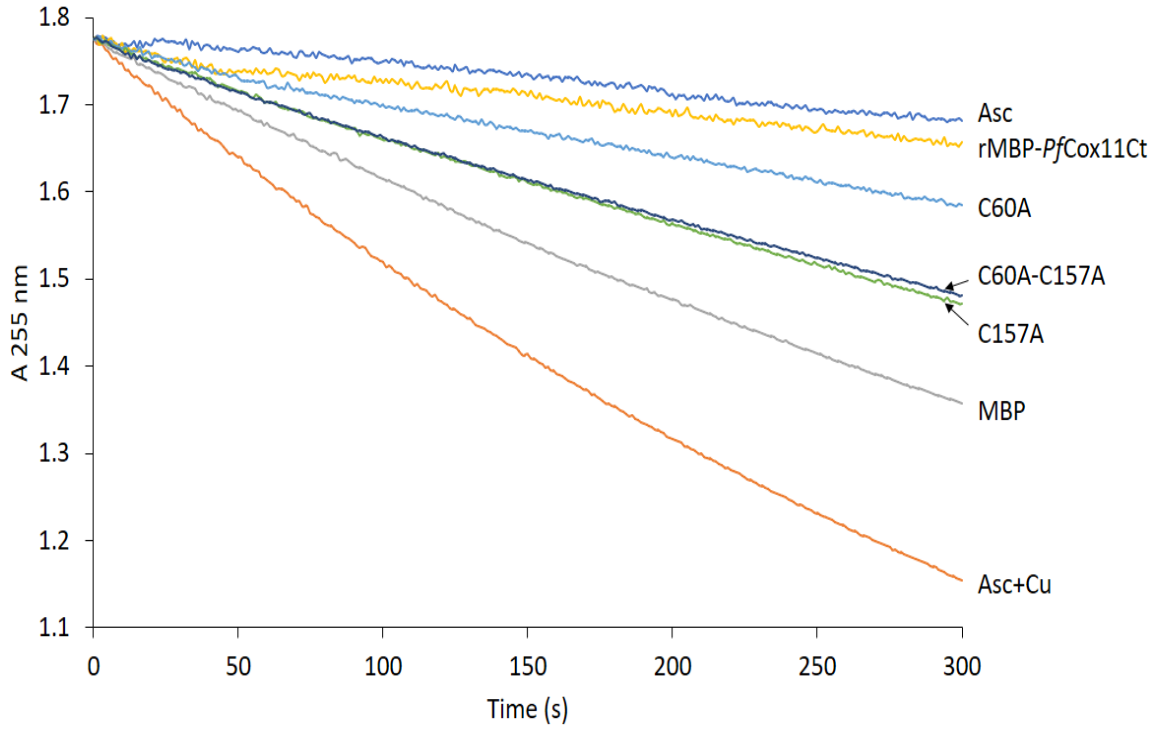

Figure 4.20. Copper-catalysed oxidative degradation of ascorbic acid in the presence of rMBP-*Pf*Cox11Ct and mutants
Measurement of the rate of ascorbic acid oxidation by 8 µM Cu^{2+} over 300 s at pH 4.5 in the presence or absence of 5 µM rMBP-*Pf*Cox11Ct and mutants. MBP was included as a control. Ascorbic acid (Asc); Ascorbic acid with copper (Asc + Cu).

4.2.10 Copper binding measured with atomic absorption spectroscopy (AAS)

Atomic absorption spectroscopy (AAS) was used to quantify the bound copper to the rMBP-*Pf*Cox11Ct. Samples from the *in vitro* BCA assay (rMBP-*Pf*Cox11Ct and MBP) were diluted 1:1 in the reaction buffer and copper content analysed at 324.5 nm. A similar pattern of data as the BCA release assay was obtained from the AAS data (Figure 4.21). The data

revealed, 1.437 µg/ml (22.63 µM) copper was bound to 5 µM MBP-*Pf*Cox11Ct, whereas 0.684 µg/ml copper was detected bound to MBP.

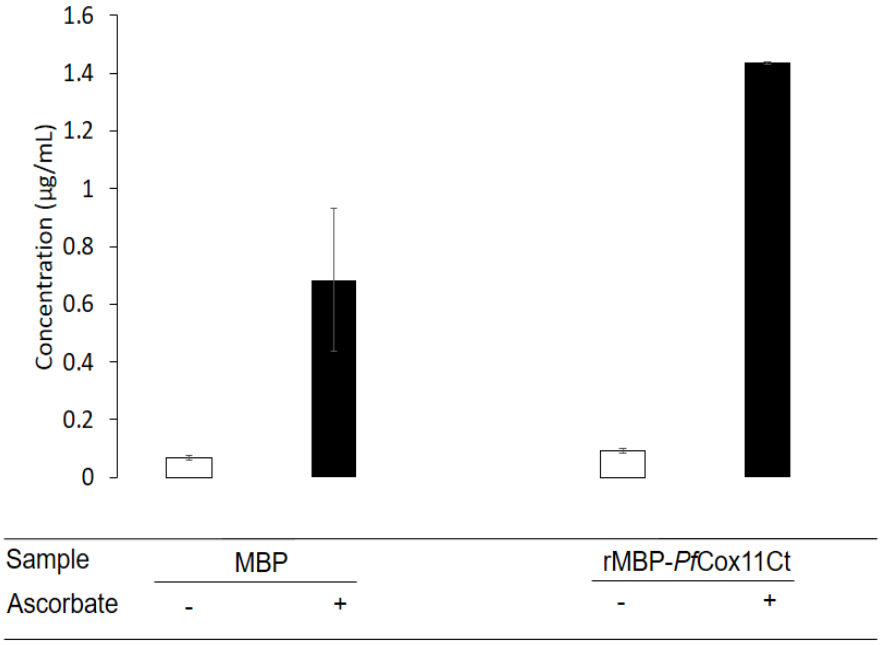

Figure 4.21. *In vitro* copper binding of rMBP-*Pf*Cox11Ct measured by atomic absorption spectroscopy
Affinity-purified rMBP-*Pf*Cox11Ct or MBP were incubated with $CuCl_2$ in the absence (open bars) or presence (solid bars) of ascorbic acid. The bound copper was quantified using atomic absorption spectrophotometer at 324.5 nm. The data presented are mean ± SD of a duplicate.

4.2.11 Copper binding measured with differential scanning fluorimetry

The melting temperature (T_m), an extrinsic property of proteins, was explored to determine the copper binding of rMBP-*Pf*Cox11Ct using the SYPRO® orange dye. The T_m of the rMBP-*Pf*Cox11Ct and MBP proteins was scanned through a range of 25 to 90°C at 0.3°C/min by monitoring the SYPRO® orange fluorescence emission.

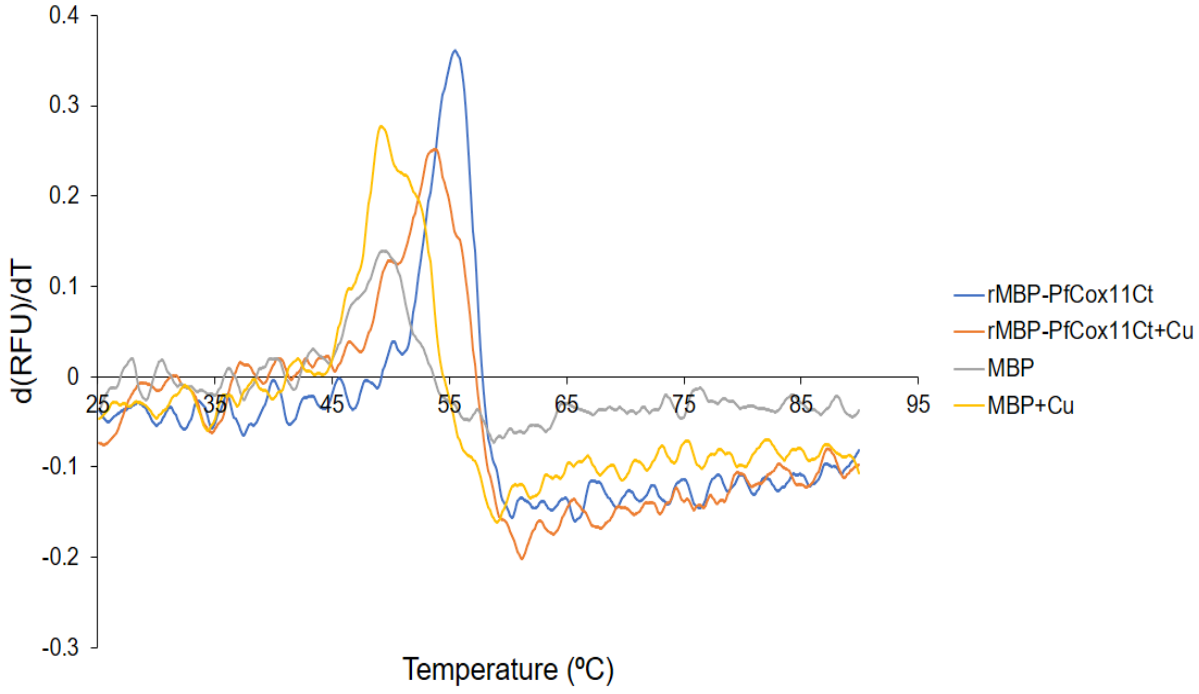

Figure 4.22. The first derivative of the differential scanning fluorimetry for rMBP-*Pf*Cox11Ct with or without copper
The figure shows the change in rMBP-*Pf*Cox11Ct and MBP melting temperatures with and without copper.

Figure 4.22 illustrates the thermal denaturation profile for the rMBP-*Pf*Cox11Ct and MBP with or without copper. MBP had a melting temperature (T_m) of 49.12 ± 0.25ºC and 49.61 ± 0.35ºC in the absence and presence of copper respectively, with a change in T_m (ΔT_m) of +0.49ºC. rMBP-*Pf*Cox11Ct had a T_m of 55.68 ± 0.12ºC and 53.42 ± 0.49ºC in the absence and presence of copper respectively, with a ΔT_m of -2.26ºC.

4.2.12 Copper tolerance of *E. coli* (BL21) host expressing rMBP-*Pf*Cox11Ct

The effect of rMBP-*Pf*Cox11Ct on the copper tolerance of the *E. coli* host cell during growth was investigated.

Firstly, the copper tolerance of an untransformed *E. coli* host (Figure 4.23A) was established using a range of copper concentrations between 0 to 20 mM (Figure 4.23A, left panel) for six hours after adding copper at the exponential growth phase. *E. coli* host-cells grew in the presence of copper below 10 mM, and 8 mM copper slows growth considerably (Figure 4.23A, right panel). This confirmed that the 0.5 mM copper used for *in vivo* copper binding studies does not affect the host-cell growth. The concentration of copper required to reduce the

E. coli host growth by 50% (IC_{50}), 7.19 mM copper, was deduced from a growth inhibition curve (data not shown) of *E. coli* host cells.

Unlike the *E. coli* cells alone, *E. coli* cells harbouring the pMal-c2x plasmid stopped growing at 8 mM copper concentration (Figure 4.23B). The experiment was repeated with the same result. The IC_{50} of 5.7 mM copper was estimated from a growth inhibition curve (data not shown) of transformed *E. coli* host expressing MBP.

When *E. coli* cells harbouring the pMal-c2x-r*Pf*Cox11Ct plasmid were grown in the presence of copper (Figure 4.24), The *E. coli* cells were able to tolerate 8 mM copper compared to the lack of growth observed in *E. coli* host expressing MBP alone. An IC_{50} of 6.72 mM was estimated from the inhibition curve. The importance of the three conserved cysteines in Cox11 to enable the *E. coli* cells to grow in the presence of 8 mM copper was determined (Figure 4.24B). Only the *E. coli* cells with the rMBP-*Pf*Cox11Ct and C60A mutant protein tolerated 8 mM copper. The C157A and C60A-C157A mutant proteins clones did not protect the cells from copper inhibition of growth.

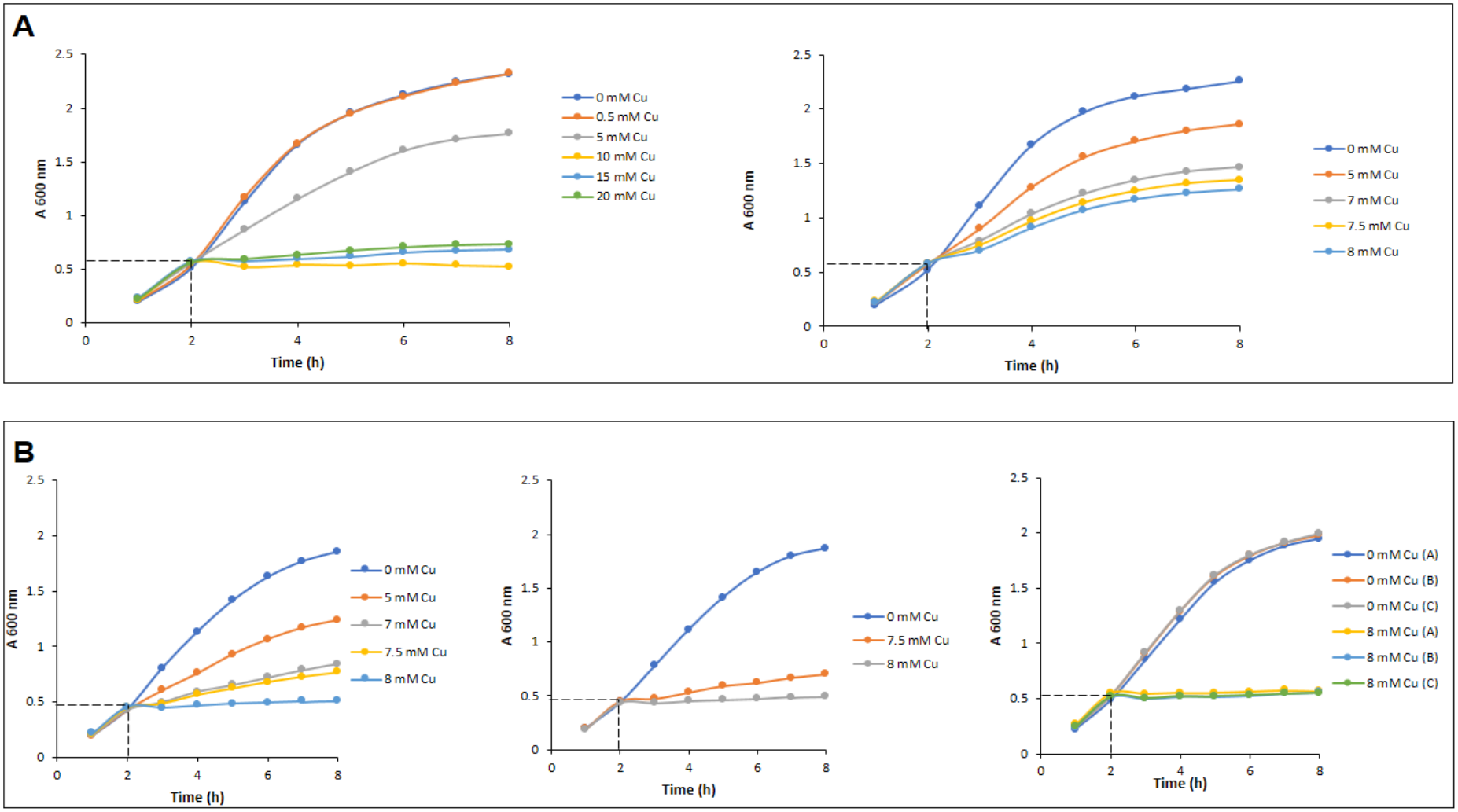

Figure 4.23. Effect of copper on growth of *E. coli* (BL21) cells

E. coli (BL21) growth was monitored by OD_{600} at an hourly interval for 6 h. (A) Cultures of untransformed *E. coli* (BL21) with 0 to 20 mM (left panel) and 0 to 8 mM (right panel) copper. (B) Cultures of *E. coli* (BL21) with pMal-c2x expression vector, with 0 to 8 mM copper. The dotted lines indicate the addition of IPTG (in transformed) and copper in *E. coli* (BL21) cultures.

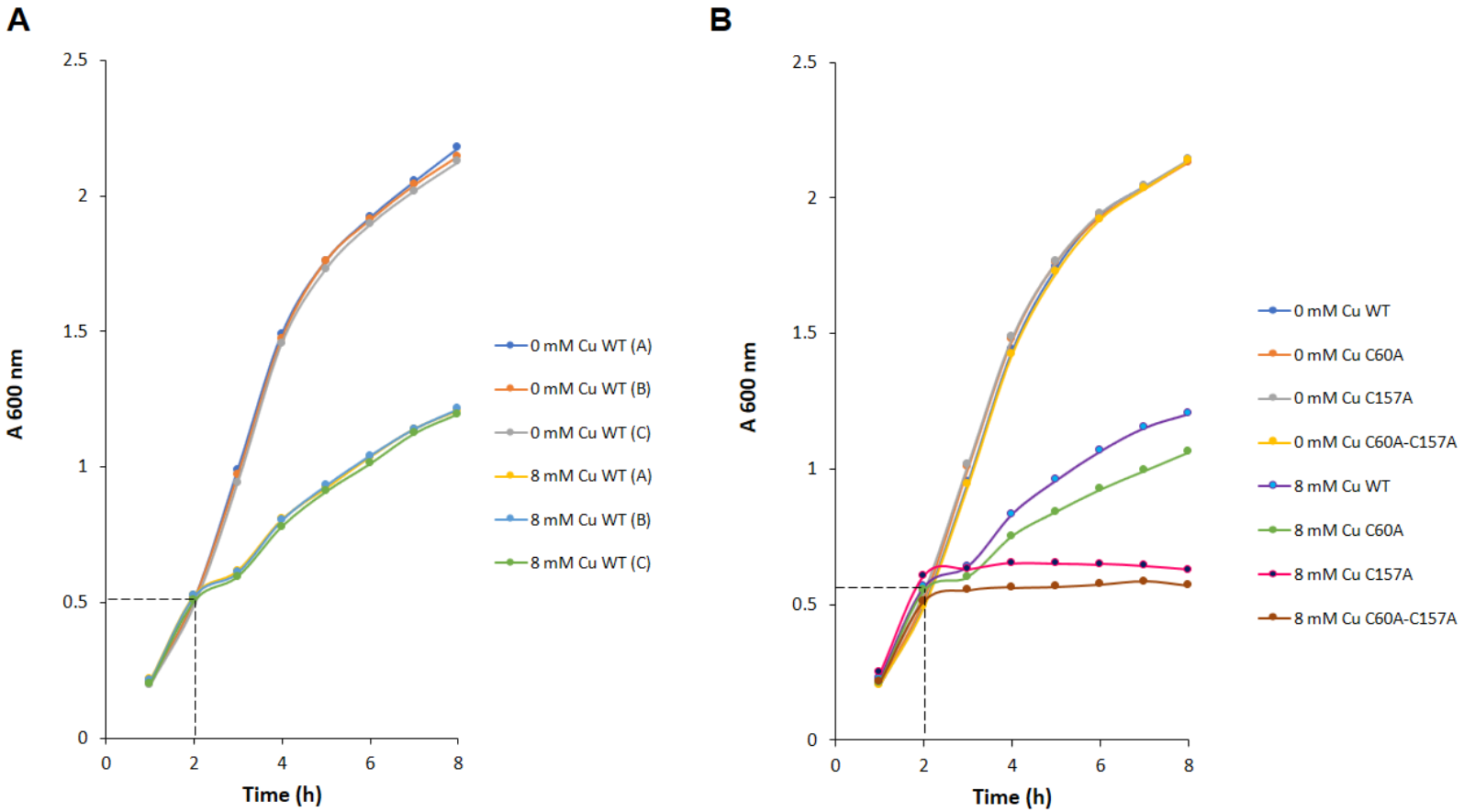

Figure 4.24. Effect of copper on the growth of *E. coli* (BL21) cells expressing rMBP-*Pf*Cox11Ct and mutants
E. coli (BL21) with the pMal-c2x-r*Pf*Cox11Ct plasmid was grown in the presence of 0 and 8 mM copper and growth was monitored at an hourly interval by OD_{600} for 6 h. (A) Triplicate *E. coli* (BL21) cultures with pMal-c2x-r*Pf*Cox11Ct, with or without copper. (B) Cultures of *E. coli* (BL21) with pMal-c2x-*Pf*Cox11Ct or mutants, with or without copper. The dotted lines indicate the addition of copper and IPTG.

4.3 Discussion

4.3.1 Cloning the *P. falciparum* Cox11 sequence

P. falciparum Cox11 is encoded by an open reading frame of 687 bp. A 486 bp encoding 162 amino acid of the C-terminal domain excluding the transmembrane N-terminal domain and 33 bp of the 3' end was amplified (Figure 4.8). The 33 bp 3' end were left out to facilitate primer design. The 486 bp sequence was amplified from *P. falciparum* genomic DNA and cloned into the pGEM®-T Easy cloning vector and subcloned into a pMal-c2x expression vector to be recombinantly expressed as an MBP fusion protein (Figure 4.2). Attempts to express the protein as a His-tagged protein (data not shown) were not successful. Others have reported difficulties expressing bacterial and yeast Cox11 as a His-tagged protein (Banci *et al.*, 2004; Carr *et al.*, 2002; Thompson *et al.*, 2010). Two methods confirmed the identity of the cloned sequence. *Alu* sequences are the most abundant middle repetitive sequences found in eukaryotic DNA sequences (Jelinek and Schmid, 1982). Only one *Alu*I site is contained within the cloned gene which was used to "fingerprint" the cloned gene sequence. The cloned insert was sequenced and had 100% identity to the *P. falciparum* Cox11 gene PlasmoDB sequence.

4.3.2 Site-directed mutagenesis of the *P. falciparum* Cox11 cysteine residues

Site-directed mutagenesis is a useful tool for deciphering protein structure-function relationships. To understand the possible role of the three conserved cysteines in the *P. falciparum* Cox11 protein, three mutants, C60A, C157A and C60A-C157A were engineered by overlap extension PCR (Heckman and Pease, 2007; Ho *et al.*, 1989). The choice of Ala residue to substitute for Cys was based on size and polarity. Substituting A for C should not affect the conformation and net charge of the proteins since the size and polarity of Ala is about that of Cys. Substituting a cysteine with an alanine at position 155 was not possible owing to constraints in the design of the two internal primers for the mutant codon. Sequencing the mutant clones confirmed the successful introduction of the two single and the double mutant. In a similar mutagenic study with yeast Cox11, amino acid substitutions in all three corresponding cysteines were obtained (Carr *et al.*, 2002; Thompson *et al.*, 2010).

4.3.3 Recombinant expression and isolation of MBP-*Pf*Cox11Ct

rMBP-*Pf*Cox11Ct expression was achieved with 0.5 mM IPTG induction in 2xYT at 30^{o}C for 4 h. The rMBP-*Pf*Cox11Ct protein eluted from the amylose affinity resin with 0.25 mM maltose and the eluted protein was detected on a western blot with an anti-MBP

antibody. The table following the purification steps of the protein records that 1.43 mg rMBP-*Pf*Cox11Ct was obtained from 400 ml (~2.91 g wet weight bacterial pellet) bacterial cultures, corresponding to about 1.17% of the soluble cell lysate. In a study with a repertoire of recombinant proteins, a yield of about 25 to 34 mg per 50 ml culture was obtained (Sivashanmugam *et al.*, 2009). The rMBP-*Pf*Cox11Ct yield is higher than the 2 mg/L yield obtained from the recombinantly expressed thioredoxin-fused soluble C-terminal domain of *Rhodobacter sphaeroides* Cox11 (Thompson *et al.*, 2010), and the yield is similar to that obtained for the *P. falciparum* copper transport protein (Ctr1) (Choveaux *et al.*, 2012).

4.3.4 Raising IgY antibodies against rMBP-*Pf*Cox11Ct

Polyclonal antibodies against the whole recombinant protein and against a specific peptide epitope were raised in chickens. Chickens are a good host for antibody production as they are evolutionarily distant from mammals and other organisms, which increases the probability of antibody production (Larsson and Sjoquist, 1990). Since antibodies are isolated from the egg yolk, and many eggs are laid by each chicken, high antibody yields can be attained which are better than antibody yields from the sera of immunised animals (Gassmann *et al.*, 1990; Lee *et al.*, 2017). About 21 mg of affinity purified IgY antibodies were obtained from a chicken. The antibody response to both the rMBP-*Pf*Cox11Ct protein and the internal peptide sequence was similar to that reported by others (Hurdayal *et al.*, 2010; Krause *et al.*, 2015). Both of the antibodies detected rMBP-*Pf*Cox11Ct protein and did not detect proteins from the uninfected red blood cell or *E. coli* host cell.

4.3.5 IgY antibodies against the rMBP-*Pf*Cox11Ct detected the native Cox11 protein

Using enhanced chemiluminescence, the anti-rMBP-*Pf*Cox11Ct IgY antibody detected a protein band which is marginally larger than the expected size of *P. berghei* Cox11 at ~28 kDa (Figure 4.15B). Helical membrane proteins have been demonstrated to run at either higher or lower than their expected sizes on SDS-PAGE gels due to the hydrophobic transmembrane domain (Rath and Deber, 2013). Thermal aggregation of membrane proteins can occur in SDS-PAGE gels, partly due to the hydrophobic transmembrane domain, which results in the formation of bands between the monomer and higher aggregates following heat treatment (Huang *et al.*, 2013; Okada *et al.*, 2011). This may explain the 58 kDa, 106 kDa and a protein aggregate above the 116 kDa bands corresponding to a dimer, tetramer and higher oligomeric forms of the *P. berghei* Cox11. An attempt to detect the protein in a *P. falciparum*

lysate was unsuccessful, possibly due to the protein not being expressed during developmental stage of the sample. Transcriptional analysis suggests *P. falciparum* Cox11 to be expressed mainly in the trophozoite stage (Aurrecoechea *et al.*, 2009; Mok *et al.*, 2007).

4.3.6 Assessing the binding of copper to rMBP-*Pf*Cox11Ct using the BCA release assay

In vitro and *in vivo* copper binding of rMBP-*Pf*Cox11Ct was demonstrated using multiple strategies which are now discussed in turns. First was the spectrophotometric based BCA copper release assay which showed that the rMBP-*Pf*Cox11Ct protein bound copper *in vitro* (Figure 4.17) and *in vivo* during *E. coli* host cell culture (Figure 4.19). Like earlier studies, rMBP-*Pf*Cox11Ct bound Cu(I) and not Cu(II) (Banci *et al.*, 2004; Carr *et al.*, 2002). *In vitro* copper binding of rMBP-*Pf*Cox11Ct was inhibited by the metal chelator, EDTA. The data from studies with the three mutants suggest that the Cys60 amino acid is not essential for copper binding in rMBP-*Pf*Cox11Ct (Figure 4.19). This implies that copper is coordinated between the Cys155 and Cys157 of the $C_{155}FC_{157}F$ (CFCF) motif. There was lower binding of copper to the C157A mutant. The binding of copper to the C60A-C157A double mutant was also low. The data for the *in vivo* copper assay like earlier findings (Banci *et al.*, 2004; Carr *et al.*, 2002; Thompson *et al.*, 2010), suggests the CFCF motif to be the likely site for copper coordination. The data here does not agree with the role of Cys60 in copper coordination as proposed by Carr *et al.* (2002).

4.3.7 Measuring rMBP-*Pf*Cox11Ct inhibition of copper-catalysed ascorbic acid oxidation

The second approach was testing rMBP-*Pf*Cox11Ct's propensity to bind copper by monitoring the rate at which copper-catalysed ascorbic acid oxidation was inhibited by the protein. Ascorbic acid is stable to atmospheric oxidation, but susceptible to copper or iron ions catalysed oxidative degradation (Martell, 1982). Metal chelators decrease the rate of metal-catalysed ascorbic acid oxidation via the formation of a mixed ligand chelate complex (Khan and Martell, 1967). The rMBP-*Pf*Cox11Ct inhibited the copper-catalysed oxidation of ascorbic acid (Figure 4.20). The mutant proteins were also assessed. The rMBP-*Pf*Cox11Ct had the highest inhibition followed by the C60A, then C157A and C60A-C157A mutants having about the same degree of inhibition. This data supports earlier findings that the CFCF domain in *P. falciparum* Cox11 like the orthologues is involved in copper binding.

4.3.8 Assessing the binding of copper to rMBP-*Pf*Cox11Ct using AAS

The third strategy to assess copper binding to rMBP-*Pf*Cox11Ct was the use of atomic absorption spectroscopy. Quantitative, as well as qualitative copper assessment using AAS, has been shown to agree with the BCA assay (Brenner and Harris, 1995). The AAS data for the assessment of the *in vitro* copper binding of rMBP-*Pf*Cox11Ct revealed a similar profile to the BCA assay (Figure 4.21).

4.3.9 rMBP-*Pf*Cox11Ct copper binding evaluated using differential scanning fluorimetry

The fourth strategy employed to measure copper binding was the use of differential scanning fluorimetry. Binding of substrate, coenzyme, or small molecules to proteins could either stabilise or destabilise proteins, leading to a change in the melting temperature of proteins (ΔT_m). From the profile (Figure 4.22), the binding of copper to rMBP-*Pf*Cox11Ct showed a destabilising effect, with a ΔT_m of -2.26^oC. This implies that binding of Cu(I) to rMBP-*Pf*Cox11Ct results in a significant change to the conformation, as $\Delta T_m \geq 2^oC$ is considered significant (Boivin *et al.*, 2013; Ericsson *et al.*, 2006; Krishna *et al.*, 2013). The $-\Delta T_m$ also implies Cu(I) binds the non-native rMBP-*Pf*Cox11Ct conformation. Although the primary form of the soluble domain of Cox11 predominantly exists as a dimer (Carr *et al.*, 2002), tetrameric and hexameric forms that bind more Cu(I) than the sum of the dimers have been purified (Thompson *et al.*, 2010). Therefore, it could be suggested that Cu(I) preferentially binds the less thermodynamically stable oligomeric conformations to the more stable conformation.

4.3.10 rMBP-*Pf*Cox11Ct enables *E. coli* host cells to tolerate harmful copper levels

A fifth approach was assessing the ability of rMBP-*Pf*Cox11Ct to confer copper tolerance to the *E. coli* (BL21) host cell. The IC_{50} value for copper is directly proportional to the copper tolerance of the *E. coli* host cell. *E. coli* cells expressing MBP (IC_{50}, 5.7 mM) or rMBP-*Pf*Cox11Ct (IC_{50}, 6.72 mM) had a reduced copper tolerance, shown by the reduced IC_{50} values compared to the IC_{50} of the untransformed *E. coli* host (IC_{50}, 7.19 mM). Since a significant amount of the *E. coli* host's resources are channelled towards heterologous recombinant protein expression (Carneiro *et al.*, 2013; Glick, 1995), this could have left the *E. coli* host vulnerable, hence, a reduced copper tolerance. The 0.5 mM copper used in the *in vivo* BCA assay does not affect the *E. coli* host growth (Figure 4.23A). Untransformed *E. coli* host cells tolerated 8 mM copper, similar to the levels tolerated by the Gram-positive bacteria

Enterococcus hirae (Solioz and Stoyanov, 2003). *E. coli* host cells expressing MBP was sensitive to 8 mM copper (Figure 4.23B). Interestingly, the expression of rMBP-*Pf*Cox11Ct enabled the growth of *E. coli* host cells in the presence of 8 mM copper (Figure 4.24A). Similar studies have demonstrated recombinantly expressed copper binding proteins can improve the levels of copper tolerated by *E. coli* expression hosts (Vita *et al.*, 2016; Yang *et al.*, 2017). To establish the role of the CFCF motif in copper binding, the growth rate of the *E. coli* host expressing the rMBP-*Pf*Cox11Ct and the mutant proteins was compared. Of the four mutant proteins, only the *E. coli* hosts expressing rMBP-*Pf*Cox11Ct and C60A tolerated 8 mM copper, while 8 mM copper killed the C157A and C60A-C157A expressing *E. coli* hosts. The observation is similar to the *in vivo* copper binding assay, where rMBP-*Pf*Cox11Ct and C60A proteins had similar copper binding characteristics that differed from that of the C157A and C60A-C157A proteins. The C157A and C60A-C157A mutant clones did not influence the growth of the *E. coli* host suggesting that the CFCF motif is the more likely site for the binding of copper.

4.3.11 Conclusion

The results in this chapter from the characterisation of the recombinant protein using; the BCA release assay, AAS, differential scanning fluorimetry, inhibition of the ascorbic acid oxidation and assessment of the *E. coli* host cell copper tolerance, established the copper binding ability of the *P. falciparum* Cox11. The Cys60 residue which is a short distance away from the CFCF motif is not involved in copper coordination. While Cys155 was not investigated, it does seems Cys157 is likely involved with copper coordination. Therefore, copper coordination is likely within the two cysteine residues, Cys155 and Cys157 of the CFCF motif. These results to the best of my knowledge are the first to characterise Cox11 in any malaria parasite.

Chapter 5

The *Plasmodium falciparum* putative Cox19 copper metallochaperone: Recombinant protein copper binding studies

5.1 Introduction

The aim of the work described in this chapter was to PCR-amplify and recombinantly express the putative *P. falciparum* Cox19 gene previously identified *in silico* (Chapter 3). The recombinant protein was expressed as an MBP-fusion protein. The second aim was to characterise the recombinant, as well as the native protein through immunochemical and copper binding studies.

5.1.1 Mitochondrial intermembrane space proteins

All mitochondrial intermembrane space (IMS) proteins are nuclear encoded and synthesised in the cytosol. Most of the IMS proteins contain internal cysteine motifs essential for import into the IMS known as the mitochondrial IMS-sorting signal (MISS) (Milenkovic *et al.*, 2009) or IMS-targeting signal (ITS) (Sideris *et al.*, 2009). The cysteine motifs are recognised by Mia40 protein (an oxidoreductase), a component of the mitochondrial import assembly (Chacinska *et al.*, 2004; Naoé *et al.*, 2004) required in the import and folding of the IMS-proteins (Banci *et al.*, 2009; Kawano *et al.*, 2009; Weckbecker *et al.*, 2012) in eukaryotes. Mia40 consists of a redox-active cysteine-proline-cysteine (CPC) motif maintained in an oxidised state by Erv1, a sulfhydryl oxidase (Banci *et al.*, 2009; Kawano *et al.*, 2009). Both Mia40 and Erv1 constitute the disulphide relay system of the mitochondria. The two primary substrates of the disulphide relay system are the twin Cx_3C and twin Cx_9C proteins. Mia40 like some of its substrates is a twin Cx_9C protein. The characteristic feature between these substrates is the [Coiled coil 1]-[Helix 1]-[Coiled coil 2]-[Helix 2] (CHCH) domain, where each helix contains two cysteine residues separated by three and nine amino acid residues in the twin Cx_3C and twin Cx_9C proteins respectively. Twin Cx_3C proteins function as chaperones facilitating the movement of hydrophobic proteins through the IMS (Koehler *et al.*, 1998; Sirrenberg *et al.*, 1996), while most of the twin Cx_9C proteins are needed in the assembly or stability of the respiratory chain complexes (Chatzi and Tokatlidis, 2013). *Plasmodium* spp. has no Mia40, and the Erv1 in *P. falciparum* did not complement the yeast Erv1 orthologue despite a successful import of IMS proteins from across the mitochondrial outer membrane (Eckers *et al.*, 2013). Perhaps an unidentified oxidoreductase is responsible for shuttling the

plasmodial IMS proteins across the mitochondrial outer membrane into the IMS (Allen *et al.*, 2008; Carrie and Soll, 2017)

5.1.2 Twin Cx_9C substrates of the IMS Mia40

As earlier stated, twin Cx_9C proteins, substrates of the Mia40 oxidoreductase are associated with the respiratory chain. The most studied of the twin Cx_9C Mia40 substrates is Cox17. Cox17 is a copper metallochaperone that delivers copper to the two cytochrome c oxidase (CcO) assembly proteins, Cox11 and Sco1, responsible for inserting copper at the Cu_B and Cu_A centres of Cox1 and Cox2 subunits respectively (Hiser *et al.*, 2000; Horng *et al.*, 2004; Lode *et al.*, 2000; Timón-Gómez *et al.*, 2018). Cox17 has been demonstrated to be essential for the survival of yeast and mammalian cells (Glerum *et al.*, 1996; Takahashi *et al.*, 2002). Malaria parasite Cox17 has been identified and characterised in the malaria parasite (Choveaux *et al.*, 2015). One of the two putative malaria parasite copper metallochaperones understudy, Cox19, an essential CcO assembly accessory protein is also a twin Cx_9C Mia40 substrate. Like Cox17, Cox19 was demonstrated to be essential for the survival of yeast cells (Bode *et al.*, 2015; Nobrega *et al.*, 2002; Rigby *et al.*, 2007).

Following the *in silico* characterisation of the *P. falciparum* Cox19 sequence (Chapter 3), the cloning, recombinant expression, purification and the characterization of the putative coding sequence is discussed in this chapter.

5.2 Results

5.2.1 Identification of the presence of a Cox19 copper metallochaperone sequence in the *Plasmodium falciparum* genome

The PF3D7_1201800 gene encoding the putative Cox19 in *P. falciparum* is localised between bases 105 483 to 106 539 of chromosome 12 of the *P. falciparum* genome (Figure 5.1A). A 556 bp sequence of the 657 bp coding region lacking twelve and 89 bases at the 5' and 3' ends respectively of the *P. falciparum* Cox19 (Figure 5.1C) was cloned. Two restriction sites, a stop codon and two adapter gene nucleotides at the 5' end of the restriction enzyme to enhance the specificity of the primers to the DNA template were added to the primer design. A 575 bp PCR-amplicon was expected.

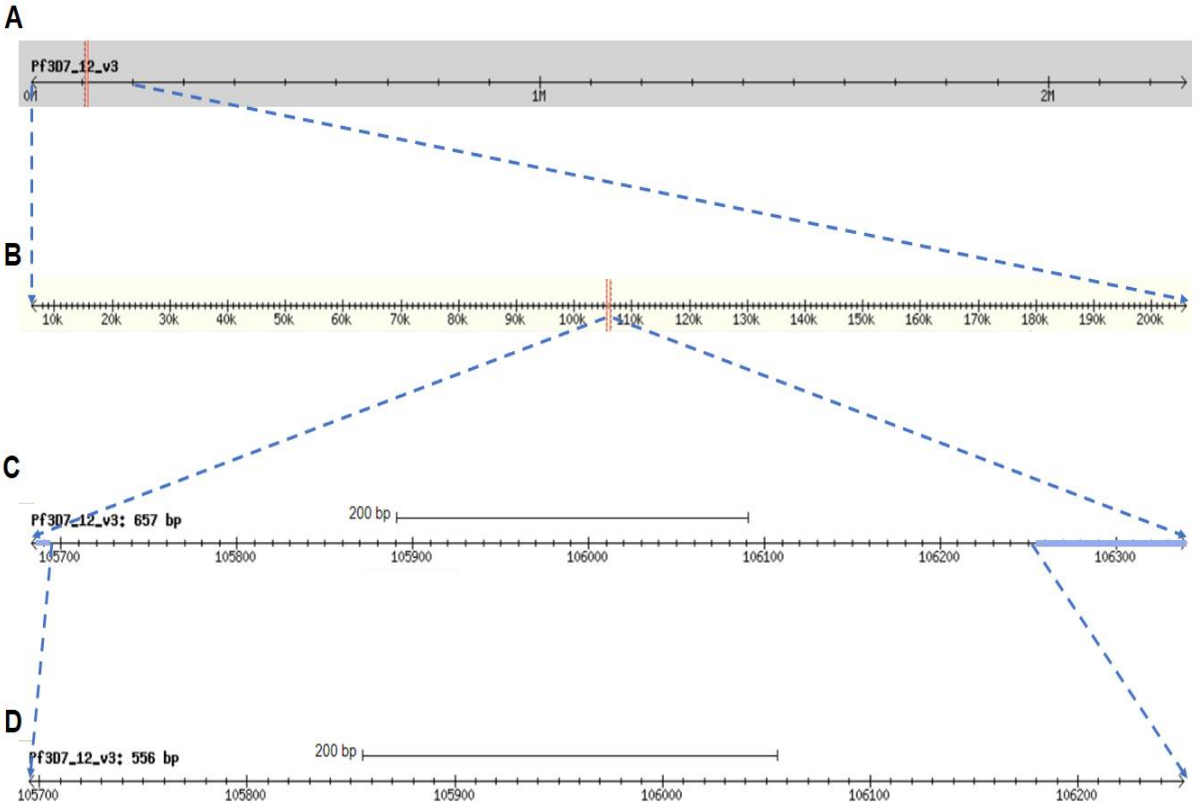

Figure 5.1. Localisation of the Cox19 coding domain in *P. falciparum* chromosome 12
PF3D7_1201800 coding domain localisation on *P. falciparum* chromosome 12 (A). An expanded view of the chromosome 12 gene organisation relative to PF3D7_1201800 (B). An exploded PF3D7_1201800 gene, 657 bp, encoding the complete protein (C). The recombinantly cloned gene segment, 556 bp (D). ▬ denotes the excluded gene segments at both N- and C-termini.

Figure 5.2 shows data from the PCR-amplification, cloning and subcloning of the *Pf*Cox19 sequence (r*Pf*Cox19). Agarose gel analysis of the PCR-amplicons from the *P.*

falciparum gDNA showed a product of ~580 bp (Figure 5.2A), corresponding to the 575 bp predicted from the gene sequence. The amplicon was cloned into a pTZ57R/T cloning vector, and colonies with the recombinant plasmid (pTZ57R/T-r*Pf*Cox19) selected. Colony-PCR from three colonies produced a ~580 bp amplicons (Figure 5.2B). The pTZ57R/T-r*Pf*Cox19 vector and the pMal-c2x expression plasmid were digested with the *Sal*I and *Pst*I restriction endonucleases. An agarose gel (Figure 5.2C) showed the undigested pTZ57R/T-r*Pf*Cox19 plasmid ran at three different estimated sizes of ~8360 bp, ~6050 bp and ~4080 bp thought to represent the multiple conformations of the circular pTZ57R/T-r*Pf*Cox19 plasmid. The product of enzyme digestion was two DNA fragments at ~2900 bp and ~580 bp corresponding to the pTZ57R/T plasmid and r*Pf*Cox19 insert respectively.

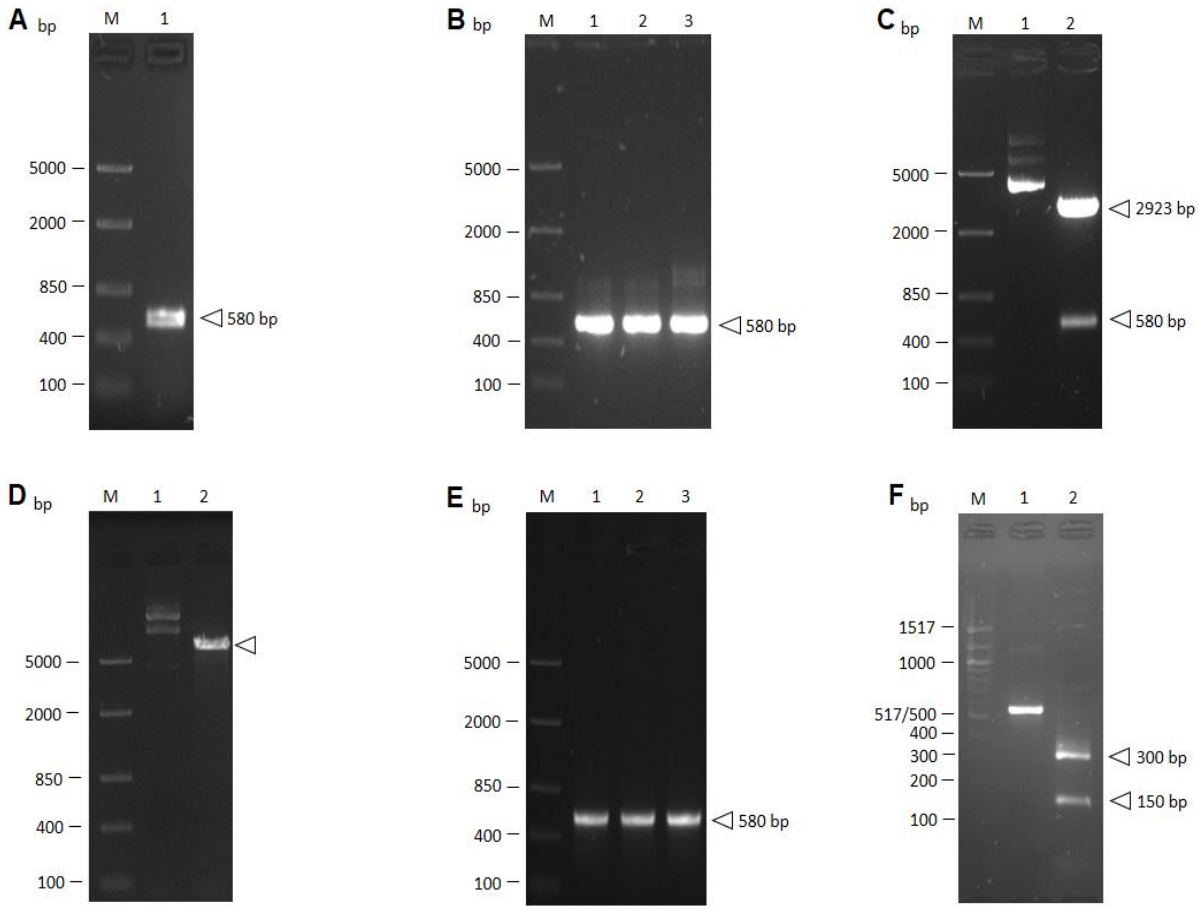

Figure 5.2. PCR-amplification, cloning and restriction enzyme digestion of r*Pf*Cox19
(A) r*Pf*Cox19 amplification product from the *P. falciparum* gDNA (lane 1). (B) r*Pf*Cox19 amplified from three pTZ57R/T-r*Pf*Cox19 plasmid-containing bacterial colonies (lanes 1-3). (C) pTZ57R/T-r*Pf*Cox19 plasmid alone (lane 1) and digested with *Sal*I and *Pst*I (lane 2). (D) pMal-c2x plasmid alone (lane 1) and digested with *Sal*I and *Pst*I (lane 2). (E) r*Pf*Cox19 amplified from three pMal-c2x-r*Pf*Cox19 plasmid-containing bacterial colonies (lanes 1-3). (F) r*Pf*Cox19 alone (lane 1) and digested with *Alu*I. Samples in A-E were analysed on a 1%, and F on a 3% (w/v) agarose gel. M in all images refers to the DNA ladder. The arrows refer to the key molecular weight band in each stance.

Figure 5.2D shows the ~6550 bp product of the pMal-c2x plasmid digested with *Sal*I and *Pst*I restriction endonucleases. r*Pf*Cox19 was cloned into the pMal-c2x expression vector at the *Sal*I and *Pst*I sites, transformed, and colonies with the recombinant plasmid (pMal-c2x-r*Pf*Cox19) were selected. Colony-PCR analysis for three colonies resulted in three ~580 bp amplicons (Figure 5.2E). A unique *Alu*I site, AGCT, occurred four times in r*Pf*Cox19 sequence enabling *Alu*I products of ~300 bp and ~150 bp to be produced. Three other products below 100 bp were not resolved on the agarose gel (Figure 5.2F).

```
PfCox19_vect      ATGTCGACAGGCAGCTTGTTAAGAAGCCTGATAGGGGGAGTTTCTTACTTGATCATAATA        60
PfCox19_pldb      --------AGGCAGCTTGTTAAGAAGCCTGATAGGGGGAGTTTCTTACTTGATCATAATA        52
                          **************************************************

PfCox19_vect      ATGAATGTACGTCAATAAAACAGAAATATTTAAAGTGTTTAAAGGAAAATAACAATGACC        120
PfCox19_pldb      ATGAATGTACGTCAATAAAACAGAAATATTTAAAGTGTTTAAAGGAAAATAACAATGACC        112
                  ************************************************************

PfCox19_vect      ATATTTGTTGTCGAGATCATTCTAAAGAATATTTCATATGTCGCATGGATAATAATTTAT        180
PfCox19_pldb      ATATTTGTTGTCGAGATCATTCTAAAGAATATTTCATATGTCGCATGGATAATAATTTAT        172
                  ************************************************************

PfCox19_vect      TGGAAAGGCAAAGCTTAAATGATTTAGGTTTTATTGAACATGAAGAAAAAAATGAAAGCC        240
PfCox19_pldb      TGGAAAGGCAAAGCTTAAATGATTTAGGTTTTATTGAACATGAAGAAAAAAATGAAAGCC        232
                  ************************************************************

PfCox19_vect      GAATAAAAAATTTTAAAGATGTATATAGTTACAATATATATAATGAAAACATGGAACGTA        300
PfCox19_pldb      GAATAAAAAATTTTAAAGATGTATATAGTTACAATATATATAATGAAAACATGGAACGTA        292
                  ************************************************************

PfCox19_vect      TATCAAGAAATATGCATGATAATATTAAAAGTAATAATTTATTGTTGAATGAGAATAATA        360
PfCox19_pldb      TATCAAGAAATATGCATGATAATATTAAAAGTAATAATTTATTGTTGAATGAGAATAATA        352
                  ************************************************************

PfCox19_vect      TGTTATCAAAATTAAATAAGAATGACCATATAAAATTTGTGGATATAAATGAAAAAAATG        420
PfCox19_pldb      TGTTATCAAAATTAAATAAGAATGACCATATAAAATTTGTGGATATAAATGAAAAAAATG        412
                  ************************************************************

PfCox19_vect      ATAGGAATGATTTTATTCTCTTAGATATTAATAATAAGGAAAATACAAATAAAAAGATAA        480
PfCox19_pldb      ATAGGAATGATTTTATTCTCTTAGATATTAATAATAAGGAAAATACAAATAAAAAGATAA        472
                  ************************************************************

PfCox19_vect      ATACAGACGATTTAAAAAATTCAGAAATTAACGATGAAAAAAAAATAGCTATAAGAAGAA        540
PfCox19_pldb      ATACAGACGATTTAAAAAATTCAGAAATTAACGATGAAAAAAAAATAGCTATAAGAAGAA        532
                  ************************************************************

PfCox19_vect      AAGAGGCTGAGGGTTATTTAGCTGTGACTGCAGAT     575
PfCox19_pldb      AAGAGGCTGAGGGTTATTTAGCTG-----------     556
                  ************************
```

Figure 5.3. Alignment of *P. falciparum* Cox19 cloned sequence with the PlasmoDB gene sequence
The *P. falciparum* Cox19 cloned sequence in pMal-c2x-r*Pf*Cox19 plasmid (*Pf*Cox19_vect) and the PlasmoDB sequence (*Pf*Cox19_pldb) (PF3D7_1201800) were aligned using Clustal Omega. The underlined nucleotide bases at the 5' and 3' ends indicate the primer sequences used to amplify *Pf*Cox19 coding region from the *P. falciparum* gDNA. The reverse complement of the underlined sequence at the 3' end was used as the reverse primer.

The sequence of r*Pf*Cox19 from the recombinant pMal-c2x-r*Pf*Cox19 plasmid was found to be identical to the PlasmoDB sequence, except for the additional stop codon at the 3' end (Figure 5.3). The cloned 556 bp sequence encodes 185 amino acids of the *P. falciparum*

Cox19 amino acid sequence, excluding the first four and the last 29 amino acid residues (Figure 5.4).

A

>*Pf*Cox19
MDIK**RQLVKKPDRGSFLLDHNNECTSIKQKYLKCLKENNNDHICCRDHSKEYFICRMDNN**
LLERQSLNDLGFIEHEEKNESRIKNFKDVYSYNIYNENMERISRNMHDNIKSNNLLLNEN
NMLSKLNKNDHIKFVDINEKNDRNDFILLDINNKENTNKKINTDDLKNSEINDEKKIAIR
RKEAEGYLAGKEYIKTLLEKKQKKTFFFLNEIFKSNNV

B

>rMBP-*Pf*Cox19
MKIEEGKLVIWINGDKGYNGLAEVGKKFEKDTGIKVTVEHPDKLEEKFPQVAATGDGPDI
IFWAHDRFGGYAQSGLLAEITPDKAFQDKLYPFTWDAVRYNGKLIAYPIAVEALSLIYNK
DLLPNPPKTWEEIPALDKELKAKGKSALMFNLQEPYFTWPLIAADGGYAFKYENGKYDIK
DVGVDNAGAKAGLTFLVDLIKNKHMNADTDYSIAEAAFNKGETAMTINGPWAWSNIDTSK
VNYGVTVLPTFKGQPSKPFVGVLSAGINAASPNKELAKEFLENYLLTDEGLEAVNKDKPL
GAVALKSYEEELAKDPRIAATMENAQKGEIMPNIPQMSAFWYAVRTAVINAASGRQTVDE
ALKDAQTNSSSNNNNNNNNNNLGIEGRISEFGSSRVD**RQLVKKPDRGSFLLDHNNECTSI**
KQKYLKCLKENNNDHICCRDHSKEYFICRMDNNLLERQSLNDLGFIEHEEKNESRIKNFK
DVYSYNIYNENMERISRNMHDNIKSNNLLLNENNMLSKLNKNDHIKFVDINEKNDRNDFI
LLDINNKENTNKKINTDDLKNSEINDEKKIAIRRKEAEGYLAAA

Figure 5.4. *P. falciparum* Cox19 amino acid sequence
(A) The cloned *Pf*Cox19 amino acid sequence derived from the *P. falciparum* gDNA is shown in bold print. (B) The recombinant MBP-*Pf*Cox19 protein amino acid sequence derived from the pMal-c2x-r*Pf*Cox19 plasmid. The four conserved cysteines are in blue.

5.2.2 Isolation of the recombinant MBP-*Pf*Cox19 protein

After expressing rMBP-*Pf*Cox19 (section 2.6.2), the protein was isolated using an amylose affinity resin and protein eluted from the matrix in a single step with maltose concentration of 0.3 mM (Figure 5.5). The unbound protein eluted over the first 15 fractions and the bound recombinant protein was eluted between fractions 36 to 41 (Figure 5.5A). Both a 45 kDa protein corresponding to the size of the MBP fusion partner and the expressed ~66 kDa band consisting of MBP and *Pf*Cox19 was observed (Figure 5.5B).

Table 5.1 is a protein purification table showing protein yield from the purification steps of the rMBP-*Pf*Cox19 protein from duplicate 400 ml cultures. About 109 mg protein was obtained in the soluble cell lysate from the lysis of 2.22 g bacterial pellet, corresponding to a

yield of ~49 mg/g bacterial pellet. About 0.44 mg/g bacterial pellet of rMBP-*Pf*Cox19 was obtained.

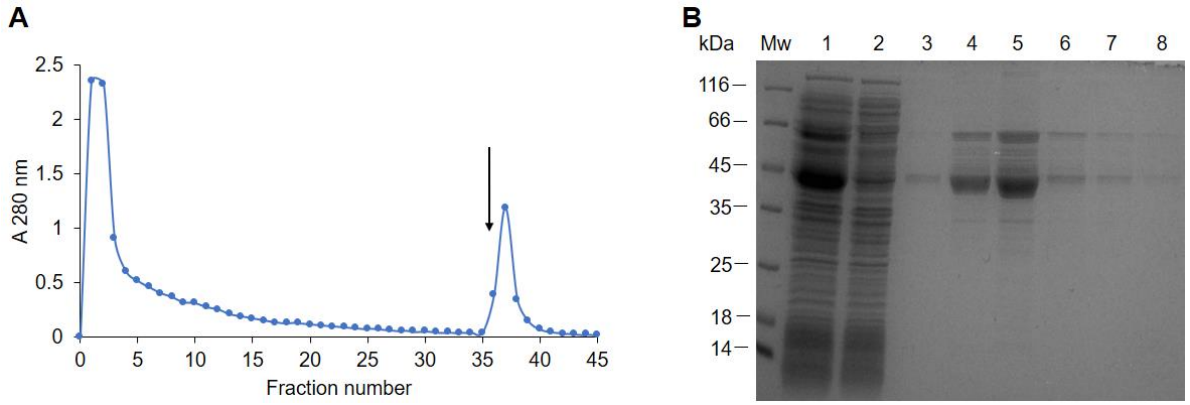

Figure 5.5. Recombinant expression and affinity purification of the rMBP-*Pf*Cox19
The rMBP-*Pf*Cox19 was purified with an amylose affinity column. (A) Elution profile from the amylose affinity matrix. Arrow indicates the point of elution with maltose. (B) Samples from the purification steps were analysed on a 12.5% reducing SDS-PAGE. Molecular weight marker (M); soluble cell lysate (lane 1); unbound fraction from the amylose affinity matrix (2); final wash (lane 3); eluents from the amylose affinity matrix (lanes 4 to 8). Lanes 4 to 8 corresponds to fractions 36 to 40 (on panel A) respectively. The arrow indicates the point of elution of rMBP-*Pf*Cox19.

Table 5.1. Purification table for the affinity purified rMBP-*Pf*Cox19

	Total vol. (ml)	**Total protein* (mg)**	**Yield (%)**	**Yield (mg/g bacterial pellet)**
Soluble cell lysate	32.50	109.50 ± 2.12	100	49.01 ± 0.94
Unbound fraction	32	100.87 ± 0.26	92.11 ± 2.05	45.44 ± 0.12
Washes	70	3.45 ± 0.06	3.15 ± 0.07	1.55 ± 0.03
Affinity purified rMBP-*Pf*Cox19	0.26 ± 0.04	0.98 ± 0.10	0.90 ± 0.11	0.44 ± 0.04

Data presented are Mean ± SD values from duplicate purifications.
Bacterial pellet = 2.22 ± 0.04 g.
* Determined with Bradford assay

Figure 5.6 illustrates that purified rMBP-*Pf*Cox19 was identified on a western blot by mouse monoclonal anti-MBP antibodies. The 66 kDa rMBP-*Pf*Cox19 and the 45 kDa MBP were both detected by the anti-MBP antibody as expected (Figure 5.6B).

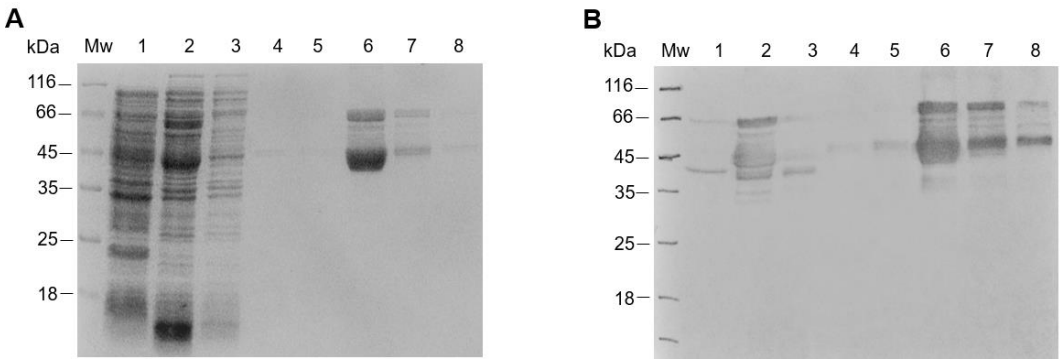

Figure 5.6. Detection of rMBP-*Pf*Cox19 by anti-MBP antibodies in a western blot
The rMBP-*Pf*Cox19 was identified on a western blot. (A) Coomassie-stained 12.5% reducing SDS-PAGE reference gel. (B) Western blot probed with mouse monoclonal anti-MBP IgG. Molecular weight marker (M); lane 1, uninduced soluble cell lysate; lane 2, induced soluble cell lysate; lane 3, unbound fraction from the amylose affinity matrix; lane 4, final wash; lanes 5 to 8, eluents from the amylose affinity matrix. Antibodies were; mouse monoclonal anti-MBP IgG (1:12000) and goat anti-mouse IgG-HRPO (1:12000).

5.2.3 IgY antibodies were raised in chicken against rMBP-*Pf*Cox19

Two chickens were immunised four times with purified rMBP-*Pf*Cox19 and IgY was isolated from the eggs of the chickens. Antibody titres in eggs were monitored by ELISA over a 14-week period (Figure 5.7A). Antibody responses increased from week two and remained high to week 14. IgY was isolated from eggs and affinity purified with a rMBP-*Pf*Cox19 AminoLink™ affinity matrix (Figure 5.7B). About 33 and 41 mg of affinity purified anti-rMBP-*Pf*Cox19 IgY were obtained from chickens one and two respectively. The chicken affinity-purified antibodies detected rMBP-*Pf*Cox11Ct and lower proteins but did not detect any protein in the uninfected red blood cell lysate or *E. coli* host cell (Figure 5.7C).

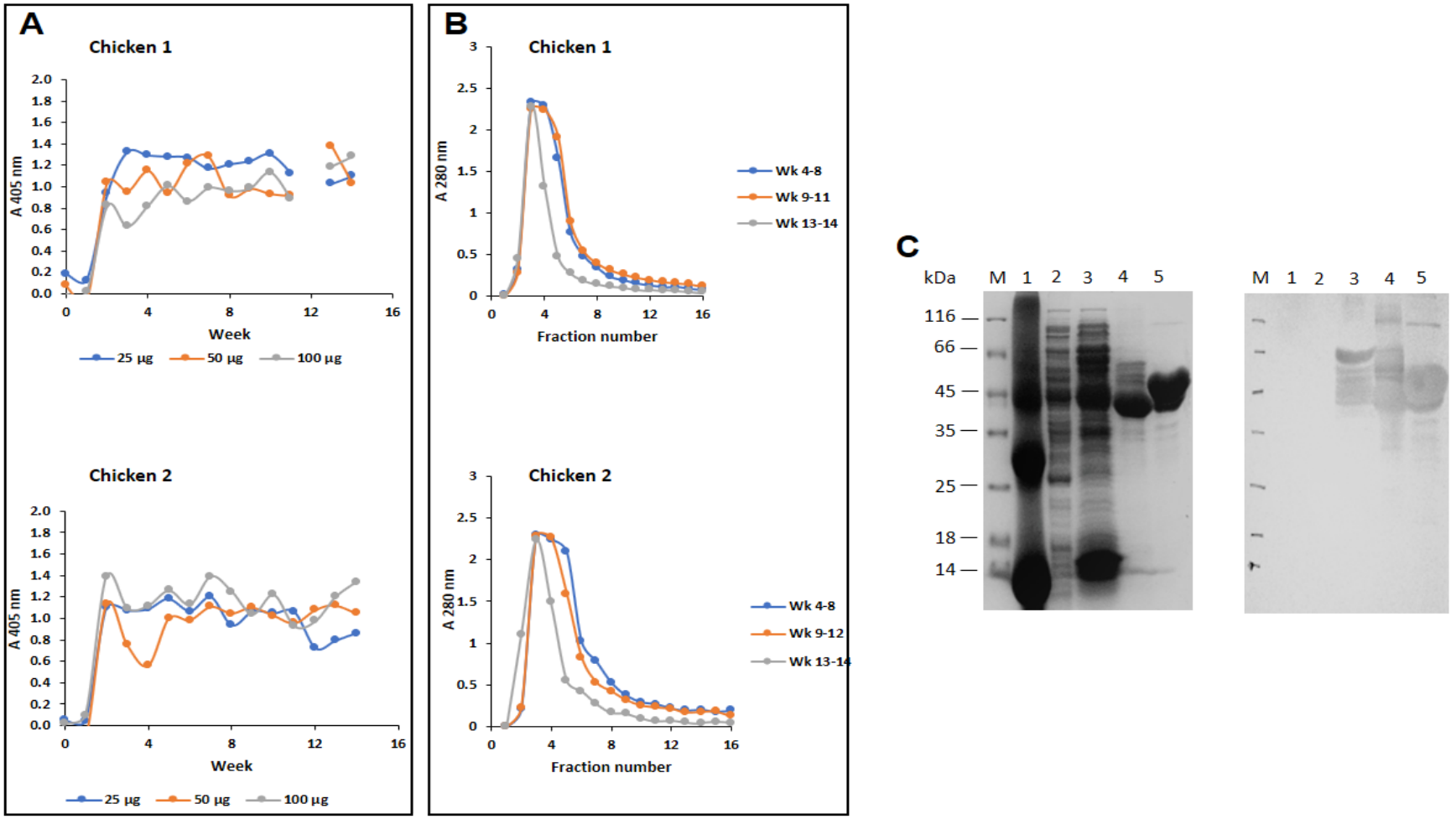

Figure 5.7. Affinity purified antibodies detected rMBP-*Pf*Cox19

Antibodies against rMBP-*Pf*Cox19 were monitored in chicken eggs by ELISA over 14 weeks. (A) Plates were coated with 150 ng/well rMBP-*Pf*Cox19. IgY (25, 50 and 100 µg/ml) primary antibody and rabbit anti-chicken IgG-HRPO (1:15 000), and plates read at OD_{405}. (B) Pools of isolated IgY from eggs were affinity purified with a rMBP-*Pf*Cox19 AminoLink™ column. (C) A 12.5% reducing SDS-PAGE Coomassie-stained reference gel (left panel). Affinity-purified IgY detected rMBP-*Pf*Cox19 on a western blot (right panel). Molecular weight marker (M); lane 1, uninfected human red blood cell lysate; lane 2, untransformed *E. coli* (BL21) lysate; lane 3, soluble rMBP-*Pf*Cox19 lysate; lane 4, affinity purified rMBP-*Pf*Cox19; lane 5, recombinant MBP.

5.2.4 Detection of the *P. berghei* Cox19 with antibodies against rMBP-*Pf*Cox19

Due to a 53% amino acid sequence identity between the cloned *P. falciparum* Cox19 region and the *P. berghei* orthologue (Figure 5.8A), the anti-rMBP-*Pf*Cox19 antibody was used to detect the presence of native Cox19 in the murine malaria parasite cell lysate. Detection of lactate dehydrogenase (LDH) with LDH antipeptide (APGKSDKEWNRDDL) antibody in the parasite lysate served as a reference and internal control.

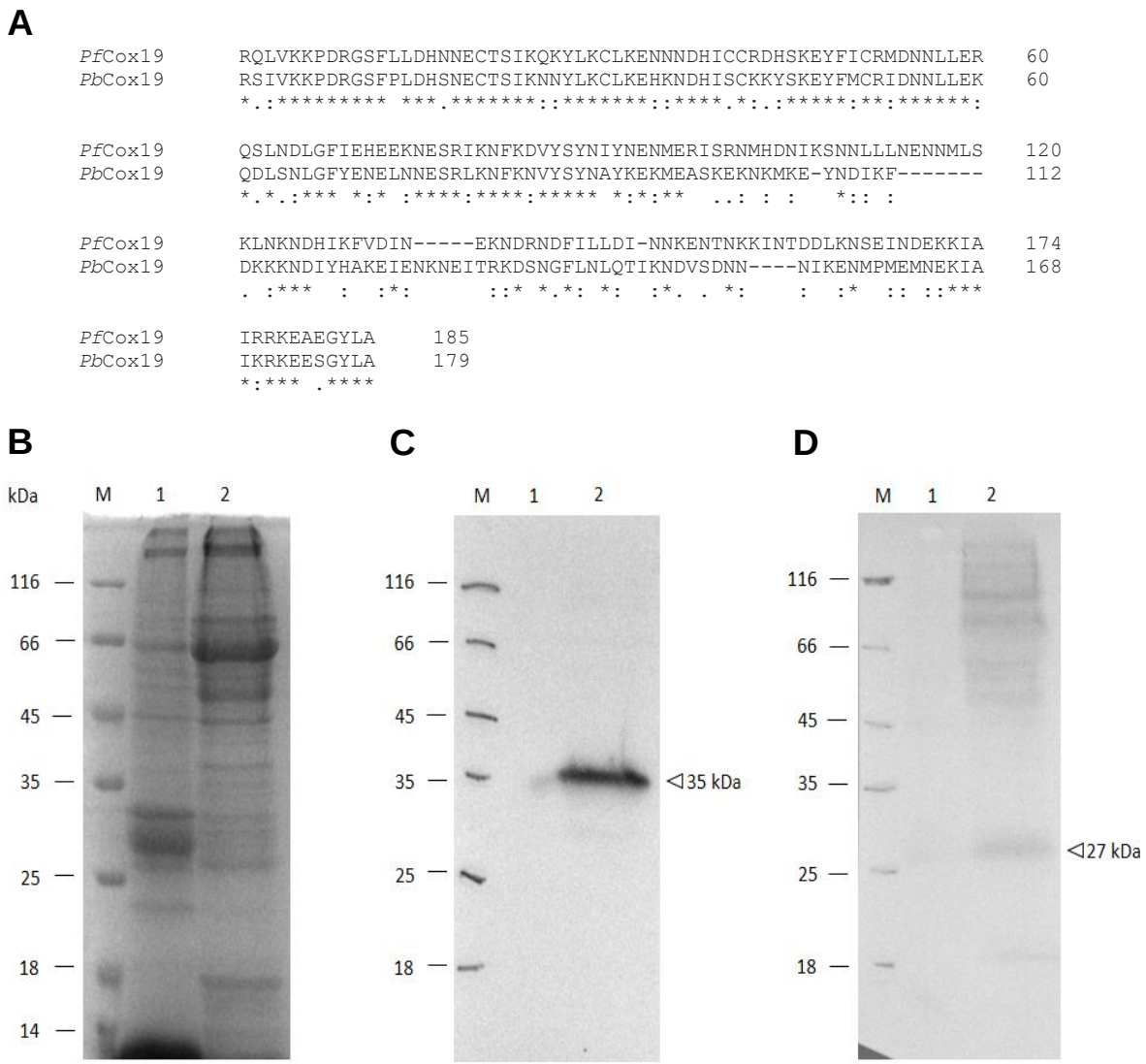

Figure 5.8. Anti-rMBP-*Pf*Cox19 antibody detection of the Cox19 in *P. berghei* infected mouse red blood cell lysate

(A) Alignment of the *P. falciparum* and *P. berghei* Cox19 amino acid sequences. The annotation "*****", denote conserved residue, while "**:**"and "**.**" denote conserved and semi-conserved substitutions respectively. Cox19 was detected in *P. berghei* infected BALB/c mouse red blood cell lysate using enhanced chemiluminescence (ECL). (B) A 12.5% reducing SDS-PAGE Coomassie-stained reference gel. (C) Western blots probed with lactate dehydrogenase antipeptide antibody or (D) IgY anti-rMBP-*Pf*Cox19, and goat anti-mouse IgG-HRPO (1:12000). Molecular weight marker (M); uninfected (lane 1) and infected (lane 2) *P. berghei* BALB/c mouse red blood cell lysates.

A 35 kDa protein corresponding to *P. berghei* LDH was detected by the pan-specific LDH antipeptide antibody in the *P. berghei* infected BALB/c mouse red blood cell lysate (Figure 5.8B). The anti-rMBP-*Pf*Cox19 antibody detected a ~27 kDa protein in the *P. berghei* infected BALB/c mouse red blood cell corresponding to the expected size, ~26.2 kDa. Proteins of molecular weight higher than 45 kDa were also detected.

5.2.5 Binding of copper to rMBP-*Pf*Cox19 measured with the bicinchoninic acid (BCA) release assay

The *in vitro* and *in vivo* copper binding potential of rMBP-*Pf*Cox19 was assessed using the BCA-release assay (section 2.8.1). The formation of a purple Cu(I)-BCA following protein-complex disruption at an alkaline pH was monitored at 354 nm as described in Figure 4.16.

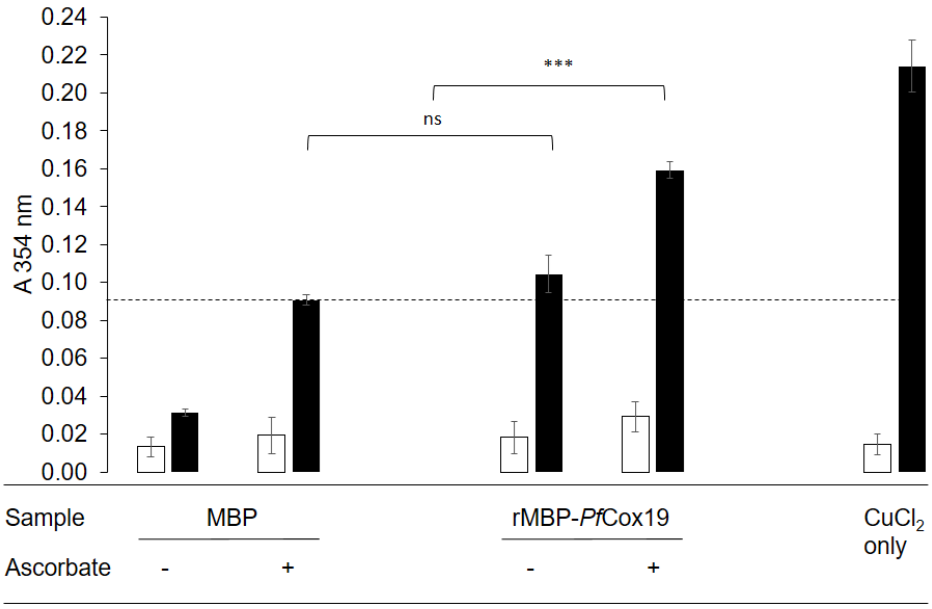

Figure 5.9. Binding of copper to rMBP-*Pf*Cox19 *in vitro* measured by BCA release assay
Affinity-purified rMBP-*Pf*Cox19 or MBP alone were incubated with $CuCl_2$ in the absence (–) or presence (+) of ascorbic acid *in vitro*. The BCA release assay was used to detect copper without (open bars) or with (solid bars) the addition of ascorbic acid. The copper standard ($CuCl_2$) was equimolar to the amount of protein. The horizontal broken line represents the cut-off for copper bound to MBP. Results are means ± S.E. of triplicate measurements from duplicate samples. *** denotes statistical significance ($P<0.001$), while, ns denotes no significant difference as determined by Student's *t*-test.

rMBP-*Pf*Cox19 binds Cu(I) and not Cu(II) as indicated in the absence and presence of ascorbate *in vitro* (Figure 5.9). The MBP control binds less copper. EDTA, which chelates copper, inhibited the Cu(I)-BCA complexation (Figure 5.10).

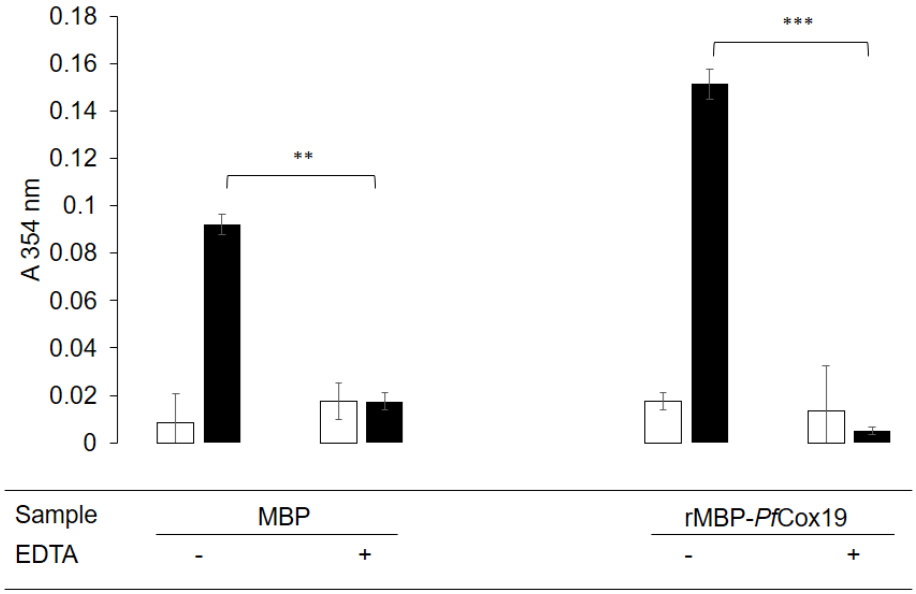

Figure 5.10. The effect of EDTA on copper binding to rMBP-*Pf*Cox19 *in vitro*
Affinity-purified rMBP-*Pf*Cox19 and MBP was incubated with $CuCl_2$ and ascorbate in the absence (-) or presence (+) of EDTA. Copper was detected without (open bars) or with (solid bars) the addition of ascorbic acid in BCA release assay at 354 nm. The data presented are mean ± SD. of a duplicate. ** and *** denotes statistical significance at P<0.01 and P<0.001 respectively, as determined by Student's t-test.

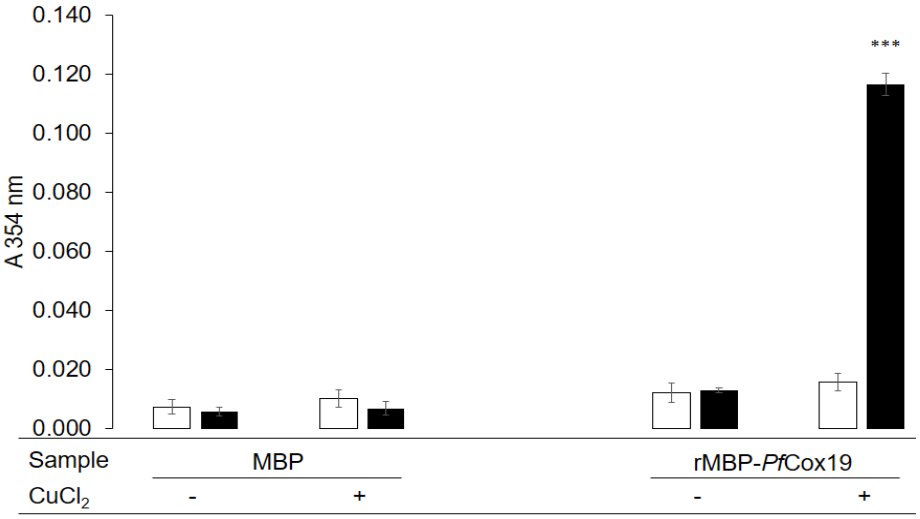

Figure 5.11. Binding of copper to rMBP-*Pf*Cox19 *in vivo* measured by the BCA release assay
0.5 mM $CuCl_2$ was added to the *E. coli* growth medium after the induction of recombinant protein expression. Following affinity purification of the recombinant proteins, copper bound *in vivo* was detected by the BCA release assay without (open bars) or with (solid bars) the addition of ascorbic acid. The BCA-Cu^+ complex was detected at 354 nm. Results are mean ± S.E. of triplicate measurements from duplicate samples. *** denotes statistical significance (P<0.001) as determined by Student's *t*-test.

In vivo copper binding of rMBP-PfCox19

Copper was added to the growth medium of *E. coli* cells expressing rMBP-*Pf*Cox19. The protein was affinity purified and the presence of copper in rMBP-*Pf*Cox19 assessed. rMBP-*Pf*Cox19 was shown to bind copper *in vivo* (P<0.001) compared to the MBP control

(Figure 5.11). The oxidation state of copper binding to rMBP-*Pf*Cox19 could not be assessed *in vivo*, however, copper is reported (Davis and O'Halloran, 2008) to be reduced inside cells.

5.2.6 rMBP-*Pf*Cox19 inhibition of copper-catalysed oxidation of ascorbic acid

The effect of rMBP-*Pf*Cox19 on copper-catalysed ascorbic acid oxidation was assessed (Figure 5.12). Ascorbic acid had a relatively sustained absorbance reading over 300 s. The addition of 8 µM copper to the solution of ascorbic acid resulted in an ascorbic acid oxidation. The oxidation of ascorbic acid with copper was inhibited by rMBP-*Pf*Cox19 and to a lesser extent by MBP.

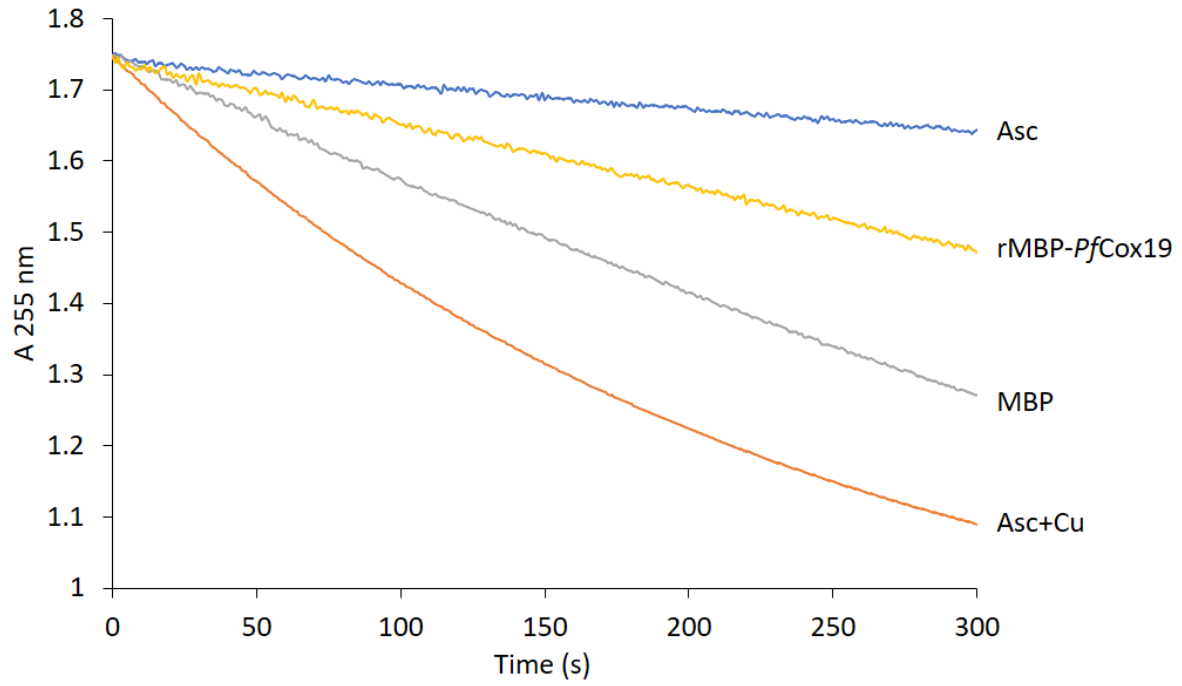

Figure 5.12. Copper-catalysed oxidative degradation of ascorbic acid in the presence of rMBP-*Pf*Cox19
Measurement of the rate of ascorbic acid oxidation by 8 µM Cu^{2+} over 300 s at pH 4.5 in the presence or absence of 5 µM rMBP-*Pf*Cox19. MBP was included as a control. Ascorbic acid (Asc); Ascorbic acid with copper (Asc + Cu).

5.2.7 Copper binding measured with differential scanning fluorimetry

The melting temperature (T_m) of rMBP-*Pf*Cox19 without or with copper was explored to determine the copper binding of rMBP-*Pf*Cox19 using SYPRO® orange dye (Figure 5.13). The T_m of affinity purified rMBP-*Pf*Cox19 and MBP was scanned through a range of 25 to 90°C at a ramp of 0.3°C/min by monitoring the SYPRO® orange fluorescence emission. The intensity of the rMBP-*Pf*Cox19 fluorescence compared to MBP control is much higher, implying the rMBP-*Pf*Cox19 has more hydrophobic regions exposed when it is heated. MBP

had a melting temperature (T_m) of 48.6 ± 0.44ºC and 48.99 ± 0.23ºC in the absence and presence of copper respectively, with a change in T_m (ΔT_m) of +0.39ºC. rMBP-*Pf*Cox19 had a T_m of 54.2 ± 0.09ºC and 55.04 ± 0.23ºC in the absence and presence of copper respectively, with a ΔT_m of +0.84ºC.

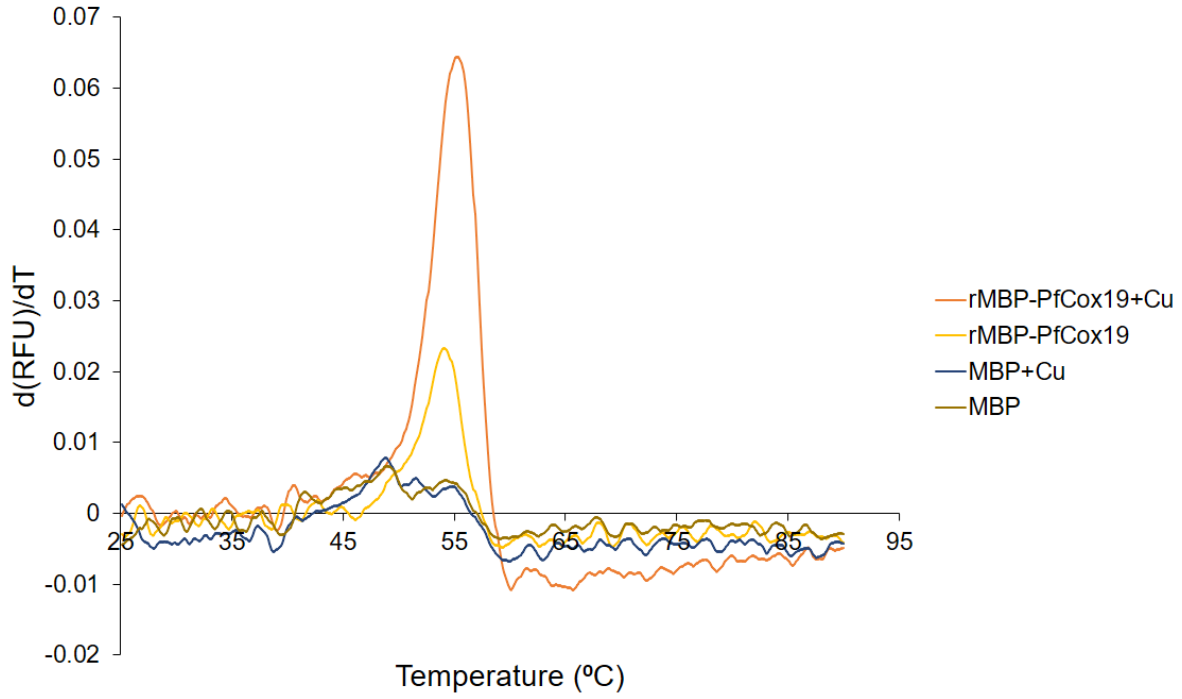

Figure 5.13. The first derivative of the differential scanning fluorimetry for rMBP-*Pf*Cox19 with or without copper
The figure shows the change in rMBP-*Pf*Cox19 and MBP melting temperatures with and without copper.

5.2.8 Copper tolerance of *E. coli* (BL21) host cells expressing MBP-*Pf*Cox19

E. coli cells harbouring the pMal-c2x-r*Pf*Cox19 plasmid were grown in the presence of 0 to 8 mM copper (Figure 5.14B). *E. coli* cells expressing rMBP-*Pf*Cox19 tolerated 8 mM copper with an IC_{50} of 7.55 mM copper (data not shown).

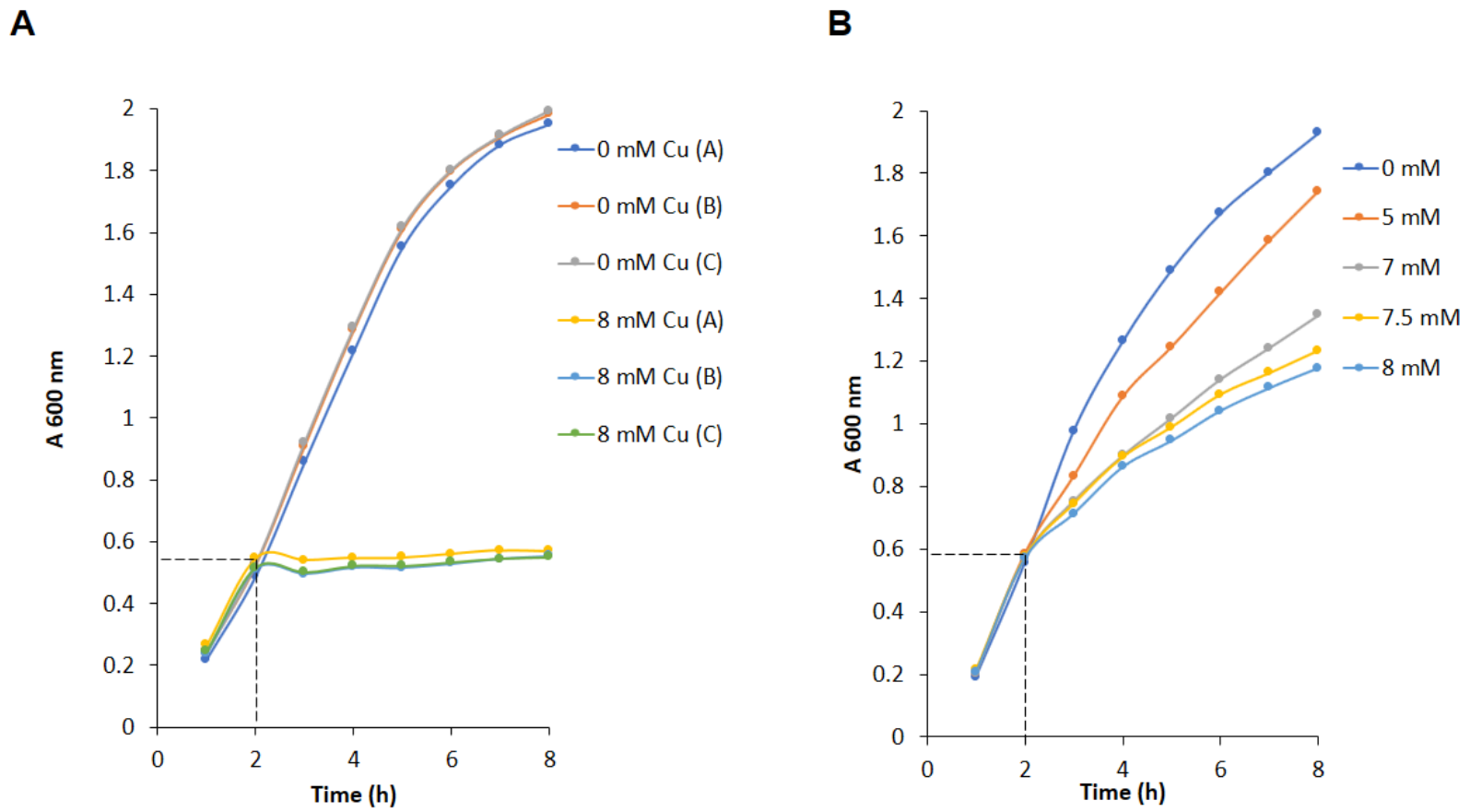

Figure 5.14. Effect of copper on the growth of *E. coli* (BL21) cells expressing rMBP-*Pf*Cox19
E. coli (BL21) with the pMal-c2x plasmid or pMal-c2x-r*Pf*Cox19 plasmid was grown in the presence of 0 and 8 mM copper and growth was monitored at an hourly interval by OD_{600} for 6 h. (A) Triplicate *E. coli* (BL21) cultures with pMal-c2x, with or without copper. (B) Cultures of *E. coli* (BL21) with pMal-c2x-r*Pf*Cox19, with 0 to 8 mM copper. The dotted lines indicate the addition of copper and IPTG.

5.3 Discussion

5.3.1 Cloning the *P. falciparum* Cox19 sequence

The *P. falciparum* Cox19 open reading frame contains 657 bp, and 556 bp encoding 185 amino acids, excluding the first four and the last 29 amino acid residues were amplified (Figure 5.4). The exclusion of these amino acid residues was to facilitate primer design. A 556 bp sequence was amplified from *P. falciparum* genomic DNA and cloned into the pTZ57R/T cloning vector, then subcloned into a pMal-c2x expression vector to be recombinantly expressed as an MBP fusion protein (Figure 5.2). Expressing the recombinant *P. falciparum* Cox19 as a His-tagged protein is likely to interfere with downstream characterisation, as His-tags have been shown to interact with copper (Watly *et al.*, 2014; Wijekoon *et al.*, 2016). MBP interacts minimally with copper (LaGier *et al.*, 2001). The cloned insert was sequenced and had 100% identity to the *P. falciparum* Cox19 gene PlasmoDB sequence.

5.3.2 Recombinant expression and isolation of MBP-*Pf*Cox19

rMBP-*Pf*Cox19 expression was induced with 0.5 mM IPTG in 2xYT medium at 30ºC for 4 h, and affinity purified with an amylose resin. The affinity-purified rMBP-*Pf*Cox19 was detected on a western blot with a monoclonal anti-MBP antibody. About 0.98 mg rMBP-*Pf*Cox19 was obtained from 400 ml (~2.22 g wet weight bacterial pellet) bacterial cultures, which is about 0.9% of the soluble cell lysate. A yield of about 25 to 34 mg per 50 ml culture was obtained in a study with a repertoire of proteins (Sivashanmugam *et al.*, 2009). The rMBP-*Pf*Cox19 yield is higher than that obtained for the recombinantly expressed strep-tag II fused yeast Cox19 (Rigby *et al.*, 2007). Choveaux *et al.* (2012) reported similar yields for the *P. falciparum* copper transport protein (Ctr1) protein.

5.3.3 Raising IgY antibodies against rMBP-*Pf*Cox19

Purified rMBP-*Pf*Cox19 served as an immunogen for the production of polyclonal antibodies in chickens. Chickens being evolutionarily distant from mammals make them a good host for antibody production against mammalian proteins (Larsson and Sjoquist, 1990). Since chicken antibodies are isolated from egg yolk, and many eggs are laid by chickens, high antibody yields are attainable compared to the sera of immunised animals (Gassmann *et al.*, 1990; Lee *et al.*, 2017). About 33 and 41 mg of affinity purified anti-rMBP-*Pf*Cox19 IgY were obtained from each chicken. The antibody response to the rMBP-*Pf*Cox11Ct protein in both chickens was similar to that reported in previous studies for other plasmodial antigens

(Hurdayal *et al.*, 2010; Krause *et al.*, 2015). The antibodies detected rMBP-*Pf*Cox19 protein and did not detect proteins from the uninfected red blood cell or *E. coli* host cell.

5.3.4 IgY antibodies against the rMBP-*Pf*Cox19 detected the native Cox19 protein

Anti-rMBP-*Pf*Cox19 IgY antibodies detected a protein band of ~27 kDa *P. berghei* Cox19 on a western blot (Figure 5.8). Protein bands above 45 kDa were also detected, and the nature of these proteins is unknown. An attempt to detect the protein in a *P. falciparum* lysate was unsuccessful, possibly due to the proteins not being expressed during developmental stage of the sample. Transcriptional analysis suggests *P. falciparum* Cox19 to be expressed mainly in the trophozoite stage (Aurrecoechea *et al.*, 2009; Mok *et al.*, 2007).

5.3.5 Assessing the binding of copper to rMBP-*Pf*Cox19 using the BCA release assay

The *in vitro* and *in vivo* copper binding of rMBP-*Pf*Cox19 was measured with different approaches. The spectrophotometric based BCA copper release assay showed that the rMBP-*Pf*Cox19 protein bound copper *in vitro* (Figure 5.9) and *in vivo* during *E. coli* host cell culture (Figure 5.11). Like an earlier study (Rigby *et al.*, 2007), rMBP-*Pf*Cox19 bound Cu(I) and not Cu(II). Similarly, the *P. falciparum* copper transport protein (Ctr1) and *P. falciparum* Cox17 bound Cu(I) and not Cu(II) (Choveaux *et al.*, 2012; 2015). Recombinant yeast Cox19 was previously shown to bind copper in a 1:1 stoichiometry, while the native protein binds variable amount of copper in the mitochondrial intermembrane space (Rigby *et al.*, 2007). *In vitro* copper binding of rMBP-*Pf*Cox19 was inhibited by the metal chelator, EDTA.

5.3.6 Measuring rMBP-*Pf*Cox19 inhibition of copper-catalysed ascorbic acid oxidation

The second approach was to assess the rate at which copper-catalysed ascorbic acid oxidation was inhibited by rMBP-*Pf*Cox19. Ascorbic acid is relatively stable to atmospheric oxidation, but undergoes metal-catalysed oxidative degradation (Martell, 1982). The rate of metal-catalysed ascorbic acid oxidation is decreased by metal chelators through the formation of a mixed ligand chelate complex (Khan and Martell, 1967). rMBP-*Pf*Cox19 inhibited the copper-catalysed ascorbic acid oxidation (Figure 5.12) as has been reported for the *P. falciparum* copper transport protein (Ctr1) and Cox17 (Choveaux *et al.*, 2012; 2015).

5.3.7 rMBP-*Pf*Cox19 copper binding evaluated using differential scanning fluorimetry

The third approach to assess copper binding was differential scanning fluorimetry. A substrate or coenzyme binding to a protein could stabilise or destabilise the protein structure, leading to a change in the melting temperature (ΔT_m) of the protein. The binding of copper to rMBP-*Pf*Cox19 appeared to stabilise the protein, with a T_m increase of 0.84^{o}C. This suggests that Cu(I) binds native rMBP-*Pf*Cox19 leading to an ordered conformation of the protein structure (Boivin *et al.*, 2013; Pace and McGrath, 1980). Although the free and copper bound Cox19 exists as stable dimeric molecules, tetrameric and higher oligomeric forms of both species have been identified (Rigby *et al.*, 2007).

5.3.8 rMBP-*Pf*Cox19 enables *E. coli* host cells to tolerate harmful copper levels

The fourth approach was to assess the ability of the rMBP-*Pf*Cox19 to confer copper tolerance to the *E. coli* (BL21) host cell. The *E. coli* cells expressing MBP were sensitive to 8 mM copper (Figure 5.14A). The expression of rMBP-*Pf*Cox19 enabled the growth of *E. coli* host cells in the presence of 8 mM copper (Figure 5.14B). This implies the rMBP-*Pf*Cox19 enables *E. coli* host cells growth despite the metabolic stress induced by the heterologous expression of recombinant proteins and the oxidant, copper (Carneiro *et al.*, 2013; Glick, 1995). An earlier study has shown the Gram-positive bacteria *Enterococcus hirae* to tolerate 8 mM copper (Solioz and Stoyanov, 2003). The overexpression of Cox19 in yeast at toxic copper levels was recently demonstrated to increase the copper tolerance of the yeast cells (Murtha *et al.*, 2018). Other studies have shown recombinantly expressed copper binding proteins improve the levels of copper tolerated by the *E. coli* host cells (Vita *et al.*, 2016; Yang *et al.*, 2017).

5.3.9 Conclusion

The results in this chapter from the characterisation of the recombinant protein using; the BCA release assay, differential scanning fluorimetry, inhibition of the ascorbic acid oxidation and assessment of the *E. coli* host cell copper tolerance, showed the *P. falciparum* Cox19 bound copper *in vitro* and in an *in vivo* setting. These results to the best of my knowledge are the first to characterise Cox19 in malaria parasite.

Chapter 6
General discussion

6.1 Brief overview

The global adoption of artemisinin-based combination therapies (ACTs) as first-line treatment for *P. falciparum* malaria has been instrumental in the success achieved in the control and cure of malaria. This success is dependent on the clinical efficacy of the first-line ACTs. Despite progress in the eradication of malaria, the disease remains a global burden, killing hundreds of thousands of individuals annually (WHO, 2016; 2017). Several novel antimalarials at different developmental stages target membrane structure and transport, nucleotide synthesis and protein translation in the parasite (Blasco *et al.*, 2017; Cowman *et al.*, 2016; Flannery *et al.*, 2013). There is a need to further explore the potential of other biological processes in the parasite as targets for novel antimalarial drugs.

6.2 Current understanding of plasmodial copper homeostasis

The genes for 14 *Plasmodium* copper-binding proteins have been identified in the plasmodial genome and four proteins have been characterised (Choveaux *et al*., 2015). The physiological processes involved in the uptake, distribution, utilisation and regulation of copper in *Plasmodia* are yet to be characterised. Orthologues of some eukaryotic copper protein genes could not be identified in the parasite (Choveaux *et al*., 2015). The unidentified copper protein orthologues may not be needed by the parasite or the parasite utilises the host proteins or the proteins have been supplanted by as yet unidentified copper proteins in a similar manner to the ADP/ATP translocase in *Encephalitozoon cuniculi* which supplants the function of the ATPase complex (Katinka *et al.*, 2001). Though *Plasmodium* lacks Cu/Zn superoxide dismutase and catalase, the parasite imports erythrocyte Cu/Zn superoxide dismutase which could be used by the parasite as a source of copper (Fairfield *et al.*, 1983). Erythrocyte Cu/Zn superoxide dismutase is digested in the parasite's food vacuole, releasing copper and zinc (Rasoloson *et al.*, 2004). *Plasmodium* Ctr1 and CuP-ATPase proteins have been proposed as two channels for copper uptake by the parasite due to their localisation to the plasma membrane and the recombinant proteins bind copper (Choveaux *et al.*, 2012; Rasoloson *et al.*, 2004). The role of CuP-ATPase in copper uptake by the parasite is debatable following evidence that the protein is localised to unidentified intracellular vesicle-like structures at the cell periphery, and not the plasma membrane in *P. berghei* (Kenthirapalan *et al.*, 2014). CuP-ATPase was then

proposed to be involved in intracellular copper redistribution and storage (Kenthirapalan *et al.*, 2014), or copper export, deduced from the decrease in intracellular copper in *P. falciparum* infected erythrocyte as the parasite develops compared to the uninfected erythrocyte (Kenthirapalan *et al.*, 2014; Rasoloson *et al.*, 2004). The *P. falciparum* Ctr1 protein is a likely channel for copper uptake by the parasite. *P. falciparum* Cox17 is found in the cytoplasm and the recombinant protein bound copper (Choveaux *et al*., 2015). Two plasmodial copper chaperones, Cox11 and Cox19 were identified and characterised in this study.

6.3 Plasmodial copper homeostasis as a potential antimalarial drug target

The increase in drug resistance in malaria outpaces efforts to develop new drugs, leading to an expanded search for novel molecular drug targets. This study focused on *Plasmodium* copper homeostasis as a possible antimalarial drug target. Copper regulation by *Plasmodium* was demonstrated with the finding that intracellular copper concentration decreased in *P. falciparum* infected erythrocyte compared to an uninfected erythrocyte (Rasoloson *et al.*, 2004). However, the mechanism involved in lowering the copper levels in the infected erythrocyte is not understood. When copper available to the parasite is decreased the parasite's fertility and development in the blood and liver stages are affected (Kenthirapalan *et al.*, 2014; 2016; Rasoloson *et al.*, 2004; Voorberg-van der Wel *et al.*, 2017). The growth of *P. falciparum* parasites was inhibited *in vitro* using the copper chelators, diethyldithiocarbamate (DDC) and neocuproine (Asahi *et al.*, 2014; Meshnick *et al.*, 1990; Rasoloson *et al.*, 2004), suggesting copper to be essential for the parasite development. Similarly, the viability of both liver schizonts and hypnozoites in *P. cynomolgi* was affected by neocuproine (Voorberg-van der Wel *et al.*, 2017). Preventing copper uptake and mobilisation by gene knockout of copper transport protein (Ctr1) and copper-transporting P-type ATPase (CuP-ATPase) in *P. berghei* impaired parasite fertility and transmission through the mosquito vector (Kenthirapalan *et al.*, 2014; 2016). Targetting plasmodial copper homeostasis could be vital to developing new antimalarial drugs.

Interestingly, copper(II) complexation to three antimalarial drug candidates; buparvaquone, pyridine-2-carboxamidrazone, and 3-arylazo-4-hydroxy-1,2-naphthoquinone potentiated their antimalarial activities (Gokhale *et al.*, 2003a; 2003b; 2006). Though the mechanism for the improved activities was not determined, it was however proposed that the four-coordinate planar geometry coupled with a positive reduction potential of the Cu(II)-

complex enhanced the internalisation and efficacy of these compounds (Gokhale *et al.*, 2003a; 2003b).

6.4 Identification of a putative *P. falciparum* Cox11 and Cox19

Some novel molecular drug targets and essential genes for the development and pathogenesis of the parasite have been identified in the *P. falciparum* genome (Jiménez-Díaz *et al.*, 2014; McNamara *et al.*, 2013; Paquet *et al.*, 2017; Spillman *et al.*, 2013; Vaidya *et al.*, 2014). Only a few of the ~5300 *P. falciparum* genes identified to date have been confirmed to code for protein (Mehlin *et al.*, 2006) and 14 have been identified as copper-binding proteins including the cytochrome c oxidase (CcO) assembly accessory proteins, Cox11 and Cox19 (

Table **3.1**) (Choveaux *et al.*, 2015; Gardner *et al.*, 2002; Rasoloson *et al.*, 2004).

The current study analysed the amino acid sequences for plasmodial Cox11 and Cox19 *in silico*. An analysis of Cox11 orthologues in multiple plasmodial species showed the presence of three conserved C-terminal cysteines (Cys60, Cys155 and Cys157), two of which (Cys155 and Cys157) span the copper-binding CFCF motif (Banci *et al.*, 2004; Carr *et al.*, 2002; Thompson *et al.*, 2010) and the third is a short distance from the motif. All *Plasmodium* Cox11 sequences, like the well characterised sequences of other species, have a single transmembrane spanning domain (Figure 3.2). The yeast Cox11 transmembrane domain was demonstrated to be essential for cellular respiration when the matrix and transmembrane domains of *S. cerevisae* Cox11 were supplanted with those of *S. cerevisae* Sco1 (Khalimonchuk *et al.*, 2005). The copper-binding Cox11 C-terminal domain in yeast and bacteria was shown to form a dimer that binds one mole equivalent of Cu(I) per monomer via the CFCF motif (Banci *et al.*, 2004; Carr *et al.*, 2002; Thompson *et al.*, 2010). The extant *Plasmodium* Cox11 genes lack a conserved N-terminal amino acid region compared to Cox11 in five other organisms (Figure 3.1). The mitochondrial matrix-localised yeast Cox11 N-terminal domain was demonstrated by mutational analysis to lack essential function (Banting and Glerum, 2006; Carr *et al.*, 2005). The *P. falciparum* Cox11 modelled structure fitted well into the β-immunoglobulin (Ig)-like fold *Sinorhizobium meliloti* Cox11 NMR-solved structure (Banci *et al.*, 2004).

Plasmodial Cox19 contained common features shared with the amino acid sequences from other organisms and a C-terminal insertion about the size of the extant Cox19 amino acid sequences in five other organisms (Figure 3.4). This implied the *Plasmodium* Cox19 amino acid sequences are twice as large as their orthologues in other organisms. This increment in plasmodial Cox19 amino acid structure is apparent, and a consequence of gene size reduction

(Aurrecoechea *et al.*, 2009; Gardner *et al*., 2002). Unlike most eukaryotic Cox19 amino acid sequences that are synthesised from mRNA transcripts comprising three to four exons, plasmodial Cox19 amino acid sequences are synthesised from a single exon gene. This phenomenon is typical of apicomplexans to loss functional redundancy in the evolution of parasitism by reducing their genomes or some gene sizes compared to the gene orthologues in other organisms, leaving only the essential genes or gene components (Jackson *et al.*, 2016; Vivares *et al.*, 2002; Wolf and Koonin, 2013). Four conserved cysteines found in twin Cx_9C motif in yeast Cox19, which are in a CHCH domain, were identified in the *Plasmodium* Cox19 (Cys24, Cys34, Cys45 and Cys55) amino acid sequences. These four cysteines have been shown to form two disulphide bridges (Cys34 – Cys45 and Cys24 – Cys55) in the yeast protein (Bode *et al.*, 2015; Fischer *et al.*, 2013; Rigby *et al.*, 2007). One of the two essential Tyr-Leu dipeptides in yeast Cox19 between the two cysteine residues in the twin Cx_9C motif (Bode *et al.*, 2015), has its Leu residue substituted with Phe in the *Plasmodium* Cox19 sequences (Figure 3.4). The mammalian Cox19 sequences have only one Tyr-Leu dipeptide found in the second Cx_9C motif, while Phe-Met dipeptide replaces the other Tyr-Leu dipeptide in the first Cx_9C motif. The variation in the conservation of Tyr-Leu dipeptide across organisms could be exploited to identify inhibitors targetting *P. falciparum* Cox19 as antimalarial drugs. Though the structure of Cox19 is not yet resolved, the *P. falciparum* Cox19 structure was modelled on the twin Cx_9C protein, human Mia40 (Bode *et al.*, 2015). The conformation of the *P. falciparum* Cox19 model agreed with the proposed Cox19 structure (Bode *et al.*, 2015; Fischer *et al.*, 2013; Rigby *et al.*, 2007).

Plasmodium Cox11 and Cox19 share amino acid sequences with several characterised Cox11 and Cox19 proteins, suggesting that the plasmodial proteins are copper chaperones in plasmodial cells.

6.5 Recombinant expression and isolation of C-terminal domain of *P. falciparum* Cox11 and Cox19 proteins

The presence of an insoluble transmembrane domain and AT-rich regions meant that only sections of the sequences coding for *P. falciparum* Cox11 and Cox19 proteins were recombinantly expressed as MBP fusion proteins. Proteins fused to MBP have improved solubility (Ahmad *et al.*, 2018). A recombinant 162-amino acid C-terminal domain of the 224 amino acids encoding *P. falciparum* Cox11 gene was cloned and expressed as an MBP fusion protein. Recombinant MBP-*Pf*Cox11Ct was isolated and identified with a mouse monoclonal anti-MBP antibody (Figure 4.12). A yield of ~1.43 mg was obtained from 400 ml (~2.91 g wet

weight bacterial pellet) of bacterial culture. Three *P. falciparum* Cox11 mutants; C60A, C157A and C60A-C157A with alanine substitutions at the corresponding cysteine residues were engineered (Heckman and Pease, 2007; Ho *et al.*, 1989) and expressed as MBP fusion proteins. The recombinant Cox11 proteins were characterised.

A 185-amino acid sequence of the 218 amino acids encoding *P. falciparum* Cox19 protein was cloned and expressed as an MBP-fusion protein. About 0.98 mg rMBP-*Pf*Cox19 was isolated from 400 ml (~2.21 g wet weight bacterial pellet) of bacterial culture. The recombinant protein was identified with a mouse monoclonal anti-MBP antibody. The rMBP-*Pf*Cox19 was characterised.

6.6 Production of polyclonal IgY used for the detection of *Plasmodium* Cox11 and Cox19

Antibodies against rMBP-*Pf*Cox11Ct and rMBP-*Pf*Cox19 were raised in chickens and affinity purified. Chicken IgY antibodies have been previously used in the characterisation of several malaria proteins (Choveaux *et al*., 2012; 2015; Hurdayal *et al*., 2010; Krause and Goldring, 2018; Krause *et al*., 2015; 2017). The three antibodies; anti-KIQXFXFEEQMLNAKEEM peptide, anti-rMBP-*Pf*Cox11Ct and anti-rMBP-*Pf*Cox19 antibodies did not detect proteins from a lysate of uninfected red blood cells or the *E. coli* host cells. The anti-rMBP-*Pf*Cox11Ct and anti-rMBP-*Pf*Cox19 antibodies both detected the native *Plasmodium* Cox11 and Cox19 respectively on a western blot of lysed *P. berghei* infected blood. An attempt to detect both proteins in a *P. falciparum* lysate was unsuccessful, possibly due to the proteins not being expressed during developmental stage of the sample. Transcriptional analysis suggests *P. falciparum* Cox11 and Cox19 to be expressed mainly in the trophozoite stage (Aurrecoechea *et al.*, 2009; Mok *et al.*, 2007). The presence of *P. berghei* Cox11 and Cox19 proteins suggests the expression of the proteins in *Plasmodium*.

6.7 Copper binds to the C-terminal domain of recombinant *P. falciparum* Cox11 and Cox19

In vitro and *in vivo* binding of copper by recombinant MBP-*Pf*Cox11Ct and MBP-*Pf*Cox19 was demonstrated using the bicinchoninic acid (BCA) copper release assay; the inhibition of copper-catalysed ascorbic acid oxidation; atomic absorption spectroscopy; differential scanning fluorimetry; and assessing the copper tolerance of *E. coli* host cells expressing the recombinant proteins. Data from the BCA copper release assay suggests that both rMBP-*Pf*Cox11Ct and rMBP-*Pf*Cox19 bind the cuprous ion (Figure 4.17 and Figure 5.9). Native *P. falciparum* Cox11 and Cox19 proteins are predicted to bind the cuprous ions as they are the

dominant intracellular copper species (Davis and O'Halloran, 2008) and considering the reducing potentials of the cell cytoplasm (Schafer and Buettner, 2001). Binding of cuprous ions was reported for *P. falciparum* Ctr1 and Cox17 (Choveaux *et al*., 2012; 2015), and the metal binding domain of *P. falciparum* CuP-ATPase (Rasoloson *et al.*, 2004). Data from studies with the three mutants; C60A, C157A and C60A-C157A proteins assessed by the BCA copper release assay suggests that the Cys157 in the CFCF motif is likely involved with copper coordination in *P. falciparum* Cox11, while Cys60 appears not to be essential for copper binding. However, data from the double mutant suggested that copper may bind to other amino acids. A possible candidate may be the Cys155 in the CFCF motif, since this motif in yeast Cox11 was shown to be the site for copper coordination (Banci *et al.*, 2004; Carr *et al.*, 2002; Thompson *et al.*, 2010). The order of importance of the cysteine residues in rMBP-*Pf*Cox11Ct copper coordination could have been validated using analytical methods like the surface plasmon resonance (SPR) but this was not done due to access and availability of instruments. The specificity of the BCA copper release assay for copper was affirmed when a similar profile was observed for the atomic absorption spectroscopy copper binding data. Binding of copper to copper proteins either increases or decreases their stability. Copper increases the stability of azurin, Cu/Zn superoxide dismutase and ascorbate oxidase, but decreases the stability of ceruloplasmin and prion protein (Baker and Agard, 1994; Milardi *et al.*, 2003; Pozdnyakova *et al.*, 2001; Rodriguez *et al.*, 2002; Savini *et al.*, 1990; Sedlák *et al.*, 2008; Stockel *et al.*, 1998). The binding of copper in differential scanning fluorimetry experiment caused a decrease (Figure 4.22) and an increase (Figure 5.13) in the T_m of rMBP-*Pf*Cox11Ct and rMBP-*Pf*Cox19 respectively. The change in T_m can be interpreted as either a decrease or an increase in the thermal stability of the protein. Both recombinant proteins chelated copper from their immediate surrounding under *in vivo* and presumably reduced conditions (Figure 4.20 and Figure 5.12). The recombinant proteins both enabled the growth of the *E. coli* bacteria host cells at toxic copper levels (Figure 4.24A and Figure 5.14B). The overexpression of Cox19 in yeast cells (Murtha *et al.*, 2018) and some copper proteins in *E. coli* host cells (Vita *et al.*, 2016; Yang *et al.*, 2017) promoted an increase in the copper tolerance of the expression host cells. *E. coli* host cells expressing the rMBP-*Pf*Cox11Ct C60A mutant grew under toxic copper levels while the *E. coli* host cells expressing the C157A and C60A-C157A did not grow. The Cys155 and Cys157 CFCF motif was considered essential for the coordination of copper within the *E. coli* host cells and possibly in *P. falciparum*.

6.8 Plasmodial copper proteins bind the cuprous ion

Six recombinant plasmodial copper proteins that have been investigated to date were shown to preferentially bind cuprous ion (Choveaux *et al*., 2012; 2015; Rasoloson *et al*., 2004). Cuprous ion being the dominant intracellular copper species (Davies and O'Halloran, 2008) contained in a reducing cytoplasmic environment (Schafer and Buettner, 2001), is likely to be the preferred copper species for binding by the native plasmodial copper proteins. Like most eukaryotes, *Plasmodium* probably obtains copper in a reduced form. Reduction may be by proteins with functions similar to those of yeast cell surface Cu^{2+}/Fe^{3+} metalloreductases and the Steap family metalloreductases in mammals (Georgatsou *et al.*, 1997; Hassett and Kosman, 1995; Martins *et al.*, 1998; Ohgami *et al.*, 2006; Rees and Thiele, 2007). However, orthologues of these proteins were not found in the plasmodial genome. Comparison of copper binding potentials between the six studied plasmodial copper proteins could not be achieved because the copper bound to the proteins was in all cases qualitatively and not quantitatively assessed. However, where the bound copper was quantitatively assessed using AAS in the case of Cox11, there was not enough supporting data to confirm any findings. This study was the first to employ multiple strategies to demonstrate the copper binding potential of plasmodial copper proteins including the assessment of copper tolerance of the *E. coli* hosts expressing the recombinant proteins.

6.9 Plasmodial Cox11 and Cox19 as potential antimalarial drug target

The significance of the electron transport chain to eukaryotes makes the pathway's enzymes attractive to antimalarial target like atovaquone, a lethal inhibitor of plasmodial cytochrome bc_1 complex (Fry and Pudney, 1992; Mather *et al.*, 2005). The three constitutive respiration pathways – glycolysis, tricarboxylic acid cycle and the electron transport chain – are essentially driven by the CcO enzyme complex which serves as the terminal electron acceptor in aerobes and facultative organisms during oxidative respiration. The plasmodial CcO donates its acquired electron for the regeneration of ubiquinone in priming for the next round of oxidative respiration (Painter *et al.*, 2007; Vaidya and Mather, 2009). Therefore, a functional CcO is critical for the parasite development. Targetting the enzyme complex or components forming the complex could be important in the development of antimalarial drugs (Krungkrai *et al.*, 1997).

The two plasmodial proteins studied in this thesis, Cox11 and Cox19, are two of the multiple CcO assembly proteins which happen to be copper proteins. With the confirmation

that copper homeostasis is essential to plasmodial development (Asahi *et al*., 2014), these proteins could prove to be vital to antimalarial drug development. Although, there is much to be done before establishing their potentials as antimalarial drug targets, findings from this study forms a basis for the exploitation of these proteins. Targetting the plasmodial Cox11 and/or Cox19 implies two biological processes, copper homeostasis and the electron transport chain, essential to the parasite's development will be inhibited (Asahi *et al*., 2014; Painter *et al.*, 2007). This could then make the inhibitor(s) potent against the parasite.

6.10 Conclusion and future studies

The present study provided an insight into the possible role of two copper chaperones in *P. falciparum* copper homeostasis. Given the importance of copper to *Plasmodium* metabolism suggested by previous studies, drug-targetted inhibition of plasmodial copper homeostasis could be effective in preventing parasite development. Having established copper binds to the recombinant *P. falciparum* Cox11 and Cox19 in this study, there is a possibility of a copper-binding role of the native proteins in the parasite. Mutational analysis of the *P. falciparum* Cox11 protein affirming the copper-binding role of the CFCF motif further consolidates the likely functional role of the protein as a copper binding protein. Mutation of key cysteines; Cys24, Cys34, Cys45 and Cys55 in the amino acid structure of *P. falciparum* Cox19 to non-polar amino acid(s) with similar structure as cysteine will help identify the amino acid residue(s) that bind copper. The limitation of this study was the fact that further empirical studies like the SPR, transmission emission microscopy or other imaging experiments validating the order and the intracellular coordination of copper by the two copper proteins studied was not done. This was largely due to access and availability of instruments. The identification of genes encoding other CcO assembly accessory proteins in *P. falciparum* (Gardner *et al.*, 2002; Painter *et al.*, 2007; Vaidya and Mather, 2009) implies that *P. falciparum* Cox11 and Cox19, like their orthologues in eukaryotes, are likely to be involved in the CcO assembly. The role of these proteins in the *Plasmodium* CcO assembly will be strengthened by establishing their mitochondrial localisation in the parasite by immunolocalisation, electron microscopy, stable isotopic labelling of proteins and pulse-chase experiments. The importance of each protein to the parasite could be inferred from gene knock-out studies using transgenic parasites (Günther *et al.*, 2009; Kanjee *et al.*, 2017; Wang *et al.*, 2017). Having established the copper binding ability of the two *P. falciparum* proteins involved in copper homeostasis, further studies are needed to assess their potentials as novel drug targets. This could be achieved

by identifying inhibitors specific to plasmodial Cox11 and Cox19 and not the human protein orthologues through *in silico* molecular docking analysis or *in vitro* inhibition kinetic studies.

Bibliography

Ahmad, I., Nawaz, N., Darwesh, N. M., ur Rahman, S., Mustafa, M. Z., Khan, S. B. and Patching, S. G. (2018). Overcoming challenges for amplified expression of recombinant proteins using *Escherichia coli*. *Protein Expression and Purification,* 144, 12-18.

Alam, M. S., Mohon, A. N., Mustafa, S., Khan, W. A., Islam, N., Karim, M. J., Khanum, H., Sullivan, D. J. and Haque, R. (2011). Real-time PCR assay and rapid diagnostic tests for the diagnosis of clinically suspected malaria patients in Bangladesh. *Malaria Journal,* 10, 175. doi:10.1186/1475-2875-10-175.

Allen, J. W., Ferguson, S. J. and Ginger, M. L. (2008). Distinctive biochemistry in the trypanosome mitochondrial intermembrane space suggests a model for stepwise evolution of the MIA pathway for import of cysteine-rich proteins. *FEBS Letters,* 582, 2817-2825.

Aller, S. G. and Unger, V. M. (2006). Projection structure of the human copper transporter CTR1 at 6-Å resolution reveals a compact trimer with a novel channel-like architecture. *Proceedings of the National Academy of Sciences of the United States of America,* 103, 3627-3632.

Amato, R., Lim, P., Miotto, O., Amaratunga, C., Dek, D., Pearson, R. D., Almagro-Garcia, J., Neal, A. T., Sreng, S., Suon, S., Drury, E., Jyothi, D., Stalker, J., Kwiatkowski, D. P. and Fairhurst, R. M. (2017). Genetic markers associated with dihydroartemisinin–piperaquine failure in *Plasmodium falciparum* malaria in Cambodia: a genotype-phenotype association study. *The Lancet. Infectious Diseases,* 17, 164-173.

Andriantsoanirina, V., Menard, D., Rabearimanana, S., Hubert, V., Bouchier, C., Tichit, M., Bras, J. L. and Durand, R. (2010). Association of microsatellite variations of *Plasmodium falciparum* Na^+/H^+ exchanger (*Pf*nhe-1) gene with reduced in vitro susceptibility to quinine: lack of confirmation in clinical isolates from Africa. *The American Journal of Tropical Medicine and Hygiene,* 82, 782-787.

Antony, H. A. and Parija, S. C. (2016). Antimalarial drug resistance: An overview. *Tropical Parasitology,* 6, 30-41.

Argüello, J. M., Raimunda, D. and González-Guerrero, M. (2012). Metal transport across biomembranes: Emerging models for a distinct chemistry. *The Journal of Biological Chemistry,* 287, 13510-13517.

Ariey, F., Witkowski, B., Amaratunga, C., Beghain, J., Langlois, A. C., Khim, N., Kim, S., Duru, V., Bouchier, C., Ma, L., Lim, P., Leang, R., Duong, S., Sreng, S., Suon, S., Chuor, C. M., Bout, D. M., Menard, S., Rogers, W. O., Genton, B., Fandeur, T., Miotto, O., Ringwald, P., Le Bras, J., Berry, A., Barale, J. C., Fairhurst, R. M.,

Benoit-Vical, F., Mercereau-Puijalon, O. and Menard, D. (2014). A molecular marker of artemisinin-resistant *Plasmodium falciparum* malaria. *Nature,* 505, 50-55.

Arnesano, F., Balatri, E., Banci, L., Bertini, I. and Winge, D. R. (2005). Folding studies of Cox17 reveal an important interplay of cysteine oxidation and copper binding. *Structure,* 13, 713-722.

Arredondo, M., Mendiburo, M. J., Flores, S., Singleton, S. T. and Garrick, M. D. (2014). Mouse divalent metal transporter 1 is a copper transporter in HEK293 cells. *Biometals,* 27, 115-123.

Asahi, H., Kobayashi, F., Inoue, S. I., Niikura, M., Yagita, K. and Tolba, M. E. M. (2016). Copper homeostasis for the developmental progression of intraerythrocytic malarial parasite. *Current Topics in Medicinal Chemistry*, 16, 3048-3057.

Asahi, H., Tolba, M. E. M., Tanabe, M. and Ohmae, H. (2013). Molecular factors that are associated with early developmental arrest of intraerythrocytic *Plasmodium falciparum*. *Canadian Journal of Microbiology*, 59, 485-493.

Asahi, H., Tolba, M. E. M., Tanabe, M., Sugano, S., Abe, K. and Kawamoto, F. (2014). Perturbation of copper homeostasis is instrumental in early developmental arrest of intraerythrocytic *Plasmodium falciparum*. *BMC Microbiology*, 14, 167. doi:10.1186/1471-2180-14-167.

Ashley, E. A., Dhorda, M., Fairhurst, R. M., Amaratunga, C., Lim, P., Suon, S., Sreng, S., Anderson, J. M., Mao, S., Sam, B., Sopha, C., Chuor, C. M., Nguon, C., Sovannaroth, S., Pukrittayakamee, S., Jittamala, P., Chotivanich, K., Chutasmit, K., Suchatsoonthorn, C., Runcharoen, R., Hien, T. T., Thuy-Nhien, N. T., Thanh, N. V., Phu, N. H., Htut, Y., Han, K.-T., Aye, K. H., Mokuolu, O. A., Olaosebikan, R. R., Folaranmi, O. O., Mayxay, M., Khanthavong, M., Hongvanthong, B., Newton, P. N., Onyamboko, M. A., Fanello, C. I., Tshefu, A. K., Mishra, N., Valecha, N., Phyo, A. P., Nosten, F., Yi, P., Tripura, R., Borrmann, S., Bashraheil, M., Peshu, J., Faiz, M. A., Ghose, A., Hossain, M. A., Samad, R., Rahman, M. R., Hasan, M. M., Islam, A., Miotto, O., Amato, R., MacInnis, B., Stalker, J., Kwiatkowski , D. P., Bozdech, Z., Jeeyapant, A., Cheah, P. Y., Sakulthaew, T., Chalk, J., Intharabut, B., Silamut, K., Lee, S. J., Vihokhern, B., Kunasol, C., Imwong, M., Tarning, J., Taylor, W. J., Yeung, S., Woodrow, C. J., Flegg, J. A., Das, D., Smith, J., Venkatesan, M., Plowe, C. V., Stepniewska, K., Guerin, P. J., Dondorp, A. M., Day, N. P. and White, N. J. (2014). Spread of artemisinin resistance in *Plasmodium falciparum* Malaria. *New England Journal of Medicine,* 371, 411-423.

Ashley, E. A., Pyae Phyo, A. and Woodrow, C. J. (2018). Malaria. *The Lancet,* 391, 1608-1621.

Aurrecoechea, C., Brestelli, J., Brunk, B. P., Dommer, J., Fischer, S., Gajria, B., Gao, X., Gingle, A., Grant, G., Harb, O. S., Heiges, M., Innamorato, F., Iodice, J., Kissinger, J. C., Kraemer, E., Li, W., Miller, J. A., Nayak, V., Pennington, C., Pinney, D. F., Roos, D. S., Ross, C., Stoeckert, J. C. J., Treatman, C. and Wang,

H. (2009). PlasmoDB: a functional genomic database for malaria parasites. *Nucleic Acids Research,* 37, D539-D543.

Babcock, G. T. and Wikström, M. (1992). Oxygen activation and the conservation of energy in cell respiration. *Nature,* 356, 301-309.

Baker, D. and Agard, D. A. (1994). Kinetics versus thermodynamics in protein folding. *Biochemistry,* 33, 7505-7509.

Baker, Z. N., Cobine, P. A. and Leary, S. C. (2017). The mitochondrion: a central architect of copper homeostasis. *Metallomics,* 9, 1501-1512.

Balabaskaran Nina, P., Morrisey, J. M., Ganesan, S. M., Ke, H., Pershing, A. M., Mather, M. W. and Vaidya, A. B. (2011). ATP synthase complex of *Plasmodium falciparum*: dimeric assembly in mitochondrial membranes and resistance to genetic disruption. *Journal of Biological Chemistry,* 286, 41312-41322.

Baldacci, P. and Ménard, R. (2004). The elusive malaria sporozoite in the mammalian host. *Molecular Microbiology,* 54, 298-306.

Balogun, E. O., Nok, A. J. and Kita, K. (2016). Global warming and the possible globalization of vector-borne diseases: a call for increased awareness and action. *Tropical Medicine and Health,* 44, 38. doi:10.1186/s41182-016-0039-0.

Banci, L., Bertini, I., Cantini, F., Ciofi-Baffoni, S., Gonnelli, L. and Mangani, S. (2004). Solution structure of Cox11, a novel type of β-immunoglobulin-like fold involved in CuB Site formation of cytochrome c oxidase. *Journal of Biological Chemistry,* 279, 34833-34839.

Banci, L., Bertini, I., Cefaro, C., Ciofi-Baffoni, S., Gallo, A., Martinelli, M., Sideris, D. P., Katrakili, N. and Tokatlidis, K. (2009). MIA40 is an oxidoreductase that catalyzes oxidative protein folding in mitochondria. *Nature Structural and Molecular Biology,* 16, 198-206.

Banting, G. S. and Glerum, D. M. (2006). Mutational analysis of the *Saccharomyces cerevisiae* cytochrome c oxidase assembly protein Cox11p. *Eukaryotic Cell,* 5, 568-578.

Baragaña, B., Hallyburton, I., Lee, M. C. S., Norcross, N. R., Grimaldi, R., Otto, T. D., Proto, W. R., Blagborough, A. M., Meister, S., Wirjanata, G., Ruecker, A., Upton, L. M., Abraham, T. S., Almeida, M. J., Pradhan, A., Porzelle, A., Martínez, M. S., Bolscher, J. M., Woodland, A., Luksch, T., Norval, S., Zuccotto, F., Thomas, J., Simeons, F., Stojanovski, L., Osuna-Cabello, M., Brock, P. M., Churcher, T. S., Sala, K. A., Zakutansky, S. E., Jiménez-Díaz, M. B., Sanz, L. M., Riley, J., Basak, R., Campbell, M., Avery, V. M., Sauerwein, R. W., Dechering, K. J., Noviyanti, R., Campo, B., Frearson, J. A., Angulo-Barturen, I., Ferrer-Bazaga, S., Gamo, F. J., Wyatt, P. G., Leroy, D., Siegl, P., Delves, M. J., Kyle, D. E., Wittlin, S., Marfurt,

J., Price, R. N., Sinden, R. E., Winzeler, E. A., Charman, S. A., Bebrevska, L., Gray, D. W., Campbell, S., Fairlamb, A. H., Willis, P. A., Rayner, J. C., Fidock, D. A., Read, K. D. and Gilbert, I. H. (2015). A novel multiple-stage antimalarial agent that inhibits protein synthesis. *Nature*, 522, 315-320.

Barcia, J. J. (2007). The Giemsa Stain: Its history and applications. *International Journal of Surgical Pathology*, 15, 292-296.

Beers, J., Glerum, D. M. and Tzagoloff, A. (2002). Purification and characterization of yeast Sco1p, a mitochondrial copper protein. *Journal of Biological Chemistry*, 277, 22185-22190.

Bien, M., Longen, S., Wagener, N., Chwalla, I., Herrmann, J. M. and Riemer, J. (2010). Mitochondrial disulfide bond formation is driven by intersubunit electron transfer in Erv1 and proofread by glutathione. *Molecular Cell*, 37, 516-528.

Blasco, B., Leroy, D. and Fidock, D. A. (2017). Antimalarial drug resistance: linking *Plasmodium falciparum* parasite biology to the clinic. *Nature Medicine*, 23, 917-928.

Bode, M., Woellhaf, M. W., Bohnert, M., van der Laan, M., Sommer, F., Jung, M., Zimmermann, R., Schroda, M. and Herrmann, J. M. (2015). Redox-regulated dynamic interplay between Cox19 and the copper-binding protein Cox11 in the intermembrane space of mitochondria facilitates biogenesis of cytochrome c oxidase. *Molecular Biology of the Cell*, 26, 2385-2401.

Boivin, S., Kozak, S. and Meijers, R. (2013). Optimization of protein purification and characterization using Thermofluor screens. *Protein Expression and Purification*, 91, 192-206.

Bousema, T. and Drakeley, C. (2011). Epidemiology and infectivity of *Plasmodium falciparum* and *Plasmodium vivax* gametocytes in relation to malaria control and elimination. *Clinical Microbiology Reviews*, 24, 377-410.

Boyce, R. M., Muiru, A., Reyes, R., Ntaro, M., Mulogo, E., Matte, M. and Siedner, M. J. (2015). Impact of rapid diagnostic tests for the diagnosis and treatment of malaria at a peripheral health facility in Western Uganda: an interrupted time series analysis. *Malaria Journal*, 14, 203. doi:10.1186/s12936-015-0725-0.

Bozdech, Z., Llinas, M., Pulliam, B. L., Wong, E. D., Zhu, J. and DeRisi, J. L. (2003). The transcriptome of the intraerythrocytic developmental cycle of *Plasmodium falciparum*. *PLoS Biology*, 1, 85-100.

Bradford, M. M. (1976). A rapid and sensitive method for the quantitation of microgram quantities of protein utilizing the principle of protein-dye binding. *Analytical Biochemistry*, 72, 248-254.

Brenner, A. J. and Harris, E. D. (1995). A quantitative test for copper using bicinchoninic acid. *Analytical Biochemistry,* 226, 80-84.

Briolant, S., Pelleau, S., Bogreau, H., Hovette, P., Zettor, A., Castello, J., Baret, E., Amalvict, R., Rogier, C. and Pradines, B. (2011). In vitro susceptibility to quinine and microsatellite variations of the *Plasmodium falciparum* Na^+/H^+ exchanger (*Pf*nhe-1) gene: the absence of association in clinical isolates from the Republic of Congo. *Malaria Journal,* 10, 37. doi:10.1186/1475-2875-10-37.

Brooks, D. R., Wang, P., Read, M., Watkins, W. M., Sims, P. F. G. and Hyde, J. E. (1994). Sequence variation of the hydroxymethyldihydropterin pyrophosphokinase: dihydropteroate synthase gene in lines of the human malaria parasite, *Plasmodium falciparum*, with differing resistance to sulfadoxine. *European Journal of Biochemistry,* 224, 397-405.

Bruce-Chwatt, L. J. (1962). Classification of antimalarial drugs in relation to different stages in the life-cycle of the parasite: commentary on a diagram. *Bullentin of the World Health Organisation,* 27, 287-290.

Burns, J. M., Parke, L. A., Daly, T. M., Cavacini, L. A., Weidanz, W. P. and Long, C. A. (1989). A protective monoclonal antibody recognizes a variant-specific epitope in the precursor of the major merozoite surface antigen of the rodent malarial parasite *Plasmodium yoelii*. *The Journal of Immunology,* 142, 2835-2840.

Burrows, J. N., Duparc, S., Gutteridge, W. E., Hooft van Huijsduijnen, R., Kaszubska, W., Macintyre, F., Mazzuri, S., Möhrle, J. J. and Wells, T. N. C. (2017). New developments in anti-malarial target candidate and product profiles. *Malaria Journal,* 16, 26. doi:10.1186/s12936-016-1675-x.

Cabrera, A., Alonzo, E., Sauble, E., Chu, Y. L., Nguyen, D., Linder, M. C., Sato, D. S. and Mason, A. Z. (2008). Copper binding components of blood plasma and organs, and their responses to influx of large doses of ^{65}Cu, in the mouse. *Biometals,* 21, 525-543.

Capaldi, R. A. (1990). Structure and function of cytochrome c oxidase. *Annual Review of Biochemistry,* 59, 569-596.

Cármenes, R. S., Freije, J. P., Molina, M. M. and Martín, J. M. (1989). Predict7, a program for protein structure prediction. *Biochemical and Biophysical Research Communications,* 159, 687-693.

Carneiro, S., Ferreira, E. C. and Rocha, I. (2013). Metabolic responses to recombinant bioprocesses in *Escherichia coli*. *Journal of Biotechnology,* 164, 396-408.

Carr, H. S., George, G. N. and Winge, D. R. (2002). Yeast Cox11, a protein essential for cytochrome c oxidase assembly, is a Cu(I)-binding protein. *Journal of Biological Chemistry,* 277, 31237-31242.

Carr, H. S., Maxfield, A. B., Horng, Y.-C. and Winge, D. R. (2005). Functional analysis of the domains in Cox11. *Journal of Biological Chemistry,* 280, 22664-22669.

Carr, H. S. and Winge, D. R. (2003). Assembly of cytochrome c oxidase within the mitochondrion. *Accounts of Chemical Research,* 36, 309-316.

Carrie, C. and Soll, J. (2017). To Mia or not to Mia: stepwise evolution of the mitochondrial intermembrane space disulfide relay. *BMC Biology,* 15, 119. doi:10.1186/s12915-017-0468-1.

Celik, A., He, F. and Jacobson, A. (2017). NMD monitors translational fidelity 24/7. *Current Genetics,* 63, 1007-1010.

Cha, S.-J., Park, K., Srinivasan, P., Schindler, C. W., van Rooijen, N., Stins, M. and Jacobs-Lorena, M. (2015). CD68 acts as a major gateway for malaria sporozoite liver infection. *The Journal of Experimental Medicine,* 212, 1391-1403.

Chacinska, A., Pfannschmidt, S., Wiedemann, N., Kozjak, V., Sanjuán Szklarz, L. K., Schulze-Specking, A., Truscott, K. N., Guiard, B., Meisinger, C. and Pfanner, N. (2004). Essential role of Mia40 in import and assembly of mitochondrial intermembrane space proteins. *The EMBO Journal,* 23, 3735–3746.

Chatzi, A. and Tokatlidis, K. (2013). The mitochondrial intermembrane space: a hub for oxidative folding linked to protein biogenesis. *Antioxidants & Redox Signaling,* 19, 54-62.

Chen, C., Huang, H. and Wu, C. H. (2017). Protein bioinformatics databases and resources. *Methods in Molecular Biology,* 1558, 3-39.

Chen, X., Qiu, J. D., Shi, S. P., Suo, S. B., Huang, S. Y. and Liang, R. P. (2013). Incorporating key position and amino acid residue features to identify general and species-specific Ubiquitin conjugation sites. *Bioinformatics,* 29, 1614-1622.

Choudhary, C., Kumar, C., Gnad, F., Nielsen, M. L., Rehman, M., Walther, T. C., Olsen, J. V. and Mann, M. (2009). Lysine acetylation targets protein complexes and co-regulates major cellular functions. *Science,* 325, 834-840.

Choveaux, D. L., Krause, R. G. E., Przyborski, J. M. and Goldring, J. P. D. (2015). Identification and initial characterisation of a *Plasmodium falciparum* Cox17 copper metallochaperone. *Experimental Parasitology,* 148, 30-39.

Choveaux, D. L., Przyborski, J. M. and Goldring, J. D. (2012). A *Plasmodium falciparum* copper-binding membrane protein with copper transport motifs. *Malaria Journal,* 11, 397. doi:10.1186/1475-2875-11-397.

Cobbold, S. A., Vaughan, A. M., Lewis, I. A., Painter, H. J., Camargo, N., Perlman, D. H., Fishbaugher, M., Healer, J., Cowman, A. F., Kappe, S. H. I. and Llinás, M. (2013). Kinetic flux profiling elucidates two independent acetyl-CoA biosynthetic pathways in *Plasmodium falciparum*. *Journal of Biological Chemistry*, 288, 36338-36350.

Cobine, P. A., Ojeda, L. D., Rigby, K. M. and Winge, D. R. (2004). Yeast contain a non-proteinaceous pool of copper in the mitochondrial matrix. *Journal of Biological Chemistry*, 279, 14447-14455.

Cobine, P. A., Pierrel, F., Bestwick, M. L. and Winge, D. R. (2006). Mitochondrial matrix copper complex used in metallation of cytochrome oxidase and superoxide dismutase. *Journal of Biological Chemistry*, 281, 36552-36559.

Coetzee, M., Kruger, P., Hunt, R. H., Durrheim, D. N., Urbach, J. and Hansford, C. F. (2013). Malaria in South Africa: 110 years of learning to control the disease. *South African Medical Journal*, 103, 770-778.

Cohen, S. N., Chang, A. C. and Hsu, L. (1972). Nonchromosomal antibiotic resistance in bacteria: genetic transformation of *Escherichia coli* by R-factor DNA. *Proceedings of the National Academy of Sciences of the United States of America*, 69, 2110-2114.

Cook, J., Aydin-Schmidt, B., González, I. J., Bell, D., Edlund, E., Nassor, M. H., Msellem, M., Ali, A., Abass, A. K., Mårtensson, A. and Björkman, A. (2015). Loop-mediated isothermal amplification (LAMP) for point-of-care detection of asymptomatic low-density malaria parasite carriers in Zanzibar. *Malaria Journal*, 14, 43. doi:10.1186/s12936-015-0573-y.

Cowman, A. F., Healer, J., Marapana, D. and Marsh, K. (2016). Malaria: biology and disease. *Cell*, 167, 610-624.

Cowman, A. F., Morry, M. J., Biggs, B. A., Cross, G. A. and Foote, S. J. (1988). Amino acid changes linked to pyrimethamine resistance in the dihydrofolate reductase-thymidylate synthase gene of *Plasmodium falciparum*. *Proceedings of the National Academy of Sciences of the United States of America*, 85, 9109-9113.

Cox-Singh, J., Davis, T. M. E., Lee, K.-S., Shamsul, S. S. G., Matusop, A., Ratnam, S., Rahman, H. A., Conway, D. J. and Singh, B. (2008). *Plasmodium knowlesi* malaria in humans is widely distributed and potentially life threatening. *Clinical Infectious Diseases*, 46, 165-171.

Cox, F. E. G. (2010). History of the discovery of the malaria parasites and their vectors. *Parasites & Vectors*, 3, 5. doi:10.1186/1756-3305-3-5.

Cui, L., Mharakurwa, S., Ndiaye, D., Rathod, P. K. and Rosenthal, P. J. (2015). Antimalarial drug resistance: literature review and activities and findings of the ICEMR network. *The American Journal of Tropical Medicine and Hygiene*, 93, 57-68.

Dancis, A., Haile, D., Yuan, D. S. and Klausner, R. D. (1994). The *Saccharomyces cerevisiae* copper transport protein (Ctr1p). Biochemical characterization, regulation by copper, and physiologic role in copper uptake. *Journal of Biological Chemistry,* 269, 25660-25667.

Daneshvar, C., Davis, T. M. E., Cox-Singh, J., Rafa'ee, M. Z., Zakaria, S. K., Divis, P. C. S. and Singh, B. (2009). Clinical and laboratory features of human *Plasmodium knowlesi* Infection. *Clinical Infectious Diseases,* 49, 852-860.

Darpo, B., Ferber, G., Siegl, P., Laurijssens, B., Macintyre, F., Toovey, S. and Duparc, S. (2015). Evaluation of the QT effect of a combination of piperaquine and a novel anti-malarial drug candidate OZ439, for the treatment of uncomplicated malaria. *British Journal of Clinical Pharmacology,* 80, 706-715.

Davies, M. J. (2016). Protein oxidation and peroxidation. *Biochemical Journal,* 473, 805-825.

Davis, A. V. and O'Halloran, T. V. (2008). A place for thioether chemistry in cellular copper ion recognition and trafficking. *Nature Chemical Biology,* 4, 148-151.

De Feo, C. J., Aller, S. G., Siluvai, G. S., Blackburn, N. J. and Unger, V. M. (2009). Three-dimensional structure of the human copper transporter hCTR1. *Proceedings of the National Academy of Sciences of the United States of America,* 106, 4237-4242.

Deng, W., Wang, C., Zhang, Y., Xu, Y., Zhang, S., Liu, Z. and Xue, Y. (2016). GPS-PAIL: prediction of lysine acetyltransferase-specific modification sites from protein sequences. *Scientific Reports,* 6, 39787. doi:10.1038/srep39787.

Dondorp, A. M. (2017). New genetic marker for piperaquine resistance in *Plasmodium falciparum*. *The Lancet Infectious Diseases,* 17, 119-121.

Drazic, A., Myklebust, L. M., Ree, R. and Arnesen, T. (2016). The world of protein acetylation. *Biochimica et Biophysica Acta - Proteins and Proteomics,* 1864, 1372-1401.

Dubinski, A. F., Camasta, R., Soule, T. G. B., Reed, B. H. and Glerum, D. M. (2018). Consequences of cytochrome c oxidase assembly defects for the yeast stationary phase. *Biochimica et Biophysica Acta - Bioenergetics,* 1859, 445-458.

Dudzik, C. G., Walter, E. D., Abrams, B. S., Jurica, M. S. and Millhauser, G. L. (2013). Coordination of copper to the membrane-bound form of α-synuclein. *Biochemistry,* 52, 53-60.

Durand, R., Jafari, S., Vauzelle, J., Delabre, J. F., Jesic, Z. and Le Bras, J. (2001). Analysis of *Pf*crt point mutations and chloroquine susceptibility in isolates of *Plasmodium falciparum*. *Molecular and Biochemical Parasitology,* 114, 95-102.

Eckers, E., Petrungaro, C., Gross, D., Riemer, J., Hell, K. and Deponte, M. (2013). Divergent molecular evolution of the mitochondrial sulfhydryl:cytochrome c oxidoreductase Erv in opisthokonts and parasitic protists. *Journal of Biological Chemistry,* 288, 2676-2688.

Egan, T. J. and Kaschula, C. H. (2007). Strategies to reverse drug resistance in malaria. *Current Opinion in Infectious Diseases,* 20, 598-604.

Eisses, J. F. and Kaplan, J. H. (2002). Molecular characterization of hCTR1, the human copper uptake protein. *Journal of Biological Chemistry,* 277, 29162-29171.

Eisses, J. F. and Kaplan, J. H. (2005). The mechanism of copper uptake mediated by human CTR1: a mutational analysis. *Journal of Biological Chemistry,* 280, 37159-37168.

Ericsson, U. B., Hallberg, B. M., DeTitta, G. T., Dekker, N. and Nordlund, P. (2006). Thermofluor-based high-throughput stability optimization of proteins for structural studies. *Analytical Biochemistry,* 357, 289-298.

Fairfield, A. S., Meshnick, S. R. and Eaton, J. W. (1983). Malaria parasites adopt host cell superoxide dismutase. *Science,* 221, 764-766.

Feagin, J. E. (1992). The 6-kb element of Plasmodium falciparum encodes mitochondrial cytochrome genes. *Molecular and Biochemical Parasitology,* 52, 145-148.

Ferdig, M. T., Cooper, R. A., Mu, J., Deng, B., Joy, D. A., Su, X. z. and Wellems, T. E. (2004). Dissecting the loci of low-level quinine resistance in malaria parasites. *Molecular Microbiology,* 52, 985-997.

Fidock, D. A., Nomura, T., Talley, A. K., Cooper, R. A., Dzekunov, S. M., Ferdig, M. T., Ursos, L. M. B., bir Singh Sidhu, A., Naudé, B., Deitsch, K. W., Su, X.-z., Wootton, J. C., Roepe, P. D. and Wellems, T. E. (2000). Mutations in the *P. falciparum* digestive vacuole transmembrane protein *Pf*CRT and evidence for their role in chloroquine resistance. *Molecular Cell,* 6, 861-871.

Field, L. S., Luk, E. and Culotta, V. C. (2002). Copper chaperones: personal escorts for metal ions. *Journal of Bioenergetics and Biomembranes,* 34, 373-379.

Fischer, M., Horn, S., Belkacemi, A., Kojer, K., Petrungaro, C., Habich, M., Ali, M., Küttner, V., Bien, M., Kauff, F., Dengjel, J., Herrmann, J. M. and Riemer, J. (2013). Protein import and oxidative folding in the mitochondrial intermembrane space of intact mammalian cells. *Molecular Biology of the Cell,* 24, 2160-2170.

Fivelman, Q. L., Butcher, G. A., Adagu, I. S., Warhurst, D. C. and Pasvol, G. (2002). Malarone treatment failure and *in vitro* confirmation of resistance of *Plasmodium falciparum* isolate from Lagos, Nigeria. *Malaria Journal,* 1, 1. doi:10.1186/1475-2875-1-1.

Flannery, E. L., Chatterjee, A. K. and Winzeler, E. A. (2013). Antimalarial drug discovery - approaches and progress towards new medicines. *Nature Reviews Microbiology,* 11, 849-862.

Flores, A. G. and Unger, V. M. (2013). Atox1 contains positive residues that mediate membrane association and aid subsequent copper loading. *The Journal of Membrane Biology,* 246, 903-913.

Fontanesi, F., Soto, I. C., Horn, D. and Barrientos, A. (2006). Assembly of mitochondrial cytochrome c-oxidase, a complicated and highly regulated cellular process. *American Journal of Physiology-Cell Physiology,* 291, C1129-C1147.

Foote, S. J., Kyle, D. E., Martin, R. K., Oduola, A. M. J., Forsyth, K., Kemp, D. J. and Cowman, A. F. (1990). Several alleles of the multidrug-resistance gene are closely linked to chloroquine resistance in *Plasmodium falciparum*. *Nature,* 345, 255-258.

Foth, B. J., Stimmler, L. M., Handman, E., Crabb, B. S., Hodder, A. N. and McFadden, G. I. (2005). The malaria parasite *Plasmodium falciparum* has only one pyruvate dehydrogenase complex, which is located in the apicoplast. *Molecular Microbiology,* 55, 39-53.

Fraga, H., Bech-Serra, J.-J., Canals, F., Ortega, G., Millet, O. and Ventura, S. (2014). The mitochondrial intermembrane space oxireductase Mia40 funnels the oxidative folding pathway of the cytochrome c oxidase assembly protein Cox19. *Journal of Biological Chemistry,* 289, 9852-9864.

Frederich, M., Dogne, J. M., Angenot, L. and Mol, P. D. (2002). New trends in anti-malarial agents. *Current Medicinal Chemistry,* 9, 1435-1456.

Frith, K.-A., Fogel, R., Goldring, J. P. D., Krause, R. G. E., Khati, M., Hoppe, H., Cromhout, M. E., Jiwaji, M. and Limson, J. L. (2018). Towards development of aptamers that specifically bind to lactate dehydrogenase of *Plasmodium falciparum* through epitopic targeting. *Malaria Journal,* 17, 191. doi:10.1186/s12936-018-2336-z.

Fry, M. and Beesley, J. E. (2009). Mitochondria of mammalian *Plasmodium* spp. *Parasitology,* 102, 17-26.

Fry, M. and Pudney, M. (1992). Site of action of the antimalarial hydroxynaphthoquinone, 2-[trans-4-(4'-chlorophenyl) cyclohexyl]-3- hydroxy-1,4-naphthoquinone (566C80). *Biochemical Pharmacology,* 43, 1545-1553.

Fujioka, H. and Aikawa, M. (2002). Structure and life cycle. *Chemical Immunology,* 80, 1-26.

Gajer, J. M., Furdas, S. D., Gründer, A., Gothwal, M., Heinicke, U., Keller, K., Colland, F., Fulda, S., Pahl, H. L., Fichtner, I., Sippl, W. and Jung, M. (2015). Histone

acetyltransferase inhibitors block neuroblastoma cell growth *in vivo*. *Oncogenesis*, 4, e137. doi:10.1038/oncsis.2014.51.

Gardner, M. J., Hall, N., Fung, E., White, O., Berriman, M., Hyman, R. W., Carlton, J. M., Pain, A., Nelson, K. E., Bowman, S., Paulsen, I. T., James, K., Eisen, J. A., Rutherford, K., Salzberg, S. L., Craig, A., Kyes, S., Chan, M. S., Nene, V., Shallom, S. J., Suh, B., Peterson, J., Angiuoli, S., Pertea, M., Allen, J., Selengut, J., Haft, D., Mather, M. W., Vaidya, A. B., Martin, D. M., Fairlamb, A. H., Fraunholz, M. J., Roos, D. S., Ralph, S. A., McFadden, G. I., Cummings, L. M., Subramanian, G. M., Mungall, C., Venter, J. C., Carucci, D. J., Hoffman, S. L., Newbold, C., Davis, R. W., Fraser, C. M. and Barrell, B. (2002). Genome sequence of the human malaria parasite *Plasmodium falciparum*. *Nature*, 419, 498-511.

Gassmann, M., Thommes, P., Weiser, T. and Hubscher, U. (1990). Efficient production of chicken egg yolk antibodies against a conserved mammalian protein. *The FASEB Journal*, 4, 2528-2532.

Georgatsou, E., Mavrogiannis, L. A., Fragiadakis, G. S. and Alexandraki, D. (1997). The yeast Fre1p/Fre2p cupric reductases facilitate copper uptake and are regulated by the copper-modulated Mac1p activator. *Journal of Biological Chemistry*, 272, 13786-13792.

Gilson, P. R. and Crabb, B. S. (2009). Morphology and kinetics of the three distinct phases of red blood cell invasion by *Plasmodium falciparum* merozoites. *International Journal for Parasitology*, 39, 91-96.

Glerum, D. M., Shtanko, A. and Tzagoloff, A. (1996). Characterization of COX17, a yeast gene involved in copper metabolism and assembly of cytochrome oxidase. *Journal of Biological Chemistry*, 271, 14504-14509.

Glick, B. R. (1995). Metabolic load and heterologous gene expression. *Biotechnology Advances*, 13, 247-261.

Gokhale, N. H., Padhye, S. B., Billington, D. C., Rathbone, D. L., Croft, S. L., Kendrick, H. D., Anson, C. E. and Powell, A. K. (2003a). Synthesis and characterization of copper(II) complexes of pyridine-2-carboxamidrazones as potent antimalarial agents. *Inorganica Chimica Acta*, 349, 23-29.

Gokhale, N. H., Padhye, S. B., Croft, S. L., Kendrick, H. D., Davies, W., Anson, C. E. and Powell, A. K. (2003b). Transition metal complexes of buparvaquone as potent new antimalarial agents. 1. Synthesis, X-ray crystal-structures, electrochemistry and antimalarial activity against Plasmodium falciparum. *Journal of Inorganic Biochemistry*, 95, 249-258.

Gokhale, N. H., Shirisha, K., Padhye, S. B., Croft, S. L., Kendrick, H. D. and McKee, V. (2006). Metalloantimalarials: synthesis, X-ray crystal structure of potent antimalarial

copper (II) complex of arylazo-4-hydroxy-1,2-naphthoquinone. *Bioorganic & Medicinal Chemistry Letters,* 16, 430-432.

Goldring, J. P. (2015). Spectrophotometric methods to determine protein concentration. *In:* Kurien, B. and Scofield, R. (eds.) *Methods in Molecular Biology.* New York, NY: Humana Press.

Grassi, B. (1901). Studi di uno zoologo sulla malaria. *Rome*.

Gray, L. W., Peng, F., Molloy, S. A., Pendyala, V. S., Muchenditsi, A., Muzik, O., Lee, J., Kaplan, J. H. and Lutsenko, S. (2012). Urinary copper elevation in a mouse model of Wilson's disease is a regulated process to specifically decrease the hepatic copper load. *PLoS One,* 7, e38327. doi:10.1371/journal.pone.0038327.

Gregson, A. and Plowe, C. V. (2005). Mechanisms of resistance of malaria parasites to antifolates. *Pharmacological Reviews,* 57, 117-145.

Gu, W. and Roeder, R. G. (1997). Activation of p53 sequence-specific DNA binding by acetylation of the p53 C-terminal domain. *Cell,* 90, 595-606.

Guan, Q., Zheng, W., Tang, S., Liu, X., Zinkel, R. A., Tsui, K.-W., Yandell, B. S. and Culbertson, M. R. (2006). Impact of nonsense-mediated mRNA decay on the global expression profile of budding yeast. *PLOS Genetics,* 2, 1924-1943.

Guex, N., Peitsch, M. C. and Schwede, T. (2009). Automated comparative protein structure modeling with SWISS-MODEL and Swiss-PdbViewer: a historical perspective. *Electrophoresis,* 30, S162-S173.

Günther, S., Matuschewski, K. and Müller, S. (2009). Knockout studies reveal an important role of *Plasmodium* lipoic acid protein ligase A1 for asexual blood stage parasite survival. *PLoS One,* 4, e5510. doi:10.1371/journal.pone.0005510.

Halliwell, B. and Gutteridge, J. M. (1984). Oxygen toxicity, oxygen radicals, transition metals and disease. *Biochemical Journal,* 219, 1-14.

Hansen, K. S., Grieve, E., Mikhail, A., Mayan, I., Mohammed, N., Anwar, M., Baktash, S. H., Drake, T. L., Whitty, C. J. M., Rowland, M. W. and Leslie, T. J. (2015). Cost-effectiveness of malaria diagnosis using rapid diagnostic tests compared to microscopy or clinical symptoms alone in Afghanistan. *Malaria Journal,* 14, 217. doi:10.1186/s12936-015-0696-1.

Hassett, R. and Kosman, D. J. (1995). Evidence for Cu(II) reduction as a component of copper uptake by *Saccharomyces cerevisiae*. *Journal of Biological Chemistry,* 270, 128-134.

He, F., Li, X., Spatrick, P., Casillo, R., Dong, S. and Jacobson, A. (2003). Genome-wide analysis of mRNAs regulated by the nonsense-mediated and 5′ to 3′ mRNA decay pathways in yeast. *Molecular Cell,* 12, 1439-1452.

Heckman, K. L. and Pease, L. R. (2007). Gene splicing and mutagenesis by PCR-driven overlap extension. *Nature Protocols,* 2, 924-932.

Heuchel, R., Radtke, F., Georgiev, O., Stark, G., Aguet, M. and Schaffner, W. (1994). The transcription factor MTF-1 is essential for basal and heavy metal-induced metallothionein gene expression. *The EMBO Journal,* 13, 2870-2875.

Hiser, L., Di Valentin, M., Hamer, A. G. and Hosler, J. P. (2000). Cox11p is required for stable formation of the Cu_B and magnesium centers of cytochrome c oxidase. *Journal of Biological Chemistry,* 275, 619-623.

Ho, S. N., Hunt, H. D., Horton, R. M., Pullen, J. K. and Pease, L. R. (1989). Site-directed mutagenesis by overlap extension using the polymerase chain reaction. *Gene,* 77, 51-59.

Hodgkinson, V. and Petris, M. J. (2012). Copper homeostasis at the host-pathogen interface. *Journal of Biological Chemistry,* 287, 13549-13555.

Horng, Y.-C., Cobine, P. A., Maxfield, A. B., Carr, H. S. and Winge, D. R. (2004). Specific copper transfer from the Cox17 metallochaperone to both Sco1 and Cox11 in the assembly of yeast cytochrome c oxidase. *Journal of Biological Chemistry,* 279, 35334-35340.

Howell, S. B., Safaei, R., Larson, C. A. and Sailor, M. J. (2010). Copper transporters and the cellular pharmacology of the platinum-containing cancer drugs. *Molecular Pharmacology,* 77, 887-894.

Howells, R. E., Peters, W. and Fullard, J. (1969). Cytochrome oxidase activity in a normal and some drug-resistant strains of *Plasmodium berghei* - a cytochemical study. I. Asexual erythrocytic stages. *Military Medicine,* 134, 893-915.

Huang, W.-C., Hsu, S.-C., Huang, S.-J., Chen, Y.-J., Hsiao, Y.-C., Zhang, W., Fidler, I. J. and Hung, M.-C. (2013). Exogenous expression of human SGLT1 exhibits aggregations in sodium dodecyl sulfate polyacrylamide gel electrophoresis. *American Journal of Translational Research,* 5, 441-449.

Hung, Y. H., Bush, A. I. and Cherny, R. A. (2010). Copper in the brain and Alzheimer's disease. *Journal of Biological Inorganic Chemistry,* 15, 61-76.

Hurdayal, R., Achilonu, I., Choveaux, D., Coetzer, T. H. and Dean Goldring, J. P. (2010). Anti-peptide antibodies differentiate between plasmodial lactate dehydrogenases. *Peptides,* 31, 525-532.

Hyde, J. E. (2005). Drug-resistant malaria. *Trends in Parasitology,* 21, 494-498.

Jackson, A. P., Otto, T. D., Aslett, M., Armstrong, S. D., Bringaud, F., Schlacht, A., Hartley, C., Sanders, M., Wastling, J. M., Dacks, J. B., Acosta-Serrano, A., Field, M. C., Ginger, M. L. and Berriman, M. (2016). Kinetoplastid phylogenomics reveals the evolutionary innovations associated with the origins of parasitism. *Current Biology,* 26, 161-172.

Jelinek, W. R. and Schmid, C. W. (1982). Repetitive sequences in eukaryotic DNA and their expression. *Annual Review of Biochemistry,* 51, 813-844.

Jiménez-Díaz, M. B., Ebert, D., Salinas, Y., Pradhan, A., Lehane, A. M., Myrand-Lapierre, M.-E., O'Loughlin, K. G., Shackleford, D. M., Justino de Almeida, M., Carrillo, A. K., Clark, J. A., Dennis, A. S. M., Diep, J., Deng, X., Duffy, S., Endsley, A. N., Fedewa, G., Guiguemde, W. A., Gómez, M. G., Holbrook, G., Horst, J., Kim, C. C., Liu, J., Lee, M. C. S., Matheny, A., Martínez, M. S., Miller, G., Rodríguez-Alejandre, A., Sanz, L., Sigal, M., Spillman, N. J., Stein, P. D., Wang, Z., Zhu, F., Waterson, D., Knapp, S., Shelat, A., Avery, V. M., Fidock, D. A., Gamo, F.-J., Charman, S. A., Mirsalis, J. C., Ma, H., Ferrer, S., Kirk, K., Angulo-Barturen, I., Kyle, D. E., DeRisi, J. L., Floyd, D. M. and Guy, R. K. (2014). (+)-SJ733, a clinical candidate for malaria that acts through ATP4 to induce rapid host-mediated clearance of *Plasmodium*. *Proceedings of the National Academy of Sciences of the United States of America,* 111, E5455-E5462.

Josling, G. A. and Llinas, M. (2015). Sexual development in *Plasmodium* parasites: knowing when it's time to commit. *Nature Reviews Microbiology,* 13, 573-587.

Kanjee, U., Grüring, C., Chaand, M., Lin, K.-M., Egan, E., Manzo, J., Jones, P. L., Yu, T., Barker, R., Weekes, M. P. and Duraisingh, M. T. (2017). CRISPR/Cas9 knockouts reveal genetic interaction between strain-transcendent erythrocyte determinants of *Plasmodium falciparum* invasion. *Proceedings of the National Academy of Sciences of the United States of America,* 114, E9356-E9365.

Kaplan, J. H. and Maryon, E. B. (2016). How mammalian cells acquire copper: an essential but potentially toxic metal. *Biophysical Journal,* 110, 7-13.

Kappe, S. H. I., Vaughan, A. M., Boddey, J. A. and Cowman, A. F. (2010). That was then but this is now: malaria research in the time of an eradication agenda. *Science,* 328, 862-866.

Kar, N. P., Kumar, A., Singh, O. P., Carlton, J. M. and Nanda, N. (2014). A review of malaria transmission dynamics in forest ecosystems. *Parasites & Vectors,* 7, 265. doi:10.1186/1756-3305-7-265.

Kasetsirikul, S., Buranapong, J., Srituravanich, W., Kaewthamasorn, M. and Pimpin, A. (2016). The development of malaria diagnostic techniques: a review of the approaches

with focus on dielectrophoretic and magnetophoretic methods. *Malaria Journal,* 15, 358. doi:10.1186/s12936-016-1400-9.

Katinka, M. D., Duprat, S., Cornillot, E., Méténier, G., Thomarat, F., Prensier, G., Barbe, V., Peyretaillade, E., Brottier, P., Wincker, P., Delbac, F., El Alaoui, H., Peyret, P., Saurin, W., Gouy, M., Weissenbach, J. and Vivarès, C. P. (2001). Genome sequence and gene compaction of the eukaryote parasite *Encephalitozoon cuniculi*. *Nature,* 414, 450-453.

Kato, N., Comer, E., Sakata-Kato, T., Sharma, A., Sharma, M., Maetani, M., Bastien, J., Brancucci, N. M., Bittker, J. A., Corey, V., Clarke, D., Derbyshire, E. R., Dornan, G. L., Duffy, S., Eckley, S., Itoe, M. A., Koolen, K. M. J., Lewis, T. A., Lui, P. S., Lukens, A. K., Lund, E., March, S., Meibalan, E., Meier, B. C., McPhail, J. A., Mitasev, B., Moss, E. L., Sayes, M., Van Gessel, Y., Wawer, M. J., Yoshinaga, T., Zeeman, A.-M., Avery, V. M., Bhatia, S. N., Burke, J. E., Catteruccia, F., Clardy, J. C., Clemons, P. A., Dechering, K. J., Duvall, J. R., Foley, M. A., Gusovsky, F., Kocken, C. H. M., Marti, M., Morningstar, M. L., Munoz, B., Neafsey, D. E., Sharma, A., Winzeler, E. A., Wirth, D. F., Scherer, C. A. and Schreiber, S. L. (2016). Diversity-oriented synthesis yields novel multistage antimalarial inhibitors. *Nature,* 538, 344-349.

Kawano, S., Yamano, K., Naoé, M., Momose, T., Terao, K., Nishikawa, S.-i., Watanabe, N. and Endo, T. (2009). Structural basis of yeast Tim40/Mia40 as an oxidative translocator in the mitochondrial intermembrane space. *Proceedings of the National Academy of Sciences,* 106, 14403-14407.

Kaypee, S., Sudarshan, D., Shanmugam, M. K., Mukherjee, D., Sethi, G. and Kundu, T. K. (2016). Aberrant lysine acetylation in tumorigenesis: implications in the development of therapeutics. *Pharmacology and Therapeutics,* 162, 98-119.

Keller, G., Bird, A. and Winge, D. R. (2005). Independent metalloregulation of Ace1 and Mac1 in *Saccharomyces cerevisiae*. *Eukaryotic Cell,* 4, 1863-1871.

Kenthirapalan, S., Waters, A. P., Matuschewski, K. and Kooij, T. W. (2014). Copper-transporting ATPase is important for malaria parasite fertility. *Molecular Microbiology,* 91, 315-325.

Kenthirapalan, S., Waters, A. P., Matuschewski, K. and Kooij, T. W. A. (2016). Functional profiles of orphan membrane transporters in the life cycle of the malaria parasite. *Nature Communications,* 7, 10519. doi:10.1038/ncomms10519.

Kermekchiev, M. B., Kirilova, L. I., Vail, E. E. and Barnes, W. M. (2009). Mutants of *Taq* DNA polymerase resistant to PCR inhibitors allow DNA amplification from whole blood and crude soil samples. *Nucleic Acids Research,* 37, e40. doi:10.1093/nar/gkn1055.

Kersting, S., Rausch, V., Bier, F. F. and von Nickisch-Rosenegk, M. (2014). Rapid detection of *Plasmodium falciparum* with isothermal recombinase polymerase amplification and lateral flow analysis. *Malaria Journal,* 13, 99. doi:10.1186/1475-2875-13-99.

Kesteman, T., Randrianarivelojosia, M. and Rogier, C. (2017). The protective effectiveness of control interventions for malaria prevention: a systematic review of the literature [version 1; referees: 1 approved, 2 approved with reservations]. *F1000Research,* 6, 1932. doi:10.12688/f1000research.12952.1

Khalimonchuk, O., Ostermann, K. and Rodel, G. (2005). Evidence for the association of yeast mitochondrial ribosomes with Cox11p, a protein required for the Cu_B site formation of cytochrome c oxidase. *Current Genetics,* 47, 223-233.

Khan, M. M. T. and Martell, A. E. (1967). Metal ion and metal chelate catalyzed oxidation of ascorbic acid by molecular oxygen. II. Cupric and ferric chelate catalyzed oxidation. *Journal of the American Chemical Society,* 89, 7104-7111.

Kim, B.-E., Nevitt, T. and Thiele, D. J. (2008). Mechanisms for copper acquisition, distribution and regulation. *Nature Chemical Biology,* 4, 176-185.

Kim, S. C., Sprung, R., Chen, Y., Xu, Y., Ball, H., Pei, J., Cheng, T., Kho, Y., Xiao, H., Xiao, L., Grishin, N. V., White, M., Yang, X. J. and Zhao, Y. (2006). Substrate and functional diversity of lysine acetylation revealed by a proteomics survey. *Molecular Cell,* 23, 607-618.

Koch, J. R. and Schmid, F. X. (2014). Mia40 targets cysteines in a hydrophobic environment to direct oxidative protein folding in the mitochondria. *Nature Communications,* 5, 3041. doi:10.1038/ncomms4041.

Koehler, C. M., Jarosch, E., Tokatlidis, K., Schmid, K., Schweyen, R. J. and Schatz, G. (1998). Import of mitochondrial carriers mediated by essential proteins of the intermembrane space. *Science,* 279, 369-373.

Korsinczky, M., Chen, N., Kotecka, B., Saul, A., Rieckmann, K. and Cheng, Q. (2000). Mutations in *Plasmodium falciparum* cytochrome b that are associated with atovaquone resistance are located at a putative drug-binding site. *Antimicrobial Agents and Chemotherapy,* 44, 2100-2108.

Kowalski, L., Bragoszewski, P., Khmelinskii, A., Glow, E., Knop, M. and Chacinska, A. (2018). Determinants of the cytosolic turnover of mitochondrial intermembrane space proteins. *BMC Biology,* 16, 66. doi:10.1186/s12915-018-0536-1.

Krause, R. G. E. and Goldring, J. P. D. (2018). Phosphoethanolamine-N-methyltransferase is a potential biomarker for the diagnosis of *P. knowlesi* and *P. falciparum* malaria. *PLoS One,* 13, e0193833. doi.org/10.1371/journal.pone.0193833.

Krause, R. G. E., Grobler, A. F. and Goldring, J. P. D. (2015). Comparing antibody responses in chickens against *Plasmodium falciparum* lactate dehydrogenase and glyceraldehyde-3-phosphate dehydrogenase with Freund's and Pheroid® Adjuvants. *Immunological Investigations,* 44, 627-642.

Krause, R. G. E., Hurdayal, R., Choveaux, D., Przyborski, J. M., Coetzer, T. H. T. and Goldring, J. P. D. (2017). *Plasmodium* glyceraldehyde-3-phosphate dehydrogenase: a potential malaria diagnostic target. *Experimental Parasitology,* 179, 7-19.

Kremsner, P. G. and Krishna, S. (2004). Antimalarial combinations. *The Lancet,* 364, 285-294.

Krishna, S. N., Luan, C.-H., Mishra, R. K., Xu, L., Scheidt, K. A., Anderson, W. F. and Bergan, R. C. (2013). A fluorescence-based thermal shift assay identifies inhibitors of mitogen activated protein kinase Kinase 4. *PLoS One,* 8, e81504. doi:10.1371/journal.pone.0081504.

Krogh, A., Larsson, B., von Heijne, G. and Sonnhammer, E. L. (2001). Predicting transmembrane protein topology with a hidden Markov model: application to complete genomes. *Journal of Molecular Biology,* 305, 567-580.

Krotoski, W. A., Collins, W. E., Bray, R. S., Garnham, P. C. C., Cogswell, F. B., Gwadz, R. W., Killick-Kendrick, R., Wolf, R., Sinden, R., Koontz, L. C. and Stanfill, P. S. (1982). Demonstration of hypnozoites in sporozoite-transmitted *Plasmodium vivax* Infection. *The American Journal of Tropical Medicine and Hygiene,* 31, 1291-1293.

Krungkrai, J., Krungkrai, S. R. and Bhumiratana, A. (1993). *Plasmodium berghei*: partial purification and characterization of the mitochondrial cytochrome c oxidase. *Experimental Parasitology,* 77, 136-146.

Krungkrai, J., Krungkrai, S. R., Suraveratum, N. and Prapunwattana, P. (1997). Mitochondrial ubiquino-cytochrome C reductase and cytochrome C oxidase: Chemotherapeutic targets in malaria paraistes. *Iubmb Life,* 42, 1007-1014.

Kuhen, K. L., Chatterjee, A. K., Rottmann, M., Gagaring, K., Borboa, R., Buenviaje, J., Chen, Z., Francek, C., Wu, T., Nagle, A., Barnes, S. W., Plouffe, D., Lee, M. C. S., Fidock, D. A., Graumans, W., van de Vegte-Bolmer, M., van Gemert, G. J., Wirjanata, G., Sebayang, B., Marfurt, J., Russell, B., Suwanarusk, R., Price, R. N., Nosten, F., Tungtaeng, A., Gettayacamin, M., Sattabongkot, J., Taylor, J., Walker, J. R., Tully, D., Patra, K. P., Flannery, E. L., Vinetz, J. M., Renia, L., Sauerwein, R. W., Winzeler, E. A., Glynne, R. J. and Diagana, T. T. (2014). KAF156 is an antimalarial clinical candidate with potential for use in prophylaxis, treatment, and prevention of disease transmission. *Antimicrobial Agents and Chemotherapy,* 58, 5060-5067.

Laemmli, U. K. (1970). Cleavage of structural proteins during the assembly of the head of bacteriophage T4. *Nature,* 227, 680-685.

LaGier, M. J., Zhu, G. and Keithly, J. S. (2001). Characterization of a heavy metal ATPase from the apicomplexan *Cryptosporidium parvum*. *Gene,* 266, 25-34.

Larsson, A. and Sjoquist, J. (1990). Chicken IgY: utilizing the evolutionary difference. *Comparative Immunology, Microbiology and Infectious Diseases,* 13, 199-201.

Laveran, A. (1881). Un nouveau parasite trouvé dans le sang de malades atteints de fièvre palustre. Origine parasitaire des accidents de l'impaludisme. *Bulletins et Mémoires de la Société Médicale des Hôpitaux de Paris,* 17, 158-167.

Le Roch, K. G., Zhou, Y., Blair, P. L., Grainger, M., Moch, J. K., Haynes, J. D., De la Vega, P., Holder, A. A., Batalov, S., Carucci, D. J. and Winzeler, E. A. (2003). Discovery of gene function by expression profiling of the malaria parasite life cycle. *Science,* 301, 1503-1508.

Leary, S. C., Cobine, P. A., Nishimura, T., Verdijk, R. M., de Krijger, R., de Coo, R., Tarnopolsky, M. A., Winge, D. R. and Shoubridge, E. A. (2013). COX19 mediates the transduction of a mitochondrial redox signal from SCO1 that regulates ATP7A-mediated cellular copper efflux. *Molecular Biology of the Cell,* 24, 683-691.

Lee, A. H., Symington, L. S. and Fidock, D. A. (2014). DNA repair mechanisms and their biological roles in the malaria parasite *Plasmodium falciparum*. *Microbiology and Molecular Biology Reviews,* 78, 469-486.

Lee, J., Peña, M. M. O., Nose, Y. and Thiele, D. J. (2002a). Biochemical characterization of the human copper transporter Ctr1. *Journal of Biological Chemistry,* 277, 4380-4387.

Lee, J., Petris, M. J. and Thiele, D. J. (2002b). Characterization of mouse embryonic cells deficient in the Ctr1 high affinity copper transporter: identification of a Ctr1-independent copper transport system. *Journal of Biological Chemistry,* 277, 40253-40259.

Lee, J., Prohaska, J. R. and Thiele, D. J. (2001). Essential role for mammalian copper transporter Ctr1 in copper homeostasis and embryonic development. *Proceedings of National Academy of Sciences of the United States of America,* 98, 6842-6847.

Lee, P. C., Chong, E. T. J., Anderios, F., Al Lim, Y., Chew, C. H. and Chua, K. H. (2015). Molecular detection of human *Plasmodium* species in Sabah using PlasmoNex™ multiplex PCR and hydrolysis probes real-time PCR. *Malaria Journal,* 14, 28. doi:10.1186/s12936-015-0542-5.

Lee, W., Syed Atif, A., Tan, S. C. and Leow, C. H. (2017). Insights into the chicken IgY with emphasis on the generation and applications of chicken recombinant monoclonal antibodies. *Journal of Immunological Methods,* 447, 71-85.

Levine, R. L. (1983). Oxidative modification of glutamine synthetase. I. Inactivation is due to loss of one histidine residue. *Journal of Biological Chemistry,* 258, 11823-11827.

Li, W., Cowley, A., Uludag, M., Gur, T., McWilliam, H., Squizzato, S., Park, Y. M., Buso, N. and Lopez, R. (2015). The EMBL-EBI bioinformatics web and programmatic tools framework. *Nucleic Acids Research,* 43, W580-W584.

Lin, W.-Z., Fang, J.-A., Xiao, X. and Chou, K.-C. (2012). Predicting secretory proteins of malaria parasite by incorporating sequence evolution information into pseudo amino acid composition via Grey system model. *PLoS One,* 7, e49040. doi:10.1371/journal.pone.0049040.

Linder, M. C. (2001). Copper and genomic stability in mammals. *Mutation Research,* 475, 141-152.

Linder, M. C. (2016). Ceruloplasmin and other copper binding components of blood plasma and their functions: an update. *Metallomics,* 8, 887-905.

Liu, X. F., Supek, F., Nelson, N. and Culotta, V. C. (1997). Negative control of heavy metal uptake by the *Saccharomyces cerevisiae* BSD2 gene. *Journal of Biological Chemistry,* 272, 11763-11769.

Lo, M. C., Aulabaugh, A., Jin, G., Cowling, R., Bard, J., Malamas, M. and Ellestad, G. (2004). Evaluation of fluorescence-based thermal shift assays for hit identification in drug discovery. *Analytical Biochemistry,* 332, 153-159.

Lode, A., Kuschel, M., Paret, C. and Rödel, G. (2000). Mitochondrial copper metabolism in yeast: interaction between Sco1p and Cox2p. *FEBS Letters,* 485, 19-24.

Lutsenko, S. (2010). Human copper homeostasis: a network of interconnected pathways. *Current Opinion in Chemical Biology,* 14, 211-217.

Lutsenko, S. (2016). Copper trafficking to the secretory pathway. *Metallomics,* 8, 840-852.

Lutsenko, S., Petrukhin, K., Cooper, M. J., Gilliam, C. T. and Kaplan, J. H. (1997). N-terminal domains of human copper-transporting adenosine triphosphatases (the Wilson's and Menkes disease proteins) bind copper selectively *in vivo* and *in vitro* with stoichiometry of one copper per metal-binding repeat. *Journal of Biological Chemistry,* 272, 18939-18944.

MacRae, J. I., Dixon, M. W., Dearnley, M. K., Chua, H. H., Chambers, J. M., Kenny, S., Bottova, I., Tilley, L. and McConville, M. J. (2013). Mitochondrial metabolism of sexual and asexual blood stages of the malaria parasite *Plasmodium falciparum*. *Bmc Biology,* 11, 67. doi:10.1186/1741-7007-11-67.

Mansilla, N., Racca, S., Gras, E. D., Gonzalez, H. D. and Welchen, E. (2018). The complexity of mitochondrial complex IV: an update of cytochrome c oxidase biogenesis in plants. *International Journal of Molecular Sciences,* 19, 662. doi:10.3390/ijms19030662.

Martell, A. E. (1982). Chelates of ascorbic acid. *Ascorbic acid: chemistry, metabolism, and uses.* American Chemical Society.

Martin-Sanchez, F., Iakovidis, I., Nørager, S., Maojo, V., de Groen, P., Van der Lei, J., Jones, T., Abraham-Fuchs, K., Apweiler, R., Babic, A., Baud, R., Breton, V., Cinquin, P., Doupi, P., Dugas, M., Eils, R., Engelbrecht, R., Ghazal, P., Jehenson, P., Kulikowski, C., Lampe, K., De Moor, G., Orphanoudakis, S., Rossing, N., Sarachan, B., Sousa, A., Spekowius, G., Thireos, G., Zahlmann, G., Zvárová, J., Hermosilla, I. and Vicente, F. J. (2004). Synergy between medical informatics and bioinformatics: facilitating genomic medicine for future health care. *Journal of Biomedical Informatics,* 37, 30-42.

Martin, R. E. and Kirk, K. (2004). The malaria parasite's chloroquine resistance transporter is a member of the drug/metabolite transporter superfamily. *Molecular Biology and Evolution,* 21, 1938-1949.

Martins, L. J., Jensen, L. T., Simon, J. R., Keller, G. L. and Winge, D. R. (1998). Metalloregulation of FRE1 and FRE2 homologs in *Saccharomyces cerevisiae*. *Journal of Biological Chemistry,* 273, 23716-23721.

Marx, G. and Chevion, M. (1986). Site-specific modification of albumin by free radicals. Reaction with copper(II) and ascorbate. *The Biochemical Journal,* 236, 397-400.

Maryon, E. B., Molloy, S. A. and Kaplan, J. H. (2013). Cellular glutathione plays a key role in copper uptake mediated by human copper transporter 1. *American Journal of Physiology - Cell Physiology,* 304, C768-C779.

Massey, N. C., Garrod, G., Wiebe, A., Henry, A. J., Huang, Z., Moyes, C. L. and Sinka, M. E. (2016). A global bionomic database for the dominant vectors of human malaria. *Scientific Data,* 3, 160014. doi: 10.1038/sdata.2016.14.

Mather, M. W., Darrouzet, E., Valkova-Valchanova, M., Cooley, J. W., McIntosh, M. T., Daldal, F. and Vaidya, A. B. (2005). Uncovering the molecular mode of action of the antimalarial drug atovaquone using a bacterial system. *Journal of Biological Chemistry,* 280, 27458-27465.

Maxfield, A. B., Heaton, D. N. and Winge, D. R. (2004). Cox17 is functional when tethered to the mitochondrial Inner membrane. *Journal of Biological Chemistry,* 279, 5072-5080.

Mayxay, M., Pukrittayakamee, S., Chotivanich, K., Looareesuwan, S. and White, N. J. (2001). Persistence of *Plasmodium falciparum* HRP-2 in successfully treated acute falciparum malaria. *Transactions of the Royal Society of Tropical Medicine and Hygiene,* 95, 179-182.

McCarthy, J. S., Lotharius, J., Ruckle, T., Chalon, S., Phillips, M. A., Elliott, S., Sekuloski, S., Griffin, P., Ng, C. L., Fidock, D. A., Marquart, L., Williams, N. S.,

Gobeau, N., Bebrevska, L., Rosario, M., Marsh, K. and Mohrle, J. J. (2017). Safety, tolerability, pharmacokinetics, and activity of the novel long-acting antimalarial DSM265: a two-part first-in-human phase 1a/1b randomised study. *Lancet Infectious Diseases,* 17, 626-635.

McNamara, C. W., Lee, M. C. S., Lim, C. S., Lim, S. H., Roland, J., Nagle, A., Simon, O., Yeung, B. K. S., Chatterjee, A. K., McCormack, S. L., Manary, M. J., Zeeman, A.-M., Dechering, K. J., Kumar, T. R. S., Henrich, P. P., Gagaring, K., Ibanez, M., Kato, N., Kuhen, K. L., Fischli, C., Rottmann, M., Plouffe, D. M., Bursulaya, B., Meister, S., Rameh, L., Trappe, J., Haasen, D., Timmerman, M., Sauerwein, R. W., Suwanarusk, R., Russell, B., Renia, L., Nosten, F., Tully, D. C., Kocken, C. H. M., Glynne, R. J., Bodenreider, C., Fidock, D. A., Diagana, T. T. and Winzeler, E. A. (2013). Targeting *Plasmodium* PI(4)K to eliminate malaria. *Nature,* 504, 248-253.

Mehlin, C., Boni, E., Buckner, F. S., Engel, L., Feist, T., Gelb, M. H., Haji, L., Kim, D., Liu, C., Mueller, N., Myler, P. J., Reddy, J. T., Sampson, J. N., Subramanian, E., Van Voorhis, W. C., Worthey, E., Zucker, F. and Hol, W. G. (2006). Heterologous expression of proteins from *Plasmodium falciparum*: results from 1000 genes. *Molecular and Biochemical Parasitology,* 148, 144-160.

Meister, S., Plouffe, D. M., Kuhen, K. L., Bonamy, G. M. C., Wu, T., Barnes, S. W., Bopp, S. E., Borboa, R., Bright, A. T., Che, J., Cohen, S., Dharia, N. V., Gagaring, K., Gettayacamin, M., Gordon, P., Groessl, T., Kato, N., Lee, M. C. S., McNamara, C. W., Fidock, D. A., Nagle, A., Nam, T.-g., Richmond, W., Roland, J., Rottmann, M., Zhou, B., Froissard, P., Glynne, R. J., Mazier, D., Sattabongkot, J., Schultz, P. G., Tuntland, T., Walker, J. R., Zhou, Y., Chatterjee, A., Diagana, T. T. and Winzeler, E. A. (2011). Imaging of *Plasmodium* liver stages to drive next-generation antimalarial drug discovery. *Science,* 334, 1372-1377.

Menard, D. and Dondorp, A. (2017). Antimalarial drug resistance: a threat to malaria elimination. *Cold Spring Harbor Perspectives in Medicine,* 7, a025619. doi: 10.1101/cshperspect.a025619.

Meshnick, S. R., Scott, M. D., Lubin, B., Ranz, A. and Eaton, J. W. (1990). Antimalarial activity of diethyldithiocarbamate: potentiation by copper. *Biochemical Pharmacology,* 40, 213-216.

Miao, J., Lawrence, M., Jeffers, V., Zhao, F., Parker, D., Ge, Y., Sullivan, W. J. and Cui, L. (2013). Extensive lysine acetylation occurs in evolutionarily conserved metabolic pathways and parasite-specific functions during Plasmodium falciparum intraerythrocytic development. *Molecular Microbiology,* 89, 660-675.

Milardi, D., Grasso, D. M., Verbeet, M. P., Canters, G. W. and La Rosa, C. (2003). Thermodynamic analysis of the contributions of the copper ion and the disulfide bridge to azurin stability: synergism among multiple depletions. *Archives of Biochemistry and Biophysics,* 414, 121-127.

Milenkovic, D., Ramming, T., Müller, J. M., Wenz, L.-S., Gebert, N., Schulze-Specking, A., Stojanovski, D., Rospert, S. and Chacinska, A. (2009). Identification of the signal directing Tim9 and Tim10 into the intermembrane space of mitochondria. *Molecular Biology of the Cell*, 20, 2530-2539.

Miller, L. H., Good, M. F. and Milon, G. (1994a). Malaria pathogenesis. *Science*, 264, 1878-1883.

Miller, R. L., Ikram, S., Armelagos, G. J., Walker, R., Harer, W. B., Shiff, C. J., Baggett, D., Carrigan, M. and Maret, S. M. (1994b). Diagnosis of *Plasmodium falciparum* infections in mummies using the rapid manual ParaSight™-F test. *Transactions of the Royal Society of Tropical Medicine and Hygiene*, 88, 31-32.

Millhauser, G. L. (2007). Copper and the prion protein: methods, structures, function, and disease. *Annual Review of Physical Chemistry*, 58, 299-320.

Mok, B. W., Ribacke, U., Winter, G., Yip, B. H., Tan, C. S., Fernandez, V., Chen, Q., Nilsson, P. and Wahlgren, M. (2007). Comparative transcriptomal analysis of isogenic *Plasmodium falciparum* clones of distinct antigenic and adhesive phenotypes. *Molecular and Biochemical Parasitology*, 151, 184-192.

Morris, N., Frean, J., Baker, L., Ukpe, I. S., Barnes, K. I., Kruger, P., Mabuza, A., Raswiswi, E., Maharaj, R., Blumberg, L. and Moonasar, D. (2013). Re-defining the extent of malaria transmission in South Africa: implications for chemoprophylaxis. *South African Medical Journal*, 103, 861-864.

Mruk, D. D. and Cheng, C. Y. (2011). Enhanced chemiluminescence (ECL) for routine immunoblotting: An inexpensive alternative to commercially available kits. *Spermatogenesis*, 1, 121-122.

Mu, J., Ferdig, M. T., Feng, X., Joy, D. A., Duan, J., Furuya, T., Subramanian, G., Aravind, L., Cooper, R. A., Wootton, J. C., Xiong, M. and Su, X. z. (2003). Multiple transporters associated with malaria parasite responses to chloroquine and quinine. *Molecular Microbiology*, 49, 977-989.

Multhaup, G., Ruppert, T., Schlicksupp, A., Hesse, L., Bill, E., Pipkorn, R., Masters, C. L. and Beyreuther, K. (1998). Copper-binding amyloid precursor protein undergoes a site-specific fragmentation in the reduction of hydrogen peroxide. *Biochemistry*, 37, 7224-7230.

Murray, C. J. L., Ortblad, K. F., Guinovart, C., Lim, S. S., Wolock, T. M., Roberts, D. A., Dansereau, E. A., Graetz, N., Barber, R. M., Brown, J. C., Wang, H., Duber, H. C., Naghavi, M., Dicker, D., Dandona, L., Salomon, J. A., Heuton, K. R., Foreman, K., Phillips, D. E., Fleming, T. D., Flaxman, A. D., Phillips, B. K., Johnson, E. K., Coggeshall, M. S., Abd-Allah, F., Abera, S. F., Abraham, J. P., Abubakar, I., Abu-Raddad, L. J., Abu-Rmeileh, N. M., Achoki, T., Adeyemo, A. O., Adou, A. K., Adsuar, J. C., Agardh, E. E., Akena, D., Al Kahbouri, M. J.,

Alasfoor, D., Albittar, M. I., Alcalá-Cerra, G., Alegretti, M. A., Alemu, Z. A., Alfonso-Cristancho, R., Alhabib, S., Ali, R., Alla, F., Allen, P. J., Alsharif, U., Alvarez, E., Alvis-Guzman, N., Amankwaa, A. A., Amare, A. T., Amini, H., Ammar, W., Anderson, B. O., Antonio, C. A. T., Anwari, P., Ärnlöv, J., Arsenijevic, V. S. A., Artaman, A., Asghar, R. J., Assadi, R., Atkins, L. S., Badawi, A., Balakrishnan, K., Banerjee, A., Basu, S., Beardsley, J., Bekele, T., Bell, M. L., Bernabe, E., Beyene, T. J., Bhala, N., Bhalla, A., Bhutta, Z. A., Abdulhak, A. B., Binagwaho, A., Blore, J. D., Basara, B. B., Bose, D., Brainin, M., Breitborde, N., Castañeda-Orjuela, C. A., Catalá-López, F., Chadha, V. K., Chang, J.-C., Chiang, P. P.-C., Chuang, T.-W., Colomar, M., Cooper, L. T., Cooper, C., Courville, K. J., Cowie, B. C., Criqui, M. H., Dandona, R., Dayama, A., De Leo, D., Degenhardt, L., Del Pozo-Cruz, B., Deribe, K., *et al.* (2014). Global, regional, and national incidence and mortality for HIV, tuberculosis, and malaria during 1990–2013: a systematic analysis for the Global Burden of Disease Study 2013. *The Lancet,* 384, 1005-1070.

Murtha, K., Hwang, M., Peccarelli, M. C., Scott, T. D. and Kebaara, B. W. (2018). The nonsense-mediated mRNA decay (NMD) pathway differentially regulates COX17, COX19 and COX23 mRNAs. *Current Genetics,* doi:10.1007/s00294-018-0892-y.

Naoé, M., Ohwa, Y., Ishikawa, D., Ohshima, C., Nishikawa, S.-i., Yamamoto, H. and Endo, T. (2004). Identification of Tim40 that mediates protein sorting to the mitochondrial intermembrane space. *Journal of Biological Chemistry,* 279, 47815-47821.

Nevitt, T., Ohrvik, H. and Thiele, D. J. (2012). Charting the travels of copper in eukaryotes from yeast to mammals. *Biochimica et Biophysica Acta,* 1823, 1580-1593.

Nkumama, I. N., O'Meara, W. P. and Osier, F. H. A. (2017). Changes in malaria epidemiology in Africa and new challenges for elimination. *Trends in Parasitology,* 33, 128-140.

Nobrega, M. P., Bandeira, S. C., Beers, J. and Tzagoloff, A. (2002). Characterization of COX19, a widely distributed gene required for expression of mitochondrial cytochrome oxidase. *Journal of Biological Chemistry,* 277, 40206-40211.

Nosten, F. and White, N. J. (2007). Artemisinin-based combination treatment of *falciparum* malaria. *The American Journal of Tropical Medicine and Hygiene,* 77, 181-192.

Ohgami, R. S., Campagna, D. R., McDonald, A. and Fleming, M. D. (2006). The Steap proteins are metalloreductases. *Blood,* 108, 1388-1394.

Öhrvik, H. and Thiele, D. J. (2015). The role of Ctr1 and Ctr2 in mammalian copper homeostasis and platinum-based chemotherapy. *Journal of Trace Elements in Medicine and Biology,* 31, 178-182.

Okada, N., Yamamoto, T., Watanabe, M., Yoshimura, Y., Obana, E., Yamazaki, N., Kawazoe, K., Shinohara, Y. and Minakuchi, K. (2011). Identification of TMEM45B as a protein clearly showing thermal aggregation in SDS–PAGE gels and dissection of its amino acid sequence responsible for this aggregation. *Protein Expression and Purification*, 77, 118-123.

Ongagna-Yhombi, S. Y., Corstjens, P., Geva, E., Abrams, W. R., Barber, C. A., Malamud, D. and Mharakurwa, S. (2013). Improved assay to detect *Plasmodium falciparum* using an uninterrupted, semi-nested PCR and quantitative lateral flow analysis. *Malaria Journal*, 12, 74. doi:10.1186/1475-2875-12-74.

Oppenheim, R. D., Creek, D. J., Macrae, J. I., Modrzynska, K. K., Pino, P., Limenitakis, J., Polonais, V., Seeber, F., Barrett, M. P., Billker, O., McConville, M. J. and Soldati-Favre, D. (2014). BCKDH: the missing link in apicomplexan mitochondrial metabolism is required for full virulence of *Toxoplasma gondii* and *Plasmodium berghei*. *PLOS Pathogens*, 10, e1004263. doi.org/10.1371/journal.ppat.1004263.

Overton, T. W. (2014). Recombinant protein production in bacterial hosts. *Drug Discovery Today*, 19, 590-601.

Pace, C. N. and McGrath, T. (1980). Substrate stabilization of lysozyme to thermal and guanidine hydrochloride denaturation. *Journal of Biological Chemistry*, 255, 3862-3865.

Painter, H. J., Morrisey, J. M., Mather, M. W. and Vaidya, A. B. (2007). Specific role of mitochondrial electron transport in blood-stage *Plasmodium falciparum*. *Nature*, 446, 88-91.

Paquet, T., Le Manach, C., Cabrera, D. G., Younis, Y., Henrich, P. P., Abraham, T. S., Lee, M. C. S., Basak, R., Ghidelli-Disse, S., Lafuente-Monasterio, M. J., Bantscheff, M., Ruecker, A., Blagborough, A. M., Zakutansky, S. E., Zeeman, A. M., White, K. L., Shackleford, D. M., Mannila, J., Morizzi, J., Scheurer, C., Angulo-Barturen, I., Martinez, M. S., Ferrer, S., Sanz, L. M., Gamo, F. J., Reader, J., Botha, M., Dechering, K. J., Sauerwein, R. W., Tungtaeng, A., Vanachayangkul, P., Lim, C. S., Burrows, J., Witty, M. J., Marsh, K. C., Bodenreider, C., Rochford, R., Solapure, S. M., Jimenez-Diaz, M. B., Wittlin, S., Charman, S. A., Donini, C., Campo, B., Birkholtz, L. M., Hanson, K. K., Drewes, G., Kocken, C. H. M., Delves, M. J., Leroy, D., Fidock, D. A., Waterson, D., Street, L. J. and Chibale, K. (2017). Antimalarial efficacy of MMV390048, an inhibitor of *Plasmodium* phosphatidylinositol 4-kinase. *Science Translational Medicine*, 9, eaad9735. doi: 10.1126/scitranslmed.aad9735.

Pearson, W. R. (2013). An introduction to sequence similarity ("homology") searching. *Current protocols in bioinformatics*, Chapter 3, Unit3.1-Unit3.1.

Peccarelli, M., Scott, T. D., Steele, M. and Kebaara, B. W. (2016). mRNAs involved in copper homeostasis are regulated by the nonsense-mediated mRNA decay pathway depending on environmental conditions. *Fungal Genetics and Biology*, 86, 81-90.

Peterson, D. S., Walliker, D. and Wellems, T. E. (1988). Evidence that a point mutation in dihydrofolate reductase-thymidylate synthase confers resistance to pyrimethamine in *falciparum* malaria. *Proceedings of the National Academy of Sciences of the United States of America,* 85, 9114-9118.

Phillips, M. A., Lotharius, J., Marsh, K., White, J., Dayan, A., White, K. L., Njoroge, J. W., El Mazouni, F., Lao, Y., Kokkonda, S., Tomchick, D. R., Deng, X., Laird, T., Bhatia, S. N., March, S., Ng, C. L., Fidock, D. A., Wittlin, S., Lafuente-Monasterio, M., Benito, F. J. G., Alonso, L. M. S., Martinez, M. S., Jimenez-Diaz, M. B., Bazaga, S. F., Angulo-Barturen, I., Haselden, J. N., Louttit, J., Cui, Y., Sridhar, A., Zeeman, A.-M., Kocken, C., Sauerwein, R., Dechering, K., Avery, V. M., Duffy, S., Delves, M., Sinden, R., Ruecker, A., Wickham, K. S., Rochford, R., Gahagen, J., Iyer, L., Riccio, E., Mirsalis, J., Bathhurst, I., Rueckle, T., Ding, X., Campo, B., Leroy, D., Rogers, M. J., Rathod, P. K., Burrows, J. N. and Charman, S. A. (2015). A long-duration dihydroorotate dehydrogenase inhibitor (DSM265) for prevention and treatment of malaria. *Science Translational Medicine,* 7, 296ra111. doi:10.1126/scitranslmed.aaa6645.

Polson, A., Coetzer, T., Kruger, J., von Maltzahn, E. and van der Merwe, K. J. (1985). Improvements in the isolation of IgY from the yolks of eggs laid by immunized hens. *Immunological Investigations,* 14, 323-327.

Pongtavornpinyo, W., Hastings, I. M., Dondorp, A., White, L. J., Maude, R. J., Saralamba, S., Day, N. P., White, N. J. and Boni, M. F. (2009). Probability of emergence of antimalarial resistance in different stages of the parasite life cycle. *Evolutionary Applications,* 2, 52-61.

Ponnudurai, T., Lensen, A. H. W., Gemert, G. J. A., Bolmer, M. G. and Meuwissen, J. H. T. (1991). Feeding behaviour and sporozoite ejection by infected *Anopheles stephensi*. *Transactions of the Royal Society of Tropical Medicine and Hygiene,* 85, 175-180.

Pope, C. R., De Feo, C. J. and Unger, V. M. (2013). Cellular distribution of copper to superoxide dismutase involves scaffolding by membranes. *Proceedings of the National Academy of Sciences of the United States of America,* 110, 20491-20496.

Pozdnyakova, I., Guidry, J. and Wittung-Stafshede, P. (2001). Copper stabilizes azurin by decreasing the unfolding rate. *Archives of Biochemistry and Biophysics,* 390, 146-148.

Price, R. N., Cassar, C., Brockman, A., Duraisingh, M., van Vugt, M., White, N. J., Nosten, F. and Krishna, S. (1999). The *pfmdr1* gene Is associated with a multidrug-resistant phenotype in *Plasmodium falciparum* from the western border of Thailand. *Antimicrobial Agents and Chemotherapy,* 43, 2943-2949.

Price, R. N., Uhlemann, A.-C., van Vugt, M., Brockman, A., Hutagalung, R., Nair, S., Nash, D., Singhasivanon, P., Anderson, T. J. C., Krishna, S., White, N. J. and Nosten, F. (2006). Molecular and pharmacological determinants of the therapeutic response to artemether-lumefantrine in multidrug-resistant *Plasmodium falciparum* malaria. *Clinical Infectious Diseases,* 42, 1570-1577.

Puig, S., Lee, J., Lau, M. and Thiele, D. J. (2002). Biochemical and genetic analyses of yeast and human high affinity copper transporters suggest a conserved mechanism for copper uptake. *Journal of Biological Chemistry,* 277, 26021-26030.

Pundir, S., Martin, M. J. and O'Donovan, C. (2017). UniProt protein knowledgebase. *In:* Wu, C. H., Arighi, C. N. and Ross, K. E. (eds.) *Protein Bioinformatics: From Protein Modifications and Networks to Proteomics.* New York, NY: Springer New York.

Raj, D. K., Mu, J., Jiang, H., Kabat, J., Singh, S., Sullivan, M., Fay, M. P., McCutchan, T. F. and Su, X.-z. (2009). Disruption of a *Plasmodium falciparum* multidrug resistance-associated protein (*Pf*MRP) alters its fitness and transport of antimalarial drugs and glutathione. *Journal of Biological Chemistry,* 284, 7687-7696.

Raman, J., Morris, N., Frean, J., Brooke, B., Blumberg, L., Kruger, P., Mabusa, A., Raswiswi, E., Shandukani, B., Misani, E., Groepe, M.-A. and Moonasar, D. (2016). Reviewing South Africa's malaria elimination strategy (2012–2018): progress, challenges and priorities. *Malaria Journal,* 15, 438. doi: 10.1186/s12936-016-1497-x.

Rasoloson, D., Shi, L. R., Chong, C. R., Kafsack, B. F. and Sullivan, D. J. (2004). Copper pathways in *Plasmodium faliciparum* infected erythrocytes indicate an efflux role for the copper P-ATPase. *Biochemical Journal,* 381, 803-811.

Rath, A. and Deber, C. M. (2013). Correction factors for membrane protein molecular weight readouts on sodium dodecyl sulfate–polyacrylamide gel electrophoresis. *Analytical Biochemistry,* 434, 67-72.

Reed, M. B., Saliba, K. J., Caruana, S. R., Kirk, K. and Cowman, A. F. (2000). Pgh1 modulates sensitivity and resistance to multiple antimalarials in *Plasmodium falciparum*. *Nature,* 403, 906-909.

Rees, E. M., Lee, J. and Thiele, D. J. (2004). Mobilization of intracellular copper stores by the Ctr2 vacuolar copper transporter. *Journal of Biological Chemistry,* 279, 54221-54229.

Rees, E. M. and Thiele, D. J. (2007). Identification of a vacuole-associated metalloreductase and its role in Ctr2-mediated intracellular copper mobilization. *Journal of Biological Chemistry,* 282, 21629-21638.

Rieckmann, K. H., Davis, D. R. and Hutton, D. C. (1989). *Plasmodium vivax* resistance to chloroquine? *The Lancet,* 334, 1183-1184.

Rigby, K., Zhang, L., Cobine, P. A., George, G. N. and Winge, D. R. (2007). Characterization of the cytochrome c oxidase assembly factor Cox19 of *Saccharomyces cerevisiae*. *Journal of Biological Chemistry,* 282, 10233-10242.

Rivett, A. J. and Levine, R. L. (1990). Metal-catalyzed oxidation of *Escherichia coli* glutamine synthetase: correlation of structural and functional changes. *Archives of Biochemistry and Biophysics,* 278, 26-34.

Rodriguez, J. A., Valentine, J. S., Eggers, D. K., Roe, J. A., Tiwari, A., Brown, R. H., Jr. and Hayward, L. J. (2002). Familial amyotrophic lateral sclerosis-associated mutations decrease the thermal stability of distinctly metallated species of human copper/zinc superoxide dismutase. *Journal of Biological Chemistry,* 277, 15932-15937.

Ross, R. (1898). The role of the mosquito in the evolution of the malaria parasite. *The Lancet*, 488-489.

Rottmann, M., McNamara, C., Yeung, B. K. S., Lee, M. C. S., Zou, B., Russell, B., Seitz, P., Plouffe, D. M., Dharia, N. V., Tan, J., Cohen, S. B., Spencer, K. R., González-Páez, G. E., Lakshminarayana, S. B., Goh, A., Suwanarusk, R., Jegla, T., Schmitt, E. K., Beck, H.-P., Brun, R., Nosten, F., Renia, L., Dartois, V., Keller, T. H., Fidock, D. A., Winzeler, E. A. and Diagana, T. T. (2010). Spiroindolones, a potent compound class for the treatment of malaria. *Science,* 329, 1175-1180.

Rutherford, J. C. and Bird, A. J. (2004). Metal-responsive transcription factors that regulate iron, zinc, and copper homeostasis in eukaryotic cells. *Eukaryotic Cell,* 3, 1-13.

Samanovic, Marie I., Ding, C., Thiele, Dennis J. and Darwin, K. H. (2012). Copper in microbial pathogenesis: meddling with the metal. *Cell Host & Microbe,* 11, 106-115.

Sambrook, J., Fritsch, E. F. and Maniatis, T. (1989). *Molecular Cloning: A Laboratory Manual,* Cold Spring Harbor, New York, Cold Spring Harbor Laboratory Press.

Saravanan, P. and Satish, K. (2010). Diagnostic and immunoprophylactic applications of synthetic peptides in veterinary microbiology. *Microbiology Research,* 1, e1. doi:10.4081/mr.2010.e1.

Sathpathi, S., Mohanty, A. K., Satpathi, P., Mishra, S. K., Behera, P. K., Patel, G. and Dondorp, A. M. (2014). Comparing Leishman and Giemsa staining for the assessment of peripheral blood smear preparations in a malaria-endemic region in India. *Malaria Journal,* 13, 512. doi:10.1186/1475-2875-13-512.

Savini, I., D'Alessio, S., Giartosio, A., Morpurgo, L. and Avigliano, L. (1990). The role of copper in the stability of ascorbate oxidase towards denaturing agents. *European Journal of Biochemistry,* 190, 491-495.

Schafer, F. Q. and Buettner, G. R. (2001). Redox environment of the cell as viewed through the redox state of the glutathione disulfide/glutathione couple. *Free Radical Biology and Medicine,* 30, 1191-1212.

Scheiber, I. F., Mercer, J. F. B. and Dringen, R. (2014). Metabolism and functions of copper in brain. *Progress in Neurobiology,* 116, 33-57.

Schlagenhauf, P. and Petersen, E. (2008). Malaria chemoprophylaxis: strategies for risk groups. *Clinical Microbiology Reviews,* 21, 466-472.

Schlitzer, M. (2008). Antimalarial drugs – what is in use and what is in the pipeline. *Archiv Der Pharmazie,* 341, 149-163.

Sedlák, E., Žoldák, G. and Wittung-Stafshede, P. (2008). Role of copper in thermal stability of human ceruloplasmin. *Biophysical Journal,* 94, 1384-1391.

Selvi, R. B. and Kundu, T. K. (2009). Reversible acetylation of chromatin: Implication in regulation of gene expression, disease and therapeutics. *Biotechnology Journal,* 4, 375-390.

Shortt, H. E. and Garnham, P. C. C. (1948). Pre-erythrocytic stage in mammalian malaria parasites. *Nature,* 161, 126.

Shrimp, J. H., Garlick, J. M., Tezil, T., Sorum, A. W., Worth, A. J., Blair, I. A., Verdin, E., Snyder, N. W. and Meier, J. L. (2017). Defining metabolic and nonmetabolic regulation of histone acetylation by NSAID chemotypes. *Molecular Pharmaceutics,* 15, 729-736.

Sideris, D. P., Petrakis, N., Katrakili, N., Mikropoulou, D., Gallo, A., Ciofi-Baffoni, S., Banci, L., Bertini, I. and Tokatlidis, K. (2009). A novel intermembrane space-targeting signal docks cysteines onto Mia40 during mitochondrial oxidative folding. *Journal of Cell Biology,* 187, 1007-1022.

Sidhu, A. B. S., Valderramos, S. G. and Fidock, D. A. (2005). *pfmdr1* mutations contribute to quinine resistance and enhance mefloquine and artemisinin sensitivity in *Plasmodium falciparum*. *Molecular Microbiology,* 57, 913-926.

Singh, B. and Daneshvar, C. (2013). Human infections and detection of *Plasmodium knowlesi*. *Clinical Microbiology Reviews,* 26, 165-184.

Singh, B., Sung, L. K., Matusop, A., Radhakrishnan, A., Shamsul, S. S. G., Cox-Singh, J., Thomas, A. and Conway, D. J. (2004). A large focus of naturally acquired *Plasmodium knowlesi* infections in human beings. *The Lancet,* 363, 1017-1024.

Singha, T. K., Gulati, P., Mohanty, A., Khasa, Y. P., Kapoor, R. K. and Kumar, S. (2017). Efficient genetic approaches for improvement of plasmid based expression of recombinant protein in *Escherichia coli*: A review. *Process Biochemistry,* 55, 17-31.

Sinka, M. E., Bangs, M. J., Manguin, S., Rubio-Palis, Y., Chareonviriyaphap, T., Coetzee, M., Mbogo, C. M., Hemingway, J., Patil, A. P., Temperley, W. H., Gething, P. W., Kabaria, C. W., Burkot, T. R., Harbach, R. E. and Hay, S. I. (2012). A global map of dominant malaria vectors. *Parasites & Vectors,* 5, 69. doi:10.1186/1756-3305-5-69.

Sirrenberg, C., Bauer, M. F., Guiard, B., Neupert, W. and Brunner, M. (1996). Import of carrier proteins into the mitochondrial inner membrane mediated by Tim22. *Nature,* 384, 582-585.

Sivashanmugam, A., Murray, V., Cui, C., Zhang, Y., Wang, J. and Li, Q. (2009). Practical protocols for production of very high yields of recombinant proteins using *Escherichia coli*. *Protein Science,* 18, 936-948.

Snow, R. W., Sartorius, B., Kyalo, D., Maina, J., Amratia, P., Mundia, C. W., Bejon, P. and Noor, A. M. (2017). The prevalence of *Plasmodium falciparum* in sub-Saharan Africa since 1900. *Nature,* 550, 515-518.

Solioz, M. and Stoyanov, J. V. (2003). Copper homeostasis in *Enterococcus hirae*. *FEMS Microbiology Reviews,* 27, 183-195.

Sørensen, H. P. and Mortensen, K. K. (2005). Advanced genetic strategies for recombinant protein expression in *Escherichia coli*. *Journal of Biotechnology,* 115, 113-128.

Soto, I. C., Fontanesi, F., Liu, J. and Barrientos, A. (2012). Biogenesis and assembly of eukaryotic cytochrome c oxidase catalytic core. *Biochimica et Biophysica Acta - Bioenergetics,* 1817, 883-897.

Spillman, N. J., Allen, R. J. W., McNamara, C. W., Yeung, B. K. S., Winzeler, E. A., Diagana, T. T. and Kirk, K. (2013). Na^+ regulation in the malaria parasite *Plasmodium falciparum* involves the cation ATPase *Pf*ATP4 and is a target of the spiroindolone antimalarials. *Cell Host & Microbe,* 13, 227-237.

Stockel, J., Safar, J., Wallace, A. C., Cohen, F. E. and Prusiner, S. B. (1998). Prion protein selectively binds copper(II) ions. *Biochemistry,* 37, 7185-7193.

Sturm, A., Amino, R., van de Sand, C., Regen, T., Retzlaff, S., Rennenberg, A., Krueger, A., Pollok, J.-M., Menard, R. and Heussler, V. T. (2006). Manipulation of host hepatocytes by the malaria parasite for delivery into liver sinusoids. *Science,* 313, 1287-1290.

Suckow, M. A., Danneman, P. and Brayton, C. (2001). *The Laboratory Mouse,* Boca Raton, CRC Press.

Swarthout, T. D., Counihan, H., Senga, R. K. and van den Broek, I. (2007). Paracheck-Pf® accuracy and recently treated *Plasmodium falciparum* infections: is there a risk of over-diagnosis? *Malaria Journal,* 6, 58. doi:10.1186/1475-2875-6-58.

Takahashi, Y., Kako, K., Kashiwabara, S.-i., Takehara, A., Inada, Y., Arai, H., Nakada, K., Kodama, H., Hayashi, J.-i., Baba, T. and Munekata, E. (2002). Mammalian copper chaperone Cox17p has an essential role in activation of cytochrome c oxidase and embryonic development. *Molecular and Cellular Biology,* 22, 7614-7621.

Tangpukdee, N., Duangdee, C., Wilairatana, P. and Krudsood, S. (2009). Malaria diagnosis: A brief review. *The Korean Journal of Parasitology,* 47, 93-102.

Tapiero, H., Townsend, D. M. and Tew, K. D. (2003). Trace elements in human physiology and pathology. Copper. *Biomedicine & Pharmacotherapy,* 57, 386-398.

Tavares, J., Formaglio, P., Thiberge, S., Mordelet, E., Van Rooijen, N., Medvinsky, A., Ménard, R. and Amino, R. (2013). Role of host cell traversal by the malaria sporozoite during liver infection. *The Journal of Experimental Medicine,* 210, 905-915.

Thompson, A. K., Smith, D., Gray, J., Carr, H. S., Liu, A., Winge, D. R. and Hosler, J. P. (2010). Mutagenic analysis of Cox11 of *Rhodobacter sphaeroides*: insights into the assembly of Cu_B of cytochrome c oxidase. *Biochemistry,* 49, 5651-5661.

Timón-Gómez, A., Nývltová, E., Abriata, L. A., Vila, A. J., Hosler, J. and Barrientos, A. (2018). Mitochondrial cytochrome c oxidase biogenesis: recent developments. *Seminars in Cell & Developmental Biology,* 76, 163-178.

Tisato, F., Marzano, C., Porchia, M., Pellei, M. and Santini, C. (2010). Copper in diseases and treatments, and copper-based anticancer strategies. *Medicinal Research Reviews,* 30, 708-749.

Tomar, D., Biswas, S., Tripathi, V. and Rao, D. N. (2006). Development of diagnostic reagents: raising antibodies against synthetic peptides of *Pf*HRP-2 and LDH using micsosphere delivery. *Immunobiology,* 211, 797-805.

Towbin, H., Staehelin, T. and Gordon, J. (1979). Electrophoretic transfer of proteins from polyacrylamide gels to nitrocellulose sheets: procedure and some applications. *Proceedings of the National Academy of Sciences of the United States of America,* 76, 4350-4354.

Tsukihara, T., Aoyama, H., Yamashita, E., Tomizaki, T., Yamaguchi, H., Shinzawa-Itoh, K., Nakashima, R., Yaono, R. and Yoshikawa, S. (1995). Structures of metal sites of oxidized bovine heart cytochrome c oxidase at 2.8 Å. *Science,* 269, 1069-1074.

Turski, M. L. and Thiele, D. J. (2009). New roles for copper metabolism in cell proliferation, signaling, and disease. *Journal of Biological Chemistry,* 284, 717-721.

Tzagoloff, A., Capitanio, N., Nobrega, M. P. and Gatti, D. (1990). Cytochrome oxidase assembly in yeast requires the product of COX11, a homolog of the *P. denitrificans* protein encoded by ORF3. *The EMBO Journal,* 9, 2759-2764.

Tzagoloff, A. and Dieckmann, C. L. (1990). PET genes of *Saccharomyces cerevisiae*. *Microbiological Reviews,* 54, 211-225.

Uyemura, S. A., Luo, S., Vieira, M., Moreno, S. N. J. and Docampo, R. (2004). Oxidative phosphorylation and rotenone-insensitive malate- and NADH-Quinone oxidoreductases in *Plasmodium yoelii yoelii* mitochondria *in situ*. *Journal of Biological Chemistry*, 279, 385-393.

Vaidya, A. B., Akella, R. and Suplick, K. (1989). Sequences similar to genes for two mitochondrial proteins and portions of ribosomal RNA in tandemly arrayed 6-kilobase-pair DNA of a malarial parasite. *Molecular and Biochemical Parasitology*, 35, 97-107.

Vaidya, A. B. and Mather, M. W. (2009). Mitochondrial evolution and functions in malaria parasites. *Annual Review of Microbiology*, 63, 249-267.

Vaidya, A. B., Morrisey, J. M., Zhang, Z., Das, S., Daly, T. M., Otto, T. D., Spillman, N. J., Wyvratt, M., Siegl, P., Marfurt, J., Wirjanata, G., Sebayang, B. F., Price, R. N., Chatterjee, A., Nagle, A., Stasiak, M., Charman, S. A., Angulo-Barturen, I., Ferrer, S., Belén Jiménez-Díaz, M., Martínez, M. S., Gamo, F. J., Avery, V. M., Ruecker, A., Delves, M., Kirk, K., Berriman, M., Kortagere, S., Burrows, J., Fan, E. and Bergman, L. W. (2014). Pyrazoleamide compounds are potent antimalarials that target Na^+ homeostasis in intraerythrocytic *Plasmodium falciparum*. *Nature Communications*, 5, 5521. doi:10.1038/ncomms6521.

van den Berghe, P. V. E., Folmer, D. E., Malingré, H. E. M., van Beurden, E., Klomp, A. E. M., van de Sluis, B., Merkx, M., Berger, R. and Klomp, L. W. J. (2007). Human copper transporter 2 is localized in late endosomes and lysosomes and facilitates cellular copper uptake. *Biochemical Journal*, 407, 49-59.

Vanachayangkul, P., Lon, C., Spring, M., Sok, S., Ta-aksorn, W., Kodchakorn, C., Pann, S.-T., Chann, S., Ittiverakul, M., Sriwichai, S., Buathong, N., Kuntawunginn, W., So, M., Youdaline, T., Milner, E., Wojnarski, M., Lanteri, C., Manning, J., Prom, S., Haigney, M., Cantilena, L. and Saunders, D. (2017). Piperaquine population pharmacokinetics and cardiac safety in Cambodia. *Antimicrobial Agents and Chemotherapy*, 61, e02000-16. doi:10.1128/AAC.02000-16.

Vander Jagt, D. L., Hunsaker, L. A., Campos, N. M. and Baack, B. R. (1990). D-lactate production in erythrocytes infected with *Plasmodium falciparum*. *Molecular and Biochemical Parasitology*, 42, 277-284.

Vest, K. E., Leary, S. C., Winge, D. R. and Cobine, P. A. (2013). Copper import into the mitochondrial matrix in *Saccharomyces cerevisiae* is mediated by Pic2, a mitochondrial carrier family protein. *Journal of Biological Chemistry*, 288, 23884-23892.

Vest, K. E., Wang, J., Gammon, M. G., Maynard, M. K., White, O. L., Cobine, J. A., Mahone, W. K. and Cobine, P. A. (2016). Overlap of copper and iron uptake systems in mitochondria in *Saccharomyces cerevisiae*. *Open Biology*, 6, 150223. doi:10.1098/rsob.150223.

Vincke, I. H. and Lips, M. (1948). Un nouveau plasmodium d'un rongeur sauvage du Congo *Plasmodium berghei* n. sp. *Annales de la Société Belge de Médecine Tropicale,* 28, 97-104.

Vita, N., Landolfi, G., Baslé, A., Platsaki, S., Lee, J., Waldron, K. J. and Dennison, C. (2016). Bacterial cytosolic proteins with a high capacity for Cu(I) that protect against copper toxicity. *Scientific Reports,* 6, 39065. doi:10.1038/srep39065.

Vivares, C. P., Gouy, M., Thomarat, F. and Metenier, G. (2002). Functional and evolutionary analysis of a eukaryotic parasitic genome. *Current Opinion in Microbiology,* 5, 499-505.

Voorberg-van der Wel, A., Roma, G., Gupta, D. K., Schuierer, S., Nigsch, F., Carbone, W., Zeeman, A.-M., Lee, B. H., Hofman, S. O., Faber, B. W., Knehr, J., Pasini, E., Kinzel, B., Bifani, P., Bonamy, G. M. C., Bouwmeester, T., Kocken, C. H. M. and Diagana, T. T. (2017). A comparative transcriptomic analysis of replicating and dormant liver stages of the relapsing malaria parasite *Plasmodium cynomolgi*. *Elife,* 6, e29605. doi:10.7554/eLife.29605.

Wang, K., Zhen, Y., Sadoski, R., Grinnell, S., Geren, L., Ferguson-Miller, S., Durham, B. and Millett, F. (1999). Definition of the interaction domain for cytochrome c on cytochrome c oxidase: II. Rapid kinetic analysis of electron transfer from cytochrome c to *Rhodobacter sphaeroides* cytochrome oxidase surface mutants. *Journal of Biological Chemistry,* 274, 38042-38050.

Wang, M., Wang, Q., Gao, X. and Su, Z. (2017). Conditional knock-out of lipoic acid protein ligase 1 reveals redundancy pathway for lipoic acid metabolism in *Plasmodium berghei* malaria parasite. *Parasites & Vectors,* 10, 315. doi:10.1186/s13071-017-2253-y.

Wang, Q., Zhang, Y., Yang, C., Xiong, H., Lin, Y., Yao, J., Li, H., Xie, L., Zhao, W., Yao, Y., Ning, Z. B., Zeng, R., Xiong, Y., Guan, K. L., Zhao, S. and Zhao, G. P. (2010). Acetylation of metabolic enzymes coordinates carbon source utilization and metabolic flux. *Science,* 327, 1004-1007.

Wang, Y., Hodgkinson, V., Zhu, S., Weisman, G. A. and Petris, M. J. (2011). Advances in the understanding of mammalian copper transporters. *Advances in Nutrition,* 2, 129-137.

Warhurst, D. C. and Williams, J. E. (1996). ACP Broadsheet no 148. July 1996. Laboratory diagnosis of malaria. *Journal of Clinical Pathology,* 49, 533-538.

Watly, J., Simonovsky, E., Wieczorek, R., Barbosa, N., Miller, Y. and Kozlowski, H. (2014). Insight into the coordination and the binding sites of Cu^{2+} by the histidyl-6-tag using experimental and computational tools. *Inorganic Chemistry,* 53, 6675-6683.

Weckbecker, D., Longen, S., Riemer, J. and Herrmann, J. M. (2012). Atp23 biogenesis reveals a chaperone-like folding activity of Mia40 in the IMS of mitochondria. *The EMBO Journal,* 31, 4348-4358.

Weiss, G. E., Gilson, P. R., Taechalertpaisarn, T., Tham, W.-H., de Jong, N. W. M., Harvey, K. L., Fowkes, F. J. I., Barlow, P. N., Rayner, J. C., Wright, G. J., Cowman, A. F. and Crabb, B. S. (2015). Revealing the sequence and resulting cellular morphology of receptor-ligand interactions during *Plasmodium falciparum* invasion of erythrocytes. *PLOS Pathogens,* 11, e1004670. doi:10.1371/journal.ppat.1004670.

White, N. J. (2004). Antimalarial drug resistance. *Journal of Clinical Investigation,* 113, 1084-1092.

White, N. J., Pukrittayakamee, S., Hien, T. T., Faiz, M. A., Mokuolu, O. A. and Dondorp, A. M. (2014). Malaria. *The Lancet,* 383, 723-735.

WHO (2010). World Malaria Report. Geneva: World Health Organisation.

WHO (2015). Guidelines for the treatment of malaria. 3rd ed.: World Health Organisation.

WHO (2016). World Malaria Report. Geneva: World Health Organisation.

WHO (2017). World malaria report. Geneva: World Health Organisation.

Wijekoon, C. J. K., Ukuwela, A. A., Wedd, A. G. and Xiao, Z. (2016). Evaluation of employing poly-lysine tags versus poly-histidine tags for purification and characterization of recombinant copper-binding proteins. *Journal of Inorganic Biochemistry,* 162, 286-294.

Wikstrom, M. K. F. (1977). Proton pump coupled to cytochrome c oxidase in mitochondria. *Nature,* 266, 271-273.

Witkowski, B., Duru, V., Khim, N., Ross, L. S., Saintpierre, B., Beghain, J., Chy, S., Kim, S., Ke, S., Kloeung, N., Eam, R., Khean, C., Ken, M., Loch, K., Bouillon, A., Domergue, A., Ma, L., Bouchier, C., Leang, R., Huy, R., Nuel, G., Barale, J.-C., Legrand, E., Ringwald, P., Fidock, D. A., Mercereau-Puijalon, O., Ariey, F. and Ménard, D. (2017). A surrogate marker of piperaquine-resistant *Plasmodium falciparum* malaria: a phenotype–genotype association study. *The Lancet. Infectious Diseases,* 17, 174-183.

Wolf, Y. I. and Koonin, E. V. (2013). Genome reduction as the dominant mode of evolution. *Bioessays,* 35, 829-837.

Wongsrichanalai, C., Barcus, M. J., Muth, S., Sutamihardja, A. and Wernsdorfer, W. H. (2007). A review of malaria diagnostic tools: microscopy and rapid diagnostic test (RDT). *The American Journal of Tropical Medicine and Hygiene,* 77, 119-127.

Xiao, G., Fan, Q., Wang, X. and Zhou, B. (2013). Huntington disease arises from a combinatory toxicity of polyglutamine and copper binding. *Proceedings of the National Academy of Sciences of the United States of America*, 110, 14995-15000.

Yang, Y., Yin, J., Liu, J., Xu, Q., Lan, T., Ren, F. and Hao, Y. (2017). The copper homeostasis transcription factor CopR is involved in H_2O_2 stress in *Lactobacillus plantarum* CAUH2. *Frontiers in Microbiology*, 8, 2015. doi:10.3389/fmicb.2017.0201.

Zhao, S., Xu, W., Jiang, W., Yu, W., Lin, Y., Zhang, T., Yao, J., Zhou, L., Zeng, Y., Li, H., Li, Y., Shi, J., An, W., Hancock, S. M., He, F., Qin, L., Chin, J., Yang, P., Chen, X., Lei, Q., Xiong, Y. and Guan, K.-L. (2010). Regulation of cellular metabolism by protein lysine acetylation. *Science*, 327, 1000-1004.

Zhou, B. and Gitschier, J. (1997). hCTR1: A human gene for copper uptake identified by complementation in yeast. *Proceedings of the National Academy of Sciences of the United States of America*, 94, 7481-7486.